APPLICATION OF SVC AND STATCOM TO IMPROVE STABILITY OF AC/DC HYBRID POWER SYSTEMS AND TO SUPPRESS SUBSYNCHRONOUS OSCILLATION

LIN YONG

Ph. D.

The Hong Kong

Polytechnic University

2012

The Hong Kong Polytechnic University

Department of Electrical Engineering

APPLICATION OF SVC AND STATCOM TO IMPROVE STABILITY OF AC/DC HYBRID POWER SYSTEMS AND TO SUPPRESS SUBSYNCHRONOUS OSCILLATION

LIN YONG

A thesis submitted in partial fulfillment of the requirements for the Degree of Doctor of Philosophy

December 2011

CERTIFICATE OF ORINGALITY

I hereby declare that this thesis is my own work and that, to the best my knowledge and belief, it reproduces no material previously published or written or material which has been accepted for the award any other degree or diploma, except where due acknowledgement has been made in the text.

__________________________(Signed)

Yong LIN (Name of student)

ABSTRACT

As the power systems continue to grow in size, large interregional AC/DC hybrid grids come into being, ultrahigh-voltage long-distance power transmission lines and ultra-large-capacity generation units are gradually put into operation, and the series capacitor compensators and High Voltage Direct Current (hereinafter referred to as HVDC) systems are adopted to improve the power system stability and transmission capability. Therefore the subsynchronous resonance/oscillation problems and the stability problems in the large-scale AC/DC hybrid power systems resulting from these factors will necessarily become the problems in the secure operation of the grids that can't be ignored. With the implementation of the "Transmission of Power from the West to the East" program, it is of obvious engineering application value to research the stability of AC/DC hybrid grids and the technologies of suppressing subsynchronous oscillations of the power system. This dissertation, in accordance with the applications of the SVC and STATCOM in the large complicated AC/DC hybrid grids, proposes novel control design theories and methods, and tests these theories and methods through calculation analyses and simulation experiments. The SVCs and STATCOMs designed according to these theories and methods have been successfully applied to the 210Mvar SVC at 500kV Wuzhou Substation in China Southern Power Grid, the four sets of SSR-DSs in Guohua Jinjie Power Plant, the 240Mvar SVCs at Chuxiong Converter Station of the Yunnan-Guangdong ±800kV ultrahigh-voltage DC power transmission project in China Southern Power Grid, and the ±200Mvar STATCOMs at 500kV Dongguan Substation in China Southern Power Grid.

This dissertation contributes to the research and engineering practice of the SVC mainly in the following aspects:

(1) Calculates the static voltage stability and transient voltage stability of China Southern Power Grid through simulation experiments, especially researches the

transient voltage stability in the cases of abrupt load increases and the faults in tie lines, builds the models for the motor loads at the receiving-end system, calculates and analyses the impact of the proportions of dynamic loads and the abrupt load increases on the stability, simulates the dynamic processes in time of AC/DC faults in the AC/DC hybrid grids, and researches the impact of bipolar block faults in the DC power transmission systems in the cases of different load models on the stability and calculates the reactive power requirements.

(2) Introduces the engineering design and calculation methods of the capacity of the SVC used to enhance the system voltage, calculates the voltage fluctuations at the 500kV side of Wuzhou Substation when the SVCs are put into operation and the swing curves of the maximum relative angles among the generator units in the system when the SVCs are in/out of operation, tests the necessity of installing the SVC accordingly, and chooses the capacity of the SVC at Wuzhou Substation according to the comparisons of the stability calculation results in the cases of typical faults.

(3) Brings forward the design method of the additional damping controller of the SVC to suppress the low-frequency oscillations, and conducts analysis and verification through time-domain simulation experiments, whose results prove that this design approach is effective, providing ground for the design of the SVC used for suppressing the subsynchronous oscillations of the power systems. The Prony analysis is introduced to get the controlled system model for the SVC damping controller tuning. The most detailed and widely used SVC control system and control strategies for the supplementary controller design and parameters tuning is modeled.

(4) Takes the SVCs at Wuzhou Substation as an example, conducts simulation experiments with the RTDS simulator in connection with the real SVC controller in accordance with the IEEE 30-bus systems and tests the concrete results of the SVC used for improving the steady and transient stability and for suppressing

low-frequency oscillations of the power system.

(5) Proposes the scheme of suppressing subsynchronous resonance/oscillation with the SVC, introduces the concrete system structure design, presents the implementation of the algorithm of introducing the subsynchronous frequency components in the process of fundamental-frequency susceptance regulations, and on the basis of the actual project at the Guohua Jinjie Power Plant and with the methods combining off-line calculation, dynamic simulation and field test, conducts comprehensive and in-depth calculation and analysis of the subsynchronous oscillations resulting from the series compensator at Jinjie Power Plant, and the four sets of SSR-DSs designed successfully accordingly have been put them into operation.

(6) Introduces the roles that the SVC plays in ameliorating the stability of the power systems containing HVDC systems, analyses the cause of reactive power oscillations in the context of two sets of SVCs in parallel operation, proposes a novel composite control structure that enables shunt 2 self-governed SVCs to achieve balanced outputs in steady states and transient states and eliminated oscillations, and tests the real SVC controller through the simulation experiments with the RTDS simulator. The SVCs at Chuxiong Converter Station of the Yunnan-Guangdong ±800kV ultrahigh-voltage DC power transmission project were designed based on this structure, and the field operation results are good. This novel composite control structure also tackle the difficult problems of current-averaging in large power electronics devices of the FACTS equipment, and the 200Mvar STATCOMs at Dongguan, the STATCOM of the largest capacity worldwide, designed based on this structure have been in operation.

(7) Researches the STATCOM in providing reactive voltage support for the grid, builds the mathematical model for the cascaded STATCOM, proposes the principle and implementation of the decoupled control of the STATCOM, builds the simulation model of the STATCOM, and tests the effectiveness of the control system

designed according to the decoupled control principle under normal and abnormal conditions through time-domain simulation experiments. The 200Mvar STATCOMs designed on the basis of this principle and algorithm are the STATCOMs with the highest voltage level of direct connection worldwide.

The works of this thesis can be also adopted to improve performance for distributed generation system such as wind farm which is sensitive to oscillation and demands dynamic reactive power support.

ACKNOWLEDGEMENT

First and foremost, I would like to express my sincere gratitude and appreciation to my supervisor, Dr. Edward W.C. Lo, for his invaluable guidance and constant encouragement throughout the challenging path towards a doctoral degree. His enthusiasm and guidance were strong sources of inspiration. He is always available for me in spite of his busy schedule and duties. It has been an honor to work under his supervision.

I am grateful to all staffs of the Department of Electrical Engineering for their support and help. I would like to acknowledge the help that I received from my friends and coworkers as well.

I would like to acknowledge the support from the China Southern Power Grid for the real data of the grid provided for the simulations, and from other organizations mentioned in this dissertation as well. Thanks are due to LI Haisheng, WANG Xing, Dr. FU Chuang, Dr. HONG Chao, Profssor JIN Xiaoming, Dr. ZHANG Jianshe, Dr. LIU Hongtao and other staffs of China Southern Power Grid Technology Research Center.

I reserve special thanks to the fate which dealt me a cruel blow. It compelled me to seek a chance of survival but it also gave me opportunities to accomplish some large engineering projects almost impossible. I don't believe in fate, whereas I revere it. Nobody knows his own destiny. This dissertation is a testament to the hard work and for that I offer the fate my deepest gratitude.

TABLE OF CONTENTS

LIST OF FIGURES, TABLES, AND ABBREVIATIONS

LIST OF FIGURES

LIST OF TABLES

LIST OF ABBREVIATIONS

AVR	Automatic Voltage Regulator
BEF	Band Elimination Filter
BPF	Band Pass Filter
CSG	China Southern Power Grid
DDAE	Difference, Differential-Algebraic Equations
EEAC	Extended Equal Area Criteria
EPRI	Electrical Power Research Institute
FACTS	Flexible AC Transmission Systems
HPF	High Pass Filter
HVDC	High Voltage Direct Current
LFO	Low-Frequency Oscillation
LOEC	Linear Optimal Excitation Control
LPF	Low Pass Filter
LPM	Liner Prediction Model
OLTC	On-Load Tap Changer
PEBS	Potential Energy Boundary Surface
PMU	Phasor Measurement Unit
PSS	Power System Stabilizer
RTDS	Real Time Digital Simulator
RUEP	Relevant Unstable Equilibrium Point
SEC	Supplementary Excitation Control
SEDC	Supplementary Excitation Damping Controller
SNB	Saddle-Node Bifurcation
SSDC	Sub-Synchronous Damping Controller
SSO	Sub-Synchronous Oscillation
SSR	Sub-Synchronous Resonance
SSR-DS	Sub-Synchronous Resonance Dynamic Stabilizer
s.t.	subject to

STATCOM	Static Synchronous Compensator
SVC	Static Var Compensator
UHV	Ultra-High Voltage
WAMS	Wide Area Measurement System
WSCC	Western Systems Coordinating Council

CHAPTER 1 INTRODUCTION

1.1 Background and Motivation

With the enlargement of the power systems, ultrahigh-voltage long-distance power transmission lines and ultra-large-capacity generation units are gradually put into operation, and the series capacitor compensators and the high voltage direct current (hereinafter referred to as HVDC) systems are adopted to improve the power system stability and transmission capability. All these contribute to bring about new problems to the secure and stable operation of the power systems, among which sub-synchronous oscillation is a typical issue.

Our country is very large with extremely unbalanced distributions energies and power loads, where the water resources are mainly concentrated in the southwest, the coal resources in Shanxi and the western parts of Inner Mongolia, and the loads in the eastern coastal areas. So, long-distance large-capacity power transmission is imperative. However, limited by the transient-state stability limits, the present grid lines in our country are characterized by obviously low transmission capabilities, and about 40 power plants of the State Grid Corporation system are blocked in terms of power outputs, such as Tuoketuo and Shangdu Power Plants in Inner Mongolia, Jinjie Power Plant in Shanxi, and Yimin Power Plant in the Northeast. Ways to tackle this problem include improvement of grid power transmission capabilities and building new lines, but owing to the limited room for developing new overhead power transmission corridors in large and medium cities, only the improvement of grid power transmission capabilities is feasible. And the series capacitor compensation is an economic and efficient way to improve the power transmission capacities of AC lines and to improve transient-state stability of the power systems. So far, there are multiple series compensation projects in operation in our country, and series compensation capacitors will gain wider applications in the construction of interconnected power grids in future. However, the large thermal power units will also continue to increase in the grids, and when integrated into the systems via series compensation lines, the large-scale steam turbine generators are liable to incur sub-synchronous resonance/oscillation in certain operation manners or at certain compensation degrees. And it has become the key technological issue of promoting and applying the series compensation capacitors to tackle the sub-synchronous resonance/oscillation problems.

The HVDC (high-voltage direct current) technology, by virtue of its technological and economic advantages, plays a very important role and gains wide applications in long-distance large-capacity power transmission and nationwide grid interconnections. In the future twenty years, there will be seven or more HVDC lines in China Southern Power Grid, and ten or more lines in Central China Power Grid. With the implementation of a large number of HVDC projects, the sub-synchronous oscillations and other direct-current security and stability problems resulting from the HVDC systems will become important practical problems.

It makes sense both in engineering applications and in practice to study the technologies of improving power system voltage stability and of suppressing the sub-synchronous resonance/oscillations of the power systems.

1.2 Primary Contributions

The main contributions of this dissertation lie in the studies and engineering practices of the SVC in improving voltage stability, suppressing sub-synchronous resonance/oscillations, and improving the stability of HVDC systems, which are summarized as follows:

(1) Bringing forward the approach to designing additional damping controller of the SVC based on Prony Identification Method, and conducting simulation calculations. The SVC in Wuzhou Substation in China Southern Power Grid was designed with this method, and results of simulation experiments with PSCAD and RTDS prove that the SVC controller can meet the grid requirements. So far, this SVC has been in operation for more than two years with good operation results.

(2) Putting forward a novel connection manner to connect the SVC (TCR+FC) to suppress sub-synchronous resonance with the 500kV bus bar of the power plant via an ordinary 500kV/35kV step-down transformer, with only the unit shafting used as the modulation and control signal of the phase-controlled reactors, and putting forward the implementation algorithm. Four sets of SVCs were designed with this method in Jinjie Power Plant, and have been in operation for two years with good operation results, greatly improving the outward transmission capabilities.

(3) Proposing a new composite control structure used for multiple sets of parallel SVCs that are controlled automatically and independently, designing a real controller accordingly, and conducting simulation experiments with RTDS for verification. The two sets of SVCs in the Chuxiong Converter Station of the Yunnan-Guangdong ±800kV ultrahigh-voltage HVDC Project have been in operation with good operation results. This control structure can tackle the current averaging problem of large-capacity power electronics devices at the device level. The 200Mvar STATCOMs also designed based on this structure have been put into operation in Dongguan Substation.

(4) This dissertation proposes the principle and implementation of the decoupled control of the STATCOM, builds the simulation model of the STATCOM, and tests the effectiveness of the control system designed according to the decoupled control principle under normal and abnormal conditions through time-domain simulation experiments. The 200Mvar STATCOMs designed on the basis of this principle and algorithm are the STATCOMs with the largest capacity and the highest voltage level of direct connection worldwide.

1.3 Organization of This Dissertation

Chapter 1 mainly introduces the background and research motivation as well as the dissertation structure and the lists of papers and patents related to the research work.

Chapter 2 is a brief review of documents, introducing the research and engineering status of grid stability, suppressing low-frequency oscillation and sub-synchronous resonance/oscillation with SVC, and the application of SVC in Ultrahigh-voltage DC power transmission.

Chapter 3 studies the underlying typical problems in the voltage stability of China Southern Power Grid, and analyses the steady-state and transient-state stability of AC/DC hybrid power transmission systems through simulation. And the calculation and analysis results are of guiding significance for future grid programming.

Chapter 4 takes the Wuzhou Substation as an example, and analyses and calculates the role that the SVC installation plays in providing dynamic reactive power support for the "Transmission of Power from the West to the East" channels in time of faults.

Chapter 5 brings forward a design approach to designing additional damping controller of the SVC based on Prony Identification Method, and conducts simulation studies in accordance with the IEEE-30 buses system, and the results indicate that this approach can effectively suppress low-frequency oscillation.

Chapter 6 conducts simulation experiments with PSCAD in accordance with the SVC controller in Wuzhou Substation that was designed with the design approach based on the Prony Identification Method, and conducts simulation experiments with RTDS in accordance with the controller hardware. Simulation results indicate that the SVC in Wuzhou Substation has the function of suppressing low-frequency oscillation, and can meet all aspects of requirements of having an SVC installed in Wuzhou substation in China Southern Power Grid.

Chapter 7 proposes a novel connection manner to connect the SVC (TCR+FC) to suppress sub-synchronous resonance with the 500kV bus bar of the power plant via an ordinary 500kV/35kV step-down transformer, with only the unit shafing used as the modulation and control signal of the phase-controlled reactors, puts forward the implementation algorithm, and enumerates the simulated and field measured waveforms and data. Results of dynamic simulations and field tests indicate that the capability of the SVC to suppress sub-synchronous resonance tallies with the expectations.

Chapter 8 calculates the role of the SVC in Chuxiong Converter Station to improve the voltage stability of the Yunnan-Guangdong Ultrahigh-voltage DC Power Transmission Lines, proposes a totally new composite control structure, realizes the balanced output of multiple parallel SVCs that are controlled independently and automatically, and enumerates the results of simulation experiments with the RTDS.

Chapter 9 proposes the principle and implementation of the decoupled control of the cascaded STATCOM, and proves that the STATCOM based on this principle can provide dynamic reactive power and voltages support for the grid through simulation experiments.

Chapter 10 summarizes the main contributions of this dissertation, and discusses some future research areas.

1.4 List of Publications

[1]. Min Zhu, Yong Lin （Min zhu & Yong Lin contributed equally to this paper）, Edward. W. C. Lo, Qiong Wang, Zhengjie Zhao and Wenhui Xie, "Electronic and magnetic properties of La_2NiMnO_6 and La_2CoMnO_6 with cationic ordering," *Applied Physical Letters* 100, 062406 (2012). （SCI indexed）.

[2]. XIA MINGCHAO, LIN YONG, EDWARD W.C. LO, "Unit Transient Based Protection for High Voltage Wind Power Transmission Lines," *Proceedings of 2011 International Conference on Instrumentation, Measurement, Circuits and Systems , ICIMCS 2011*, December 13-14, 2011, Hong Kong.

[3]. Yong Lin, MingChao Xia, Edward W.C. Lo, "SVC Additional Damping Controller Design Using Prony Identification," *Asian Transactions on Engineering* (ATE ISSN: 2221-4267), Volume 01 Issue 05, November 2011, pp.45-48

[4]. Chun Shang, Yong Lin, Zhengxiang Zhang, Tiansen Gongi, Rong Hu, "The Method of Reducing Voltage Oscillation in Feedforward Controlled SVC," *ELECTRICAL ENGINEERING*，2011(1)，pp.74-78

[5]. Chun Shang, Yong Lin, Zhengxiang Zhang, Tiansen Gongi, Rong Hu, "Self-regulating Control Reference Voltage Method in SVC System," *ELECTRICAL ENGINEERING*，2010(12), pp.74-76

[6]. LIN Yong, Edward. W. C. Lo, "Study on the grid-connected wind power plant caused effects on power quality," *ELECTROTECHNICAL APPLICATION*, 2009, 28(21), pp.42-45

[7]. LIN Yong，YU Cang Bi，WANG Qiang, "Principle and Application of the Static Transfer Switch," *Proceedings of National Conference on Power Quality*, August 2009, pp.526-533

[8]. LIN Yong, "Wind Power and Grid Integration," *China Wind Power Information*, August 2009, pp.29-32

[9]. LIN Yong, "Development and operation of a wind farm," *ELECTRIC AGE*, June 2009, pp.92-93

[10]. LIN Yong, "Identification of Non-linear Load and Quantitative Analysis of Pollution in Grid," *ELECTRIC POWER SYSTEM EQUIPMENT*, May 2009, pp.60-64

[11]. PANG Huey, LO Edward W.C. and LIN Yong, "Computer simulation and performance of a low concentration ratio hybrid solar parabolic trough concentrator system with DC output," *The International Conference on Electrical Engineering* 2008, No. O-048.

[12]. Xia Mingchao, Lin Yong, "A Novel Voltage Transients Based Protection Criterion fort-Type High Voltage Transmission Lines," *POWERENG 2007, International Conference on Power Engineering, Energy and Electrical Drives*,

2007.4 (ISBN: 978-1-4244-0895-5) pp.377-380

[13]. Lin Yong, Xia Mingchao, Wu Jun, Wang Chen, Ao Ran, "Study on measurement and simulation evaluation of large wind power plant caused effects on power quality," *Proceedings of ISES World Solar Congress* 2007, Beijing, China, 2007, pp.2318-2323

[14]. Jun Wu and Yong Lin, "Economic dispatch including wind power injection," *Proceedings of ISES World Solar Congress* 2007, Beijing, China, 2007, pp.2343-2347.

CHAPTER 2 LITERATURE REVIEW

2.1 Grid Stability and Its Theoretical Research

2.1.1 Origin and Development of Voltage Stability Research

2.1.1.1 Origin of Voltage Stability Research

In the processes of power system programming, design and operation, stability has been an important topic of research. Currently, the power system is developing towards ultrahigh voltage, long distance and large capacity, and large increase of electricity demand and the relative lagging of power generation and transmission facilities make the operation margins of the power systems smaller, or even near the boundaries of stability; meanwhile, the introduction of computer technologies and the emergence of emerging power electronics rectification deices introduce new mechanisms for the dynamic behaviors of the power systems, and also pose rigorous ordeals for the power system stability.

For a long time, both the classical and modern theories and analytical methods of power system stability have been focused on the angle stability of the systems, especially on the transient-state behavior characteristics after the systems undergo large disturbances or faults. The mechanism of this problem has been very clear, and a complete set of analytical methods and control measures have been developed, but for some faults that happened in recent years, the original analytical methods can't provide satisfactory explanations. The common characteristics of such faults is that, in time of system disturbances, the system frequencies and angles remain constant on the whole, and in some cases, the system frequencies may even increase, but the voltages of certain buses will continue to drop beyond control, so much as to force the systems to lose a great deal of loads or even collapse. Such incidents are referred to as voltage instability or voltage collapse.

The frequency occurrences of voltage collapse faults have drawn attention of the scholars, and given impetus to the research of voltage stability problem. In 1982, the US EPRI Power Transmission Group, when programming the research areas of power system operation, listed voltage collapse and abnormal voltage problems as the most important research topics. And the IEEE and the CIGRE also organized special working groups to investigate and discuss voltage stability problems. In March 1987, the 38.01 Working Group of the CIGRE specially proposed the programming and design of the guideline for the power systems to prevent voltage collapse, and its current research work mainly concentrates on the discussion of voltage collapse mechanism and on the research of security calculation and research models, analytical methods and prevention measures of voltage collapse. In a word, the research of voltage stability has been booming in the recent more than years, almost making the voltage stability problem an independent research area.

2.1.1.2 History and Status of Voltage Stability Research

The research of voltage stability problems started at the beginning of 1950's, and has not made great progress until the 1970's owing to the limitations of research methods and system sizes. In early documents, voltage stability and angle stability were studied respectively as two independent problems and with distinctive models; the angle stability researches the synchronous operations of the generators under various circumstances, while the insufficiency of reactive power of the power systems to meet the requirements of the loads will lead to voltage stability problems. In normal cases, the voltage stability problems result from the system insufficiency of reactive power, usually categorized as the static stability category, and the research mainly concentrates on discussing the mechanism of voltage instability in the static point of view, or on finding the operation limit conditions on the basis of flow equations; meanwhile, to facilitate the research, the voltage stability analyses usually ignore nonlinearity.

But in recent years, the development of our cognition of voltage stability indicates that voltage stability problems are actually much more complicated than we imagine. On one hand, voltage instability and power angle instability should be two typical forms of nonlinear dynamic system instability, and they are important parts of stability research. A large number of faults show that, in many cases, they are mutually related and affected, and are hard to differentiate. So, the mathematical models for power system power angle stability research and those for power system voltage stability research are consistent at the highest level, and the differences lies in that the crux of the research of voltage stability is to uncover the factors and main characteristics related to voltage stability problem to provide proper models for analysis and to provide ground for the voltage stability analysis of practical power systems. Artificially dividing them may lead to ex parte conclusions. On the other hand, with the deepening of research, people are gradually recognizing the necessity of dynamic research. The power system is a nonlinear kinetic system, stability belongs to dynamic category, voltage collapse is essentially dynamic [2.1-2.5], and voltage instability or voltage collapse is a dynamic process. The dynamic components in the system, such as the generator and its control system, load types and characteristics, transmission characteristics, reactive power compensation equipment, operator's operations and operations of automatic devices have impact on voltage instability. Static analysis methods, incapable of taking into account the impact of dynamic components, can't research the mechanism and development process of voltage instability. Meanwhile, when the power systems undergo short-circuits or other types of large impulses, the mathematical expressions of the dynamic behavior of the power system must preserve their nonlinear characteristic so as to uncover the development mechanism and characteristics under large disturbances of power system voltage instability.

With the further development of power system voltage stability research, more in-depth research of definitions and classifications of voltage stability is required. So far, the definitions and classifications of voltage stability are still very confusing, and there are still no generally accepted strict and scientific classifications and definitions.

Roughly speaking, there are roughly the following definitions:

C.Concordia defined the voltage stability as "the capability of the power system to maintain the load voltages within a defined range, i.e. when the load admittance increases, the load power also increases, and the power and voltages are controllable". Accordingly, C.W.Taylor [2.3] defined voltage instability as "the process of gradual voltage attenuation resulting from the loss of voltage stability", and voltage collapse as "the bus voltage falls out of acceptable ranges after faults or disturbances".

P.Kundur [2.5] defined voltage stability as "the capability of the power system to maintain the voltages of all the buses as acceptable values when the power system is in normal operation or undergoes disturbances", voltage instability as ""the continuous and uncontrollable dropping process of voltage", and voltage collapse as the "the process of part voltage dropping beyond acceptable ranges resulting from a series of events accompanied by voltage instability". And there were also similar definitions in the 1993 annual report of CIGRE TF 38.02.10[2.6].

The diversity of voltage stability definitions also indicates the large divergence with respect to voltage stability in the present power system engineering circles. For example, on one hand, CIGRE defined the voltage stability in time of small disturbances as the phenomenon that the load voltage is close to the pre-disturbance voltage of the equilibrium point, the case that there are no voltage equilibrium points after disturbances as voltage instability, and the case that there are voltage equilibrium points after disturbances but the voltages are too low as voltage collapse. But meanwhile, CIGRE regarded the two terms of voltage instability and voltage collapsed as exchangeable.

And there are also different opinions about the classifications of voltage stability:

Starting from the magnitude of disturbances, Kundur [2.5] and Taylor [2.3] followed the classifications of angle stability problems to classify voltage stability into small-disturbance voltage stability and large-disturbance voltage stability, and their definitions tally with the definitions of the stability of general linear systems and nonlinear systems. The small-disturbance voltage stability is about the research of the stability of the system undergoing small disturbances under normal conditions, and on the contrary, the large-disturbance voltage stability is the stability of the system after the system undergoes short-circuits or grid operations.

According to the time frame, Taylor [2.3] classified voltage stability into transient voltage stability, mid-term voltage stability and long-term voltage stability. Transient voltage stability ranges from 0 to 10s in duration, mainly about the voltage instability resulting from the fast load restoration characteristics of induction motor and HVDC system, especially about the voltage instability resulting from the acceleration of motors after short-circuits or about the voltage instability of asynchronous motor asynchronization resulting from weak grid ties. Mid-term voltage stability (also referred to as post-disturbance or post-transient voltage stability) ranges from 1 to 5min in category, including the roles of the maximum current limits of OLTCs, voltage regulators and generators. Long-term voltage stability ranges from 20 to 30min in time category, whose main relevant factors include: limits of overload time of power transmission lines, roles of load characteristics and various control measures (such as load shedding) and so on.

According to the research methods, the voltage stability problems can be classified into static voltage instability, dynamic voltage instability and transient voltage stability.

Static voltage stability means that the slow increases of the loads result in the slow drops of the bus voltages at the load side until the voltages become unstable when the power system reaches the critical values to bear load increases, and the rotor angles and bus voltage angles do not change obviously during the whole process before the voltages drop abruptly.

Dynamic voltage instability means that, after faults occur, to maintain transient angle stability and system frequency, the system may also trip the generators and shed the loads besides grid operations. The slow load restoration process may lead to voltage instability for the system structure becomes weak or the whole (or part) system becomes weak in load support capability, and the generators, their control mechanism and the load characteristics will have impact on the dynamic voltage instability.

Transient voltage stability means the instability process of the voltages at certain load buses dropping irreversibly and abruptly accompanied by the reactive swings of generators during the fault handling process of the system after faults or other types of large disturbances occur in the power system, when the relative swings among the generators may not exceed the degree of power system angle stability.

In the past several decades, the scholars attached importance to the research of the analysis methods of voltage stability, but their research of the mechanisms of voltage collapse and voltage instability are far from satisfactory. Voltage collapse comprises two stages of voltage instability and collapse, and there are usually slow voltages instability processes before voltage collapse. To understand the system behavior and the mutual effect of various components so as to take voltage control measures to prevent voltage collapse, we first need to understand the mechanism of voltage instability so as to gain a clear idea of the essence and cause of voltage collapse, know about the relationships between voltage stability problems and other stability problems of power system, analyze the impact of various components of the power system on voltage stability, build the system models that are suitable for the analyses of voltage stability problems, and bring forward voltage stability criteria, voltage stability margin indices, and measures to control voltage collapse. The initial voltage collapse usually occurs in the case of heavy loads, so voltage collapse is regarded as caused by overload, but there are different opinions about how the system develops into voltage collapse after overload. On one hand, this is owing to the complexity of the voltage stability research; one the other hand, this is because the research and analysis methods of voltage instability mechanism are closely related, and the different simplifications of the system models and the different analysis methods are the radical causes of the disputes about the voltage instability mechanism.

2.1.2 Explanations of Voltage Stability Mechanism

2.1.2.1 Explanations of Static Mechanism of Voltage Instability

Voltage stability was initially regarded as a static problem, so the mechanism of voltage instability was explained from the static point of view. For example, in early 1950's, П М Malkovich [2.7] from former Soviet Union proposed the first voltage criterion - dQ/dV criterion on the basis of single-machine infinite system. As the classic and intuitional physical explanation of voltage stability problems, this criterion is popular and has been adopted by many textbooks.

The dQ/dV was proposed based on the following thinking: the high x/r ratio of the system makes the voltages of various buses in the system are mainly related to the reactive power. Meanwhile, seeing that the induction motor loads are the main loads, we research the voltage stability with the stability of induction motor, where the voltage stability means the system can maintain the load voltages at certain levels in the cases of small disturbances. For the system shown in Fig. 2.1, the Q_L in Fig. 2.2 is the static reactive power-voltage characteristic curve of the loads, Q_G is the static reactive power-voltage characteristic curve of power sources, and $Q= Q_G - Q_L$, where the intersections A and B of Q_G and Q_L are equilibrium points. Small-disturbance analyses of point A indicate that, when the voltage drops slightly by V, we have $Q_G > Q_L$ and $dQ/dV<0$, i.e. the system maintains a certain margin of reactive power when there are small disturbances with the loads, so voltage at point A is stable, and voltage at point B is unstable.

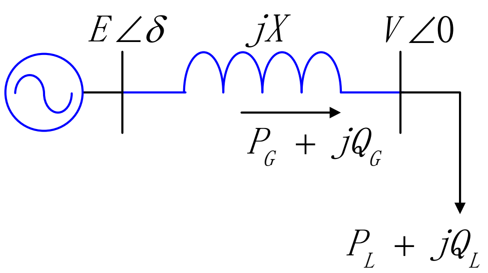

Fig. 2.1 Connection diagram of single-source single-load system

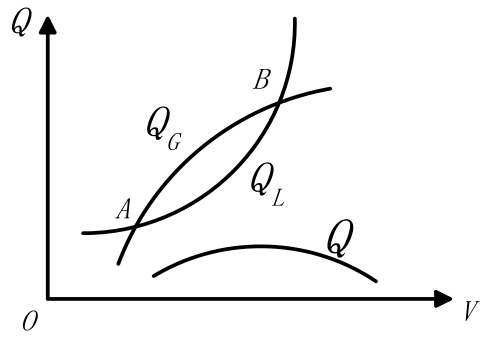

Fig. 2.2 Static reactive power-voltage characteristic curves

The criterion of dQ/dV is to estimate the stability of induction motor loads with their static voltage characteristics, and is equivalent to the criteria of dE/dU and dU/dE [2.8] that were proposed later in the case of single-source single-load system. But in the multi-machine systems, its applications are conditional: only when the system frequency changes are ignored, reactive power is insufficient, and the relative angles among generators are small in the time of voltage drops, i.e. angle stability damage unlikely to occur, the above criteria are applicable, and meanwhile the mutual impact of various loads are unlikely to be taken into account. But in practical systems, angle stability and voltage stability are mutually overlapping and influential, in many cases it is hard to judge who results in the stability damage, and the loads are mutually influential, so this criterion can't be generalized to multi-machine systems.

More often, people are concerned about the voltage instability and the loading capability of the system, and in view of these drawbacks of dQ/dV, some scholars propose dP/dV criterion, explaining the mechanism of voltage instability with the PV and QV curves.

For the system shown in Fig. 2.1, the grid transmission characteristics are

$$\begin{cases} \dfrac{P_L X}{E^2} = \dfrac{V}{E}\sin\delta \\ \dfrac{Q_L X}{E^2} = \dfrac{V}{E}\cos\delta - \left(\dfrac{V}{E}\right)^2 \end{cases} \tag{2.1}$$

Combining the above equation yields

$$\left(\frac{P_L X}{E^2}\right)^2+\left[\frac{Q_L X}{E^2}+\left(\frac{V}{E}\right)^2\right]^2=\left(\frac{V}{E}\right)^2 \tag{2.2}$$

Assume the source potential E and grid reactance A to be constant. Then a cluster of PV curves in the context of constant load power factors and a cluster of QV curves in the context of constant load PL, as are shown in Fig. 2.3 and Fig. 2.4.

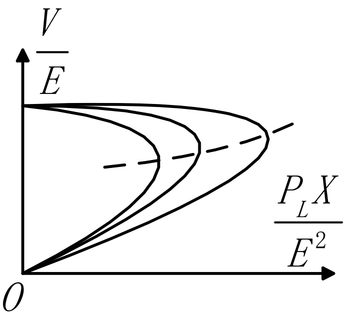

Fig. 2.3 PV curves of a single-source single-load system

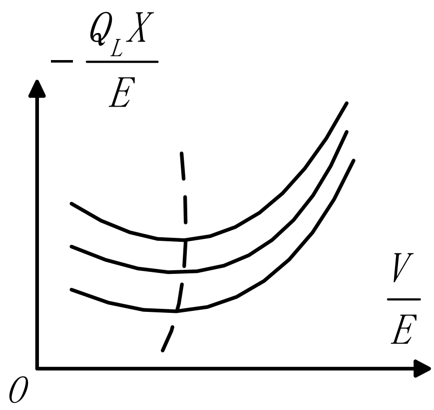

Fig. 2.4 QV curves of a single-source single-load system

The dashes in Fig. 2.3 and Fig. 2.4 connect the apexes of the PV and QV curves, corresponding to the limits of the system loading capacities. These points are regarded as the critical points with the following several kings of explanations:

One explanation is that when the system loads gradually increase to the limits, additional increases will make the system lose steady equilibrium and become unstable. But it is still uncertain whether this instability corresponds to voltage instability, and it cannot explain how the system becomes unstable. On the other hand, even if there is a balance point with the system, that does not mean voltage is stable at this point, because it only ensures that this point is s stable operating point, but it is uncertain whether the voltage is stable in time of disturbance, and this is just what stability requires (at least required by small-disturbance stability).

Another explanation is that, the points at the upper part of the PV curves and the right part of the QV curves are balance points where the system can operate stably, and the points at the other parts are unstable balance points. When the system operating points transfer from the upper part of the PV curves or the right part of the QV curves to the other parts, it begins to become unstable at the inflection point, so this point is the critical point of voltage stability.

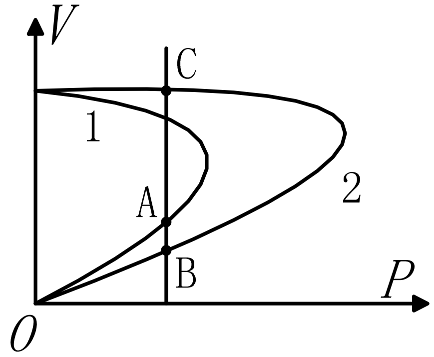

Fig. 2.5 Causality of voltage control

There are multiple explanations of why the system is unstable at points of the lower half of the PV curves: one explanation is that when the system operates at points of the lower half of the PV curves, voltage control loses causality and is thus unstable. As shown in Fig.2.5, curves 1 and 2 are both the PV curves of the system shown in Fig1.1, and the only difference is that the source potential E corresponding to curve 2 is larger than that corresponding to curve 1. Suppose the system originally operated at point A in the lower part of curve 1. If the source potential increases to the value corresponding to curve 2, then, according to the constant-power characteristic of the load, the system operation point will transfer to point B in the lower part of curve 2. So, we can conclude that when the system operates in the lower half, the increase of the source voltage will lead to the drop of the voltage at the load bus, and the voltage control loses causality.

The dP/dV criterion explains the mechanism of voltage instability from the static point of view, just like the dQ/dV criterion, holding that the unbalances of active power and reactive power causes the system voltage instability, while overlooking the impact of the dynamic components in the system. Actually, at the critical points of PV curve and QV curve, the Jacobi matrices are singular, but after the generators, their control systems and other components are taken into account, the singularity of the Jacobi matrices may change. The research of P.W Sauer and M.A Pai [2.9] shows that only under the two very special simplification conditions that the roles of the dynamic components at the generator side are simplified and integrated into the classic swing equations of the generator will the singularity of the Jacobi Matrix of the standard flow equations be equivalent to that of the dynamic model. In 1994, Taylor [2.2] pointed out in his works that the PV curve or QV curve can't be used as the decision –making basis in multi-machine systems. Since the system stability requires the system to have flow solution and to be dynamically stable, the conclusions drawn simply by taking the flow state that causes the Jacobi Matrix of the standard flow equations to be singular as the criterion for stability tend to be optimistic.

2.1.2.2 Explanation of the Dynamic Mechanism of Voltage Instability

With the development of the voltage stability research, the dynamic instability mechanism that takes the dynamic role of the generators and their regulation systems and the impact of loads and other dynamic components came into being.

H.G Kwatny [2.10] discussed the bifurcation of the dynamic systems that correspond to the standard flow equations and that are integrated into the swing equations of the generators, and proposes the voltage instability mechanism that the mathematical model of the system, part of the local solutions of whose algebraic equation groups are not unique.

More scholars research the system voltage stability from the angle of load stability [2.11]. But actually, if there are reactive power unbalances in the system, the system will be unstable. The research of H.D. Chiang [2.12] and Y.Sekine [2.13] hold that voltage instability may be caused by the insufficiency of the active power that the system provides for the loads to meet the active power requirements of the loads, or may be caused by reactive power shortage.

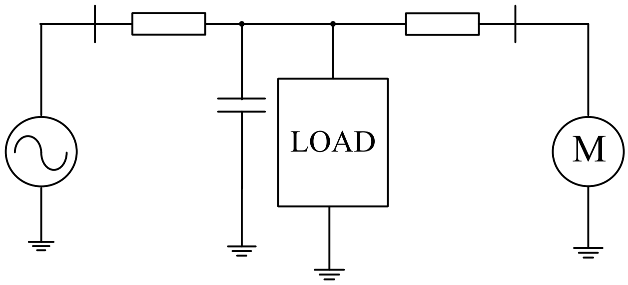

Fig. 2.6 Connection diagram of a simple system

Ha.Lee Byung [2.3] et al. proposed the explanation of the dynamic mechanism of voltage collapse form the angle of time domain simulation, holding that the mutual impact of the generators and the grid (including the voltage regulator and voltage control components) results in voltage collapse. For the model of a simple system shown in Fig. 2.6, the dynamics of the generator, excitation system and the motor are taken into account. Assume that the stable operating point of the system lies near the SNB bifurcation point, and then the excitation current of the generator is close to the over-limit state, when the motor terminal voltage will drop if there is a small disturbance. And we can know through analysis that

1) Suppose the mechanical loads of the motor to be constant-power loads, and then the terminal voltage drop will lead to the increase of the rotor currents of the motor;

2) The increases of the rotor currents enlarge the voltage drops in the power transmission lines, and further reduce the motor terminal voltage;

3) Since the equivalent shunt capacitance of the lines is in direct proportion to the square of the voltage, the terminal voltage drop will result in the reduction of reactive power compensation of the capacitors, and in the increasing shortage of reactive power in the system;

4) The increase of the rotor currents of the motor will lead to the increase of the generator output currents. When the generator excitation current reaches the limit, the terminal voltage and the reactive power output of the generator will decrease, further reducing the voltages at all buses of the system.

Through such a vicious cycle, the voltages drop continuously or even collapse under certain conditions.

This dynamic mechanism explains the development process of voltage collapse vividly without taking other components that impact voltage stability (such as OLTC, SVC)in the system or the effect of load characteristics into account. Meanwhile, the components of the system generally reserve certain margins, and it does not reflect how the generator reaches the limits in practical operation and how the generator impacts voltage stability when returning from the limits to take the generator as lying at the excitation limit state directly. For a practical power system, the following factors shall also be taken into account:

(1) if there is the OLTC in the system, then the operation of the OLTC may result in the decrease of the equivalent admittance of the primary side and in the further drop of the generator terminal voltage;

(2) Consider the load characteristics. If the OLTC operates to restore the voltage of the secondary side, then it will lead to the recovery of the load power at this bus and have negative impact on the voltage of the primary side;

(3) The increase of the stator currents of the motor will make the motor in greater need of reactive power support, and make the SVC gradually saturated. Once the SVC is saturated, then it will inevitably cause the generator to transmit more reactive power through the power transmission lines, while the transmission of a large quantity of reactive power will result in the increases of the voltage drops along the power transmission lines, and in the significant reduction of terminal voltage of the motor;

(4) The large increases of the need for reactive power from the generator will lead to the significant increase of the excitation currents of the generator, making the generator in a strong excitation state. Owing to the limits of the thermal capacity of the excitation windings, it the generator returns from the strong excitation state after some time, then it will cause the excitation to drop suddenly, resulting in the large shortage of reactive power in the grid and the large voltage drops at the buses of the system.

(5) A more severe case is that, when the stator currents of the generator exceed the limits, the generator will be tripped generally, causing the significant shortage of active power and reactive power in the system and finally resulting in voltage

collapse.

2.1.2.3 Impact of Component Characteristics on Voltage Stability

(1) Load characteristics

The load characteristics are the crux of voltage stability research, and scholars generally hold that the load characteristics have remarkable impact on the system voltage stability, and load characteristic should be taken into account in analysis [2.14-2.20]. A.Borghetti [2.14] et al. maintains that different load models correspond to different conditions of system voltage stability after researching the impact of various load characteristics on voltage stability in detail. Robert [2.15] and F.P DeMello [2.16] researched the voltage instability resulting from the asynchronization of induction motors and maintain that the motor loads play an important role in voltage instability. Y.N. Yu [2.17] and EL-Sadek [2.18] researched the voltage instability process with more detailed induction motor models, and the research results indicate that the influential factors of voltage stability mainly include the weight of induction motor loads in the composite loads, the characteristics of induction motors and of their driven mechanical loads. Y.N Yu [2.17] pointed out that the approximate models of induction motor may reflect its voltage stability characteristics generally. Presently, the load models for voltage stability research are many, but it remains a difficulty how to determine the load characteristic parameters.

(2) OLTC

Many scholars [2.21-1.25] maintain that OLTC (On-Load Tap Changer) plays an important role in the voltage instability process, and the negative voltage regulation or continuous regulations of the OLTC in the unstable regions are one of the main reasons of voltage instability. Sekine [2.21] holds that the incontinuous operation of the OLTC may lead to voltage collapse, while W.R Larchs [2.22] holds that when the continuous operation of the OLTC makes the reactive power of the generators beyond the limits or makes the dynamic load unstable, the voltage level will drop dramatically and voltage collapse will occur. Y.Sekine [2.13] holds that the dynamics of OLTC may aggravate the voltage stability of the induction motor loads, while Y.N Yu's [2.23] simulation calculations indicate that the OLTC can enhance the voltage stability of the induction motor loads. In accordance with the negative voltage regulations of the OLTC, Sekine [2.21] proposed the strategy of blocking the OLTC when the voltage is close to instability. W.R Larchs [2.22] maintains that at low voltages, the continuous operations of the OLTC will cause the voltage levels to drop dramatically and result in voltage collapse. Y.Sekine [2.13] shows with his simulation calculation that the dynamics of the OLTC will aggravate the voltage stability of the induction motor loads., while Y.N Yu et al. [2.23] holds that the OLTC can enhance the voltage stability of the induction motor loads. Sekine [2.21] proposes the strategy to block the OLTC when the voltage is close to instability.

(3) Generator characteristics

The excitation limits, load characteristics of the generators and the OLTC are generally regarded as the important factors that are related to voltage instability. After the generator reaches the limits, it losses strong excitation and causes the system to be in shortage of reactive power and the local voltages to drop significantly until finally the voltage collapses.

(4) SVC and HVDC

The rectifier and inverter of the HVDC system will consume a great deal of reactive power and have impact on voltage stability, while the SVC injects reactive power into the system and is conducive to voltage stability. R.J Koessler [2.26] holds that the SVCs are advantageous to voltage stability. Y.Sekine [2.13] pointed out that sufficient reactive power compensation helps the voltages of the load buses with low voltage solutions to recover to normal.

Besides, some other components in the system (such as low voltage/frequency load shedding devices and secondary voltage control) and control measures will have fairly large impact on the voltage stability.

In a word, so far the research of the voltage instability mechanism is far from in-depth, and it is still unclear how the system components impact the voltage stability, but there are some basic agreements:

(1) Voltage instability and voltage collapse are essentially dynamic processes, or even large disturbance processes. The maximum bearing capability of the grid is not

necessarily the voltage stability limit;

(2) Of all the influential factors of voltage stability, the load characteristics are the key links and the causes of voltage instability, while the large disturbances in the system, the sudden outage of generators, abrupt reduction of excitation and the sudden increases of loads are the direct causes of the system instability;

(3) Voltage instability corresponds to the damage of the dynamic balance of the system, and PV and QV curves only reflect the static balance relationships, i.e. reflect the grid constrains. And they are the necessities of stability,. After the roles of the dynamic components in the system are taken into account, the active and reactive power balance relationships at the static balance points may be damaged by them and be unstable;

(4) Voltage instability is mainly determined by the contradiction between the increase of load requirements and the limited capabilities of active power and reactive power transmissions of the grid;

(5) In practical systems. The small-disturbance voltage stability limits correspond to the limits of the system loads, i.e. the system returns to the original balance point after disturbances; while the large-disturbance voltage stability correspond to whether the system will be capable of reaching a new stable balance point after disturbances.

2.1.3 Technologies of Enhancing Voltage Stability

(1) Generators

In time of casual faults or when the operation of new lines or transformers is delayed, put the uneconomic generator in operation to change the flow or provide voltage support.

(2) Series capacitors

Series capacitors can effectively reduce the reactance of the lines and thus reduce the net reactive power losses. So the lines can transmit more reactive power from the strong system at one end to the system with reactive power shortage at the other end.

(3) Shunt capacitors

Shunt capacitors can help tackle the voltage instability problems, for the reactive power is mostly compensated for locally.

(4) Static Var Compensator (SVC)

The coordinated use of SVC and STATCOM are effective in controlling voltages and preventing voltage collapse.

(5) Operation at high voltage

Operation at high voltage can reduce reactive power requirements of the system.

(6) Load shedding at low voltage

A certain amount of load reduction may avoid voltage collapse. In static stability problems, it is the most effective to shed the loads at the receiving-end systems.

(7) Low power factor generators

When the newly added generators are close to the regions that are short of reactive power or to the regions that may require large reactive power reserves occasionally, it is proper to adopt the generator with a power factor of 0.85 or 0.8.

(8) Reactive power overload capacity of generators

The overload capabilities of the generator and exciters can be used to delay voltage collapse.

2.1.4 Summary and Outlook of Voltage Stability Research

By summing up the research work of voltage stability, we can see

(1) The static analysis method based on flow equations has made great progress, and the margin indices describe the operation conditions of current system and the distance from the stability boundaries. The results are of a certain degree of practical value, but have not touched the essence of voltage stability problems.

(2) The research with nonlinear kinetic methods is booming, but it is still unknown whether the bifurcation of the mathematical model of the power system.

(3) Dynamic voltage stability analysis methods, system models and effective

numeric calculation technologies are the development direction in future.

However, there are still several aspects for further in-depth research:

(1) In-depth research of the mechanism of voltage collapse and voltage instability;

(2) The selection of system models is the basis of voltage stability research, and it is the key of future research to propose reasonable mathematical models, especially the load models.

(3) Research the relationships between the angle stability and voltage stability and, on this basis, build a uniform and effective model and method for the research of nonlinear power system.

(4) Introduce more effective mathematical methods to improve calculation efficiency and provide reasonable explanations for the phenomena of the power system.

2.2 Research of SVC in Suppressing Low-frequency Oscillations

2.2.1 Background of Power System Low-frequency Oscillations Problem

To achieve the holistic energy development plan in our country, we have set the "Transmission of West Power to the East, Mutual Supply between the South and the North, Nationwide Grid Interconnection, and Separation of Power Plants and the Grids" as our direction. While the grid interconnection technologies can greatly improve the economy and reliability, they may also bring about some problems. It the grid structures are imperfect and short of necessary safety measures, then a local small disturbance or abnormal operation may also result in the chain reactions throughout the system, or even bring about the large-area system collapse and catastrophic losses [2.27]. In this regard, the US, Russia, Canada, Europe, Japan and so on has undergone disastrous lessons [2.28, 2.29]. And there have been many low-frequency oscillation incidents from home and abroad, such as the Northern Europe system [2.30], Scotland-England system [2.31], and Southeastern system of Australia [2.32] and so on. On August 10, 1996, a power blackout fault occurred in the US, and the recorded curves by the WSCC (Western System Coordinating Council) indicated that the negative damping low-frequency oscillations finally caused the whole system to separate and to collapse with large-area power blackout [2.33].

In recent years, many times of power oscillations have taken place in Anhui, Hubei, Hebei, and Guangdong grids in our country, posing threats to the stability of the systems and to the power system equipment. And many times of low-frequency oscillations were detected in China Southern Power Grid in 2001 [2.34].

The low-frequency oscillations of the grid means that, for the generators that operate in parallel through power transmission lines in the power system, the disturbances will result in the relative swings among the rotors of the generators, and when there are sufficient dampings in the system, such oscillations will calm down soon, otherwise, if the system is short of necessary dampings, then oscillations will continue to occur, when the power along the power transmission lines will oscillate accordingly. Since the frequencies of the oscillations are as low as 0.2 to 2.5 Hz, the oscillations are referred to as low-frequency oscillations.

The low-frequency oscillations in the grid may be either local or global. The local problems involve a small part of the system, while the global problems are caused by the mutual impact of a large number of generator units, taking the shapes of the oscillations of swings between the generators in one region and those in another region and referred to as regional oscillation pattern [2.35]. In large interconnected systems, there are usually two kinds of different interregional oscillations: the low-frequency pattern at an order of magnitude ranging from 0.1 to 0.3Hz[2.36] and higher frequency pattern ranging from 0.4 to 0.7 Hz.

It is notable that low-frequency oscillations with unclear mechanisms occurred many times under the conditions of sufficient dampings in our country. These low-frequency oscillations can't be well explained with the traditional theories of low-frequency oscillations. So it is becoming increasingly important to perform more in-depth research of the mechanisms and suppression measures of power system low-frequency oscillations.

In a word, by analyzing the mechanisms of low-frequency oscillations in large interconnected grids and researching and proposing preventive and control measures accordingly, we can direct the power system interconnections among different regions, improve the control level of the grids, and promote the development of control systems for which we own independent intellectual property. This research will build the system of theory and methods for the analysis and control of low-frequency oscillations in large interconnected grids and improved the security and stability of the power system operations.

2.2.2 Mechanism and Analysis Methods of Power System Oscillations

The low-frequency oscillations in the interconnected systems that were reported earliest were observed before the founding of the WSCC in the US. The low-frequency oscillations caused the tie lines to be tripped because of overcurrent, and brought about around 0.05Hz and 0.18Hz oscillations in the systems. And the low-frequency oscillations also occurred in our country in 1984.

2.2.2.1 Several Theories of Oscillation Mechanism

Starting from the beginning of the low-frequency oscillations, the research of the mechanism mainly centers on the following aspects.

(1) Mechanism of Negative Damping

In 1969, F. Demello [2.37] analyzed the mechanism of the low-frequency oscillations in accordance with a single-machine infinite system, and pointed out that, owing to the inertia of the excitation system, with the increase of the amplification factor of the excitation regulator, the real part of the eigenvalue corresponding to the mechanical oscillations of the rotor increases from a negative value gradually and, with the large amplification factor, becomes a positive value such that the generator generate oscillations with decreasing amplitudes.

So, the cause of the low-frequency oscillations is that, with the increase of the amplification factor of the excitation system, negative dampings are generated to offset the positive damping inherent in the system, and to make the total damping of the system be negative of be small. Thus, once there are disturbances, oscillations with decreasing amplitudes will emerge in the system shaftings. This is the most important explanation of the mechanism of the low-frequency oscillations, and future work will be centered on this mechanism [2.38, 2.39].

After many years of perfection and practice, the mechanism of negative damping is fairly mature, and becomes commonly accepted mechanism of low-frequency oscillations. The power system stabilizers (PSS) designed according to this philosophy has been widely used on site and function well in suppressing the low-frequency oscillations.

(2) Resonance theory or forced oscillation theory [2.40, 2.41]

For the nonlinear dynamic systems, when the frequencies of outside disturbances coincide with the inherent natural oscillation frequencies of the system, resonance/oscillation will take place. Since the inherent oscillation frequencies of the large grids are generally low, so the frequencies of the resonance/oscillation resulting from the resonance/oscillation are generally within the low-frequency regions. So low-frequency oscillations come into being.

(3) Bifurcation theory

Owing to the impact of the nonlinear characteristics of the system, when the parameters or disturbances change within a certain range, the system structure may become unstable such that oscillations take place, and its mathematical basis is the bifurcation chaos theory of the nonlinear dynamic systems [2.42]. Since there is still no strict ground for whether the chaos phenomena are observed in the power system, such research is still in the theoretical research stage.

In a word, in the research of the mechanism of low-frequency oscillations, the negative damping mechanism research is the earliest and the most mature with a set of complete system. And the existence of so many theories indicate that there is still no unified theory to explain the mechanism of low-frequency oscillations, and that further research is necessary.

2.2.2.2 Classifications of Analysis and Research Methods

Usually, the low-frequency oscillation problems are classified into the small-disturbance stability analysis, and there are many approaches to the small-disturbance stability analysis of the power system [2.5]. According to the mathematical models that the analysis is based on, these approaches can be roughly classified into two categories, i.e. numeric simulation method (time domain method) and eigenvalue analysis method (frequency domain method).

The numeric simulation method is widely used in the analysis and research of transient stability of the power system, which calculates the complete time responses of the system variables with the numeric calculation approaches of nonlinear equations in accordance with the special disturbances. But the applications of this method are limited by the practical problems.

(1) The results of the analysis of the damping characteristics of various oscillation patterns simply with the time domain response of the system variables are not quite convincing, because the selections of disturbances and the measurement quantities impacts the results a lot. And there may be multiple patterns in the responses, and the responses of weak damping pattern may not be obvious.

(2) It usually takes the dynamic process of as long as tens of seconds to simulate and calculate, and the calculation amount is quite large.

(3) Time domain responses can't fully reveal the essence of small-disturbance stability problems, so it is hard to find out the cause of system instability directly with the simulation results and look for corresponding improvement countermeasures.

The eigenvalue analysis method is the basic method to research the low-frequency oscillation problems of the power system, comprising the whole eigenvalue method and the partial eigenvalue method. The whole eigenvalue method finds all the eigenvalue with the QR algorithm at the same time, while the partial eigenvalue method main includes the SMA, AESOPS, S matrix method and the fraction transform method. These methods only calculate part of eigenvalues that are critical to the stability criteria to ensure that the precision and speed can meet the requirements of large-scale power systems.

For the eigenvalue method, there are two research philosophies at present: one is to calculate al the eigenvalues with the decomposed algorithm on the basis of the QR algorithm, which is still at the research stage but has a bright future; the other is to continue to research the partial eigenvalue method in the context of new principles.

To sum up, the present analysis methods have achieved some results, but they also have some deficiencies. Facing the increasing complicated system dynamics, we find it necessary to conduct further research to find new efficient analysis methods. The digital simulation of the power system has become the main tool of design, programming and operation of the power system, and the accuracy of the simulation results is important to the secure, reliable and economic operation of the power system.

2.2.3 Research Status of Low-frequency Oscillations Control

Concretely speaking, the suppression strategies of low-frequency oscillations mainly concentrate on the following two aspects: generator excitation control technology, and the applications of TACTS technology.

1. Generator excitation control technology [2.43, 2.44]

As early as in 1960's, people began to recognize the extreme importance of the analysis and control of low-frequency oscillations to the secure and stable operation of the power system. In the past several decades, great achievements have been made in the dynamic stability area, such as eigenvalue analysis method, negative damping mechanism of single-machine system, and the applications of power system stabilizer. Now, simulation effectiveness verification, nonlinear theories, new approaches to signal processing and the research of advanced control strategies have been the main directions of low-frequency oscillations research.

(1) Single-parameter supplementary control

In the 1960's, low-frequency oscillations (LFO) occurred in the grids of the United States. And in 1969, deMelloF et al. proposed using the supplementary excitation control (SEC) to improve the system damping and referred to this single-parameter ($\Delta\omega$ or ΔP_e) supplementary excitation control as the Power System Stabilizer (PSS). After that, the generator units in the US, China and other countries have been equipped with the power system stabilizers [2.45].

But it is notable that there are three problems with the PSS:

1) Although most generators have been furnished with the PSS, the low-frequency oscillations still occur occasionally;

2) Since this design is essentially based in the single-machine single-parameter phase compensation method, its applicable band of system oscillations is very narrow;

3) In the South China power grid, PSSs were intended to be used to improve the small-disturbance stability of the system, but calculations indicated that it is hard for the PSSs with certain constant parameters to tally with the different operation manners of the system.

(2) Linear optimal excitation controller (LOEC)

In 1970's to 1980's, some Chinese scholars successfully developed the linear optimal excitation controller (LOEC). Compared with the PSS, the LOEC has the following innovations: 1) it improves the single-parameter supplementary feedback into multi-parameter feedback; 2) it finds the most appropriate matching relationship of the amplification factors among multiple feedback quantities and realizes the "optimal control" with the mature "linear, quadratic, and Riccati" (LQR) control method.

The LOEC widens the applicable oscillation band (i.e. improves the robustness to oscillation frequency changes), and suppresses the low-frequency oscillations more effectively.

(3) Nonlinear robust PSS（NR-PSS）

The main characteristics of the nonlinear robust PSS (NR-PSS) are: 1)distributed control manner, i.e. the excitation control quantity u_F of the generator is related to its output quantities Q_e, u_t, ω only, and irrelevant to the output quantities of other machines; 2)the control law is irrelevant to the power transmission grid parameters, i.e. the control quantities of the generator are related to its own parameters $T_J, T_{d0}^{''}, x_d^{'}, x_d$ only, excluding the power transmission grid parameters. The nonlinear control law can achieve the complete decoupled distributed control among various generators, and is strictly robust to the grid parameters. And these two advantages are just what the nonlinear excitation control manner does not have [2.46].

2. Suppressing low-frequency oscillations with the FACTS device[2.47]

The roles of the power electronics devices in suppressing low-frequency oscillations have been taken seriously. The HVDC, SVC, and TCSC can suppress the low-frequency oscillations and how to coordinate the controls of various devices and the controls of various devices and the PSS has been a hot spot. The application of the FACTS technology to suppressing the low-frequency oscillations will transfer the focus of research low-frequency oscillations from the power generation side to the power transmission side.

In the way of signal processing, Prony Analysis has been paid attention to and applied in recent years. It may estimate the oscillation frequencies, attenuation, amplitudes, and relative phases by the responses to the given signals. Just because of this characteristic, and of the vigorous promotion and in-depth research of experts and scholars Hauer, Trudnowski and so on [2.48, 2.49], this algorithm has been used to tackle some problems of the power system and shown bright future [2.36].

It is also an effective way to discuss the low-frequency oscillation problems from the angle of system damping distributions. by analyzing the damping coupling phenomena among the different generator units in the multi-generator system, we can draw the following valuable conclusions: in the multi-machine system, the damping coupling among the different generator units may enable the generator units to have the same attenuation factor; during the oscillation process of any oscillation pattern, the oscillation modals play deterministic role in the damping magnitude, so, to increase the oscillation modal damping, we must exert damping on the generator units with large eigenvectors. For simplicity, this dissertation proposes an algorithm of fast estimation of the electromechanical modal eigenvalues in the multi-machine system, which divides the machine clusters by the participation factors and eigenvectors, and uses a two-machine system as the equivalent of a multi-machines system. Meanwhile, this dissertation researches the impact of the changes of the system excitation operation manners on the damping of the multi-machine system.

Nowadays, scholars are beginning to research some advanced intelligent analysis methods.

To sum up, the research of the mechanism and control methods of low-frequency oscillations in the large-scale interconnected power grids has been a hotspot and a difficult point of the research in the power system area. This research may be applied to the dynamic security evaluation of the interconnected grids in our country, and advanced SVC devices may be used to improve the system damping and suppress low-frequency oscillations so that the security, stability, and power transmission capability of the interconnected grids in our country can be improved remarkably and the social and economic benefits can be greatly increased.

2.2.4 Direction of Future Research of Low-frequency Oscillations

Presently, there have occurred many low-frequency oscillations in the grids, but their dynamic processes can't be well repeated by digital simulation experiments. It is crucial to analyze the degree of the impact that the load models have on the system low-frequency oscillations, and this includes two aspects of research: one is the research of the impact of the different load models on the low-frequency oscillations, focusing on the degree of the impact of the load model uncertainties on the system; the other is the research of the mutual effect of the load models and the controllers. And it requires further research whether the linear controllers widely used in the grids at present can enhance the system dampings and suppress low-frequency oscillations effectively under the uncertainties of the load models.

CHAPTER 3 TYPICAL PROBLEMS OF VOLTAGE STABILITY IN CHINA SOUTHERN POWER GRID

China southern power grid is complicated because it is a grid comprising sending ends and receiving ends, a multi-infeed AC/DC hybrid power system, and a system with numerous complicated dynamic components. The research problems of China southern power grid mainly include: static voltage stability problems of the system, transient-state voltage stability problems of receiving-end grids with a large proportion of induction motors in time of abrupt load increases, transient-state voltage stability problems caused by the power shortage resulting from the faults of the tie lines of the "Transmission of Power from the West to the East" channels, and low-frequency oscillation problems of the systems caused by small disturbances.

3.1 Static Voltage Stability of China Southern Power Grid System

3.1.1 Simulation and Calculation Conditions

To study the static voltage stability of China southern power grid, this dissertation conducts calculations and analyses with the forecasted data of 2010 in "the Eleventh Five-year" Power System Design of China Southern Power Grid and with the BPA simulation software.

3.1.2 Calculation and Simulation Methods and Results

The aim of static voltage stability analysis is to evaluate the static voltage stability degree of the system, and to determine the weak regions of voltage stability. The static power transmission limit is closely related to static voltage stability of the power system, and can be used to measure the static voltage stability of the system.

The specific calculation method of static power transmission limits is to determine the maximum loads and static voltage stability margins by increasing the loads of a certain region or a certain substation in Guangdong progressively according to the constant power factors. To maintain power balance, the generators must increase output to balance the load increases. To consider the severe case of voltage stability, assume that the units of all the power plants in Guangdong and Guangxi are in full outputs, and the load increases in Guangdong and Guangxi must be balanced by the power transmitted from the West to the East. Assume that the power outputs of Yunnan Dazhaoshan Power Plant, Yunnan Xuancheng Power Plant, Guizhou Dafang Power Plant, and Guizhou Qianbei Power Plant can be automatically regulated according to the power supply-demand balance of the whole grid, each supplying 20 percent of the load increases, and assign Yunnan Manwan Power Plant as the balancing machine to supply other load increases and power losses.

In the Guangdong Grid of 2008, the loads of the districts and cities in Guangdong are increased respectively while maintaining the power factors constant. The load increases are balanced by the increases of the power transmitted from the West to the East. The results of static voltage stability calculations of all the districts and cities are shown in Table 3.1, where Kcr=(maximum load-present load) /present *100%

Table 3.1 Static Voltage Stability of the Grids of the Districts and Cities in Guangdong (Provided by China Southern Power Grid)

District/city	Kcr
Dongguan	14 .90%
Foshan	21 .28%
Guangzhou	15 .25%
Shenzhen	18 .79%
Chaozhou	71. 76%
Jiangmen, Yangjiang	38. 60%
Meizhou, Heyuan	67.82%
Shaoguan, Qingyuan	66 .79%
Shanwei, Jieyang	63.58%
Shantou	67 .09%
Zhuhai	67. 56%
Zhanjiang, Maoming	57.02%
Zhongshan	40.23%
Zhaoqing, Yunfu	47.18%
Huizhou	42.43%

As can be seen from the above table, Shenzhen, Dongguan, Guangzhou and Foshan are four grids of the weakest static voltage stability, and it is necessary to conduct more detailed and in-depth research of them.

3.2 Voltage Instability Caused by Reactive Power Demand Increases Resulting from Abrupt Motor Load Increases at the Receiving-end System

China southern power grid is a typical system with power sending ends and power receiving ends, and in the power receiving ends in Guangdong district, the support of power sources are relatively insufficient while the induction motors are increasing in proportion, posing ordeals to the grid stability. So, it is necessary to study the impact of the proportion and sudden start-up of motor loads on the transient-state voltage stability of the grid.

3.2.1 Simulation Calculation Conditions

Now, this dissertation will calculate and analyze the interconnected grids of 220kV and above in Yunnan, Guizhou, Guangxi and Guangdong (including Hong Kong) with the data of 2005 and with the software of NETOMAC (Network Torsion Machine Control).

3.2.2 Introduction of Simulation Software

Modern power systems are increasing continuously in size with tens of thousands of lines and generators, complicated and varied operation manners, and such emerging new equipment as novel FACTS devices, and all these pose higher requirements to the functionality and precision of the simulation software. NETOMAC is power system simulation software developed by Siemens AG. After more than 30 years of development and application starting from 1970's, NETOMAC is becoming consummate continuously with increasingly powerful functions. NETOMAC is characterized by:

(1) Complete component models. NETOMAC can simulate in detail almost all the components, including such nonlinear components as arrester, thyristor and so, and such FACTS devices as HVDC and static var compensator (SVC).

(2) Wide simulation frequency bands. NETOMAC can simulate both 10-2Hz regulation process of steam turbine generator and the 106Hz thunder power wave process, and can perform simulations and calculations of various electromagnetic transient-state power system processes like EMTDC and EMTP, and of various electromechanical transient-state and steady-state power system processes like PSS/E and BPA. It is especially notable that NETOMAC can partition the grids to build different models with the embedded algorithm of real-time data transition between the electromagnetic transient-state models and the electromechanical transient-state models.

(3) Numerous powerful functions. NETOMAC can perform such various calculations as flow, short circuit, stability, dynamic equivalent, analysis of motor

startup, parameter identification, torsional vibration of unit shafting and optimized flow.

The design and modeling of the controllers are the most distinctive features of NETOMAC, which provides an extremely plentiful library of basic controller modules. As of now, all the controllers of the power system, such as the AVR and PSS of the generator and the controllers of various FACTS devices, can be modeled by the basic control modules in the module library.

On the basis of the above advantages, this research work chooses NETOMAC as the tool for grid analysis.

3.2.3 System Modeling

3.2.3.1 Generator Model

In this research work, the generators apply the six-order precise model based on the PARK formulae, and the corresponding model takes into account the one damping winding along the d-axis and the two damping windings along the q-axis as well as the impact of magnetic saturation, i.e. the model of changing E_q'', E_q', E_d'' and E_d' in consideration of magnetic saturation.

According to the actual application conditions in China southern power grid and in reference of relevant research achievements, the simulations and calculations consider eight types of excitation regulators, which are the EA type, EC type, EG type, EK type, FC type, FF type, FJ type, and FK type.

3.2.3.2 Load Modeling

(1) Static Load Model

$$P = P_0 \bullet \left[p_1 \left(\frac{V}{V_0}\right)^2 + p_2 \left(\frac{V}{V_0}\right) + p_3 \right] \tag{3.1}$$

In the above Equation (3.1), the constant-power load, constant-current load, and constant-impedance load are set up in a proportion of 3:4:3.

(2) Dynamic Load Models

In actual systems, the load characteristics are very complicated. When the systems are analyzed with a purely static load, the response characteristics are largely different from the characteristics of the actual systems. Comparisons of recorded post-fault real-time waveforms of the systems both home and abroad with the simulation results indicate that simulations with the static load models are unable to reflect the post-fault dynamic processes of the actual systems precisely for voltage stability analysis, and that, to better approximate the post-fault dynamic processes of the simulated systems, simulations must be performed with the dynamic models.

However, owing to the characteristics of complexity, dispersity, and randomicity of the loads, it is rather hard to describe the load characteristics of the systems precisely, and this problem has not yet been well tackled. In power system programming and simulations, the actually dispersed industrial and civil loads are usually referred to the 110kV side or even 220kV side for their equivalents, but the simulation and calculations may be performed at the 500kV grid. How to determine the equivalent reactance between the loads and the high-voltage grids? This adds to the difficulty of load modeling. However, owing to the importance of load models in power system simulations, research must be done with the load models so that load models that are close to the actual conditions can be progressively built.

In the present analysis and calculations of power systems, the equivalent induction motors are often selected to describe the dynamic loads of the systems. It is rather difficult to select equivalent induction motors to describe the dynamic loads. In dynamic simulations, there are commonly two models of induction motors: one is the three-order model, ignoring the transient states of the induction motor rotors, including the transient-state electrical process and mechanical motion equation of the rotor; the other is the simpler one-order model comprising the steady-state equivalent circuit and mechanical motion equation of the induction motor. In general research of voltage stability, the latter model can meet the requirements. Fig. 3.1 shows the equivalent induction motor applied by most simulation programs.

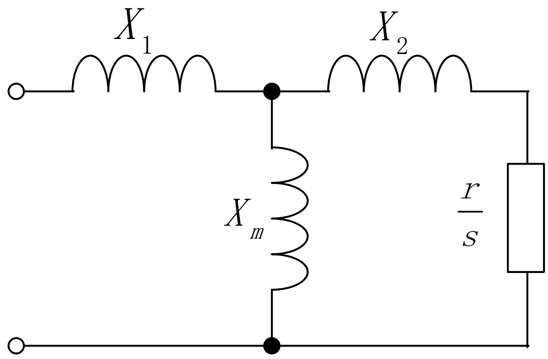

Fig. 3.1 Equivalent circuit of common induction motor

In Fig. 3.1, X_1, X_2 and X_m are the equivalent leakage reactance of the stator respectively, r is the equivalent resistance of the rotor, and s is the slip.

However, it is also hard to select the equivalent induction motor models. The actual induction motors in the systems take different forms with different capacities and operation characteristics. It remains to be further studied in power system programming and simulations how to represent the holistic characteristics of the dynamic loads with one large-capacity equivalent unit at the higher voltage side and how to select the induction motor parameters.

In the US, about sixty percent of the electricity is consumed by the motor loads, where ninety per are induction motor loads. Other surveys indicate that the cases of larger selected motor capacities than necessary are prevalent, and about half of motors operate at power levels below sixty percent of the rated power. This may bring about very large deviations to the load forecasts of the programming and operation departments, and thus make the programming and operation departments underestimate the quantities of abrupt load increases in some cases.

As for the modeling of dynamic loads and the selection of dynamic load parameters, the US Electrical Power Research Institute has done a great deal of empirical research. On the basis of this research work, the IEEE suggested applying the induction motor model and recommended part of the parameters, which are shown in Table 3.2. In Table 3.2, $R_s, X_{s0}, X_m, R_r, X_{r0}$ and H are the stator resistance, stator leakage reactance, excitation reactance, rotor resistance, rotor reactance, and inertial time constant respectively.

Table 3.2 Motor Model parameters recommended by the IEEE Load Modeling Working Group

Type	R_s	X_{s0}	X_m	R_r	X_{r0}	H	Load factor
1	0.031	0.1	3.2	0.018	0.18	0.7	0.6
2	0.013	0.067	3.8	0.009	0.17	1.5	0.8
3	0.013	0.14	2.4	0.009	0.12	0.8	0.7
4	0.013	0.14	2.4	0.009	0.12	1.5	0.7
5	0.077	0.107	2.22	0.079	0.098	0.74	0.46
6	0.035	0.094	2.8	0.048	0.163	0.93	0.6
7	0.064	0.091	2.23	0.059	0.071	0.34	0.8

Type1 - small industrial motor
Type2 - large industrial
Type3 - water pump
Type4 - auxiliary power
Type5 - composite civil motor
Type6 - composite civil and industrial motor
Type7 - composite air conditioning motor

3.2.3.3 Quasi-steady-state Modeling of HVDC System

1. Model of HVDC System

The principle and equivalent circuit of the HVDC system connecting two AC systems are shown in Fig. 3.2:

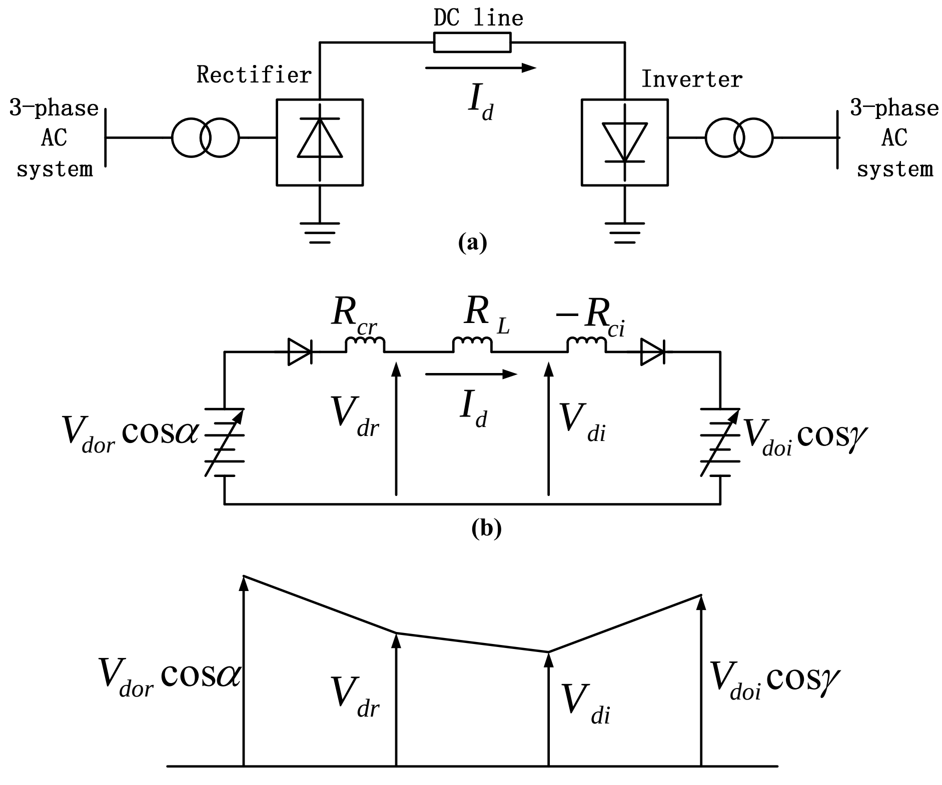

Fig. 3.2 Schematic diagram of HVDC system (Provided by CSG)
(a) Principle diagram (b) Equivalent circuit (c) Voltage distribution diagram

In flow and stability calculation and research, the quasi-steady-state model of the DC converter is based on the following assumptions:

(1) The AC systems of the rectification side and the inversion side contain constant-frequency symmetrical voltage sources behind the symmetrical impedances;

(2) The voltages and currents of the DC lines are completely straight;

(3) The conversion transformers are loss-free and unsaturated.

On the basis of the above assumptions, the steady-state operation characteristics of the conversion stations can be expressed by the following equations:

$$V_{d0i} = \frac{3\sqrt{2}}{\pi} BT_i E_{aci} \tag{3.2}$$

$$V_{d0i} = \frac{3\sqrt{2}}{\pi} BT_i E_{aci} \tag{3.3}$$

$$V_{di} = V_{d0i}\cos\gamma - R_{ci}I_d = V_{d0i}\cos\beta + R_{ci}I_d \tag{3.4}$$

$$R_{ci} = \frac{3}{\pi} BT_i X_{ci} \tag{3.5}$$

$$\cos\phi \approx \frac{V_d}{V_{d0}} \tag{3.6}$$

$$P = V_d I_d = P_{ac} \tag{3.7}$$

$$Q = P\tan\varphi \tag{3.8}$$

$$V_{dr} = V_{di} + R_d I_d \tag{3.9}$$

$$\beta = \gamma + \mu \tag{3.10}$$

In the above equations,

E_{ac} is the RMS line voltage of the high-voltage buses,

T is the turn ratio of the conversion transformer,

B is the number of series bridges,

P is the active power,

Q is the reactive power,

V_d and I_d are the DC voltage and DC current per pole respectively,

$X_c = \omega L_c$ is the commutation reactance per bridge/phase,

$R_c = \frac{3}{\pi} X_c$ is the equivalent phase resistance,

R_d is the DC line resistance,

α is the firing angle,

β is the leading firing angle,

γ is the arc extinguishing angle,

μ is the commutation angle, and

ϕ is the power factor angle.

2. Control Manners and Switching of HVDC System

The controllable parameters of the control system of double-end HCDC system include the firing angle α of the rectification side and the leading firing angle β of the inversion side.

The controlled parameters of the rectification side are the DC line power P_d or DC line current I_d, referred to as power regulator and current regulator respectively. These two approaches are similar in that they are usually implemented through constant-current control or the constant-power control for the dispatchers.

The controlled parameters of the inversion side are the DC line voltage V_d, angle γ and the DC line current I_d, referred to as voltage regulator, angle γ regulator and current regulator respectively. In the case of normal flow, the HVDC system is controlled by the voltage regulator and the angle γ regulator jointly, and the regulator with larger value of β is selected to control the inverter so that commutation failure can be avoided. Only when the firing angle of the rectifier reaches the minimum of $\alpha_{\min}$ will the current regulator function, when the rectification side operates at the constant firing angle $\alpha_{\min}$, and the inversion side is controlled in the constant-current way with the current instruction as $I_{ord} - I_m$, where I_m is the current margin.

In every kind of regulator, there is an amplitude-limiting PD link, and the control block diagram is shown in Fig. 3.3 and Fig. 3.4:

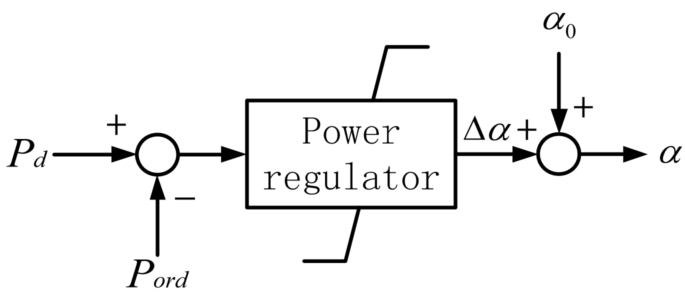

Fig. 3.3 Block diagram of constant-power control system of the rectification side. (Provided by CSG)

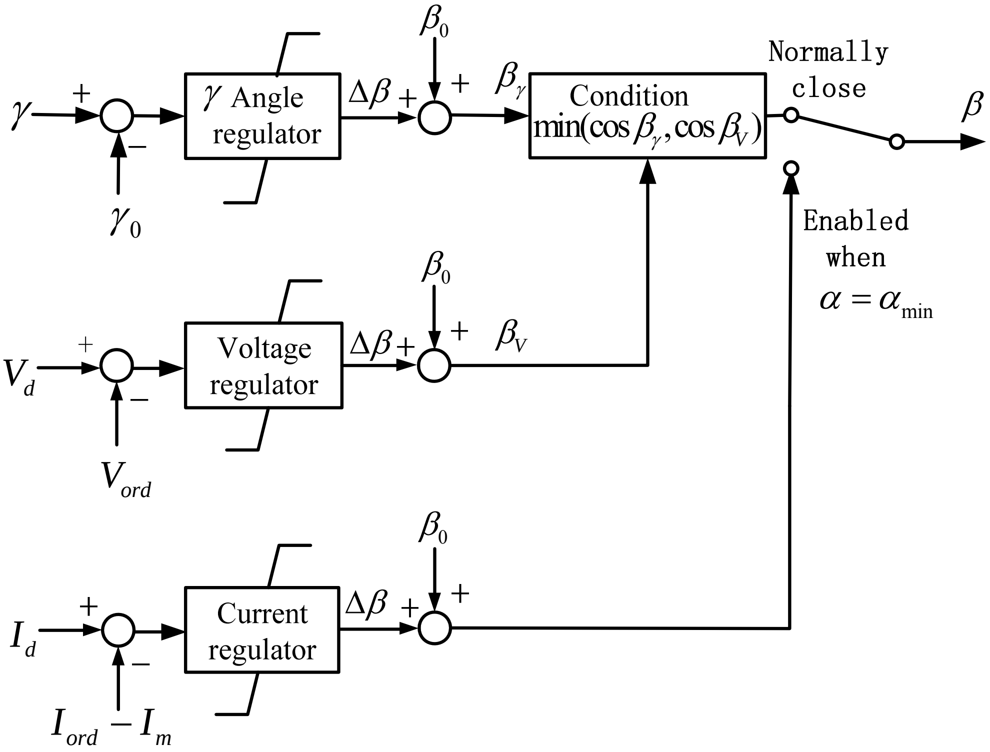

Fig. 3.4 Block diagram of control system of the inversion side. (Provided by CSG)

3.2.4 Impact of Proportion of Dynamic Loads on Voltage Stability

The proportion of dynamic loads also has impact on the system stability, and the larger the proportion, the weaker the system voltage stability.

As can be seen from the analysis of the simulation results of the double-pole fault in Three Gorges-Guangdong HVDC system, when the proportion of dynamic loads is forty percent, the Luodong voltage will drop continuously after the fault occurs, with the voltage dropping to 0.7p.u. in 10s, and the active power load of the motor drops oscillatorily while the reactive power load increases oscillatorily with increasing amplitudes, bringing about voltage instability of the system. But when the proportion of dynamic loads is fifty percent, the Luodong voltage will drop to 0.7p.u. in 1.5s, and the active power load of the motor drops to zero in 10s while the reactive power load increases to more than twice, bringing about more serious voltage stability problems of the system.

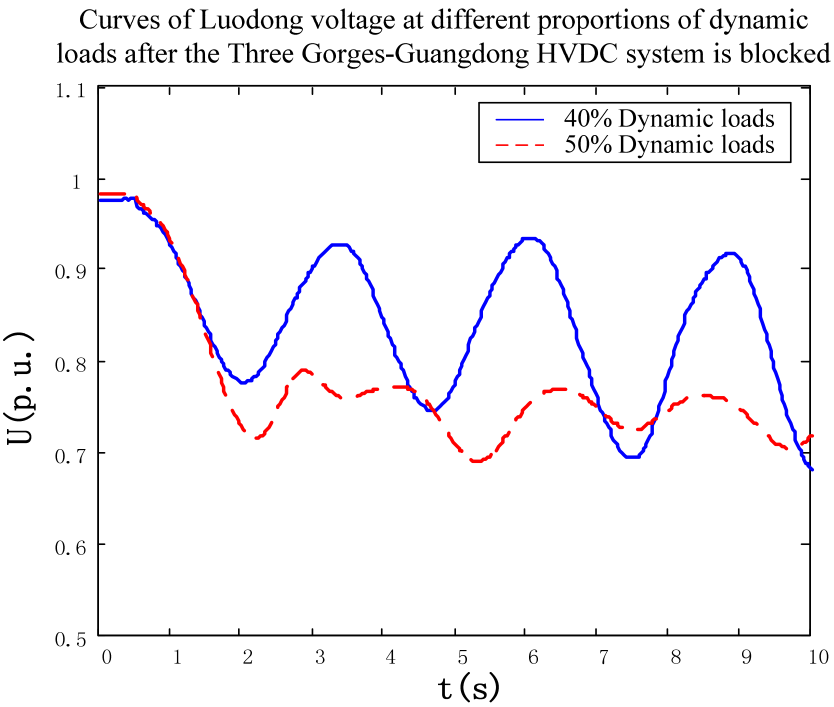

Fig. 3.5 Curves of Luodong voltage at different proportions of dynamic loads after the Three Gorges-Guangdong HVDC system is blocked. (Simulation based on the data provided by CSG)

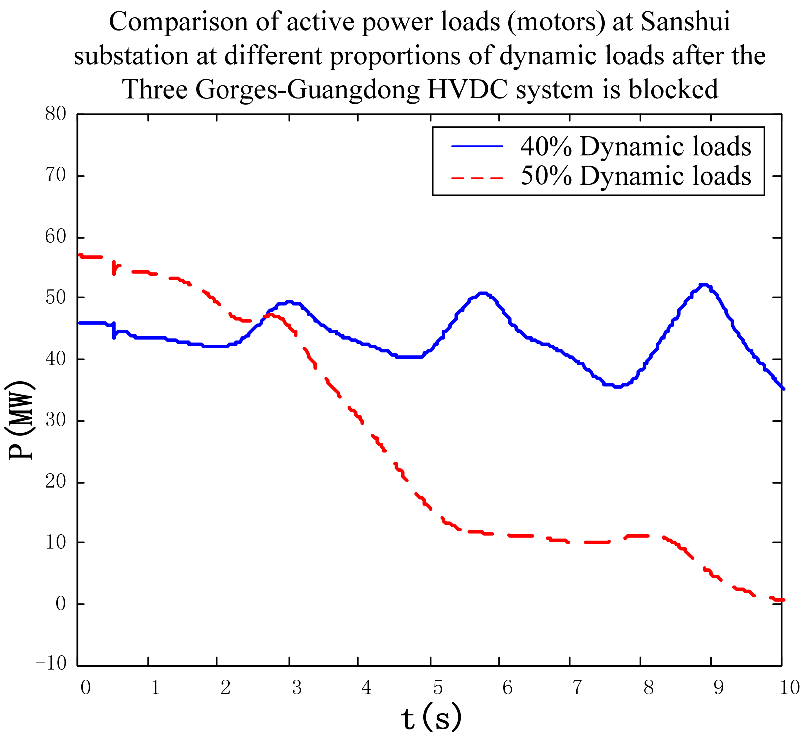

Fig. 3.6 Comparison of active power loads (motors) at Sanshui substation at different proportions of dynamic loads after the Three Gorges-Guangdong HVDC system is blocked. (Simulation based on the data provided by CSG)

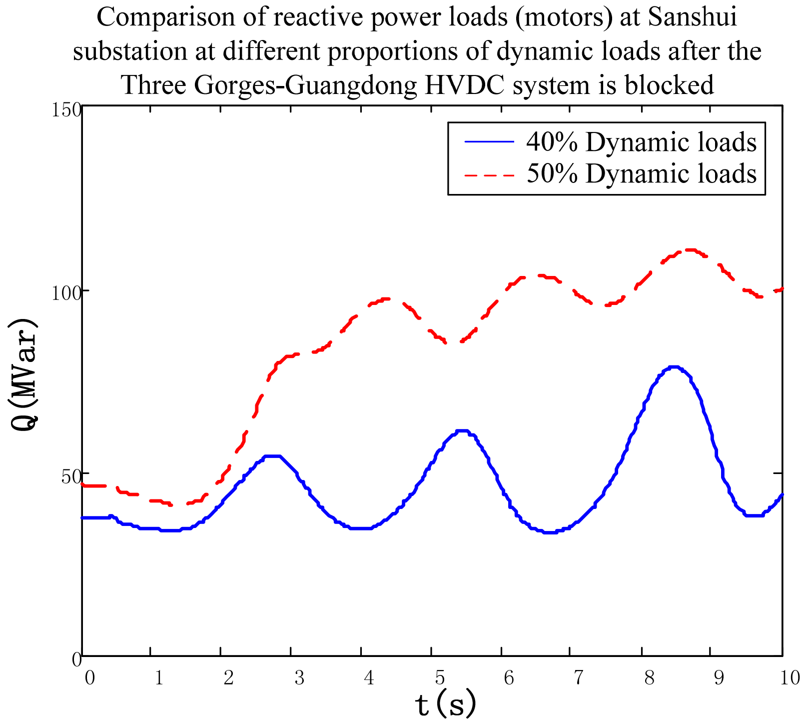

Fig. 3.7 Comparison of reactive power loads (motors) at Sanshui substation at different proportions of dynamic loads after the Three Gorges-Guangdong HVDC system is blocked. (Simulation based on the data provided by CSG)

As can be seen from the simulation results, the higher the proportion of dynamic loads is, the weaker the system voltage stability is.

3.2.5 Voltage Stability in Time of Abrupt Increases of Dynamic Load

The system voltage stability resulting from the startup of motor load is a category of voltage stability problem incurred by non-faults. In the receiving-end system with a large proportion of induction motors and with heavy loads, the sudden increases of loads will lead to voltage stability problem.

3.2.5.1 Analysis of the Mechanism of System Voltage Collapse Resulting from Sudden Increase of Loads

The sudden increase of loads means the fast load increase beyond plan and estimation (such as the sudden increase of air conditioning loads in very hot or cold weather).

Incidents of large-area power failure resulting from the system voltage collapse incurred by the sudden increase of loads have taken place many times worldwide, of which typical incidents include the power failure in Paris, France in 1978 and the power failure in Tokyo, Japan in 1987. Analyses show that these voltage collapse incidents share the following common characteristics:

All the voltage collapse incidents happened in the networks of large cities. The grids are characterized by high density of loads, and a large amount of power relies on outside supply owing to the limitations of environmental protection and the small number of power sources in the load regions. For example, the French grid, where the voltage collapse incident took place, is supplied by 3700MW by other countries, and the voltage support capability was weak in the load regions.

The direct cause of voltage collapse is that the high growth speed of the loads far exceeds the original expectation, and the total capacity of abruptly increasing loads reaches a certain proportion. No one can ensure that such case will not happen again in the future. Owing to the shortage of sufficient dynamic reactive power sources for voltage support, the rapidly increasing loads will result in the system voltage drop; meanwhile, the proportion of the original motor loads in the grid has been high, and the low-voltage operation characteristics of such loads with the characteristics of the motor loads as the air conditioner and heat pump further aggravate the system stability.

Voltage collapse is usually accompanied by high utilization rate of equipment in the load center, and the shortage of reactive power reserve, especially of the dynamic reactive power reserve, is an important cause of voltage collapse incidents. In the present power system, there are usually parallel capacitors at the secondary side or the power distribution side of large-power key substations used as reactive power compensators. But these capacitor banks are generally used for "reactive power management" other than for direct voltage control, and in practical operation, the reactive power capacitor banks for system voltage regulation are switched manually according to the plan changes of the load forecast so that unnecessary repetitive operations of the automatic devices resulting from voltage fluctuations and equipment damage can be avoided. The reactive power output of the compensation capacitors is in direct proportion to the square of the voltage, and the same capacitors will generate twenty percent less of reactive power at a ninety percent of normal voltage level than that at the normal voltage level. The low voltage resulting from the overload is unbalanced, and the local low voltage may result in the increases of line currents, the increases of reactive power losses of the lines in direct proportion to the square of the currents, and further the shortage of reactive power and voltage drop and even voltage collapse by vicious cycle. In this case, the switching of capacitors will sooner or later determine whether voltage collapse will take place. Generally speaking, the operators don't dare to determine whether to switch the capacitors at their sole discretion under abnormal circumstances. So, it is inadequate just to increase the number of manually switched capacitors, and the reactive power regulators that can automatically and dynamically change the output according to the voltage are needed, such as the SVC.

On the other hand, the common consequence of faults in the grids of large cities is high costs. For example, the voltage collapse incident in Tokyo resulted in a load loss of 8 million kW, lasted for four hours, and incurred a loss of 32 million kWh, amounting to about 1.6 million dollars by the electricity price of 0.05 dollor per kWh, or 48 million dollars of direct economic loss. And this is only the economic loss.

3.2.5.2 Possibility of Large-scale Abrupt Load Increases in Domestic Power Systems

Currently, with the economic development of our country, the grids are enlarging in size continuously, and large-scale load centers come into being progressively, such as Beijing, Shanghai and Guangzhou-Shenzhen city group. These load centers have the structural characteristics of the grids of general large cities. For example, most loads of Guangdong grid focus in Pearl River Triangle (Guangzhou, Dongguan, Shenzhen, Zhuhai, Foshan districts) and Chaozhou-Shantou region, and the loads comprise static loads and dynamic motor loads with a high proportion of dynamic loads; meanwhile, the local power sources are insufficient in the load focusing regions, quite a proportion of power is supplied by the outside, and the ten million kW power transmitted from the West to Guangdong accounts for more than one third of the total loads of Guangdong grid. So, large load increases beyond plan and forecast are highly possible in the load focusing regions in Guangdong grid with a high probability of resulting in voltage collapse, and the overseas voltage collapse faults are worth borrowing. And also, voltage stability faults have also occurred in our country. For example, faults have ever taken place in Shanghai grid, causing low voltage and a load shedding of about one million kW.

Although there have taken place such voltage stability faults both home and abroad, the theoretical analysis and practical measurement of the voltage of large grid in time of abrupt load increases are still very hard, and there are still no powerful theoretical tools for the analysis and prediction of such faults. So, the system simulation has become the most important means of analysis and forecast.

Precise digital models of power system components need to be built to reflect the practical operation conditions in the system simulation, where the load models are the most important, and the load properties, capacities, growth speed also have great impact on the simulation results. Besides, the relevant control operations, or even the impact of the dispatcher's commands on the system, must be taken into account so that the operation characteristics of the system can be reflected, or the actual system conditions can "reoccur". In this chapter, the simulation tool of NETOMAC will be used to simulate the case of abrupt load increases that may take place in Guangdong grid.

3.2.5.3 Model of Abruptly Increasing Load

The abruptly increasing load is simulated by the startup of equivalent induction motor with the following parameters:

```
const static double Rr = 0.048；          //Rr=Rr
static double Xs = 0.194；                //Xs=Xs equivalent stator reactance if the system side
const static double Xr = 0.163；          //Xr=Xr
const static double A = 1.0；
const static double B = 0.0；
const static double sl0 = 0.04；          // slip
const static double Xm = 2.8；            // td0l=(Xr+Xm)/(100*M_pie*Rr)
const static double H = 0.93；            // tj1=2*H
const static double Sbr = 24.0；          // average capacity
const static double LF =0.6；             //power factor
```

Fig. 3.10 shows the simulation curves of the equivalent induction motor in the process of startup. Simulation results of the motor startup characteristics indicate that the active power consumption continues to increase in nearly 5s until it reaches the steady-state value, while the reactive power consumption reaches the maximum value at the instant of startup and then drop gradually. This tallies with the practical case of load increases, especially of the increases of such load as air conditioner. So, the increasing load will need to absorb a great deal of reactive power, leading to the system voltage drop or even voltage collapse under some conditions.

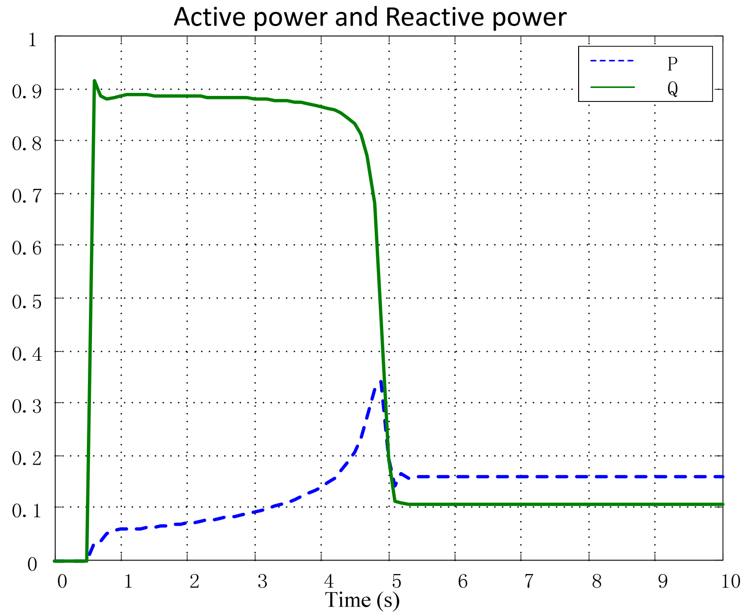

Fig. 3.8 Curves of bus voltage, active power and reactive power at the time of induction motor startup.

3.2.5.4 Patterns of Putting Abruptly Increasing Loads into Operation

The loads in the simulation mean the aggregate system load seen from the high-voltage power transmission lines to the load side, with all the system loads concentrating at the110kV bus in an equivalent way, and so the abruptly increasing loads for simulation are also supplied by the 110kV bus. There are two patterns of putting the abruptly increasing loads into operation for simulation: one is to start up the equivalent induction motor loads of the whole grid at 0s, a pattern of simulating the large impulses of the abruptly increasing loads to the system; the other is to divide the abruptly increasing loads into three batches and start up the equivalent induction motor loads of every batch of abruptly increasing loads stepwise every 2 seconds, with the total amount of the abruptly increasing loads equal to that of the former pattern. Every batch of loads is dispersed in the Pearl River Triangle and the Chaozhou-Shantou region with roughly equal capacities. The first batch of loads start up at 0s, and the following two batches start up successively every 2 seconds.

3.2.5.5 Scheme of Simulating Abruptly Increasing Loads

In the simulation and calculation, the proportions of dynamic loads to static loads can be selected as 20%:80%, 30%:70%, 40%:60% and so on. To reflect the practical case of increasing proportion of dynamic loads in the receiving-end grid, and to test the voltage stability under the most rigorous conditions, we select 35%:60% as the proportion of dynamic loads to static loads, with a 10% of abruptly increasing dynamic loads. The specific simulation scheme is shown in Table 3.3.

Table 3.3 Scheme of abruptly increasing loads simulation

proportion of static loads	proportion of dynamic loads	proportion of abruptly increasing loads	abruptly increasing manner
60%	35%	10%	once
			three times

3.2.5.6 Simulation Results and Analysis

(1) Simulation results of 60%static loads+35%dynamic loads+ 10% abruptly increasing loads that increase in one batch

After the induction motors start up in one batch to bring about impulses to the system, the voltages of the system buses are shown in Table 3.9.

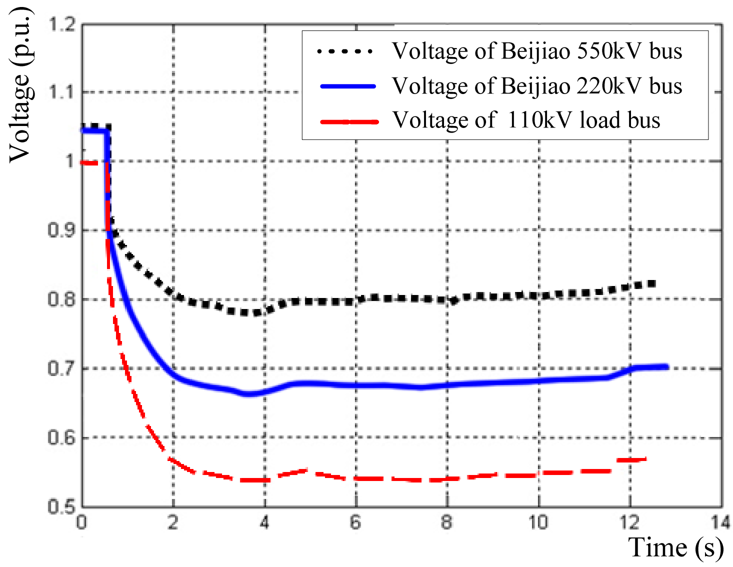

Fig. 3.9 Curves of system voltages after the abrupt load increases. (Simulation based on the data provided by CSG)

The three curves in Fig. 3.9 are of the voltage of 500kV bus of the Beijiao

Substation, of the 220kV bus voltage and of the voltage of 110kV load point (Tianhe) in Guangzhou. As can be seen from the above figure, owing to the impulses of the startup of a high capacity of equivalent induction motors, the voltages of the buses of different voltage levels show a trend of dropping, among which the load-side bus voltage drops the most dramatically. At this time, the dynamic voltage of the 220kV bus has been below 0.70p.u. for a long time, the steady-state voltage reaches 0.70p.u., and the steady-state voltage of the 500kV bus maintains only at around 0.80p.u. The steady-state voltage of the load-side bus drops to below 0.60 p.u., and the voltage of this load point shown in the above figure is the minimum of the voltages of all the load points. Observation of the changing processes of dynamic voltages of other load points shows that the biggest difference from case 1 lies in that the load voltages of Dongguan and Chaozhou-Shantou region have dropped to below 0.65p.u. (above 0.65p.u. in other districts), and that there have been large-area voltage instability phenomena at the load side with voltage sag degrees higher than that of case 1.

The key reason of these phenomena is that there are an increasing number of motor loads in the system, and the abruptly increasing loads, after being put into operation, need to absorb a great deal of reactive power from the system, leading to large voltage drops. The operation characteristics of the original induction motors at low voltages are as follows: the active power will drop a great deal, while the reactive power increases a great deal, and further aggravating the load-side voltage.

The abrupt load increases usually have smaller impact on the bus voltages of high-voltage levels than on the load-side bus voltage, so the voltage sags at the high-voltage levels are less serious than those at the load side. Meanwhile, the angle curves of the units within and outside Guangdong system are shown in Fig. 3.10, with the angles of all the units of Guangdong system remaining stable.

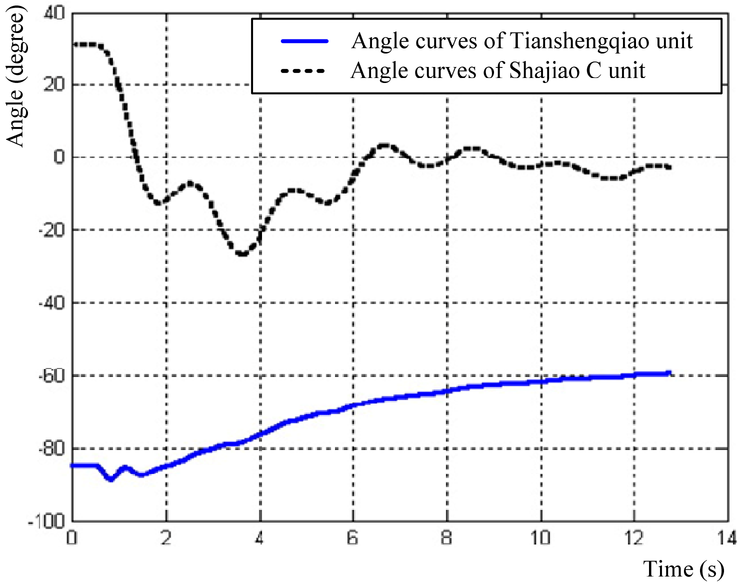

Fig. 3.10 Angle curves of the system units after abrupt load increases. (Simulation based on the data provided by CSG)

As can be seen from the above angle curves, in the cases of the disturbances of abrupt load increases, the power plants both within and outside the region will remain angle stability.

As shown below, Fig. 3.11a through Fig. 3.11d show the schematic diagrams of the 500kV bus voltages, 220kV bus voltages, 110kV bus voltages, and the angles of main units within the grid in the cases of abrupt load increases.

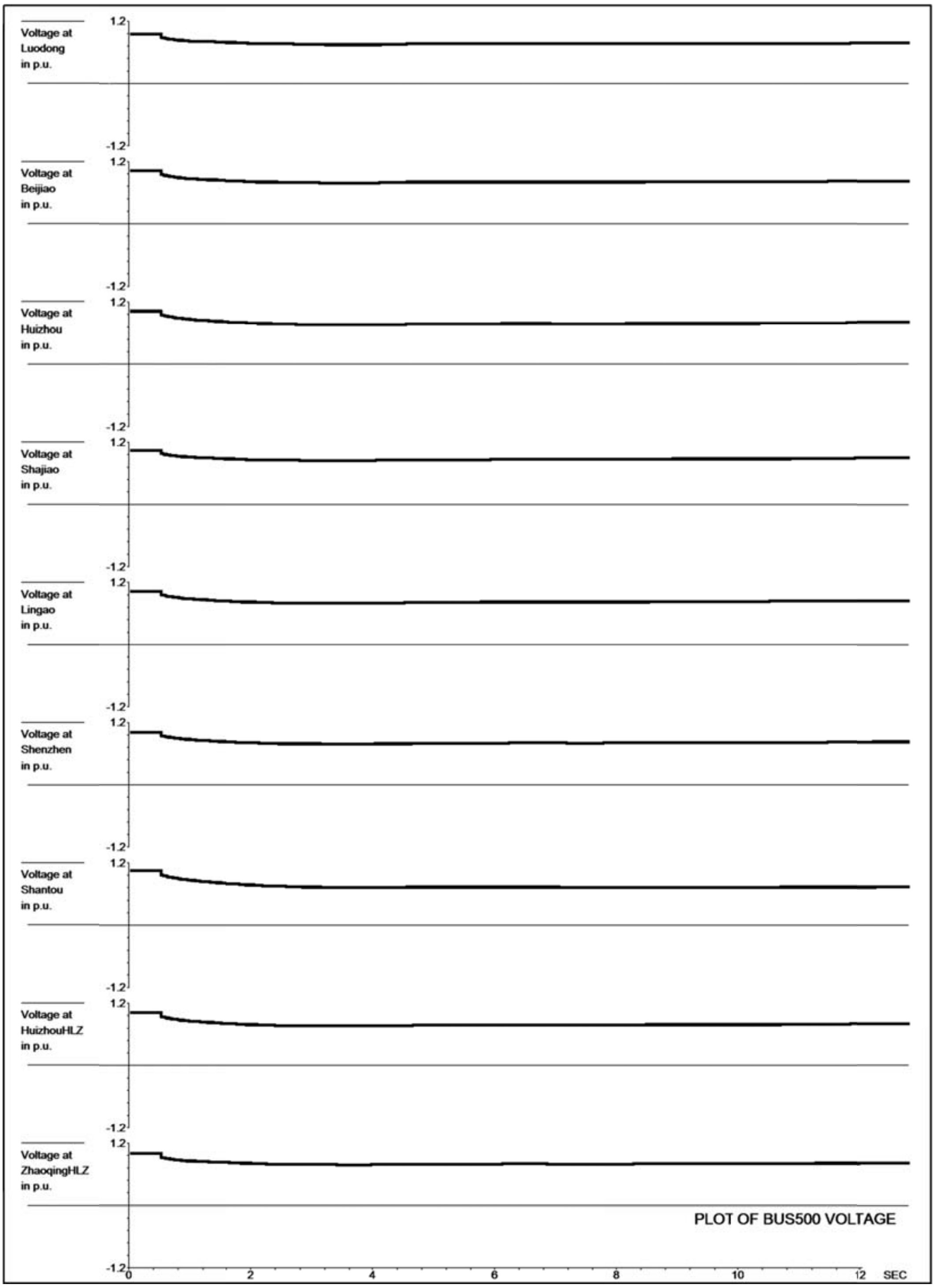

Fig. 3.11a Curves of 500kV bus voltages after abrupt load increases. (Simulation based on the data provided by CSG)

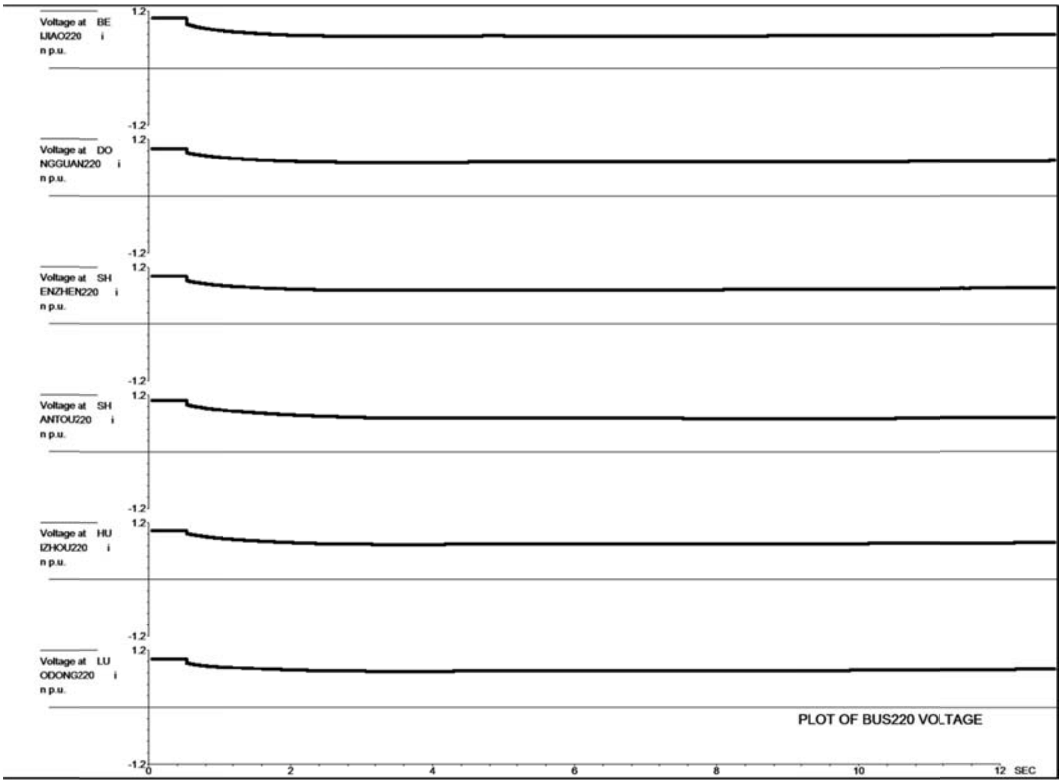

Fig. 3.11b Curves of 220kV bus voltages after abrupt load increases. (Simulation based on the data provided by CSG)

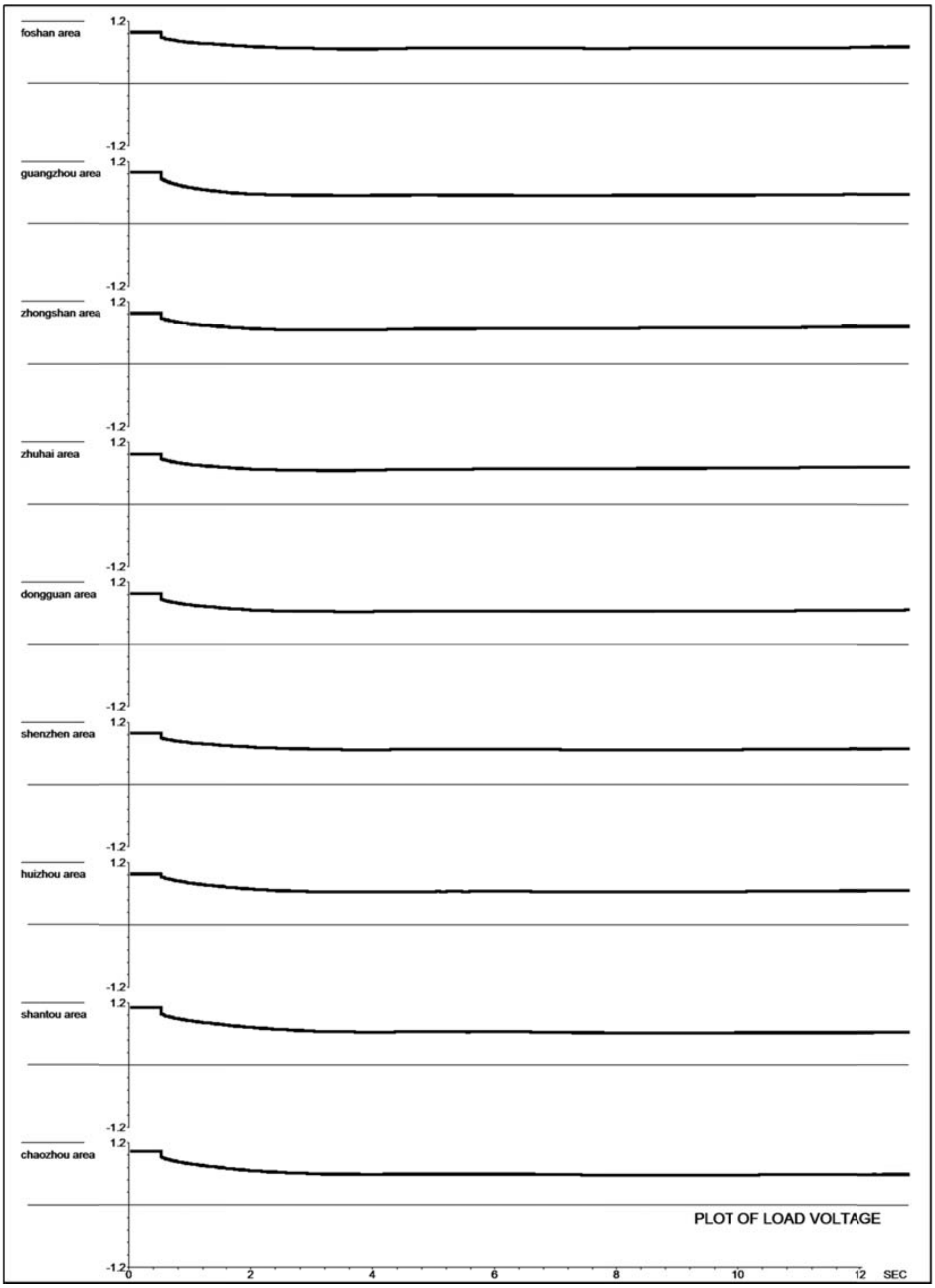

Fig. 3.11c Curves of 110kV bus voltages after abrupt load increases. (Simulation based on the data provided by CSG)

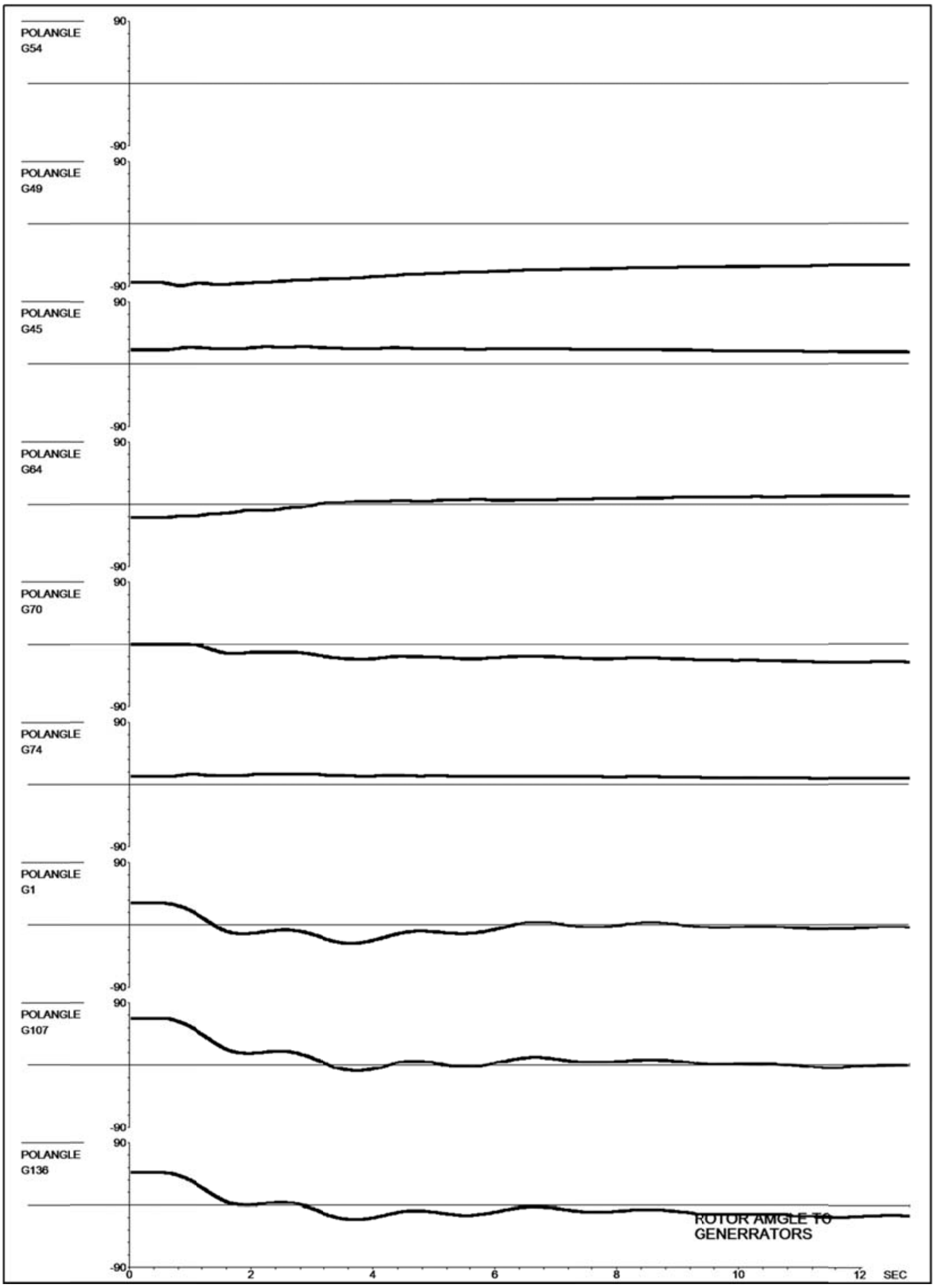

Fig. 3.11d Curves of angles of main units after abrupt load increases. (Simulation based on the data provided by CSG)

2) Simulation results of 60％static loads＋35％dynamic loads+ 10% abruptly increasing loads that increase in three batches

After the induction motors start up in three batches to bring about impulses to the system, the voltages of the system buses are shown in Table 3.12.

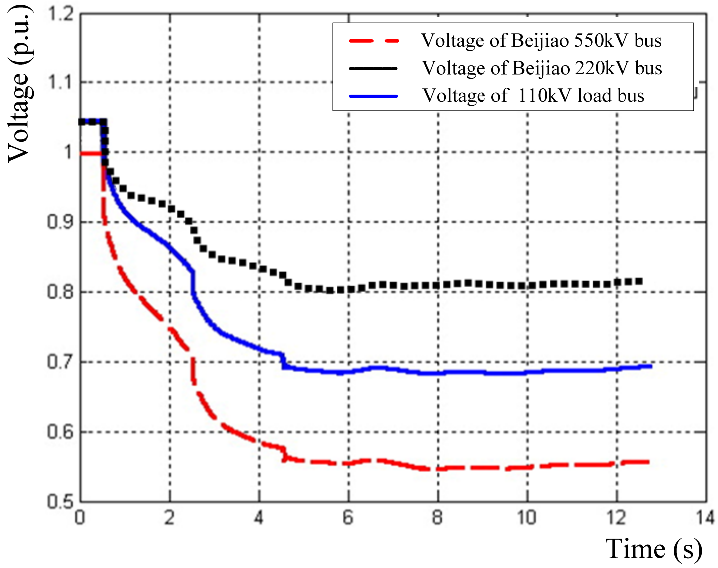

Fig. 3.12 Curves of system voltages after the abrupt load increases. (Simulation based on the data provided by CSG)

The three curves in Fig. 3.12 are of the voltage at the 500kV bus of the Beijiao Substation, of the 220kV bus voltage and of the voltage of 110kV load point (Tianhe) in Guangzhou. As can be seen from the above figure, owing to the impulses of the startup of a high capacity of equivalent induction motors, all the voltages of the buses of different voltage levels show a trend of dropping, among which the load-side bus voltage drops the most dramatically. At this time, the dynamic voltage of the 220kV bus has been below 0.70p.u. for a long time, the steady-state voltage is close to 0.70p.u., and the steady-state voltage of the 500kV bus maintains only at around 0.80p.u. The steady-state voltage of the load-side bus drops to below 0.60p.u., and the voltage of this load point shown in the above figure is the minimum of the voltages of all the load points. Observation of the changing processes of dynamic voltages of other load points shows that the biggest difference from case 2 lies in that the load voltages of Dongguan and Chaozhou-Shantou region have dropped to around 0.65p.u. (above 0.65p.u. in other districts), and that there have been large-area voltage instability phenomena at the load side with voltage sag degrees higher than that of case 2. The key reason of these phenomena is that there are an increasing number of motor loads in the system, and the abruptly increasing loads, after being put into operation, need to absorb a great deal of reactive power from the system, leading to large voltage drops. In comparison with case 5, it takes a longer time for the voltages to drop to the steady states when the abrupt load increase are put into operation in three batches than in one batch, but the steady-state voltage levels are equal.

The abrupt load increases usually have smaller impact on the bus voltages of high-voltage levels than on the load-side bus voltage, so the voltage sags at the high-voltage levels are less serious than those at the load side. Meanwhile, the angle curves of the units within and outside Guangdong system are shown in Fig. 3.13, with the angles of all the units of Guangdong system remaining stable.

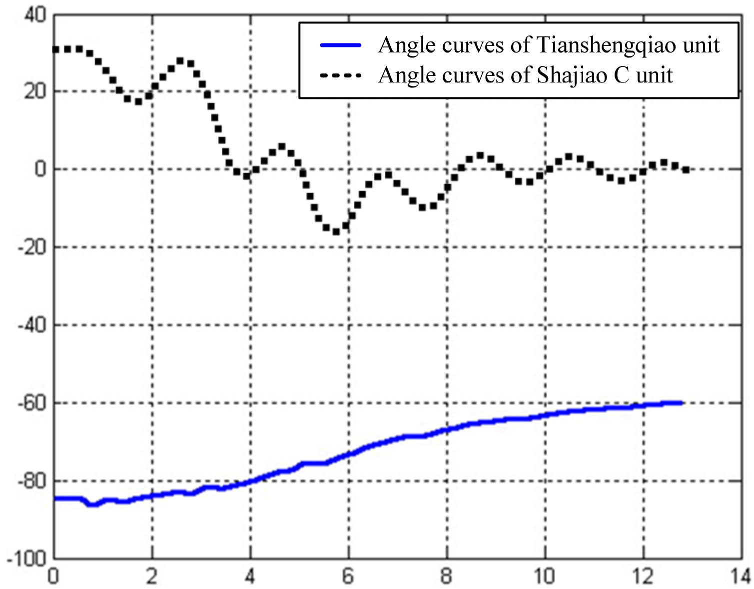

Fig. 3.13 Angle curves of the system units after abrupt load increases. (Simulation based on the data provided by CSG)

As can be seen from the above angle curves, in the cases of the disturbances of abrupt load increases, the power plants both within and outside the region will remain angle stability.

As shown below, Fig. 3.14a to Fig. 3.14d show the schematic diagrams of the 500kV bus voltages, 220kV bus voltages, 110kV bus voltages, and the angles of main units within the grid in the cases of abrupt load increases.

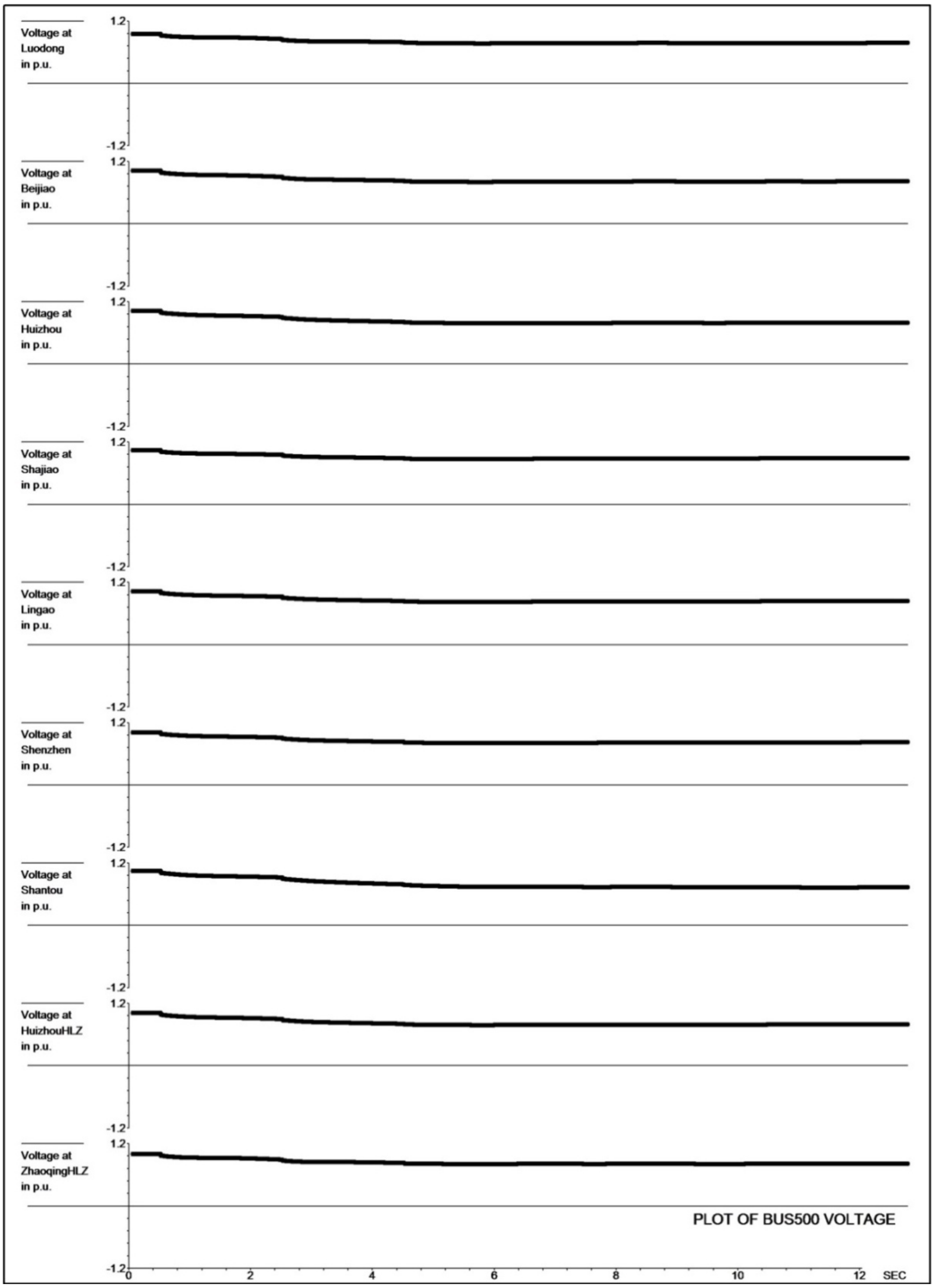

Fig. 3.14a Curves of 500kV bus voltages after abrupt load increases. (Simulation based on the data provided by CSG)

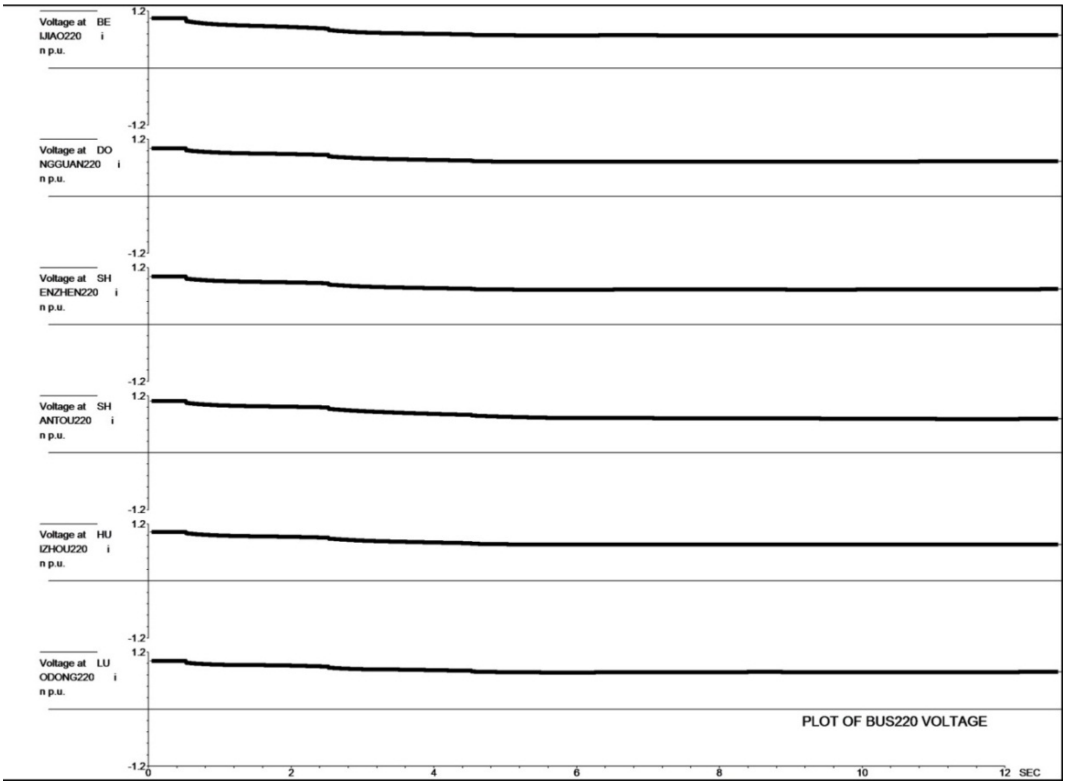

Fig. 3.14b Curves of 220kV bus voltages after abrupt load increases. (Simulation based on the data provided by CSG)

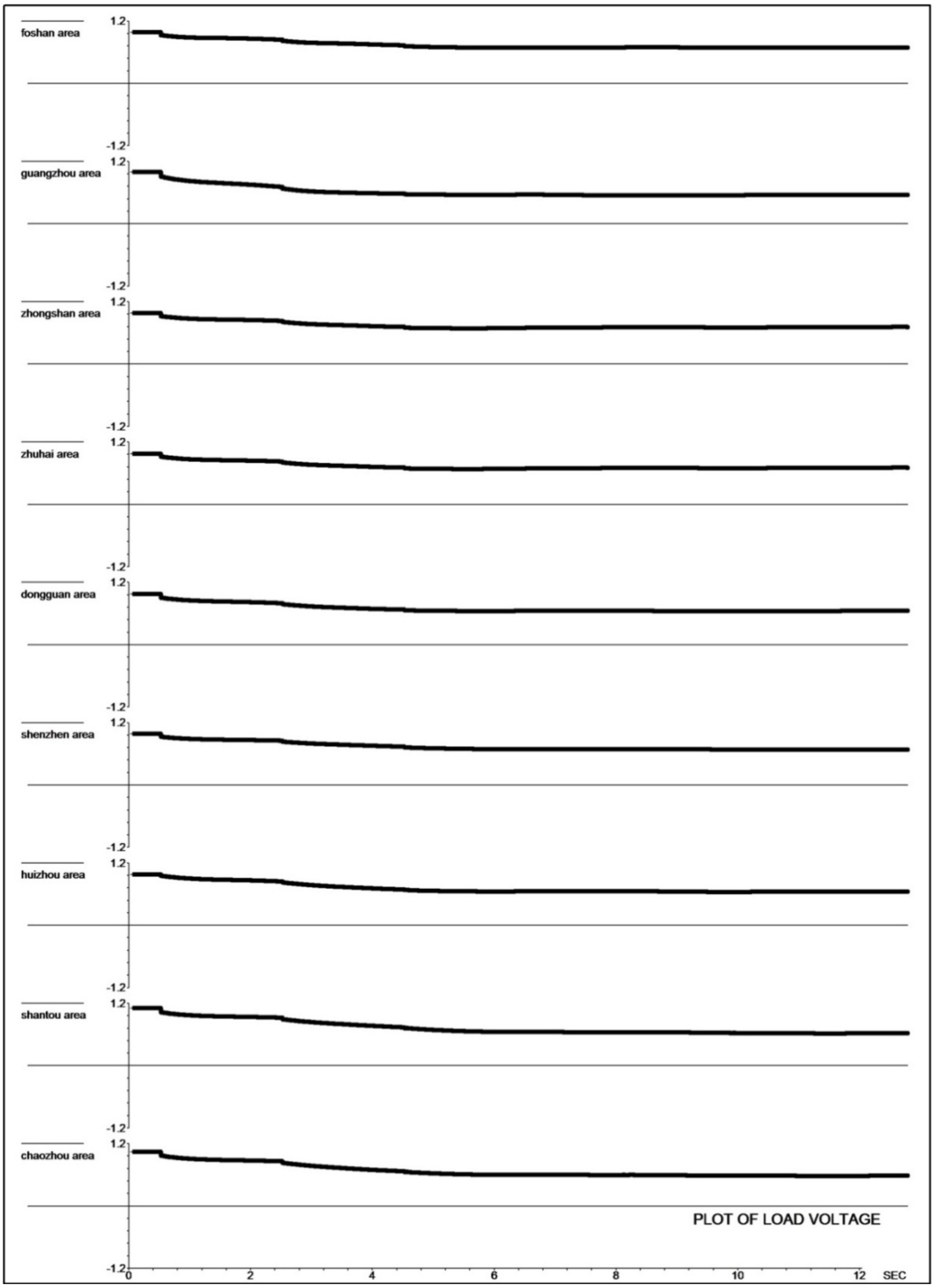

Fig. 3.14c Curves of 110kV bus voltages after abrupt load increases. (Simulation based on the data provided by CSG)

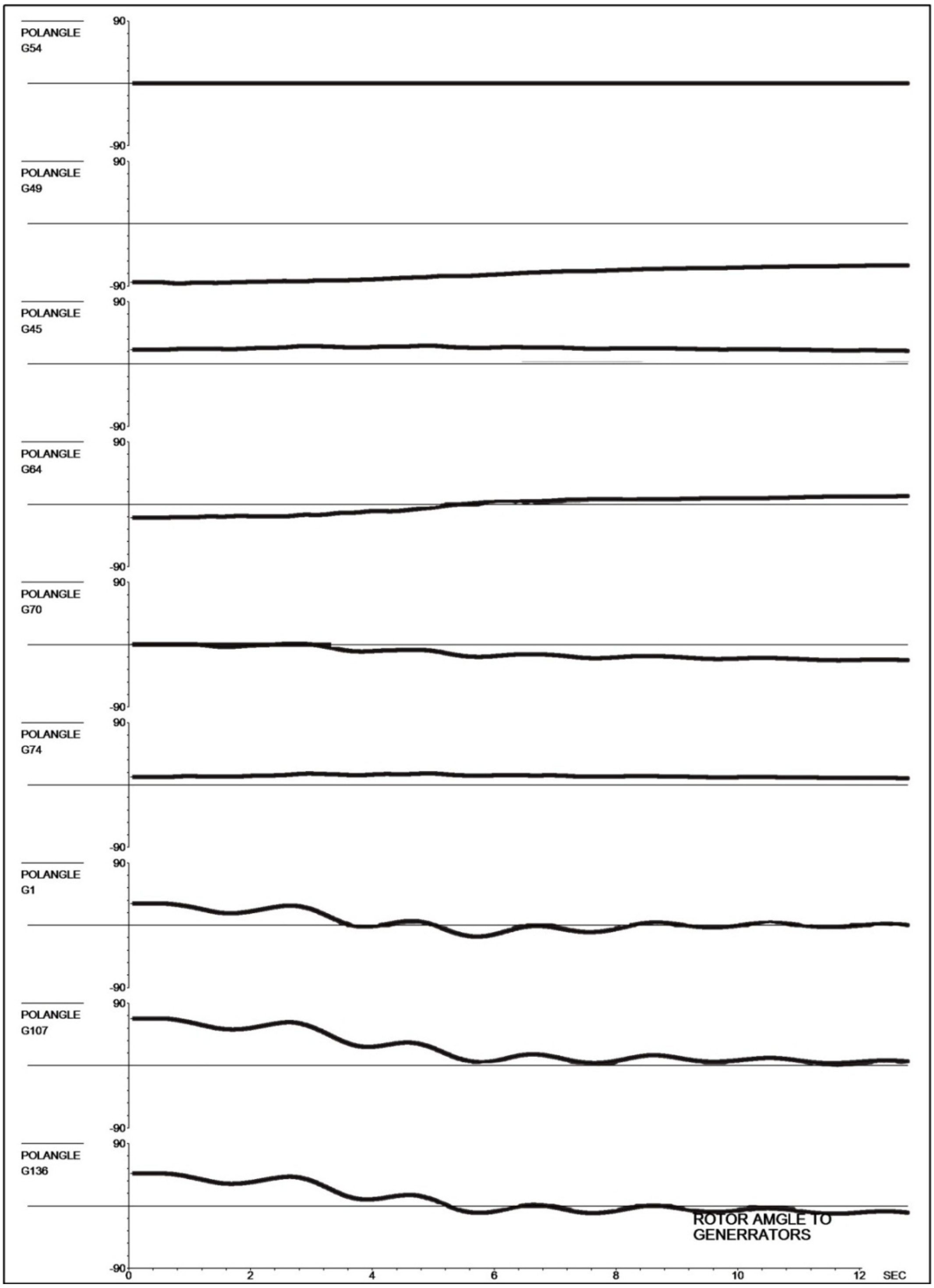

Fig. 3.14d Curves of angles of main units after abrupt load increases. (Simulation based on the data provided by CSG)

3.2.5.7 Summary of Simulation Conclusions

In 3.2.5.6, simulation experiments are conducted in accordance with every case shown in Table 3.3, the dynamic voltage processes of all the voltage levels of the whole grid are analyzed and compared, and the angle characteristics of the units within and outside Guangdong grid are observed. Simulation experiments and analyses yield the following conclusions:

(1) In time of abruptly increasing loads in the heavy load regions in Guangdong system, there are large voltage sag phenomena in the regions of abruptly increasing loads, with the minimum of dynamic voltages below 0.75p.u. lasting for more than 1s, which can be regarded as voltage instability.

(2) As can be seen from the simulation results, the region that is most prone to voltage instability is Guangzhou district, where the load-side voltage is the lowest in all cases, and the 220kV bus voltage of Beijiao Substation is also the lowest out of the voltages of all the 220kV buses. Additionally, the regions with low voltage levels also include Dongguan and Shenzhen districts, and there may be voltage instability in Chaozhou-Shantou region in some cases.

(3) The abruptly increasing loads in one batch may have more serious impact on voltage stability than those in three batches, which is embodied by faster voltage sags and lower steady-state voltages.

(4) Different manners of abruptly increasing loads may have impact on voltage stability as shown in Table 3.4.

Table 3.4 Impact of different manners of abruptly increasing loads on voltage stability (Simulation based on the data provided by CSG)

Proportion of static loads	Proportion of dynamic loads	Proportion of abruptly increasing loads	Manner of abrupt increases	Minimum dynamic voltage of 220kV bus at Beijiao Substation (p.u.)	Steady-state voltage of 220kV bus at Beijiao Substation(p.u.)	Angle of grid-wide units
60%	35%	10%	in one batch	below 0.7	0.7	synchronous
			in three batches	below 0.7	0.68	synchronous

3.3 Transient Stability Problems Incurred by Faults in Tie Lines

3.3.1 Simulation Calculation Conditions and Stability Criteria

Calculations are performed with the NETOMAC software developed by SIEMENS and with the programming data of China Southern Power Grid in 2015. The stability criteria are defined as follows:

(1) Transient-state stability

The criterion of transient-state stability is that, after the grid experiencing large disturbances each time, the angles of all the units will become larger, remain synchronous in one or two oscillation cycles, and then oscillate in a synchronous and damping way, and the voltages of key system buses will gradually recover.

(2) Dynamic stability

The criterion of dynamic stability is that, in the case of a fault with any component of the system, the protection system and switchgears operate correctly, and the system damping is no less than 0.03, i.e. the oscillation amplitudes reduce to below 10% after 12 oscillations; in the case of small disturbances, the system damping is no less than 0.04, i.e. the oscillation amplitudes reduce to below 10% after 9 oscillations.

(3) Voltage stability

The criteria of voltage stability are determined as follows: when the voltage of key bus is lower than 0.75 p.u. and lasts for less than 0.8s, it is stable; when the voltage of the key bus is lower than 0.75 p.u. and lasts for more than 0.8s, it is unstable or critical.

3.3.2 Dynamic Processes of Faulty AC/DC System

Assume the faults leading to power loss to be bipolar block fault in DC lines or three-phase short-circuit fault in AC lines. The first fault is a typical DC one, and the second is a typical AC one. They can represent the main faults in the tie lines. And the schematic diagrams of these two faults are shown in Fig. 3.15a and Fig. 3.15b. Now, the dynamic processes of the systems will be expounded on and analyzed in the cases of these two faults below.

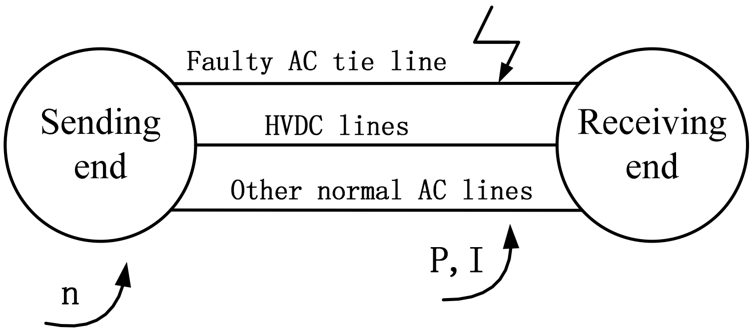

Fig. 3.15a Three-phase short-circuit fault in AC lines

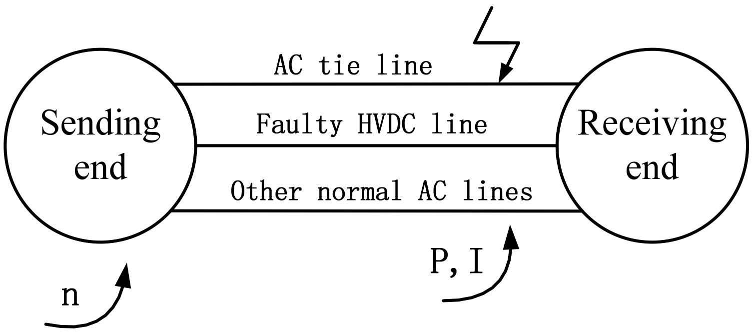

Fig. 3.15b Bipolar block fault in DC lines

When a three-phase short-circuit fault in AC lines or a bipolar block fault in DC lines occurs, a great deal of active power will not be transmitted through these DC or AC lines instantaneously, and the system flow will be re-distributed. This amount of power shortage will be assumed by the AC tie lines that are in normal operation. The transmitted power P along the AC tie lines will increase, and the current I injected from the lines to the receiving-end grid will also greatly increase, which are shown in Fig. 3.16. With $Q = I^2 \bullet X$ the reactive power requirements of the receiving-end grid increase dramatically. The original network is short of additional reactive power compensation, causing the receiving-end voltages to drop initially, the power at the sending end is unable to be sent out, and the generators at the sending end to increase in rotation speed or even to be asynchronous. Once the voltages begin to drop, the reactive power compensation provided by the fixed capacitors at the receiving end begins to decrease, leading to the shortage of reactive power compensation and further drop of voltages. So, the fault at the tie lines causes the transient-state voltage stability at the receiving end. The power transmission capacity of a double-circuit AC transmission line is about 40% to 60% of that of DC lines. So, the impact of fault on AC lines is weaker than on DC lines because of the smaller power transmission capacity of AC lines, although the post-fault dynamic processes are identical for AC lines and DC lines. Below this dissertation will study the system stability in the context of faults in accordance with the bipolar block fault in DC system.

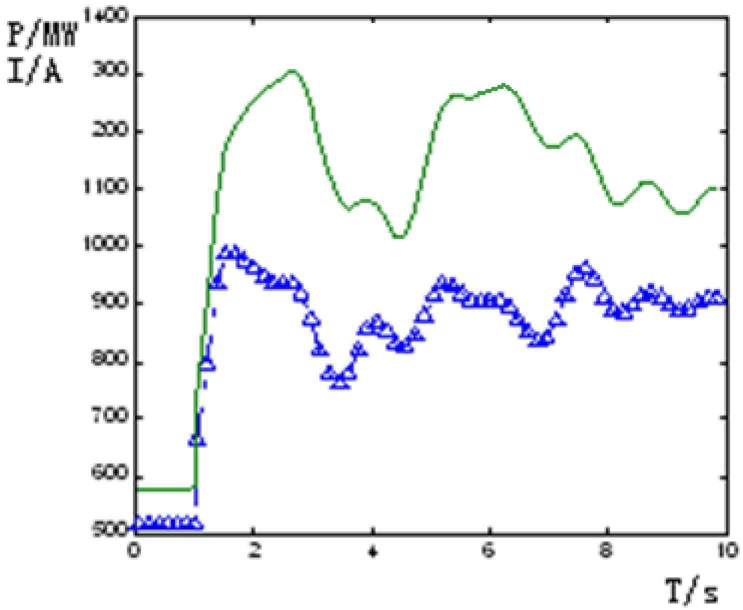

Fig. 3.16 Post-fault power and current of AC lines in normal operation(Blue line: Power, green line: Current)

3.3.3 Impact of Bipolar block in DC System on System Stability in the Context of Different Load Models

The dynamic processes in correspondence with different load models are different even in the context of identical system faults. This dissertation studies the dynamic processes in accordance with two different load models in time of power deficiency in the tie lines, and arrives at conclusions concerning the impact of the proportion of dynamic loads on the grid stability. Also, this dissertation perform comparative analyses of voltage stability in the maximum operation manner of China Southern Power Grid in 2015 in accordance with the two load combinations of 100% static loads and 70% static loads + 30% dynamic induction motor loads in time of bipolar block of the DC system.

According to the stipulations of China Southern Power Grid, the criterion of voltage stability is as follows: after the system disturbances are cleared, if the duration when the bus voltage is lower than 0.75p.u. is less than 1s, and the bus voltages of key substations can restore to above 0.8p.u., then the voltages can be judged to be stable.

3.3.3.1 Impact of Faults on System Voltage Stability in the Case of 100% Static Loads

In the case of 100% static loads, bipolar block faults are set up in six HVDC lines, and the system bus voltages at the receiving ends are shown in Fig.3.17a to Fig. 3.17f.

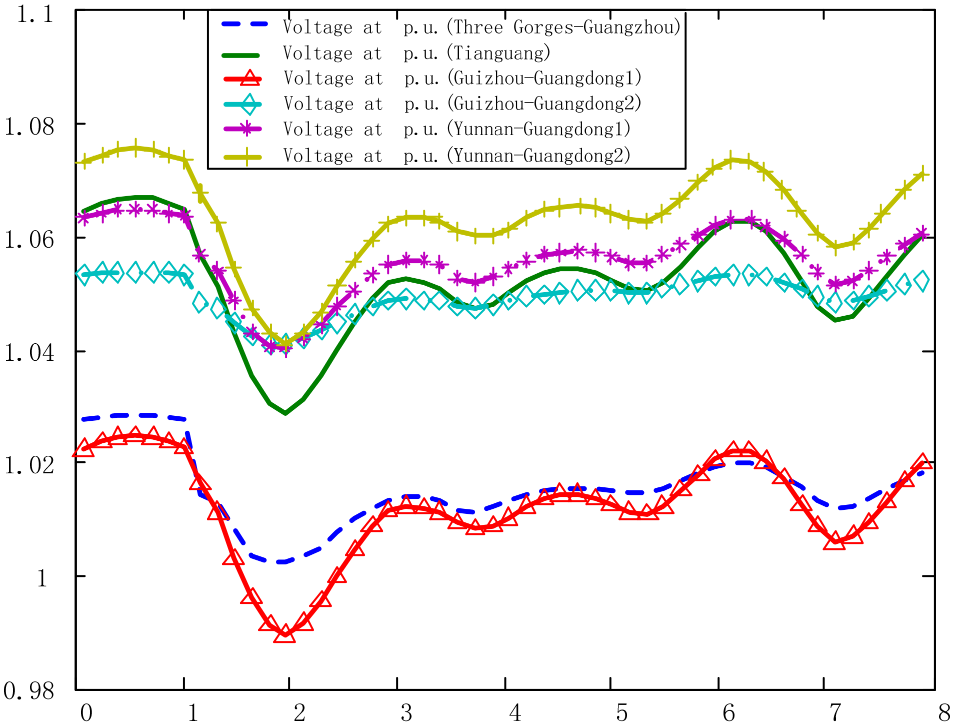

Fig. 3.17a Voltages in the context of bipolar block in Three Gorges-Guangzhou HVDC system (100% static loads) (Simulation based on the data provided by CSG)

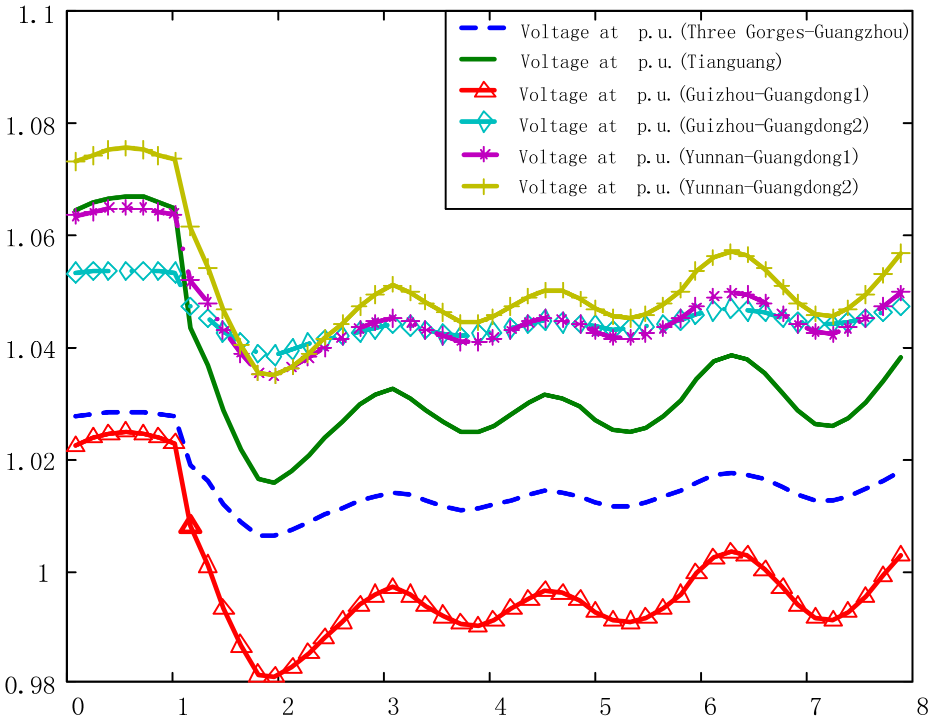

Fig. 3.17b Voltages in the context of bipolar block in Tianshengqiao-Guangzhou HVDC system (100% static loads) (Simulation based on the data provided by CSG)

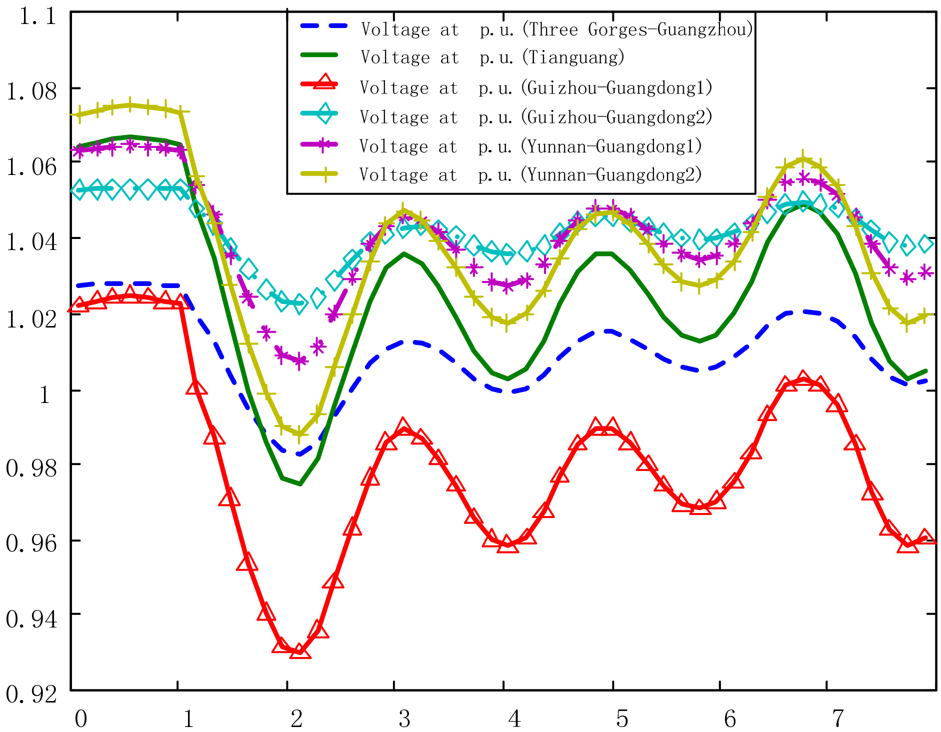

Fig. 3.17c Voltages in the context of bipolar block in Guizhou-Guangzhou HVDC system1 (100% static loads) (Simulation based on the data provided by CSG)

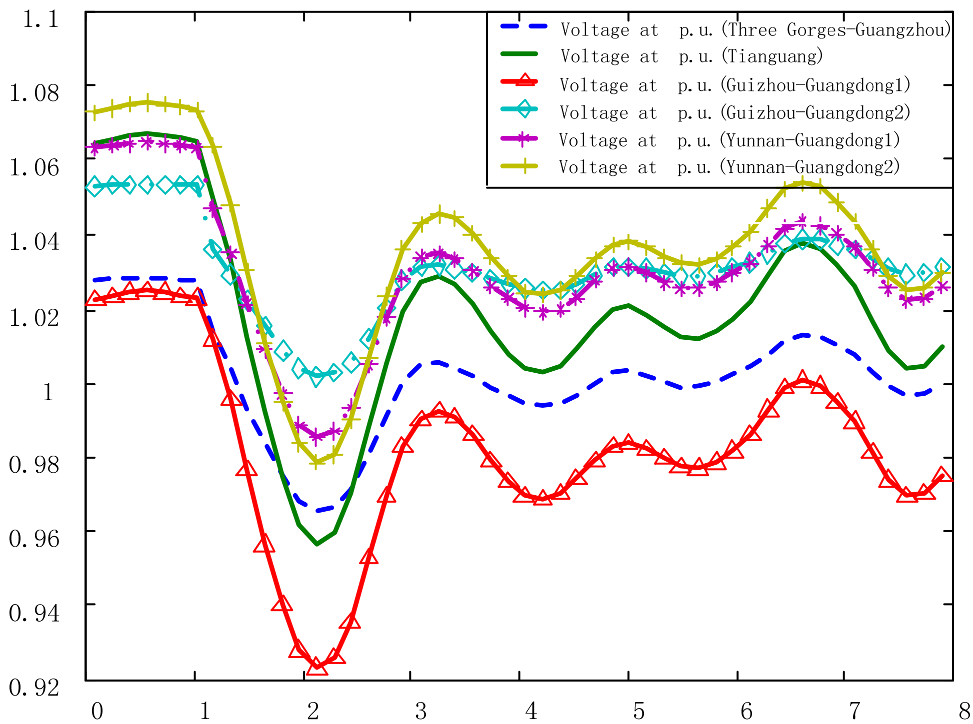

Fig. 3.17d Voltages in the context of bipolar block in Guizhou-Guangzhou HVDC system2 (100% static loads) (Simulation based on the data provided by CSG)

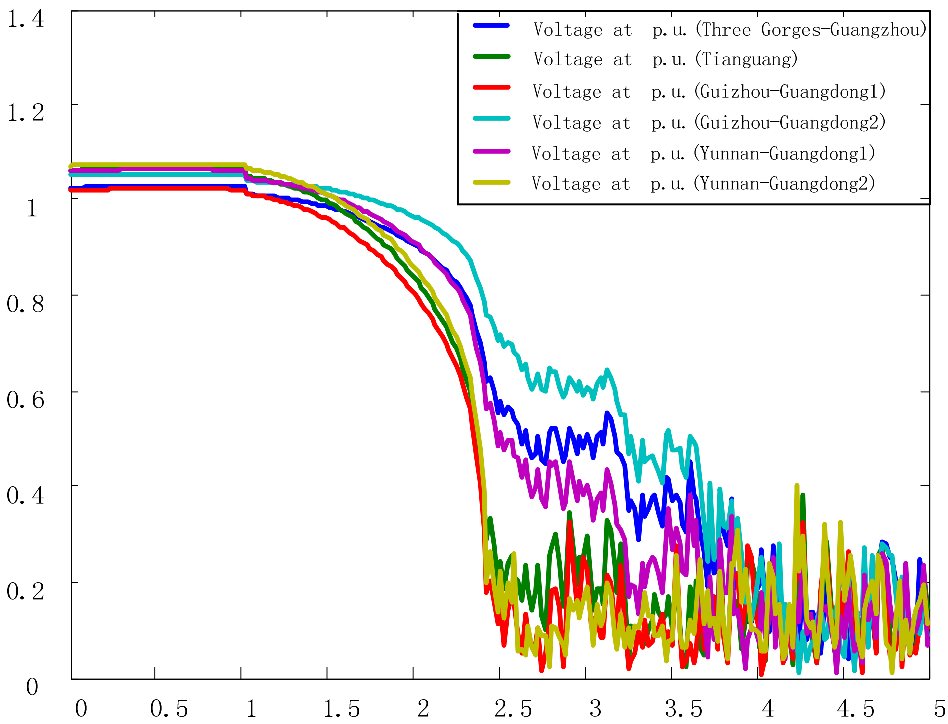

Fig. 3.17e Voltages in the context of bipolar block in Yunnan-Guangdong HVDC system1 (100% static loads) (Simulation based on the data provided by CSG)

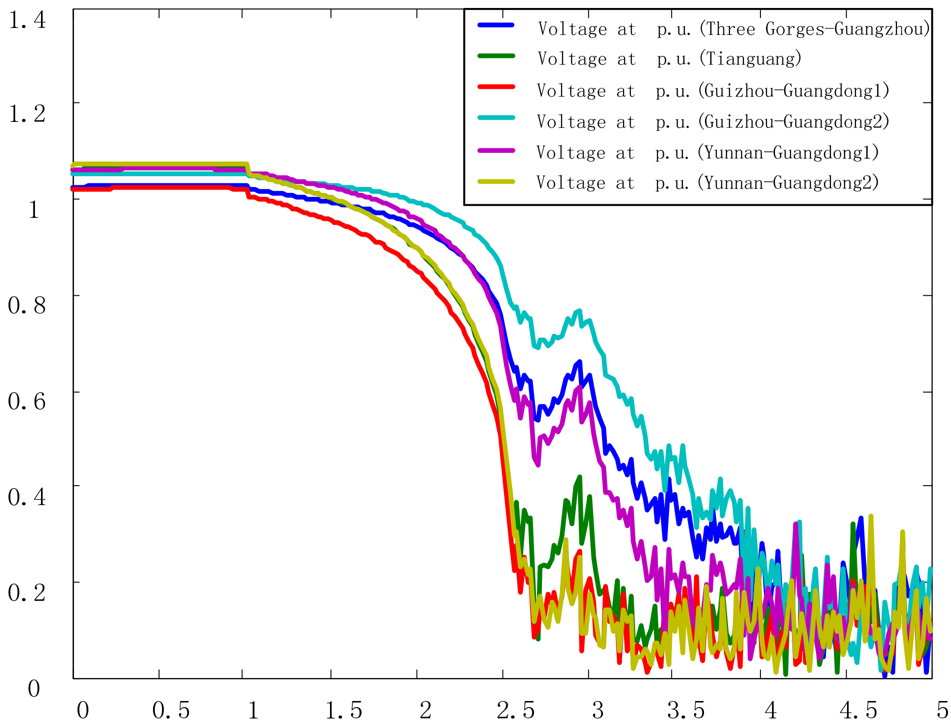

Fig. 3.17f Voltages in the context of bipolar block in Yunnan-Guangdong HVDC system2 (100% static loads) (Simulation based on the data provided by CSG)

In accordance with the stability guidelines, the above results can be tabulated as

follows:

Table 3.5 System stability in the context of 100% static loads in time of HVDC faults

faulty lines	Three Gorges - Guangzhou	Tiaoshengqiao - Guangzhou	Guizhou – Guangzhou 1	Guizhou – Guangzhou 2	Yunnan-Guangzhou 1	Yunnan-Guangzhou 2
voltage stability standards	compliant	compliant	compliant	compliant	incompliant	incompliant
voltage collapse	no	no	no	no	yes	yes

As can be seen from Table 3.5, for the four lines of Three Gorges – Guangzhou, Tiaoshengqiao – Guangzhou, Guizhou – Guangzhou 1 and Guizhou – Guangzhou 2 with a rated capacity below 3000MW, the system voltages will remain stable after the bipolar block occurs. But for the two lines of Yunnan- Guangzhou 1 and Yunnan-Guangzhou 2 with a rated capacity of 5000MW, the system voltages will collapse after the bipolar block occurs.

3.3.3.2Impact of Faults on System Voltage Stability in the Case of 70% Static Loads +30% Dynamic Loads

In the case of 70% static loads + 30% dynamic loads, bipolar block faults are set up in six HVDC lines, and the system bus voltages at the receiving ends are shown in Fig. 3.18.

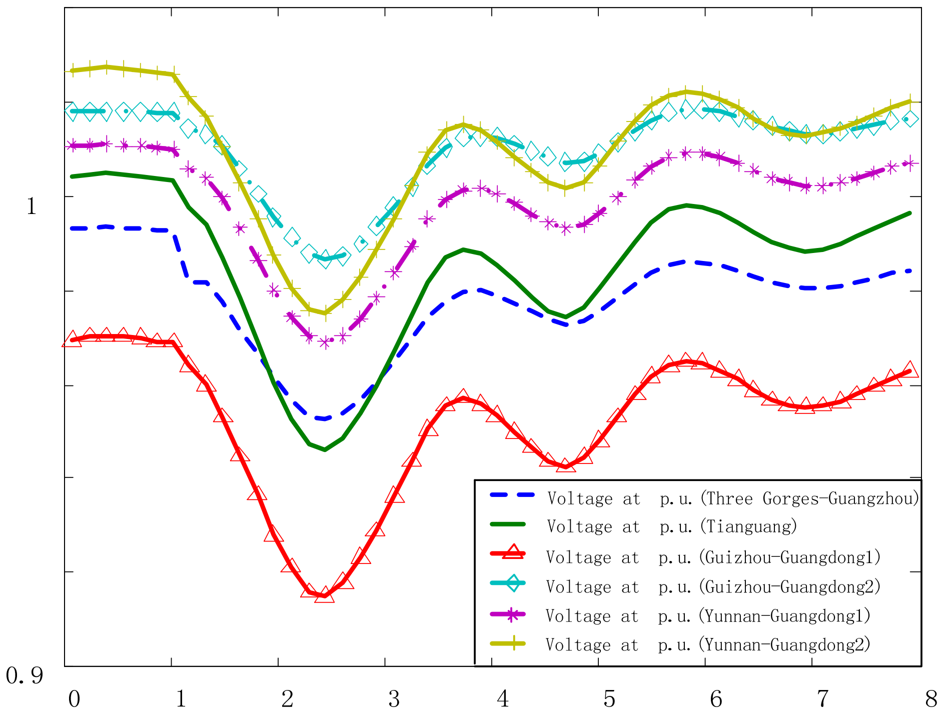

Fig. 3.18a Voltages in the context of bipolar block in Three Gorges-Guangzhou HVDC system (70% static loads + 30% induction motor loads) (Simulation based on the data provided by CSG)

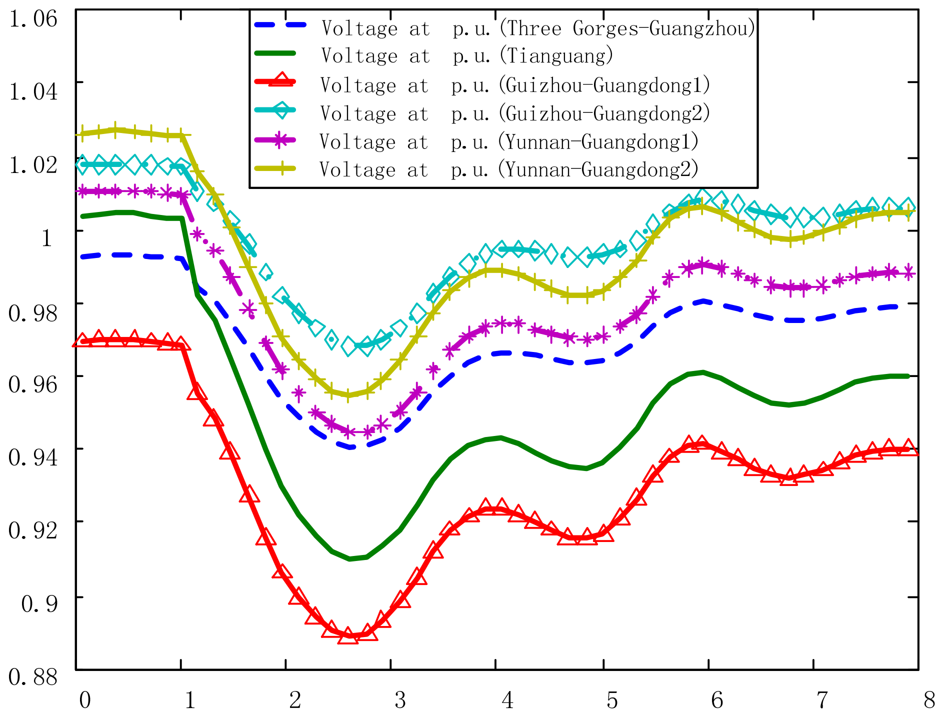

Fig. 3.18b Voltages in the context of bipolar block in Tianshengqiao-Guangzhou HVDC system (70% static loads + 30% induction motor loads) (Simulation based on the data provided by CSG)

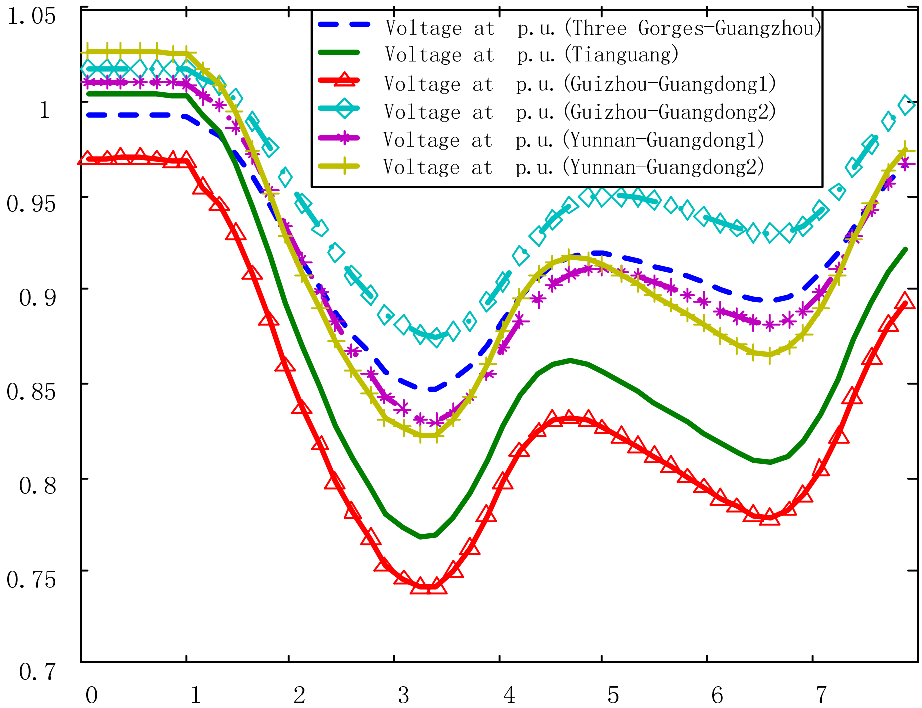

Fig. 3.18c Voltages in the context of bipolar block in Guizhou-Guangzhou HVDC system1 (70% static loads + 30% induction motor loads) (Simulation based on the data provided by CSG)

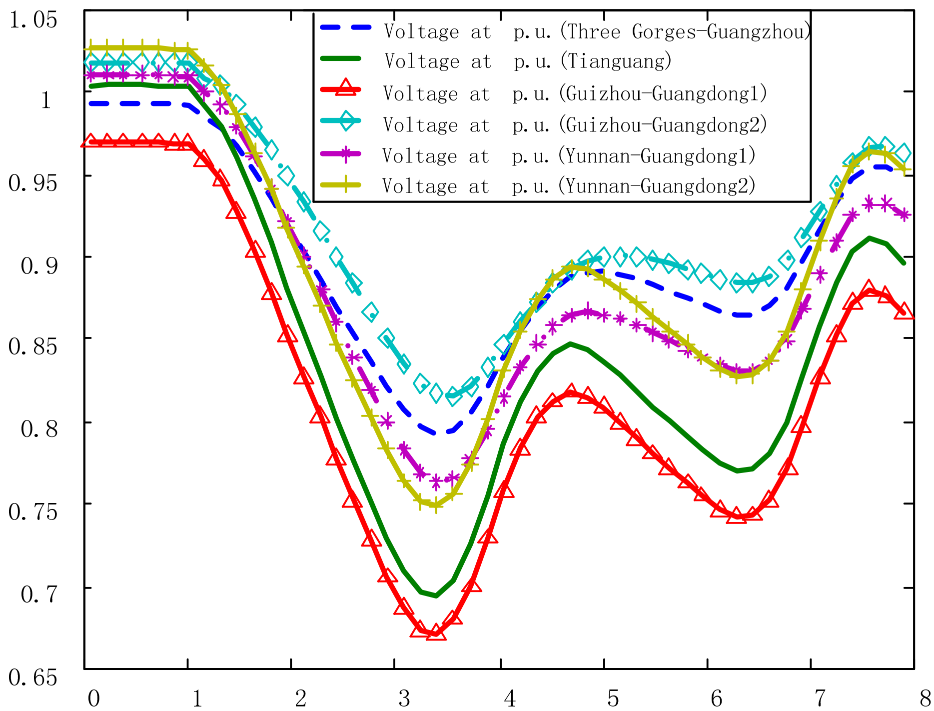

Fig. 3.18d Voltages in the context of bipolar block in Guizhou-Guangzhou HVDC system2 (70% static loads + 30% induction motor loads) (Simulation based on the data provided by CSG)

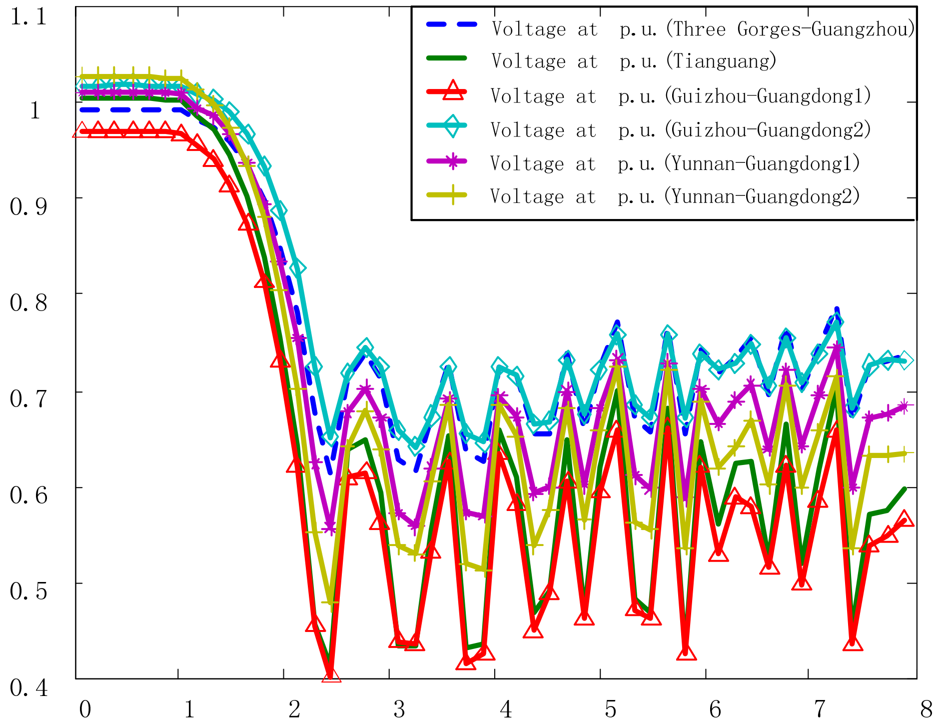

Fig.3.18e Voltages in the context of bipolar block in Yunnan-Guangdong HVDC system1 (70% static loads + 30% induction motor loads) (Simulation based on the data provided by CSG)

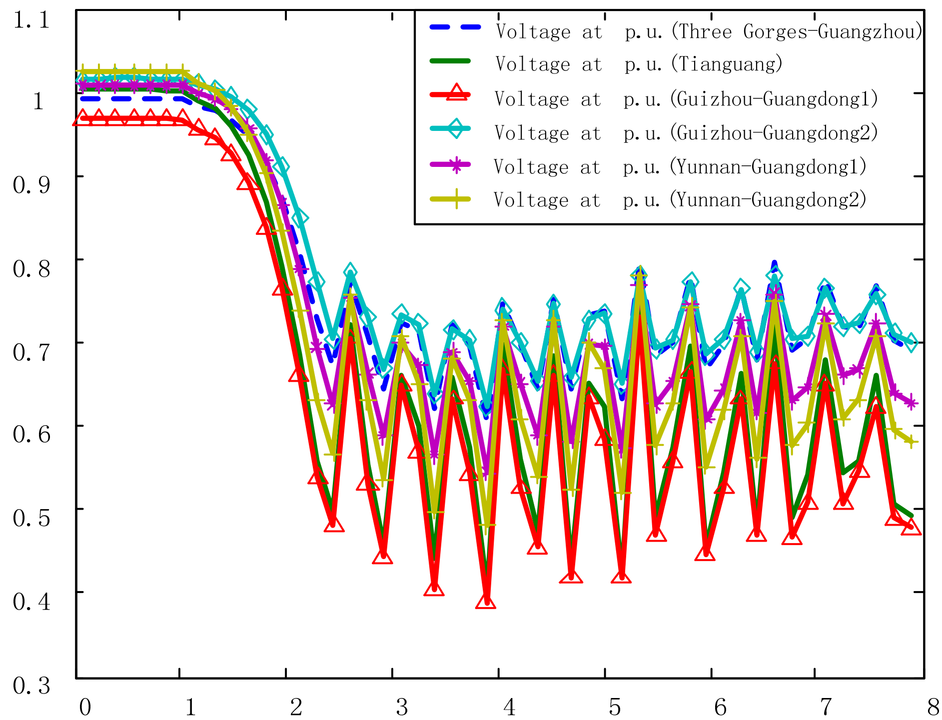

Fig.3.18f Voltages in the context of bipolar block in Yunnan-Guangdong HVDC system2 (70% static loads + 30% induction motor loads) (Simulation based on the data provided by CSG)

In accordance with the stability guidelines, the above results can be tabulated as

follows:

Table 3.6 System stability in the context of 70% static loads + 30% induction motor loads in time of HVDC faults (Simulation based on the data provided by CSG)

faulty lines	Three Gorges - Guangzhou	Tiaoshengqiao - Guangzhou	Guizhou – Guangzhou 1	Guizhou – Guangzhou 2	Yunnan-Guangzhou 1	Yunnan-Guangzhou 2
voltage stability standards	compliant	compliant	compliant	incompliant	incompliant	incompliant
voltage collapse	no	no	no	no	yes	yes

As can be seen from Table 3.6, for the four lines of Three Gorges – Guangzhou, Tiaoshengqiao – Guangzhou, Guizhou – Guangzhou 1 and Guizhou – Guangzhou 2 with a rated capacity below 3000MW, the system voltages will become unstable but will not collapse after the bipolar block occurs. But for the two lines of Yunnan-Guangzhou 1 and Yunnan- Guangzhou 2 with a rated capacity of 5000MW, the system voltages will collapse after the bipolar block occurs.

3.3.3.3 Conclusions

The following conclusions can be drawn:

(1) The larger the capacity of the faulty line is, the greater the impact of the fault on stability is. For the two lines of Yunnan- Guangzhou 1 and Yunnan- Guangzhou 2 with a large rated capacity, the system voltages will not only be unstable but also collapse after the bipolar block occurs.

(2) The load properties have remarkable impact on the system stability. The model of 100% static loads yields the best system voltage stability. When 30% induction motor loads are added, the system voltage is more prone to instability. The explanation is that the initial voltage drops result from the increases of current injections and reactive power requirements in the AC tie lines in normal operation; once the voltages begin to drop, if there are induction motors in the loads, then the reactive power requirements begin to increase instead with the voltage drops. This causes the system to be in need of more reactive power, and the voltages to drop more

rapidly in the default of reactive power compensation, forming a position feedback. But there is no such a problem with the 100% static loads.

(3) In the practical systems, the proportion of induction motor loads is very high, so the fault of large disturbances in the tie lines will lead to serious problems of transient-state voltage stability. And the systems are in need of a great deal of dynamic reactive power support in time of faults.

(4) The transmission power of the power transmission lines is related to the angles, voltages at the sending end and the receiving end, and the reactance of the power transmission lines. When the double circuits are tripped by fault in time of three-phase fault in one loop of the "Transmission of Power from the West to the East" channels, the generators in Yunnan and Guizhou will accelerate while the generators in Guangdong Grid will reduce their speeds, and the angles between the generators at the sending end and those at the receiving end will increase, causing the voltages of the buses in the channels to drop, the power transmission capacity of the lines to decrease, and the reactive power transmission of the lines to increase. Meanwhile, when a double-circuit channel is tripped, its transmission capacity will transfer to other lines, causing the transmission power of other lines to increase dramatically. When the transmission power of the lines exceeds their natural power, it will consume a great deal of reactive power to transmit 1MW more active power. So, the dramatic increase of reactive power transmission will result in greater voltage drops of the lines, reduction of power transmission capabilities of the lines, and further enlargement of the system angles.

3.3.4 Analysis of Reactive Power Requirements in Time of Faults

Concrete analysis will be performed below in accordance with conclusion 4 in 3.3.3.3, i.e. when the transmission power of the lines exceeds their natural power, it will consume a great deal of reactive power to transmit 1MW more active power.

3.3.4.1 Simulation Analyses

The AC tie lines comprise four double-circuit circuits, which are Hezhou-Luodong, Wuzhou-Luodong, Maoming-Yangjiang, and Huishui-Hechi. When a double-circuit three-phase short-circuit grounded fault occurs in the Huishui-Hechi AC lines, comparisons of the changes of reactive power absorbed by the drop points at the receiving end of the tie lines from the system before and after the HVDC power increases in Guizhou-Guangzhou HVDC system 1 will be performed below. The simulation results are shown in Fig. 3.19.

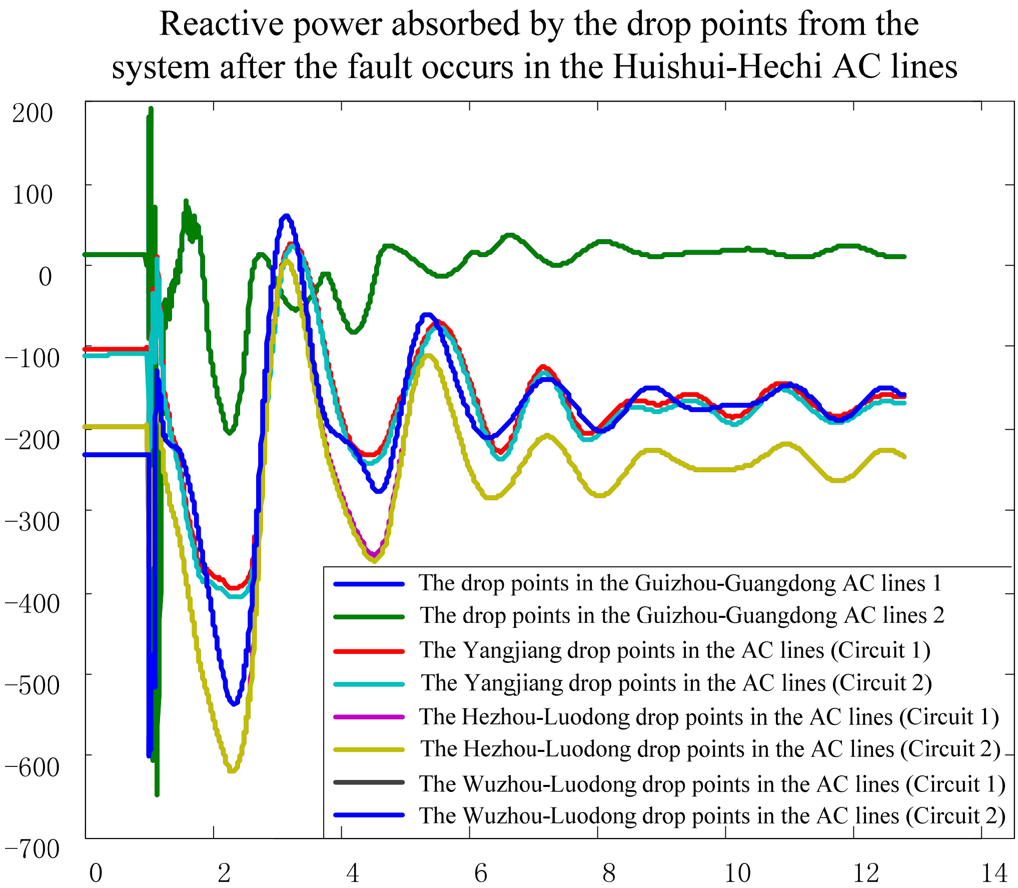

Fig. 3.19 Reactive power absorbed by the drop points from the system after the fault occurs in the Huishui-Hechi AC lines (Simulation based on the data provided by CSG)

The total reactive power requirements before and after the fault occurs in the Huishui-Hechi AC lines are 1054.9Mvar and 1105.5Mvar respectively, with the maximum requirement of reactive power being 3526.7Mvar during the fault.

Table 3.7 Changes of reactive power absorbed by the drop points from the system before and after the fault occurs in the Huishui-Hechi AC lines (Simulation based on the data provided by CSG)

total reactive power requirement of the drop points before the fault	total reactive power requirement of the drop points after the fault becomes stable	maximum reactive power requirement of the drop points during the fault
1054.9Mvar	1105.5Mvar	3526.7Mvar

When a bipolar block fault occurs in the DC lines of the Guizhou-Guangzhou HVDC system 2, comparisons of the changes of reactive power absorbed by the drop points at the receiving end of the tie lines from the system before and after the HVDC power increases in Guizhou-Guangzhou HVDC system 1 will be performed below. The simulation results are shown in Fig. 3.20.

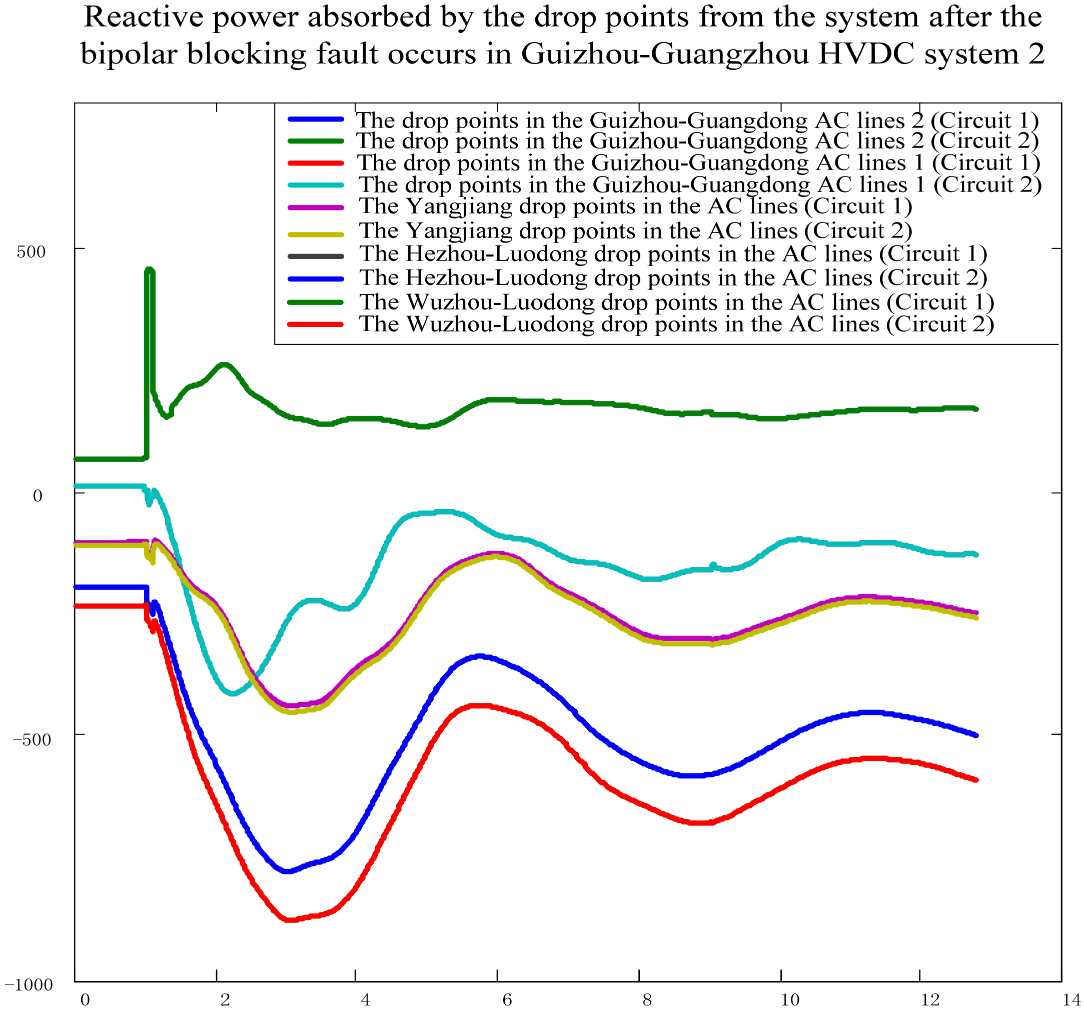

Fig. 3.20 Reactive power absorbed by the drop points from the system after the bipolar block fault occurs in Guizhou-Guangzhou HVDC system 2 (Simulation based on the data provided by CSG)

The total reactive power requirements before and after the fault occurs in the Guizhou-Guangzhou HVDC system 2 are 921.9Mvar and 2610.6Mvar respectively, with the maximum requirement of reactive power being 4400.9Mvar during the fault. And they are tabulated in Table 3.8.

Table 3.8 Changes of reactive power absorbed by the drop points from the system before and after the bipolar block fault occurs in Guizhou-Guangzhou HVDC system 2 (Simulation based on the data provided by CSG)

total reactive power requirement of the drop points before the fault	total reactive power requirement of the drop points after the fault becomes stable	maximum reactive power requirement of the drop points during the fault
921.9Mvar	2610.6Mvar	4400.9Mvar

As can be seen from the above simulation results, after a fault occurs either in the AC lines or in the DC lines, the system need absorb a great amount of dynamic reactive power in the dynamic processes. So, in the systems, especially in the power transmission channels, dynamic reactive power compensators are of great significance in improving the transient-state voltage stability of the AC/DC systems in China Southern Power Grid.

3.3.4.2 Theoretical Calculations

The mechanism of transient-state voltage stability resulted from large disturbance faults is that, under normal operation conditions, active power and reactive power balance at all buses of the system.

When faults (three-phase AC grounding fault, bipolar block fault of DC system) occur in the tie lines, power balance between the sending end and the receiving end will be broken, resulting in the redistribution of flow. In the case that no generators are tripped at the sending end, the current and power will flood into the AC lines that are free from faults. After the flow becomes heavier in the lines in normal operation, the requirements for inductive reactive power will be more than those for capacitive reactive power. Meanwhile, with the dramatic increases of currents injected into the grid at the receiving end, according to $Q = I^2 \bullet X$, the reactive power requirements of the grid at the receiving end will also increase dramatically. With the increases of reactive power requirements in the lines and at the drop points, dynamic reactive power support is required to stabilize the voltages at the drop points.

Calculation of reactive power consumed by the AC lines is as following.

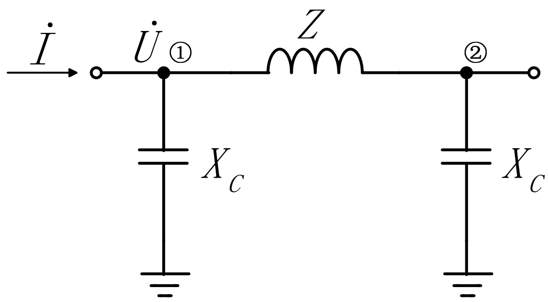

Fig. 3.21 Π-type equivalent circuit of AC lines

Assume the current flowing into the circuit to be $\dot{I}$, and the voltage at bus① to be $\dot{U}$. Then $P + jQ = \dot{U}\dot{I}$.

(1) After flowing through bus①, $P + jQ$ becomes $P + j(Q - \frac{|\dot{U}|^2}{|X_C|})$, where $X_C = \frac{1}{j\omega C}$

(2) The current is $\dot{I}^{'} = \dot{I} + \frac{\dot{U}}{X_C}$, where $X_C = \frac{1}{j\omega C}$

(3) The voltage drop along the power transmission lines is: $\Delta\dot{U} = \dot{I}^{'}Z = (\dot{I} + \frac{\dot{U}}{X_C})Z$, where $Z = R_L + jX_L$.

(4) The reactive power consumed by the lines is: $\Delta Q = \Delta\dot{U}\dot{I}^{*}\sin\varphi$

(5) The reactive power injected into the lines at bus ② is:

$$Q_{\text{in}} = -Q + \frac{|\dot{U}|^2}{|X_C|} - \Delta Q + \frac{|\dot{U} - \Delta\dot{U}|^2}{|X_C|}$$

[Example 1]

R=4.6856Ω

X =70.008Ω

C_b =322.73nF

I' =1173.35∠16.96°A

U =508.61∠18.42°kV

Then,

$$X_C = \frac{1}{j\omega C} = -j \bullet \frac{1}{2\pi fC} = -j \bullet \frac{1}{2\pi \times 50 \times 322.73 \times 10^{-9}} = -j9860.3\Omega$$

$$\frac{U}{X_C} = \frac{508.61\angle 18.42° \times 1000}{-j9860.3} = 51.57\angle 108.42°\text{A}$$

$$I = I' - \frac{U}{X_C} = 1175\angle 14.45°\text{A}$$

$$P + jQ = \sqrt{3}U\hat{I}$$
$$= \sqrt{3}\left[508.61 \times 1175.8\cos\left(18.42° - 14.45°\right) + j508.61 \times 1175.8\sin\left(18.42° - 14.45°\right)\right]$$
$$= \sqrt{3}\left(596.6 + j277.5\right)\text{MVA} = 1033.3 + j71.77\text{MVA}$$

Since the inductive reactive power is consumed in the lines, denote the reactive power as

$$Q = -71.77\text{Mvar}$$

$$\sqrt{3} \bullet \frac{|U|^2}{|X_C|} = 45.43\text{Mvar}$$

$$\Delta U = 82.33\angle 103.13°\text{kV}$$

$$\Delta Q = \sqrt{3} \bullet \Delta U \bullet I' \bullet \sin\varphi = \sqrt{3} \times \left(-96.38\right) = -170\text{Mvar}$$

$$\sqrt{3} \bullet \frac{|U - \Delta U|^2}{|X_C|} = \frac{\sqrt{3} \times 507.68\angle 9.13° \times 10^3}{-j9860.3} = 45.26\text{Mvar}$$

The reactive power consumed in the lines is: -170+45.43+45.26=-79.31Mvar

[Example 2]

Assume that the active power increases by in the AC power transmission lines. Calculate the consumed reactive power.

I' =1561.6∠-128.03°A

U =464.98∠-128.20°kV

Then

$$\frac{U}{X_C}=\frac{464.98\angle-128.20°\times1000}{-j9860.3}=47.2\angle-38.20°\text{A}$$

$$I=I'-\frac{U}{X_C}=1562.2\angle-129.76°\text{A}$$

$$\begin{aligned}P+jQ&=\sqrt{3}U\hat{I}\\&=\sqrt{3}\left[464.98\times1562.2\cos\left(-128.2°+129.76°\right)+j464.98\times1562.2\sin\left(-128.2°+129.76°\right)\right]\\&=1258.1\angle1.56°=1257.67786+j34.52\text{MVA}\end{aligned}$$

Since inductive reactive power is consumed in the lines, denote the reactive power as

$$Q=-34.52\text{Mvar}$$

$$\sqrt{3}\bullet\frac{|U|^2}{|X_C|}=\sqrt{3}\times21.93=37.98\text{Mvar}$$

$$\Delta U=109.57\angle-41.86°\text{kV}$$

$$\Delta Q=\sqrt{3}\bullet\Delta U\bullet I'\bullet\sin\varphi=-295.7\text{Mvar}$$

$$\sqrt{3}\bullet\frac{|U-\Delta U|^2}{|X_C|}=\frac{\sqrt{3}\times470.86\angle-141.63°\times10^3}{-j9860.3}=38.95\text{Mvar}$$

The reactive power consumed in the lines is: -295.7+37.98+38.95=-218.2Mvar

Conclusions:

After the active power increases by ΔP=224.38MW in the AC lines, the consumed reactive power increases from -79.31Mvar to -218.2Mvar, I'=139Mvar, so $\Delta Q\approx0.62\frac{U}{X_C}=\frac{498.9\angle53.34°\times1000}{-j9860.3}=50.6\angle143.34°\text{A}$. This means that, it will consume 0.62Mvar reactive power to transmit 1MW active power in the case of this power increment (ΔP=224.38MW) at this operation point.

[Example 3]

Assume the active power increment to be ΔP=70.3MW in the lines. Calculate the consumed reactive power.

$$I' = 1277.2\angle 52.47°\text{A}$$

$$U = 498.9\angle 53.34°\text{kV}$$

$$\frac{U}{X_C} = \frac{498.9\angle 53.34° \times 1000}{-j9860.3} = 50.6\angle 143.34°\text{A}$$

$$I = I' - \frac{U}{X_C} = 1279\angle 50.2°\text{A}$$

$$\begin{aligned} P + jQ &= \sqrt{3}U\hat{I} \\ &= \sqrt{3}\left[498.9 \times 1279 \times \cos\left(-53.34° - 50.2°\right) + j498.9 \times 1279 \times \sin\left(-53.34° - 50.2°\right)\right] \\ &= 1105.2\angle 3.14° = 1103.6 + j60.5\text{MVA} \end{aligned}$$

As inductive reactive power is consumed in the lines, denote the reactive power as

$$Q = -60.5\text{Mvar}$$

$$\sqrt{3} \bullet \frac{|U|^2}{|X_C|} = \sqrt{3} \times 25.24\text{Mvar} = 43.72\text{Mvar}$$

$$\Delta U = 89.62\angle 138.64°\text{kV}$$

$$\Delta Q = \sqrt{3} \bullet \Delta U \bullet I' \bullet \sin\varphi = -197.8\text{Mvar}$$

$$\sqrt{3} \bullet \frac{|U - \Delta U|^2}{|X_C|} = \frac{\sqrt{3} \times 499.62 \times 10^3}{9860.3} = 43.85\text{Mvar}$$

The reactive power is consumed in the lines is: -197.8+43.72+43.85=-110.23Mvar

Conclusions:

After the active power increases by ΔP=70.3MW in the AC lines, the consumed reactive power increases from -79.31Mvar to -110.23Mvar, ΔQ=30.92Mvar, so $\Delta Q \approx 0.44\Delta P$. This means that, it will consume 0.44Mvar reactive power to transmit each 1MW active power in the case of this power increment (ΔP=70.3MW) at this operation point.

CHAPTER 4 IMPROVING SYSTEM VOLTAGE STABILITY WITH SVC

4.1 Overview of Measures to Improve Voltage Stability

The capability of the power system to provide reactive power and the voltage-reactive power characteristics of the loads are key factors to determine voltage stability, and improving the capability of the power system to provide reactive power and ameliorating the voltage-reactive power characteristics of the loads are the main measures to improve voltage stability. Owing to the losses resulting from the reactive power transmission in the power lines, reactive power of the power system is generally compensated for locally. These measures of reactive power compensation can be regarded either as measures to improve reactive power capability of the system, or as measures to meliorate the voltage-reactive power characteristics of the loads. The present measures to improve the system voltage stability include:

(1) Ameliorating the excitation control systems of generators

If the excitation control systems of generators are ameliorated so that the high-voltage terminal voltage of output transformers of the generators are kept constant, then the reactance X of the lines are reduced equivalently. Thus, the reactive power losses of the transmission system will be reduced, and the capability of the system to provide reactive power and the system voltage stability will be improved.

(2) Compensating the long-distance power transmission lines for reactive power losses

Modern power systems have entered a phase pf large capacity and long-distance transmission, and long-distance AC power transmission lines will consume a great amount of reactive power. If such reactive power losses are reduced, or the long-distance power transmission lines are compensated for reactive power losses at the middle, then the system voltage stability will be improved. The FACTS technologies provide technological support for these measures. The former can be achieved by TCSC, which reduces the total reactance X of the lines and thus reduces the reactive power losses; the latter may be achieved by the SVC, which, when installed at the middle the power transmission lines, can compensate the lines for reactive power losses and improve the system stability.

Such dynamic reactive power compensators as switchable capacitor bank, static var compensator (SVC) or static synchronous compensator (STATCOM) can be installed at the load centers. Dynamic reactive power compensators can ameliorate the reactive power-voltage characteristics of the loads, and thus greatly improve the system voltage stability. By virtue of the high speed of control, the SVC installations can greatly improve the dynamic and transient-state voltage stability of the system.

(3) Reforming the load characteristic

Reforming the load characteristics of the power system, especially the reactive power characteristics of the loads, can effectively improve the voltage stability of the systems. For example, by reforming the motor loads and installing high-voltage VFDs for high-voltage large-capacity asynchronous motors, we can greatly improve the reactive power-voltage characteristics of the asynchronous motors in time of startup, greatly reduce the impact of asynchronous motors on the system voltages when the motors start up, and improve the system voltage stability.

(4) Protection measures

Various protection measures, such as undervoltage release, and undervoltage load shedding.

(5) Regulating functions of HVDC systems

When important power transmission channels are tripped in time of faults, we can consider reducing the increases of the power of AC lines with the overvoltage regulating functions of the DC systems so as to reduce the reactive power losses and improve the system voltage stability.

However, there are costs with the DC power overload. As can be known from the analysis of the voltage-reactive power characteristics of the DC converter stations, when the system voltages drop, if the active power transmitted by the DC system increases, then according to Equation (4.1), the power factor of the converter station will decrease. That is, the converter station will absorb additional reactive power for circulating current losses, and this is harmful for the system voltage stability.

$$\cos\varphi_i \approx \frac{V_{di}}{V_{doi}} = \frac{\cos\gamma_i + \cos(\gamma_i + u)}{2} = \cos\gamma_i - \frac{R_{ci} I_d}{V_{doi}} \tag{4.1}$$

Let's take the Tianshengqiao-Guanzhou HVDC system as an example. We can approximately derive the relations between the increase of active power and that of reactive power when the inversion side is overloaded and regulated according to the formula above. Concrete calculation results are tabulated in Table 4.1.

Table 4.1 Proportions of reactive power increases when the HVDC system is overloaded and regulated (Simulation based on the data provided by CSG)

Active power overload	0%	10%	20%	30%	40%	50%
Power factor	0.8650	0.8533	0.8415	0.8298	0.8181	0.8063
Reactive power increase	0%	15.89%	32.79%	50.71%	69.66%	89.66%

The reactive power losses of the HVDC converter stations can be compensated for by the dynamic reactive power compensators installed at the buses near the converter stations.

4.2 Introduction of the SVC

The Static Var Compensator (SVC) is a parallel static reactive power generator or absorber, and its output changes with the specific control parameters of the power system. "Static" means that SVC has no moving or rotating components, different from the synchronous condenser. By regulating the TCR and TSC, the SVC improves the power system performance in various ways. By controlling the reactive power output rapidly, the SVC can regulate the system voltage, improve transient-state stability, increase power transmission capacity, reduce the instantaneous overvoltage, increase the damping of system oscillation and dampen subsynchronous resonance/oscillation. In the HVDC system, the SVC can be used to provide reactive power for the converters, and ameliorate the dynamic regulations of AC power transmission at the converter side, so that the whole installation can output continuously-changing reactive power, the static and the system voltage stability can be improved.

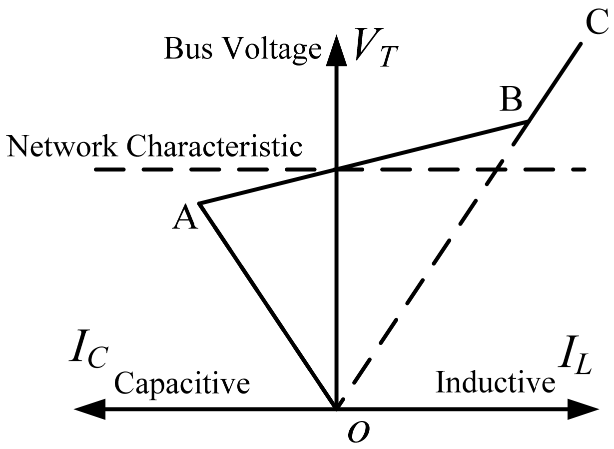

Fig. 4.1 Operation characteristics of typical SVC installation

The typical SVC installation can be denoted by the shunts of fixed capacitors and variable reactors, whose V-I characteristic curve is plotted in Fig. 4.1. In Fig. 4.1, segment OA corresponds to the minimum reactance, where the SVC is equivalent to a fixed capacitor; segment BC corresponds to the maximum reactance, where the SVC is equivalent to a fixed inductor; segment AB corresponds to the adjustable reactance, where the SVC is equivalent to a variable susceptance, with its slope contingent on the control system; point A corresponds to the capacitive reactive power rating of the SVC, and point B corresponds to the inductive reactive power rating of the SVC.

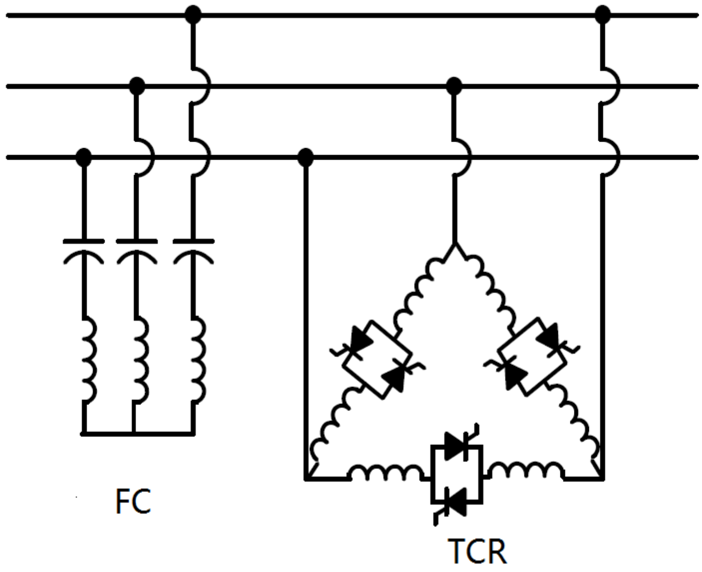

Fig. 4.2 Structure of TCR-based SVC

The principle of the commonly used SVC based on TCR+FC is shown in Fig. 4.2. The operation characteristics of such a compensation installation are dependent on the range of operation voltage and the system voltage at the site of the installation. When the system voltage is lower than the minimum voltage stipulated by the installation, the capacitors will output reactive power to the system, with the reactors absorbing no reactive power; when the system voltage is higher than the minimum voltage stipulated by the installation, the inductors will absorb part of reactive power unbtil the system reaches the voltage stipulated by the installation; when the system exceeds the voltage stipulated by the installation, the inductors will continue to absorb reactive power until the absorption reaches the reactive power rating of the reactors, and this rating determines the highest level of operation voltage of the SVC; when the system voltage exceeds the maximum voltage stipulated by the installation, the capacity of the reactors to absorb reactive power depends on the overload capacity of the compensation installation. Such kind of SVC applies the saturated reactors or silicon-controlled reactors, and has a smooth voltage/current characteristic curve.

4.3 SVC Siting and Reactive Power Checking

As can be seen from stability analyses of the "Transmission of Power from the

West to the East" channels in China Southern Power Grid in accordance with various faults, after faults occur in the channels, the lowest voltages of the system lie in the 500kV buses in Hezhou Substation and Wuzhou Substation during the transient-state processes. And analyses of the mechanism of the harmful faults in the "Transmission of Power from the West to the East" channels in 2008 show that Hezhou Substation and Wuzhou Substation are the oscillation center of the whole China Southern Power Grid, but the two substations are short of reactive power compensation. Any fault in the "Transmission of Power from the West to the East" channels may cause the angle between the sending end and the receiving end to enlarge, and the voltages of Hezhou Substation and Wuzhou Substation to drop., which will lead to the drop of power transmission capabilities of the north channel and middle channel of the "Transmission of Power from the West to the East" project, and further enlarge the angle between the sending end and the receiving end. Calculations and analyses of the stability of the receiving-end grid of 2008 in the context of a single fault show that any one fault in Guangdong Grid may result in the commutation failure of the HVDC system, drop of transmission power, transfer of part of transmitted power from the HVDC system to the AC channels, remarkable increase of reactive power losses in the AC channels, and, furthermore, remarkable voltage drops in Hezhou Substation and Wuzhou Substation during the oscillation processes.

Currently, the power factor within the power supply ranges of Hezhou Substation and Wuzhou Substation is 0.95, meaning that there is much potential to reduce reactive power losses. But careful analyses of the direction of the transmission flow in Wuzhou Substation indicate that the reactive power flows from the low-voltage side to the medium-voltage side, meaning that reactive power is basically balanced at the 220kV voltage level, and slight surplus goes to the 500kV voltage level. The shortage of reactive power compensation in Hezhou Substation and Wuzhou Substation mainly lies in the 500kV side, and improving the power factors in the 220kV grids in Hezhou and Wuzhou will result in overvoltage at the 220kV level without helping much in alleviating the shortage of reactive power compensation in 500kV grids, violating the principle of gradational and regional compensation and local balancing of reactive power. So, capacitor compensator and dynamic reactive power compensators can be installed in Hezhou Substation and Wuzhou Substation to compensate the two substations for their deficiencies of reactive power, and to improve the transient-state stability of China Southern Power Grid.

So, dynamic reactive power compensators can be installed in Hezhou Substation and Wuzhou Substation such that in the case of any one fault in the "Transmission of Power from the West to the East" channels and Guangdong Grid, on one hand, the dynamic reactive power compensators can prevent the voltages from dropping too much in Hezhou Substation and Wuzhou Substation and improve their capabilities of withstanding voltage collapse; on the other hand, the dynamic reactive power compensators can prevent the power angles between the units at the sending ends and those at the receiving ends, and, to some extent, improve the system angle stability.

To sum up, Hezhou Substation and Wuzhou Substation are the oscillation center of China Southern Power Grid, so the 500kV substations in Hezhou and Wuzhou are preliminarily selected as the candidate sites for reactive power compensation in China Southern Power Grid. According to the present mastery, a large power source will be integrated into Hezhou Substation, and is expected to provide strong reactive power support for Hezhou Substation; Changzhou Hydropower Plant near Wuzhou Substation is impeded in output during the flood period, causing Wuzhou Substation to be short of dynamic reactive power. So, comparisons of the two sites of Wuzhou and Hezhou indicate that it is more necessary and imperative to install an SVC installation in Wuzhou Substation.

4.4 Analyses of Reactive Power Balance at Main Stations of "Transmission of Power from the West to the East" Channels

4.4.1 Analyses of Reactive Power Balance of "Transmission of Power from the West to the East" channels

The 500kV power transmission lines have large charging power, and require wide ranges of reactive power in time of active power changes. High-voltage reactors are required to be installed in long-distance 500kV power transmission lines so that power-frequency overvoltage and secondary arc currents in the lines can be reduced. In the maximum operation manner, when the transmitted power along the high-voltage power transmission lines is greater than or equal to the natural power, the charging reactive power in the lines is equal to the reactive power consumed by the lines, the reactive power generated by the high reactance brings about a surplus of inductive reactive power in the 500kV grid, and, more capacitive reactive power is required to be generated for compensation so that reactive power can be balanced.

The relationships between the high-voltage reactors and low-voltage capacitors in the main 500kV substations of the "Transmission of Power from the West to the East" channels of 2008 show that the inductive reactive power generated by the high-voltage reactors is unable to be balanced by the existing low-voltage capacitors in accordance with the programming in most substations, ant there is a deficiency of a certain amount of inductive reactive power in the 500kV grid in the maximum summer operation manner. In 2008, the transmitted power exceeded the natural power of the transmission lines, the charging power of the lines offset the reactive power losses along the lines, and the capacity reactive power resulting from large reactors could not be compensated for by the low-voltage capacitors. As a result, the 500kV grids in multiple 500kV substations were short of capacitive reactive power.

In the maximum summer operation manner, the 500kV grid in Guangxi Grid is short of capacitive reactive power compensation mainly because the inductive reactive power resulting from large reactors cannot be balanced. If more low-voltage capacitors are added to the 35kV buses at the 500kV substations, then overvoltage will occur at the 220kV buses of the 500kV substations. Besides, owing to the limits of transformers, only a limited number of capacitors can be added to the 35kV buses at the 500kV substations, unable to fully balance the inductive reactive power resulting from large reactors. So, there are problems with compensating for the inductive reactive power resulting from large reactors with low-voltage capacitors both in theory and in practice. Theoretically, the most promising approach is to substitute controllable or switchable large reactors for large reactors so that the large reactors can be reduced in capacity or tripped in the maximum summer operation manner, and be increased in capacity or switched on in the minimum operation manner. So, we suggest carrying out special research of optimizing the installation locations large reactors, of checking the power-frequency overvoltage and secondary arc current levels, and of the feasibility of substituting controllable or switchable large reactors for large reactors.

4.4.2 Checking Calculations of Reactive Power Balance near Wuzhou Substation

1. Principles of reactive power balance calculations

The checking calculations of inductive reactive power balance must follow the following principles:

(1) The charging reactive power of the nearby lines must be taken into account when the capacitive reactive power required for balance is determined.

(2) The large reactance and the low reactance inside the substation must be taken into account when the required capacity of inductive reactive power near the substation is determined.

Checking calculations of the capacitive reactive power required for balance must be carried out in maximum operation manner subject to the following principles:

(1) The charging reactive power of the nearby lines and the capacitive reactive power compensation inside the substations must be taken into account when the reactive power sources are determined; the reactive power losses along the nearby lines, the reactive power losses of the transmissions as well as the compensation provided by the large reactors near the substation must be taken into account when the reactive power loads are determined.

(2) The reactive power losses of the lines and the transformers are calculated in accordance with the flow calculation results.

(3) The reactive power provided by the substations for the 220kV grids will not be considered.

In the above calculations of the charging power and reactive power losses along the lines near the substations, half of the total charging power and the total reactive power losses will be considered.

2. Configuration of reactive power compensators in Wuzhou Substation

According to the "Eleventh Five-year" Development Program of Guangxi Grid, as of 2010, the configuration of reactive power compensators in Wuzhou Substation is:

2×150Mvar compensator installed at the Wuzhou side of 500kV Laibin-Wuzhou double-circuit lines: large reactance

3×45Mvar low reactors and 2×60Mvar low capacitors configured at the low-voltage side of transformer #2;

2×60Mvar low reactors and 2×60Mvar low capacitors configured at the low-voltage side of transformer #1;

3. Checking calculations of reactive power balance near Wuzhou Substation

According to the principles of reactive power balance calculations mentioned above, the results of inductive and capacitive reactive power balance near Wuzhou Substation in 2010 are tabulated in Table 4.2 and 4.3.

As can be seen from the balance results, when Wuzhou Substation is extended according to the original program, the configured inductive active power compensators can compensate for the charging power near the substation, and the reactive power is basically balanced; the configured capacitive active power compensators provide a surplus of about 100Mvar in addition to compensating for the reactive power losses near the substation.

Because the SVC installation can generate part of inductive reactive power, the originally programmed 2×60Mvar low reactors and 2×60Mvar low capacitors can be adjusted wherever necessary.

Table 4.2 Results of inductive reactive power balance calculations in Wuzhou Substation in 2010 (Mvar) (Calculation based on the data provided by CSG)

Line name	Line length (km)	Charging power/2 (Mvar)	Capacity of large reactor (Mvar)	Capacity of low reactor (Mvar)	Compensation degree
Wuzhou-Luodong (doubly-circuit)	420	248	—	—	—
Laibin-Wuzhou (doubly-circuit)	476	281	300	—	—
substation	—	—	—	255	—
total	896	529	273	255	100%

Table 4.3 Results of capacitive reactive power balance calculations in Wuzhou Substation in 2010 (Mvar) (Calculation based on the data provided by CSG)

Line name	Line length (km)	Charging power/2 (Mvar)	Capacity of large reactor (Mvar)	Capacity of LV capctitor (Mvar)	Surplus of capacitive reactive power (+: deficit, -: surplus)
Wuzhou-Luodong (doubly-circuit)	210	248	—	—	—
Laibin-Wuzhou (doubly-circuit)	238	281	273	—	—
substation	—	—	—	240	—
total	448	529	273	—	-105

4.5 Simulation of Reactive Power Compensation by SVC in Wuzhou Substation

4.5.1 Conditions of System Studies

(1) Target year of research and operation manner: 2010, maximum load manner during flood period

Simulation software: BPA

(2) Grid for calculation:

The grid optimized and adjusted in the "Eleventh Five-yea" Grid Optimization Research of China Southern Power Grid is taken as the basis, and the preliminary scheme recommended by Research on the Feasibility of Series Compensators Installation and Reactive Power Optimization and Compensation Project in China Southern Power Grid during the "Eleventh Five-year" is also applied, i.e. 50% Guixian series compensation, 40% Liuhe series compensation, 50% Yumao series compensation, 50% Mohong series compensation, and 60% Wenda series compensation.

(3) Means of stability calculations

To analyze the system swings and voltage fluctuations in the cases of a three-phase permanent fault occurring at the Wuzhou side of Laibin-Wuzhou 500kV lines, a unipolar block fault occurring in Yunnan-Guangdong HVDC system, and a three-phase permanent fault occurring at the Heping side of Heping-Chuxiong lines when the SVCs are out of operation and the SVC are in operation with different capacities.

To calculate the impact of different capacities of SVCs in operation on the power transmission capabilities at the limits of "Transmission of the West Power to the East" channels (including the limits of Guangxi-Guangdong HVDC system, of Yunnan-Guangdong system, and of Guizhou-Guangzhou).

(4) SVC operation conditions: the output of the SVC in Wuzhou is zero under

normal operation conditions, and the capacitive output can be adjusted smoothly within the ranges of 0~120Mvar/0~180Mvar/0~210Mvar; the control strategy is to maintain the voltage at the 500kV side of Wuzhou Substation at a certain level.

4.5.2 Results of System Studies and Analyses

Results of system studies and analyses are as following.

(1) Analyses of typical faults near Wuzhou Substation

Fig. 4.3,4.4 and 4.5 show the voltage fluctuations and SVC outputs in the cases of three-phase permanent faults occurring at the Wuzhou side of Laibin-Wuzhou 500kV lines, Fig. 4.6 shows the voltage fluctuations at the 500kV side of Wuzhou Substation when the SVCs are in/out of operation, and Fig. 4.7 shows the swing curves of the maximum relative angles of the units within the system when the SVCs are in/out of operation. Fig 4.3 ～ 4.7 are screen snapshots of the power recorders.

As can be seen from the above figures,

SVC can suppress voltage fluctuations; when the voltage of Wuzhou Substation is at the bottom of the valley, the SVC provide the maximum amount of capacitive reactive power for the system to improve the bus voltage; while when the voltage of Wuzhou Substation is at the peak, the reactive power output of the SVC is at the bottom of the valley.

After faults occur, the SVC can provide emergency support of reactive power such that the voltages restore more rapidly without smaller fluctuations.

The SVC in operation may reduce the swing angles of the units, but its impact on the angle stability is small on the whole.

When faults occur in Laiwu lines, the SVCs of the capacities of 120/180/210Mvar play almost the same roles in suppressing voltage fluctuations, because the required dynamic reactive power support is fairly small (basically smaller than 120Mvar).

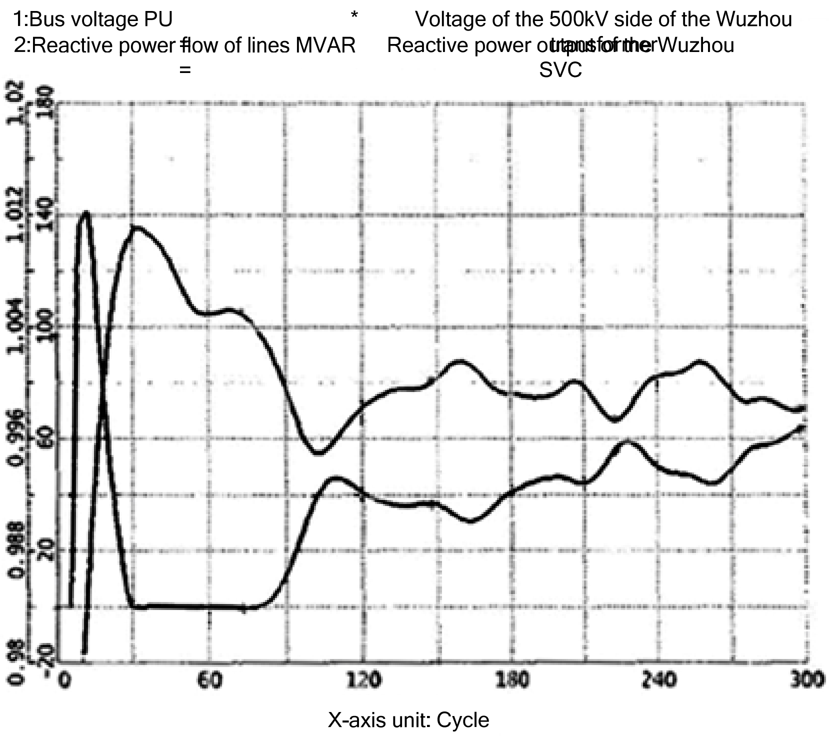

Fig. 4.3 Curves of voltages and reactive power outputs in the case of a three-phase permanent fault at the Wuzhou side of Laiwu lines with an SVC of 120Mar installed in Wuzhou (Simulation based on the data provided by CSG)

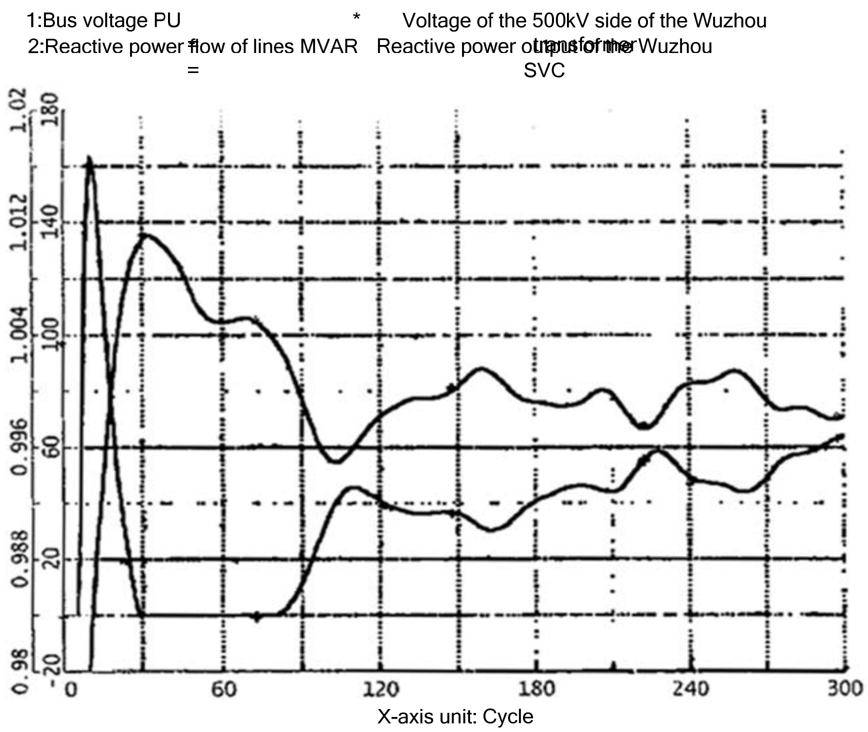

Fig. 4.4 Curves of voltages and reactive power outputs in the case of a three-phase permanent fault at the Wuzhou side of Laiwu lines with an SVC of 180Mar installed in Wuzhou (Simulation based on the data provided by CSG)

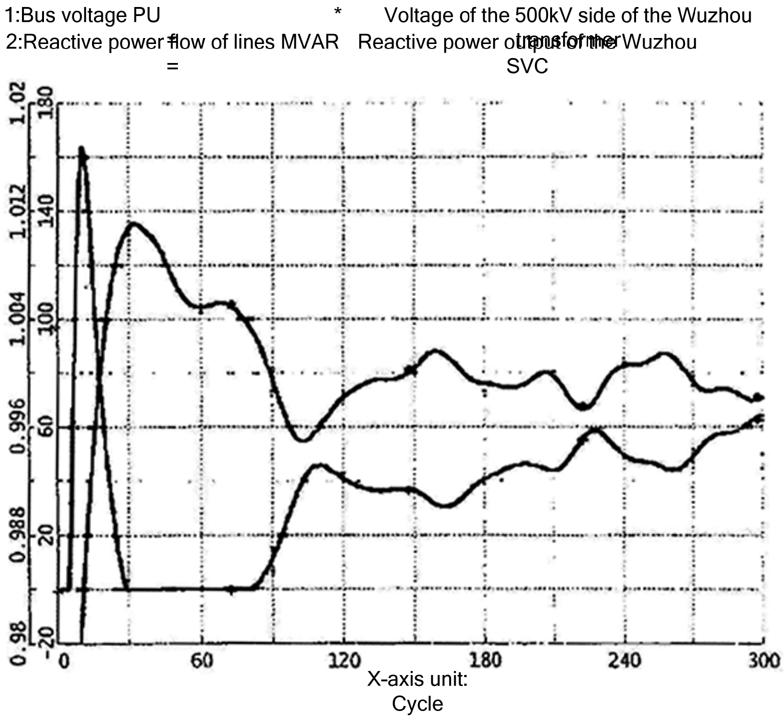

Fig. 4.5 Curves of voltages and reactive power outputs in the case of a three-phase permanent fault at the Wuzhou side of Laiwu lines with an SVC of 210Mar installed in Wuzhou (Simulation based on the data provided by CSG)

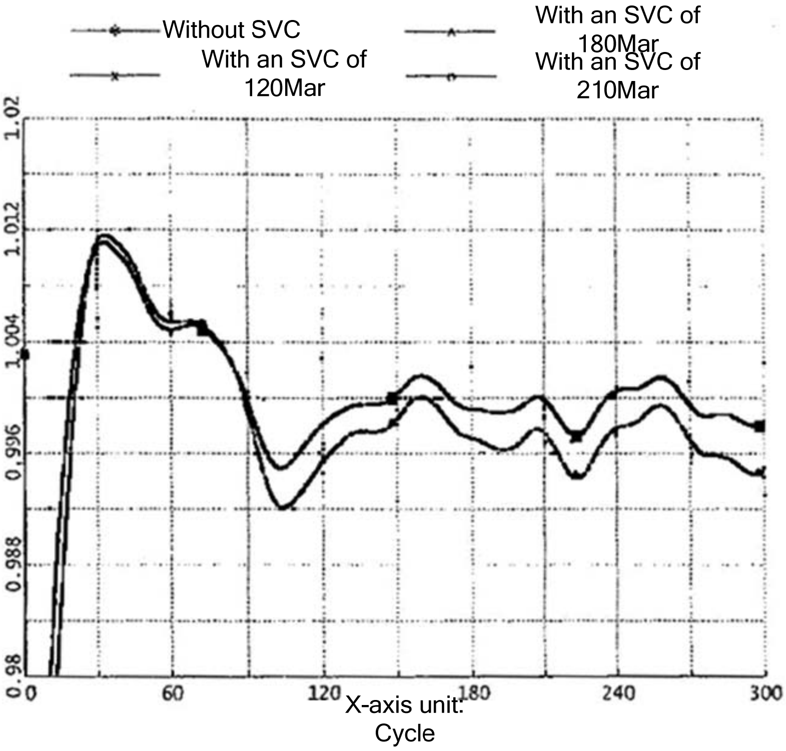

Fig. 4.6 Curves of voltage fluctuations at the 500kV side of Wuzhou in the case of a three-phase permanent fault at the Wuzhou side of Laiwu lines with an SVC of different capacities installed in Wuzhou (Simulation based on the data provided by CSG)

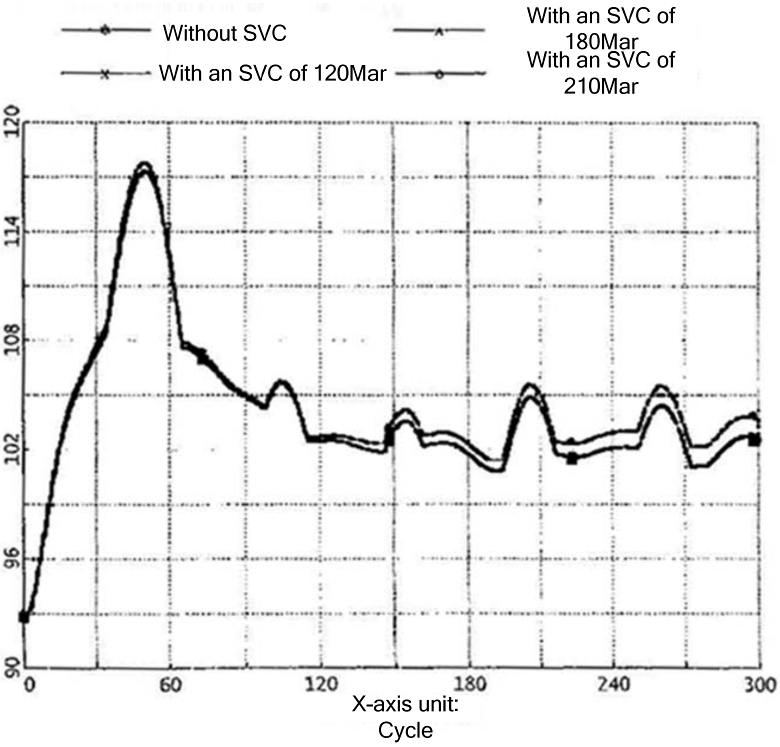

Fig. 4.7 Curves of the maximum relative angle swings of the units in the case of a three-phase permanent fault at the Wuzhou side of Laiwu lines with an SVC of different capacities installed in Wuzhou (Simulation based on the data provided by CSG)

(2) Analyses of unipolar block faults in Yunnan-Guangdong HVDC system

Fig. 4.8, Fig. 4.9 and Fig. 4.10 show the voltage fluctuations and SVC outputs in the cases of a unipolar block fault occurring in Yunnan-Guangdong HVDC system, and Fig. 4.11 shows the voltage fluctuations at the 500kV side of Wuzhou Substation when the SVC is in/out of operation.

As can be seen from comparisons of the above figures,

When a unipolar block fault occurs in Yunnan-Guangdong HVDC system, the voltage of Wuzhou drops fairly much, and cannot recover to the rated voltage level during the post-fault oscillation process; the SVC operates with full output of spare reactive power since the control strategy is to maintain the voltage at the 500kV side of Wuzhou Substation at a certain level.

The emergency support capability of the SVC as a reactive power source can help to accelerate the voltage restoration process of Wuzhou Substation, and the larger the SVC capacity, the faster the voltage restores. The SVC can reduce the magnitude of post-fault voltage drops in 500kV bus by 4 to 6kV, as shown in Fig.4.11.

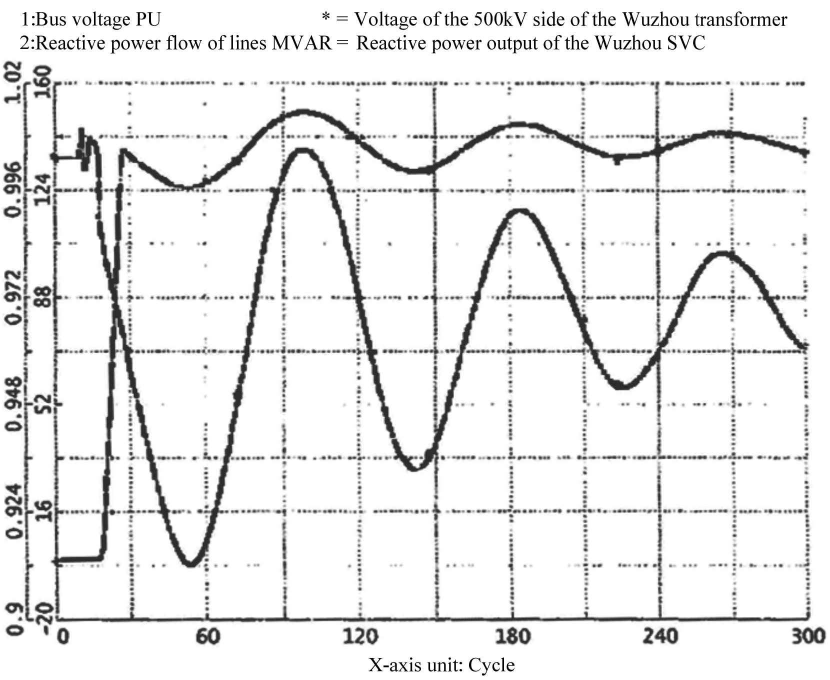

Fig. 4.8 Curves of voltages and reactive power outputs in the case of a unipolar block fault in Yunnan-Guangdong HVDC system with an SVC of 120Mar installed in Wuzhou (Simulation based on the data provided by CSG)

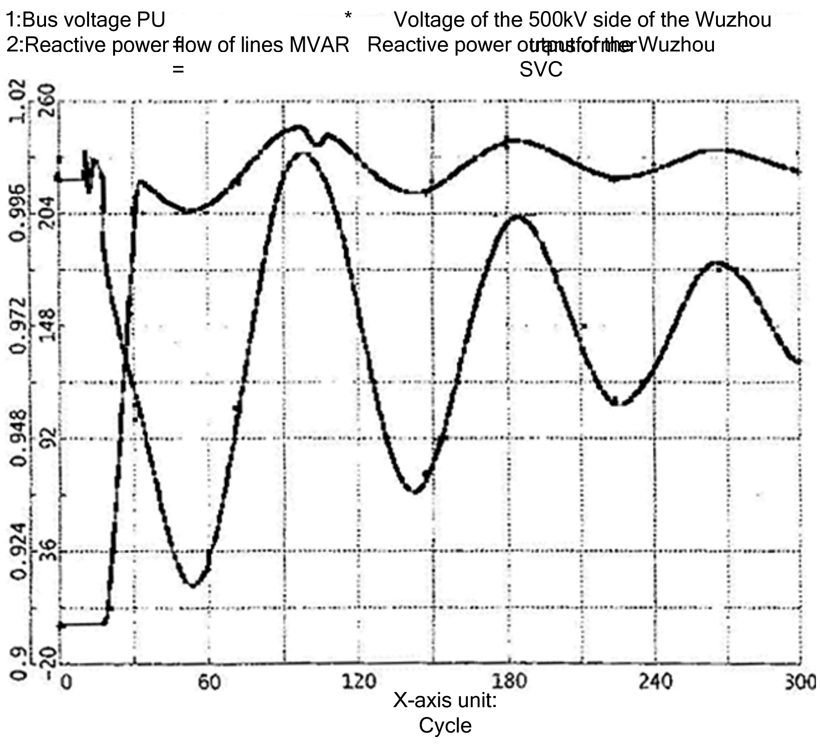

Fig. 4.9 Curves of voltages and reactive power outputs in the case of a unipolar block fault in Yunnan-Guangdong HVDC system with an SVC of 180Mar installed in Wuzhou (Simulation based on the data provided by CSG)

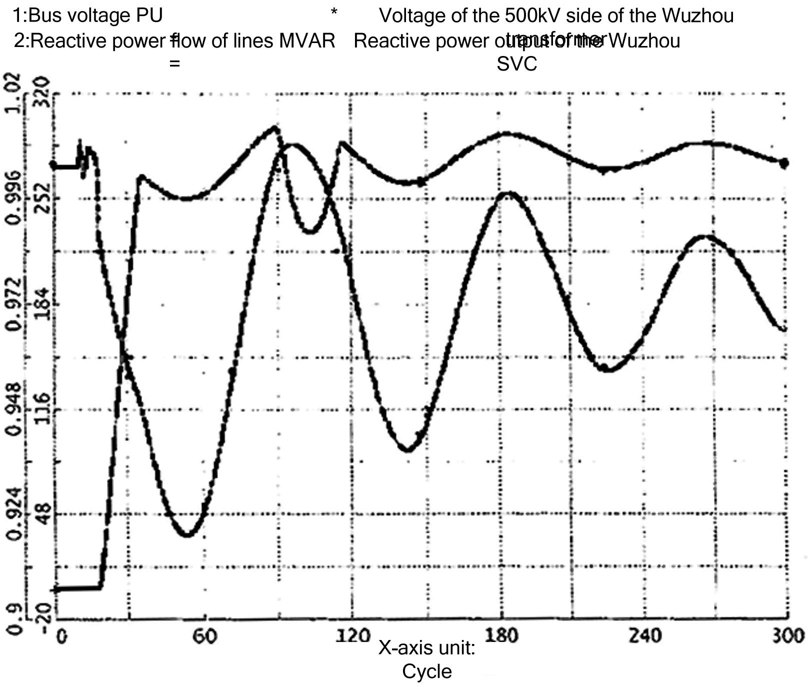

Fig. 4.10 Curves of voltages and reactive power outputs in the case of a unipolar block fault in Yunnan-Guangdong HVDC system with an SVC of 210Mar installed in Wuzhou (Simulation based on the data provided by CSG)

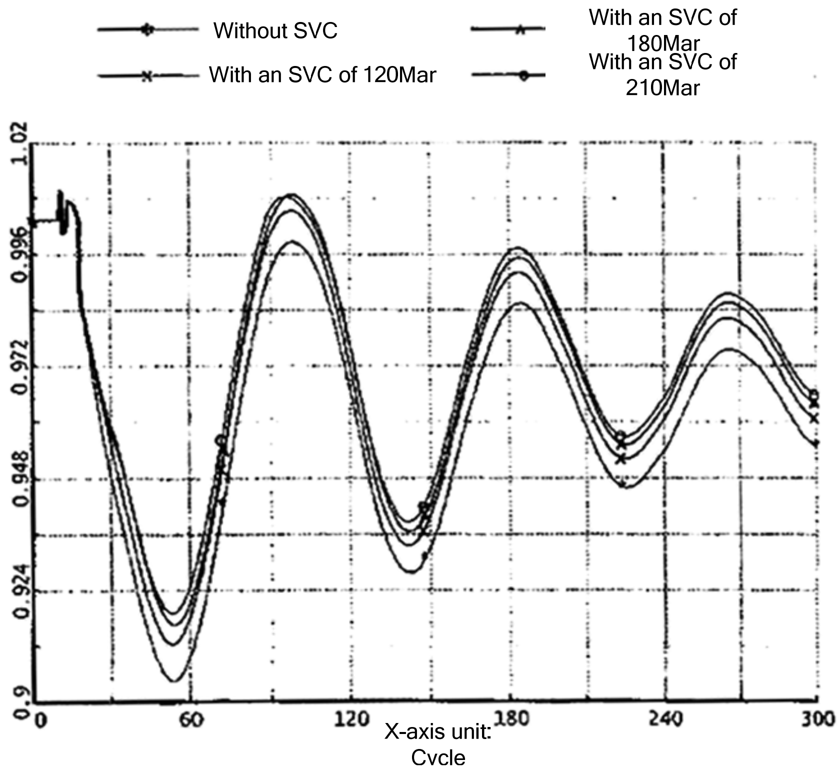

Fig. 4.11 Curves of voltage fluctuations at the 500kV side of Wuzhou in the case of a unipolar block fault in Yunnan-Guangdong HVDC system with an SVC of different capacities installed in Wuzhou (Simulation based on the data provided by CSG)

(3) Analyses of three-phase permanent faults in Heping-Chuxiong lines

Fig.4.12, Fig. 4.13 and Fig. 4.14 show the voltage fluctuations and SVC outputs in the cases of three-phase permanent faults occurring in Heping-Chuxiong lines, and Fig. 4.15 shows the voltage fluctuations at the 500kV side of Wuzhou Substation when the SVC is in/out of operation.

As can be seen from the above figures:

When a three-phase permanent fault occurs in Heping-Chuxiong lines, the flow transferring from the HVDC system to the AC system is fairly large with large fluctuations, bringing about fairly large voltage fluctuations at Wuzhou Substation. And since the control strategy is to maintain the voltage at the 500kV side of Wuzhou Substation at a certain level, the reactive power output of the SVC swings between zero and the maximum value, with zero output in time of high voltage and maximum reactive power output in time of low voltage.

The emergency support capability of the SVC as a reactive power source can help to accelerate the voltage restoration process of Wuzhou Substation, and the larger the SVC capacity, the faster the voltage restores. The SVC can reduce the magnitude of post-fault voltage drops in 500kV bus by 4 to 6kV, as shown in Fig.4.15.

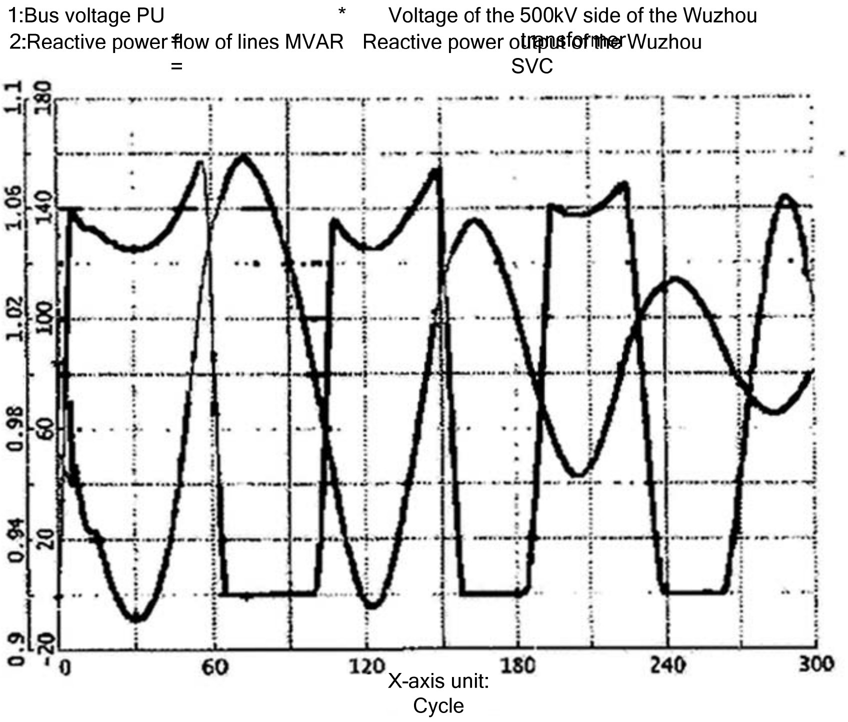

Fig. 4.12 Curves of voltages and reactive power outputs in the case of a three-phase permanent fault in Heping-Chuxiong lines with an SVC of 120Mar installed in Wuzhou (Simulation based on the data provided by CSG)

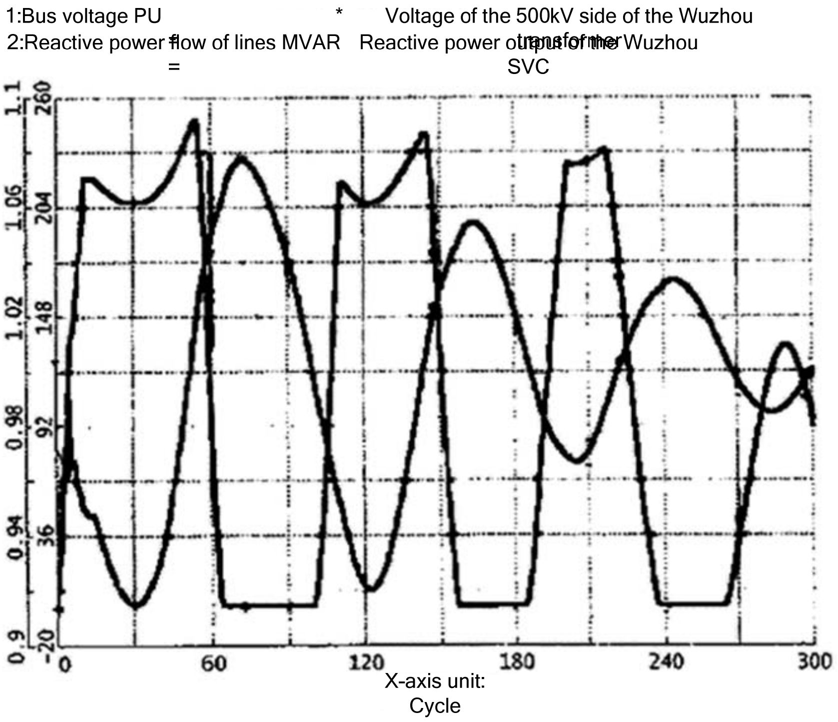

Fig. 4.13 Curves of voltages and reactive power outputs in the case of a three-phase permanent fault in Heping-Chuxiong lines with an SVC of 180Mar installed in Wuzhou (Simulation based on the data provided by CSG)

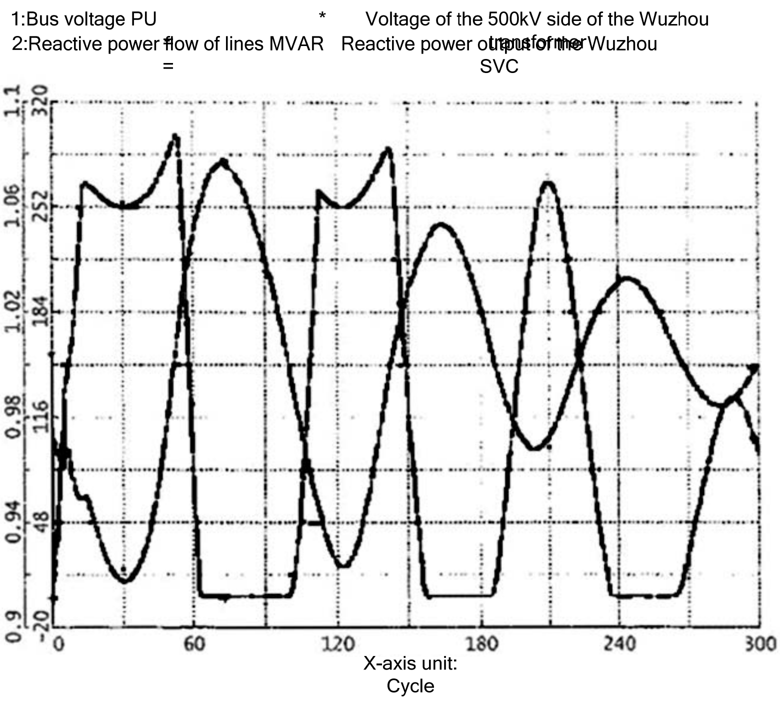

Fig. 4.14 Curves of voltages and reactive power outputs in the case of a three-phase permanent fault in Heping-Chuxiong lines with an SVC of 210Mar installed in Wuzhou (Simulation based on the data provided by CSG)

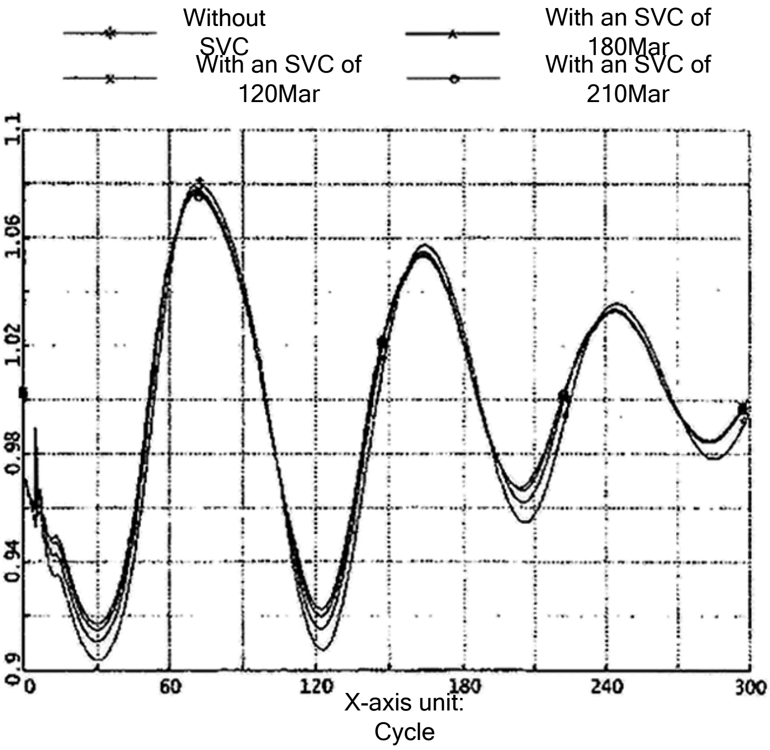

Fig. 4.15 Curves of the voltage fluctuations at the 500kV side of Wuzhou in the case of a three-phase permanent fault in Heping-Chuxiong lines with an SVC of different capacities installed in Wuzhou (Simulation based on the data provided by CSG)

(4) Analysis of power transmission capability improvement

When no SVC or an SVC of 120, 180 or 210Mvar is in operation, checking calculations are performed in accordance with the limits of "Transmission of Power from the West to the East" channels in China Southern Power Grid, and the results are tabulated in Table 4.4.

As the calculation results show, the SVC installed in Wuzhou contributes little to improving the limits of the "Transmission of Power from the West to the East" channels; when an SVC of 120Mvar is installed, the power transmission limits of Guangxi-Guangdong, Yunnan-Guangdong, and Guizhou-Guangzhou HVDC systems are improved by 70, 10 and 10MW respectively; when an SVC of 180Mvar is installed, the power transmission limits of Guangxi-Guangdong, Yunnan-Guangdong, and Guizhou-Guangzhou HVDC systems are improved by 90, 30 and 20MW respectively; when an SVC of 210Mvar is installed, the power transmission limits of Guangxi-Guangdong, Yunnan-Guangdong, and Guizhou-Guangzhou HVDC systems are improved by 100, 30 and 30MW respectively. And the larger the capacity of the SVC installation is, the larger the magnitude of stability level increases is.

Table 4.4 Calculation results of stability limits in 2010 (unit: MW) (Calculation based on the data provided by CSG)

Examinee cross-section	SVC capacity (Mvar)	AC (MW)	HVDC (MW)	Total (MW)	Increment (MW)
Guangxi - Guangdong	N/A	10670	12100	22770	—
	120	10740	12100	22840	70
	180	10760	12100	22860	90
	210	10770	12100	22870	100
Yunnan - Guangzhou	N/A	4410	50000	54410	—
	120	4420	50000	54420	10
	180	4440	50000	54440	30
	210	4440	50000	54440	30
Guizhou - Guangzhou	N/A	4660	6000	10660	—
	120	4670	6000	10670	10
	180	4680	6000	10680	20
	210	4690	6000	10690	30

According to the calculation results of power transmission limits of the "Transmission of Power from the West to the East" channels in China Southern Power Grid, the SVC installation can help to improve the power transmission capabilities to some extent, and the larger the capacity of the SVC installation, the greater the improvement is, but with the increase of the capacity of the SVC installation, the magnitude by which the power transmission capability increases decreases gradually.

To sum up, according to the results of stability calculations in the case of typical faults, of the calculations of limits of the "Transmission of Power from West to East" channels, and of the calculations of reactive power balance near the substations, it is feasible to select the capacity of the SVC installation as 120, 180 or 210Mvar; the larger the capacity of the SVC installation, the stronger the capability of suppressing voltage fluctuations and the more the improvement of power transmission capability. So, the SVC installation of 210Mvar can yield the best results of reactive power compensation.

CHAPTER 5 ADDITIONAL DAMPING CONTROL DESIGN OF SVC

The low frequency oscillation is becoming the major problem of the inter-connection power systems. This problem lowered the transmission limits and the dynamic stability level. In China the problem is even significant as gigas of power electric is transmitted from the West to the East through both HVAC and HVDC lines. Several approaches are studied or applied for solving this problem, including the PSS tuning on the generation side, the HVDC modulation and the FACTs damping controller design on the transmission side [5.1]. SVC as the one of the typical representatives of the FACTs family is installed worldwide. The SVC installation is mainly for the voltage regulation and reactive power compensation. But the SVC additional control function can solve the oscillation problem and improve the small signal stability of the system [5.2].

This chapter proposed a way that selects Prony identification to get the order reduced control system module and uses optimal controller design method for the SVC damping parameter tuning.

We apply the Prony identification to get the reduced order linear description of the power system, and then select the input and output channels to add the SVC to get the closed loop. Thus, by tuning the SVC controller parameters the power system can be controlled and the oscillation can be damped.

5.1 Fundamentals of Low-frequency Oscillation Analysis

5.1.1 Eigenvalue, eigenvector, and solutions of differential equation group

Characteristic equation, characteristic determinant, eigenvector and eigenvalue of matrix are important concepts in linear control theory. First, let's discuss the control quantity in the general form of the state equation of constant linear control system

$$\dot{X} = AX(t) + BU(t) \tag{5.1}$$

When $U = 0$, state equation (5.1) becomes a first-order linear differential equation group with constant coefficients

$$\dot{X} = AX(t) \tag{5.2}$$

Equation (5.2) can be expanded into

$$\begin{bmatrix} \dot{x}_1(t) \\ \dot{x}_2(t) \\ \vdots \\ \dot{x}_n(t) \end{bmatrix} = \begin{bmatrix} a_{11} & a_{12} & .. & a_{1n} \\ a_{21} & a_{22} & .. & a_{2n} \\ .. & .. & .. & .. \\ a_{n1} & a_{n2} & .. & a_{nn} \end{bmatrix} \begin{bmatrix} x_1(t) \\ x_2(t) \\ \vdots \\ x_n(t) \end{bmatrix} \tag{5.3}$$

Assume the solutions of homogeneous differential equation group (5.3) to take the following form:

$$x_1 = c_1 e^{\lambda t}; x_2 = c_2 e^{\lambda t}; \ldots x_n = c_n e^{\lambda t}; \tag{5.4}$$

Substituting Equation (5.4) into Equation (5.3) yields

$$\begin{bmatrix} c_1 \\ c_2 \\ \vdots \\ c_n \end{bmatrix} \lambda e^{\lambda t} = \begin{bmatrix} a_{11} & a_{12} & .. & a_{1n} \\ a_{21} & a_{22} & .. & a_{2n} \\ .. & .. & .. & .. \\ a_{n1} & a_{n2} & .. & a_{nn} \end{bmatrix} \begin{bmatrix} c_1 \\ c_2 \\ \vdots \\ c_n \end{bmatrix} e^{\lambda t} \tag{5.5}$$

Reducing both sides of the equality sign by factor $e^{\lambda t}$, we get the following homogeneous linear algebraic equation group

$$\begin{bmatrix} c_1 \\ c_2 \\ \vdots \\ c_n \end{bmatrix} \lambda = \begin{bmatrix} a_{11} & a_{12} & .. & a_{1n} \\ a_{21} & a_{22} & .. & a_{2n} \\ .. & .. & .. & .. \\ a_{n1} & a_{n2} & .. & a_{nn} \end{bmatrix} \begin{bmatrix} c_1 \\ c_2 \\ \vdots \\ c_n \end{bmatrix} \tag{5.6}$$

i.e.

$$AC = \lambda C \tag{5.7}$$

or

$$\begin{aligned} &(a_{11} - \lambda)c_1 + a_{12}c_2 + \ldots + a_{1n}c_n = 0 \\ &a_{21}c_1 + (a_{22} - \lambda)c_2 + \ldots + a_{2n}c_n = 0 \\ &\ldots\ldots\ldots\ldots\ldots\ldots\ldots\ldots\ldots\ldots\ldots \\ &a_{n1}c_1 + a_{n2}c_2 + \ldots + (a_{nn} - \lambda)c_n = 0 \end{aligned} \tag{5.8}$$

Obviously we will find the non-zero solutions of $c_1, c_2 \ldots c_n$, According to the basic theorems of homogeneous linear equation in Linear Algebra, the adequate and necessary condition that Equation (5.8) has non-zero solutions is that its coefficient determinant

$$D = \begin{vmatrix} a_{11} - \lambda & a_{12} & .. & a_{1n} \\ a_{21} & a_{22} - \lambda & .. & a_{2n} \\ .. & .. & .. & .. \\ a_{n1} & a_{n2} & .. & a_{nn} - \lambda \end{vmatrix} = |A - \lambda I| \tag{5.9}$$

is equal to zero. Thus, we get the n-th-order algebraic equation to find $(-\lambda)^n$

$$|A - \lambda I| = 0 \tag{5.10}$$

where I is the unit matrix.

Equation (5.8) is referred to as the characteristic equation of linear system $\dot{X} = AX$; determinant $|A - \lambda I|$ at the left side of the characteristic equation is referred to as characteristic determinant or characteristic polynomial. Vector C in Equation (5.7) is referred to as eigenvector. Characteristic equation (5.10) is an n-th-order algebraic equation with n roots, which can be expressed by a vector as follows:

$$\Lambda^* = [\lambda_1^* \quad \lambda_2^* \quad \ldots \quad \lambda_n^*]^T$$

Λ^* can be referred to as eigenvalue or eigenvalue vector, where every component

$\lambda_i^*(i=1,2,...,n)$ is referred to as the eigenvalue of the characteristic equation or as the eigenvalue of matrix A.

To sum up, the eigenvector and eigenvalue can be defined as follows.

If a certain dynamics system can be expressed by a first-order constant-coefficient linear homogeneous differential equation group

$$\dot{X} = AX$$

and there exists a non-zero vector

$$C = \begin{bmatrix} c_1 \\ c_2 \\ \vdots \\ c_n \end{bmatrix}$$

and a complex number $AC = \lambda C$ such that

$$AC = \lambda C$$

stands, then λ is the eigenvalue of matrix A; C is referred to as the eigenvector of matrix A corresponding to eigenvalue λ. Determinant $|A - \lambda I| = 0$ is the characteristic equation of state equation $\dot{X} = AX$. So the eigenvalues are also those of the characteristic equation.

As we know, if matrix A is a diagonal matrix, i.e. $A = diag(a_{11}, a_{22}, ..., a_{nn})$, then $a_{11}, a_{22}, ..., a_{nn}$ are the eigenvalues of matrix A. This is because in this case, the characteristic polynomial is

$$|A - \lambda I| = (a_{11} - \lambda)(a_{22} - \lambda)...(a_{nn} - \lambda)$$

So, the eigenvalue $\lambda_i = a_{ii}(i=1,2,...,n)$ 。

According to Equation (5.10), we can find the eigenvector $\Lambda^* = [\lambda_1^* \quad \lambda_2^* \quad ... \quad \lambda_n^*]^T$, and substitute every value of $\lambda = \lambda_i^*$ (totally n) into Equation (5.6). Then we can find a group of eigenvector C_i corresponding to λ_i^*, whose general form is

$$C_i = k\begin{bmatrix} c_{1i}^* \\ c_{2i}^* \\ \vdots \\ c_{ni}^* \end{bmatrix} (i = 1, 2, ..., n)$$

where k is an arbitrary constant, and $\begin{bmatrix} c_{1i}^* & c_{2i}^* & ... & c_{ni}^* \end{bmatrix}^T$ is the basic set of solutions. Thus we get n basic sets of solutions. And we have found eigenvector C. According to Equation (5.3), we obtain the solutions of the differential equation (5.3) as

$$X(t) = \begin{bmatrix} x_1(t) \\ x_2(t) \\ \vdots \\ x_n(t) \end{bmatrix} = k_1\begin{bmatrix} c_{1i}^* \\ c_{2i}^* \\ \vdots \\ c_{ni}^* \end{bmatrix} e^{\lambda_1^* t} + k_2\begin{bmatrix} c_{1i}^* \\ c_{2i}^* \\ \vdots \\ c_{ni}^* \end{bmatrix} e^{\lambda_2^* t} + ... + k_n\begin{bmatrix} c_{1i}^* \\ c_{2i}^* \\ \vdots \\ c_{ni}^* \end{bmatrix} e^{\lambda_n^* t} \tag{5.11}$$

Substituting the boundary conditions, we get n arbitrary constants $k_1, k_2, ..., k_n$.

However, in some cases, especially when mainly studying the stability of the linear control system, we don't necessarily need to find the eigenvector C, rather, we just need to find the eigenvalues C of matrix A, for, once A is determined, the characteristics (stability, dynamic properties, and free oscillation frequency) of the transitional process of the dynamics system in study are roughly determined. As we know, the eigenvalue vector, or the eigenvalue vector Λ^* of matrix A determines the form of the solutions of the corresponding differential equations. For example, the root of the characteristic equation of a second-order system is

$$\Lambda^* = \begin{bmatrix} \lambda_1^* \\ \lambda_2^* \end{bmatrix} = \begin{bmatrix} \alpha + j\beta \\ \alpha - j\beta \end{bmatrix}$$

Then the general solution of the differential equation takes the following form

$$x_1 = A_1 e^{\alpha t} \sin(\beta t + \varphi_1)$$
$$x_2 = A_2 e^{\alpha t} \sin(\beta t + \varphi_2)$$

As can be seen, the real part of eigenvalue λ_i^* determines the attenuation index of the state variables, and the imaginary part determines the free oscillation frequency of the state variables in the transitional process.

To sum up, in the system expressed by the linear constant-coefficient differential equation group

$$\dot{X} = AX(t)$$

the eigenvalues of matrix A determine the behavior of the system in the transitional process.

Now, let's discuss the eigenvalues of the closed-loop linear constant-coefficient control system with feedback of state variables. In this case, the standard form of the state equation of the system is

$$\dot{X}(t) = (A - BK)X(t) \tag{5.12}$$

when Equation (5.12) has turned into the same form as Equation (5.2). Once the gain matrix K in the above equation is found, all the above discussions and descriptions concerning the characteristic equation and eigenvalues of Equation (5.2) will apply to the Equation (5.12) of linear control system feedback of state variables.

The main task of pattern analysis is to find the eigenvalue and eigenvectors of matrix $\mathbf{A}$. As mentioned above, the eigenvalue λ and eigenvector $\mathbf{u}$ of matrix $\mathbf{A}$ meet

$$\mathbf{Au} = \lambda\mathbf{u}, \quad \lambda \in R, \quad \mathbf{u} \in R_n \tag{5.13}$$

where $\mathbf{u}$ is also referred to as the right eigenvector. In the complex region, $\mathbf{A}$ must have n eigenvalues, denoted as $\lambda_1, \lambda_2, \cdots, \lambda_n$, and the corresponding right eigenvector are $\mathbf{u}_1, \mathbf{u}_2, \cdots, \mathbf{u}_n$. Denote $\mathbf{\Lambda} = diag(\lambda_1, \lambda_2, \cdots, \lambda_n)$, and $\mathbf{U} = [\mathbf{u}_1, \mathbf{u}_2, \cdots, \mathbf{u}_n]$. Then we have

$$\mathbf{AU} = \mathbf{U\Lambda} \tag{5.14}$$

Performing transform $\mathbf{X} = \mathbf{UZ}$, and in consideration of Equation (5.13), we can change Equation (5.14) into

$$\dot{\mathbf{Z}} = \mathbf{U}^{-1}\mathbf{AUZ} = \mathbf{\Lambda Z} \tag{5.15}$$

As can be seen from Equation (5.15), the system after transformation is decoupled, and its solution takes a simple form

$$z_i = c_i e^{\lambda_i t} \tag{5.16}$$

where $\mathbf{\Lambda} = diag(\lambda_1, \lambda_2, \cdots, \lambda_n)$ is the initial value of $\mathbf{U} = [\mathbf{u}_1, \mathbf{u}_2, \cdots, \mathbf{u}_n]$. Substituting Equation (5.16) into $\mathbf{X} = \mathbf{UZ}$, we get

$$\begin{aligned}\mathbf{X} &= \begin{bmatrix} x_1 \\ x_2 \\ \vdots \\ x_n \end{bmatrix} = \mathbf{UZ} = \mathbf{u}_1 z_1 + \mathbf{u}_2 z_2 + \cdots + \mathbf{u}_n z_n \\ &= c_1 \begin{bmatrix} u_{11} \\ u_{12} \\ \vdots \\ u_{1n} \end{bmatrix} e^{\lambda_1 t} + c_2 \begin{bmatrix} u_{21} \\ u_{22} \\ \vdots \\ u_{2n} \end{bmatrix} e^{\lambda_2 t} + \cdots + c_n \begin{bmatrix} u_{n1} \\ u_{n2} \\ \vdots \\ u_{nn} \end{bmatrix} e^{\lambda_n t}\end{aligned} \tag{5.17}$$

As can be seen from the above equation, the right eigenvectors $\mathbf{u}_i$ corresponding to eigenvalues λ_i $(i = 1, 2, \cdots, n)$ reflect the relative amplitudes and phases of the observation pattern of state variables x_i $(i = 1, 2, \cdots, n)$. The larger the modulus of $\mathbf{X} = \mathbf{UZ}$, the stronger the relations between x_k and λ_i. So u_{ki} reflects the observability of x_k to λ_i.

The left eigenvector of λ_i is defined as

$$\mathbf{v}_i^T \mathbf{A} = \mathbf{v}_i^T \lambda_i \tag{5.18}$$

Transposing Equation (5.18), we have

$$\mathbf{A}^T \mathbf{v}_i = \lambda_i \mathbf{v}_i \tag{5.19}$$

As can be seen from Equation (5.19), $\mathbf{v}_i$ is the right eigenvector of $\mathbf{A}^T$ corresponding to λ_i. Denote $\mathbf{V} = [\mathbf{v}_1, \mathbf{v}_2, \cdots, \mathbf{v}_n]$, and we have

$$\mathbf{A}^T \mathbf{V} = \mathbf{V\Lambda} \tag{5.20}$$

i.e.

$$\mathbf{V}^{-1} \mathbf{A}^T \mathbf{V} = \mathbf{\Lambda} \tag{5.21}$$

Transposing Equation (5.21) again, we get

$$\mathbf{V}^T \mathbf{A} \mathbf{V}^{-1} = \mathbf{\Lambda} \tag{5.22}$$

Comparing Equation (5.22) with Equation (5.14), and letting $\mathbf{V}^T = \mathbf{U}^{-1}$, we have

$$\mathbf{V}^T \mathbf{U} = \mathbf{I} \tag{5.23}$$

$\mathbf{V}$ 、 $\mathbf{U}$ shown in Equation (5.23) are referred to as the normalized left and right eigenvector matrices.

Considering Equation (5.23), and we can rewrite transform $\mathbf{X} = \mathbf{UZ}$ as

$$\mathbf{Z} = \mathbf{V}^T \mathbf{X} \tag{5.24}$$

The i-th equation in Equation (5.24) is

$$z_i = \mathbf{v}_i^T \mathbf{X} = [v_{1i}, v_{2i}, \cdots, v_{ni}] \bullet \begin{bmatrix} x_1 \\ x_2 \\ \vdots \\ x_n \end{bmatrix} \tag{5.25}$$

As Equation (5.25) shows, if the modulus of v_{ki} is very large, then that means that a slight change of x_k may result in the large change of z_i, and z_i corresponds to λ_i. So v_{ki} reflects the controllability of x_k to λ_i.

5.1.2 Participation Factor, Damping Ratio, Electromechanical Loop Ratio, Sensitivity of Eigenvalue to Parameters

The correlation factor between the k -th state variable with the i -th pattern is

$$p_{ki} = \frac{v_{ki} u_{ki}}{\mathbf{v}_i^T \mathbf{u}_i} \tag{5.26}$$

where v_{ki} and u_{ki} are the k -th row i -th column elements of the left and right eigenvector matrices $\mathbf{V}$ and $\mathbf{U}$. When $\mathbf{V}$ and $\mathbf{U}$ are normalized, the denominator Equation (5.26) is 1.

Since v_{ki} reflects the controllability of x_k to λ_i, and u_{ki} reflects the observability of x_k to λ_i, the correlation factor defined by Equation (5.21) has obvious physical significance. A large correlation factor means the strong observability and controllability of x_k to λ_i, and the correlation factor is of guiding significance for the selection of the installation site of the control equipment to suppress low-frequency oscillation.

Assume the eigenvalues of the linear system at the balance point to be

$$\lambda_i = \sigma_i + j\omega_i\ ,\quad i = 1, 2, \cdots, n \tag{5.27}$$

According to the judging approach to the stability of linear system, when the real parts of all the eigenvalues are less than 0, the balance points of the system are asymptotically stable; if only one eigenvalue has a real part greater than 0, then the system balance point is unstable. The damping ratio corresponding to oscillation frequency ω_i is defined as

$$\xi_i = \frac{-\sigma_i}{\sqrt{\sigma_i^2 + \omega_i^2}} \tag{5.28}$$

As can be seen from the definition of damping ratio, that the real parts of all the eigenvalues are less than 0 is equivalent to that all the damping ratios $\xi_i > 0$ （$i = 1, 2, \cdots, n$）. The damping ration integrates the information of the real and imaginary parts of the eigenvalue, and can reflect the oscillation properties of the system time-domain response. For a practical physical system that can operate stably, the damping ratio is generally required to be greater than a certain value so that a certain stability margin can be ensured. For the power system, the damping ration of the low-frequency oscillation pattern (the oscillation pattern of 0.2~2.5Hz) is generally expected to be no less than 0.1~0.3.

The electromechanical loop correlation ratio ρ_i of eigenvalue λ_i is defined as

$$\rho_i = \left| \frac{\sum\limits_{k \in (\Delta\delta, \Delta\omega)} p_{ki}}{\sum\limits_{k \notin (\Delta\delta, \Delta\omega)} p_{ki}} \right| \tag{5.29}$$

where $k \in (\Delta\omega, \Delta\delta)$ means that p_{ki} is the participation factors of generator angle and angular speed in pattern λ_i, and $k \notin (\Delta\omega, \Delta\delta)$ denotes the participation factors of state variables except generator angle and angular speed in pattern λ_i. The electromechanical loop correlation ratio ρ_i is used to judge whether pattern λ_i is an electromechanical oscillation, and if $\rho_i > 1$, then pattern λ_i is regarded as a low-frequency oscillation one.

To sum up, if pattern λ_i meets the following conditions

$$\begin{cases} \omega_i = 0.2 \sim 2.5Hz \\ \xi_i < 0.3 \\ \rho_i > 1 \end{cases} \tag{5.30}$$

then λ_i is a low-frequency oscillation pattern with insufficient damping.

Assume the system matrix is a function of parameter α, and $\lambda_i, \mathbf{u}_i$ is an eigenvalue-eigenvector pair. Then

$$\mathbf{A}(\alpha)\mathbf{u}_i = \lambda_i \mathbf{u}_i \tag{5.31}$$

Different values of α result in different $\lambda_i, \mathbf{u}_i$, so $\lambda_i, \mathbf{u}_i$ are implicit function of α. Finding the partial derivative of both sides of Equation (5.31) with respect to α, we get

$$\frac{\partial \mathbf{A}(\alpha)}{\partial \alpha}\mathbf{u}_i + \mathbf{A}(\alpha)\frac{\partial \mathbf{u}_i}{\partial \alpha} = \frac{\partial \lambda_i}{\partial \alpha}\mathbf{u}_i + \lambda_i \frac{\partial \mathbf{u}_i}{\partial \alpha} \tag{5.32}$$

Left multiplying both sides of Equation (5.32) by λ_i the transposed left eigenvector $\mathbf{v}_i^T$, and considering $\mathbf{v}_i^T \mathbf{A} = \mathbf{v}_i^T \lambda_i$, we have

$$\frac{\partial \lambda_i}{\partial \alpha} = \frac{\mathbf{v}_i^T \dfrac{\partial \mathbf{A}(\alpha)}{\partial \alpha} \mathbf{u}_i}{\mathbf{v}_i^T \mathbf{u}_i} \tag{5.33}$$

Equation (5.33) yields the sensitivity of eigenvalue λ_i to parameter α.

In the practical application of the power system, the eigenvalues distribution near the imaginary axis is defined as the critical region, as shown in Fig. 5.1.

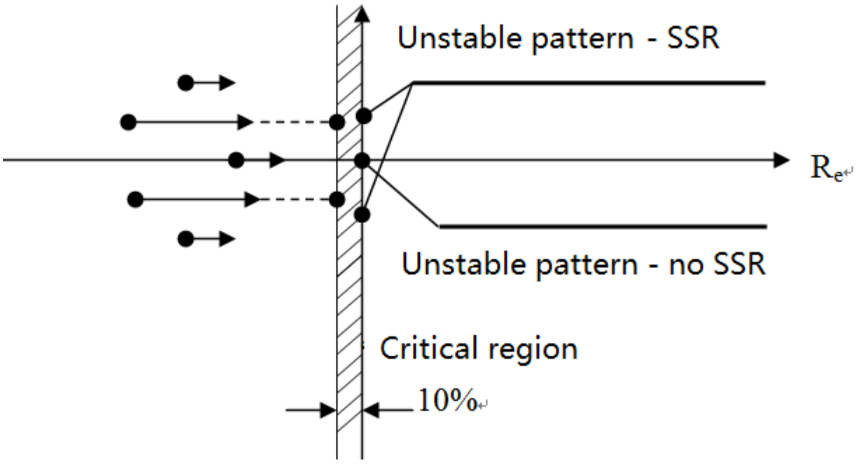

Fig. 5.1 Schematic diagram of critical region

The whole complex plane, according to the different distributions of eigenvalues, is divided into three regions: stable region, weak-damping region and unstable region, which are shown in Fig. 5.2.

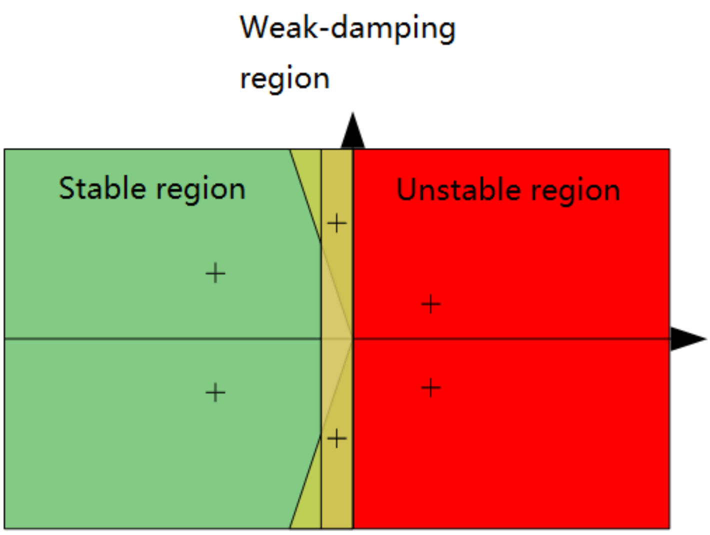

Fig. 5.2 The three regions in the complex plane

5.1.3 Approach of Pattern Analysis

The QR method is effective in finding all the eigenvalues of the matrix, but when the matrix size is large, usually when the number of the order of the matrix exceeds 1000, the QR method no longer applies. For the large matrix, we can only find the characteristic roots and eigenvectors within a certain range with such partial pattern analysis approaches as pattern selection method, power iteration method, inverse power iteration method, Rayliegh quotient iteration method, Newton method Amoldi method, and Jacobi-Davidson method. Even so, all the eigenvalues within a specified range can't ensure to be found exhaustively in theory currently. For the East China Power Grid, if the generator and its controller apply the detailed models, the number of the order of the coefficient matrix of the linearized models is about 2000 to 3000. So, it remains a problem in need of detailed research which algorithm to use to find all the characteristic roots within the low-frequency oscillation (oscillation frequency of 0.2 ~ 2.5Hz, damping ratio less than 0.3) accurately and reliably. The Rice University Parallel Computation Research Center in the US developed a tool for computing the eigenvalues of large-size matrix, which applies the implicit restart Arnoldi method and is open sourced, and is used for the analysis of eigenvalues of large-size matrix by MATLAB.

5.2 Conventional Approaches to Suppressing Power System Oscillations

5.2.1 Approach to Suppressing Low-frequency Oscillations in Accordance with the Negative Damping Theory

As the essence of low-frequency oscillations is the insufficient damping of the relative swings in the generator rotors, on the prerequisite that the generator structures are not changed, an obvious way to suppress low-frequency oscillations is to supplement damping for the generators from outside the generators, including the damping control provided for the generator terminals and that for the power system. As can be seen from Fig. 5.3, this additional damping may come from the self-excitation side at the generator terminal, from the speed-regulating side at the generator terminal, or from such regulators as the FACTS equipment in the power system, for the FACTS equipment also suppresses the low-frequency oscillations through the electromagnetic interactions between the stator and the rotor.

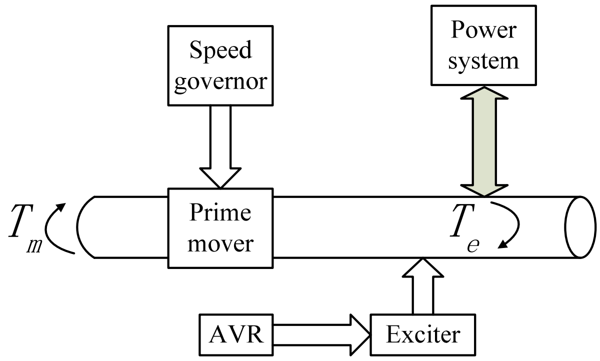

Fig. 5.3 Sources of additional dampings borne by the generator shaftings

As can be seen, in addition to the controlled at the generator terminal, the controller in the grid and such FACTS equipment as SVC, STATCOM and SSSC are also effective ways to suppress all kinds of oscillations. Currently, the costs of the FACTS equipment and of the power electronics components are gradually decreasing, and the enterprises in our country has made continuous progress in the research of this area and has mastered multiple core technologies. All these factors have made it possible to take advantage of the FACTS technologies in a large scale. And the FACTS equipment will be an indispensable part of the grid in the future.

5.2.2 Analysis of the Mechanism of Low-frequency Oscillations with the Negative Damping Theory

The power system mainly comprises the generator and its controller, transformer, switchgear, load and power transmission lines, and is a large-scale nonlinear system. From the perspective of control, there are many inherent oscillation patterns in the power system, and the patterns will be excited under specific conditions. Generally speaking, owing to the existence of various electromagnetic and mechanical dampings, most of the oscillation patterns will be dampened in a short time without causing impact on the stable operation of the power system; but owing to the inherent complexity of the power system, in certain electromechanical patterns, there may be weak damping or negative damping, causing the relative swings of the angles of the respective generators and the continual oscillation of such parameters as the bus voltage and the power along the transmission lines, or even leading to very serious consequences. In the eigenvalue analysis, these patterns are embodied by a negative or positive value with small absolute value and by the eigenvalues strongly correlated to $\Delta\omega$ and $\Delta\delta$.

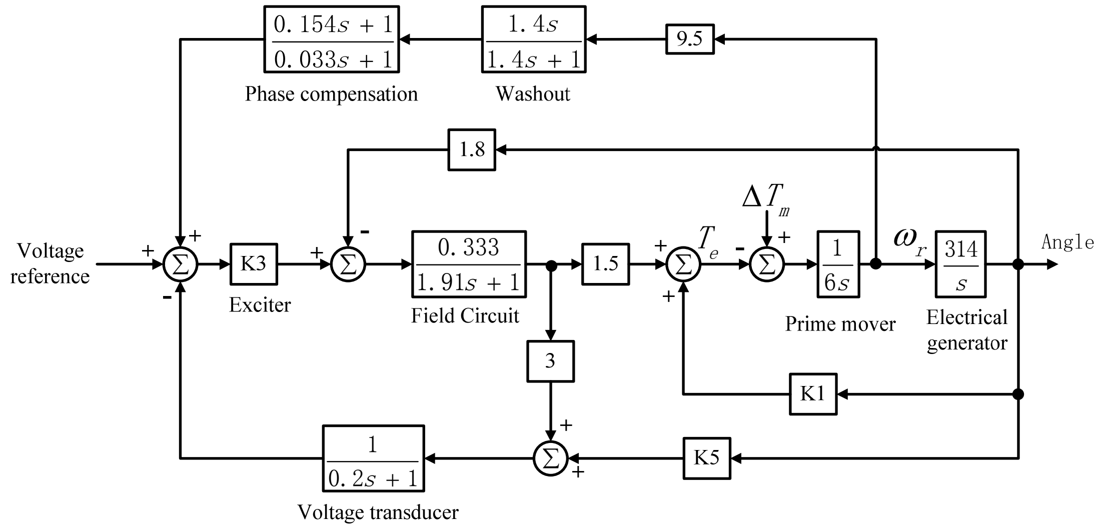

Fig. 5.4 A single-machine infinite system with AVR and PSS

Theoretical analysis shows that, for a generator with modern Automatic Voltage Regulator, even only in the conditions of a single-machine infinite system, when the generator has a high output and a large equivalent reactance of the outside, the excitation system may also provide negative damping for a certain low-frequency pattern (i.e. K5<o in Figure 5.4).

In consideration of the generator under the impact of the excitation system

$$\Delta T_e'' = \frac{-K_5 K_2 K_E}{(1+T_E p)(K_3 + T_{d0}' p) + K_6 K_E}\Delta\delta$$

and $\Delta T_e'' = K_e''\Delta\delta + D_e''\Delta\omega$, we know that, when the system is heavily loaded, K5<0, making the damping of the power system negative.

We may draw the following conclusions:

1) In the case of heavy load, the impact of the excitation system on the transient-state stability and that on the dynamic stability are contradictory.

2) The heavily loaded long-distance interconnected electrical systems are prone to low-frequency oscillations.

In the modern power system, owing to the large number of excitation system and interregional large-capacity power transmissions, the low-frequency oscillations are becoming a main influential factor of the stable operation of the power system. For example, after the nationwide grid interconnection in September 2003, ultralow-frequency oscillation of 0.13Hz and transient unbalanced interregional propagation phenomena emerged in the system, and the amplitudes of power oscillations far exceeded the expected calculation results, resulting in the obvious decrease of dampings all over the interconnected grid.

In the default of effective suppression measures, to avoid the low-frequency oscillations and, especially, the catastrophic faults of nation-side voltage collapse resulting from the global problems, we can only avoid the overload of the long-distance power transmission lines, such that the power for interregional transmission is lower than the designed capability. For example, owing to the insufficient suppression of low-frequency oscillations, the built Northeast-North China tie lines have a power transmission capacity of below 800MW per loop, lower than the natural power of about 1.2GW, which is obviously uneconomic.

Now let's analyze the small-signal stability with respect to the system shown in Fig. 5.5, where the synchronous machine applies the traditional model.

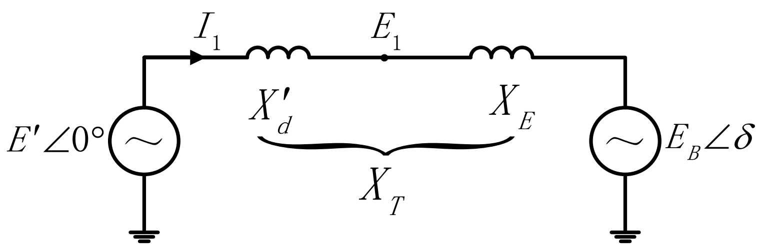

Fig. 5.5 equivalent system for small-signal stability research

Taking $E^{'}$ as the reference vector, we have

$$\tilde{I}_t = \frac{E'\angle 0^o - E'\angle -\delta}{jX_T} = \frac{E' - E_B(\cos\delta - j\sin\delta)}{jX_T} \tag{5.34}$$

$$X_T = x_d + X_E \tag{5.35}$$

$$\tilde{E}' = \tilde{E}_{t0} + jX'_d\tilde{I}_{t0} \tag{5.36}$$

The complex power of the generator is

$$S' = P + jQ = \tilde{E}'\tilde{I}_t^* = \frac{E'E_B \sin\delta}{X_T} + j\frac{E'(E' - E_B\cos\delta)}{X_T} \tag{5.37}$$

The air gap moment is

$$T_e = P = \frac{E'E_B}{X_T}\sin\delta \tag{5.38}$$

When $\delta = \delta_0$, i.e. under the initial conditions, linearization yields

$$\Delta T_e = \frac{\partial T_e}{\partial\delta}\Delta\delta = \frac{E'E_B}{X_T}\cos\delta_0(\Delta\delta) \tag{5.39}$$

The motion equations in the context of the p.u. values are

$$p\Delta\omega_r = \frac{1}{2H}(T_m - T_e - K_D\Delta\omega_r) \tag{5.40}$$

$$p\delta = \omega_0\Delta\omega_r \tag{5.41}$$

Linearizing the above two equations yields

$$p\Delta\omega_r = \frac{1}{2H}(\Delta T_m - K_s\Delta\delta - K_D\Delta\omega_r) \tag{5.42}$$

$$p\Delta\delta = \omega_0\Delta\omega_r \tag{5.43}$$

where

$$K_s = (\frac{E'E_B}{X_T})\cos\delta_0 \tag{5.44}$$

Expressing with the vector matrices yields

$$\frac{d}{dt}\begin{bmatrix}\Delta\omega_r \\ \Delta\delta\end{bmatrix} = \begin{bmatrix}-\frac{K_D}{2H} & -\frac{K_S}{2H} \\ \omega_0 & 0\end{bmatrix}\begin{bmatrix}\Delta\omega_r \\ \Delta\delta\end{bmatrix} + \begin{bmatrix}\frac{1}{2H} \\ 0\end{bmatrix}\Delta T_m \tag{5.45}$$

Simplifying the state equation yields the following transfer function equation:

$$s^2(\Delta\delta) + \frac{K_D}{2H}s(\Delta\delta) + \frac{K_S}{2H}\omega_0(\Delta\delta) = \frac{\omega_0}{2H}\Delta T_m \tag{5.46}$$

The natural frequency is

$$\omega_n = \sqrt{K_S\frac{\omega_0}{2H}} \tag{5.47}$$

The damping ratio:

$$\zeta = \frac{1}{2}\frac{K_D}{2H\omega_n} = \frac{1}{2}\frac{K_D}{\sqrt{K_S 2H\omega_0}} \tag{5.48}$$

The following conclusions can be drawn from the above two equations:

(1) The larger the system size (electrical distance), the lower the oscillation frequency, and the worse the damping;

(2) The larger the inertia of the units in the system (the more the number of the units), the lower the oscillation frequency, and the worse the damping.

On the basis of the foregoing derivations, we can conclude the following characteristics of the system with frequent low-frequency oscillations:

(1) Long-distance heavily loaded power transmission lines;

(2) Application of modern fast, multiple excitation systems with high top values

5.3 Suppressing Low-frequency Oscillations with Additional Damping Control of SVC

The SVC is a typical representative of the FACTS equipment, characterized by mature technology and relatively low cost, and is an effective way of suppressing power system low-frequency oscillations. As is known to all, the SVC, characterized by fast response and multiple control manners, can be used to compensate the power system for dynamic reactive power, to support the voltages, and to improve the system voltage stability [5.4]. In recent year, studies on the additional control of the SVC show that proper design of additional controller can make the SVC suppress the oscillations in addition to improving voltage stability [5.5]. The power system low-frequency oscillations are essentially a small-signal stability problem of the system, and the additional damping control of the SVC can help to improve the small-signal stability problem of the system, to suppress the system low-frequency oscillations, and to improve power transmission limits.

As the installation of the SVC is an effective scheme to suppress the low-frequency oscillations, its control manner is the most important. To achieve different results of control, the SVC has multiple control manners, such as voltage control, reactive power control and constant-admittance control. And these control manners are different in terms of objectives and strategies, and the SVC takes the rotor angle between the generators as the control objective when used to suppress the low-frequency oscillations. But if the above control manners are applied mechanically, then there may be aggravated oscillations under some conditions. Besides, research shows that the pure reactive power compensation will bring about negative damping. So, it is necessary to add additional damping controller in accordance with the low-frequency oscillations.

5.3.1 Principle of Additional Damping Control of the SVC

The SVC can not only provide dynamic voltage support, but also provide damping for the system through additional control [5.6]. The principle is as follows:

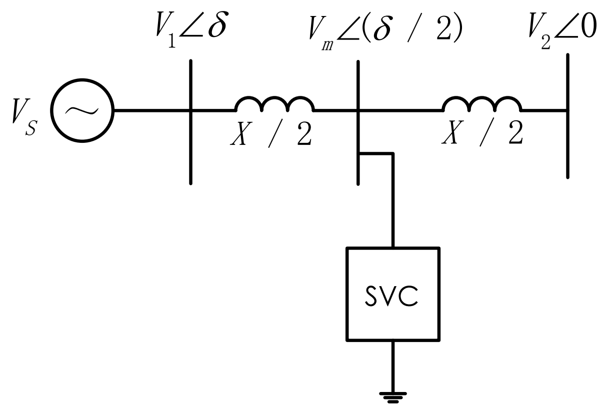

Fig. 5.6 A single-machine infinite system

A single-machine infinite system is shown in Fig. 5.6, where the SVC is installed at the middle of the transmission lines.

The relationships of unit terminal voltage V_1, tail terminal voltage V_2 and the voltage at the middle of the lines V_m are as follows:

$$\begin{cases} V_1 = |V_1|\sin(\omega t + \delta) \\ V_2 = |V_2|\sin\omega t \\ V = |V_1| = |V_2| \\ V_m = |V_m|\sin\left(\omega t + \dfrac{\delta}{2}\right) \end{cases} \tag{5.49}$$

The transmission power is

$$P_E = \frac{V \bullet V_m}{0.5X}\sin\frac{\delta}{2} \tag{5.50}$$

Linearizing Equation (5.50) yields

$$\Delta P_E = \frac{\partial P_E}{\partial V}\Delta V + \frac{\partial P_E}{\partial V_m}\Delta V_m + \frac{\partial P_E}{\partial \delta}\Delta\delta \tag{5.51}$$

$$M\frac{d^2(\Delta\delta)}{dt^2}\Delta V + \frac{\partial P_E}{\partial V_m}\Delta V_m + \frac{\partial P_E}{\partial \delta}\Delta\delta = 0 \tag{5.52}$$

As can be seen, if

$$\Delta V_m = K\frac{d(\Delta\delta)}{dt} \tag{5.53}$$

i.e. if the voltage V_m at the midpoint varies linearly with the power angle deviation $\Delta\delta$, then the SVC plays a role in damping oscillations.

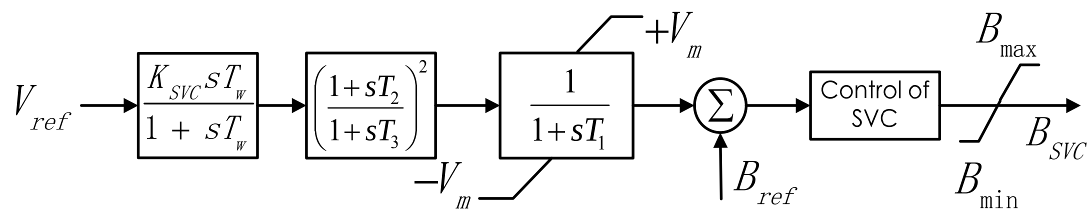

Fig. 5.7 Additional damping control of the SVC

The block diagram of the additional damping control of the SVC is shown in Fig. 5.7. There are four factors included, proportional factor K_{SVC}, wash out factor $\frac{sT_w}{1+sT_w}$, lag factor $\frac{(1+sT_2)^2}{(1+sT_3)^2}$ and mass factor $\frac{1}{1+sT_1}$.

The feedback signals of the additional control are generally the physical quantities reflecting low-frequency oscillations, such as slip, angle difference, and power changes.

5.3.2 Approach to Designing Additional Damping Controller of the SVC Based on Prony System Identification

5.3.2.1 Overview of Power System Identification Methods

At present, the identification method of model linearization, by virtue of its maturity, reliability and facility, is still used the most widely. This identification method has the following advantages:

(1) To a certain extent, the model obtained through identification can reflect the internal structure of the system, and this is especially precious for complicated large systems, for, under such conditions, the system matrices are almost unlikely to be obtained through calculations.

(2) This identification method linearizes the nonlinear system locally, and the obtained model can use some mature analytical approaches and control means for linear models. Its effectiveness has been proved in practice.

(3) In contrast with the dynamic simulation experiments and time-domain simulation experiments of nonlinearized models, the linearized models can greatly accelerate the simulations.

The commonly used identification approaches to analyzing low-frequency oscillations of the power system include Steiglitz-McBride (SM) algorithm, Prony algorithm, Eigensystem Realization Algorithm (i.e. ERA， also referred to as Experimental Module Analysis) and N4SID/PEM (Numerical Algorithms for Subspace State-space System Identification/Prediction Error Method) algorithm. These algorithms are realized in different ways: the SM algorithm performs iterations and adjustments for the coefficients of a transfer function, the Prony algorithm finally obtains the combination of power functions with different weights, the ERA algorithm expands the impulse response identification based on the singular values decomposition of the Hankel matrix to other excitation signals and continuous systems, and the N4SID algorithm is a kind of state model identification method based on subspace, whose results can usually be treated as the initial values of PEM method based on power spectrum estimations.

The results of the Prony algorithm directly include the initial amplitudes and attenuation coefficients of various oscillation patterns, and the Prony algorithm is the most intuitional identification approach to analyzing power system low-frequency oscillations. The improved Prony algorithm further improves the anti-noise performance and spectrum resolution, and has gained preliminary application in the online identification of the power system. Besides, the Prony identification is characterized by a high speed and real-time property.

5.3.2.2 Brief Introduction of Prony Identification

The Prony Algorithm assumes the model of the signals to be a linear combination of a series of exponential functions with arbitrary amplitudes, phase frequencies and damping coefficients. For discrete time series $x(i)\,(i=1,2,\cdots,n)$, we have

$$\hat{x}(n)=\sum_{m=1}^{p} b_m {z_m}^n \tag{5.54}$$

where $b_m = A_m e^{j\theta_m}$, A_m is the amplitude, θ_m is the phase, $z = e^{(\alpha_m + j2\pi f_m)\Delta t}$, α_m is the damping coefficient, f_m is the corresponding oscillation frequency, Δt is the sampling interval, and p is the order of the model. It is a kind of identification approach in accordance with sampling data of equal intervals. The basic procedure of the algorithm is:

(1) Evaluating the liner prediction model (LPM) shown by Equation (5.55) to find parameter α_m, where $m=1-p$;

$$x(p+k)=a_1 x(p+k-1)+\cdots+a_p x(k) \tag{5.55}$$

(2) Evaluating the polynomial of Equation (5.56) constructed by the LPM parameters to find root z_m

$$1+a_1 z^{-1}+\cdots+a_p z^{-p}=0 \tag{5.56}$$

(3) Simplifying model (5.54) into a linear equation group with respect to

parameter b_m with the z_m found in step 2. We can find such parameters as amplitude, phase frequency and damping coefficient according to the definitions of Prony model parameters.

The Prony Algorithm is characterized by high-frequency resolutions for the model parameters include the oscillation frequency, attenuation coefficient, and the information of the amplitude and phase of the pattern. Meanwhile, the system low-frequency oscillations usually take the form of the linear combination of multiple oscillation patterns with different frequencies, different attenuation coefficients and different phases, which tallies with the model of Prony signals. So, the Prony identification is suitable for the analysis of low-frequency oscillations.

As can be seen from the above analyses, the analyses of low-frequency oscillations require the signals including the order-reduced model of its dominant low-frequency pattern and parameter identification results.

5.3.2.3 Principle of Design of SVC Damping Controller Based on System Identification

Prony method is a fast system identification method, it directly gives the initial amplitudes and attenuation coefficients of the oscillation modes, based on the damping controllers design using nonlinear constrained optimization [5.3].

The principle of the design of SVC damping controller based on system identification is shown in Fig. 5.8.

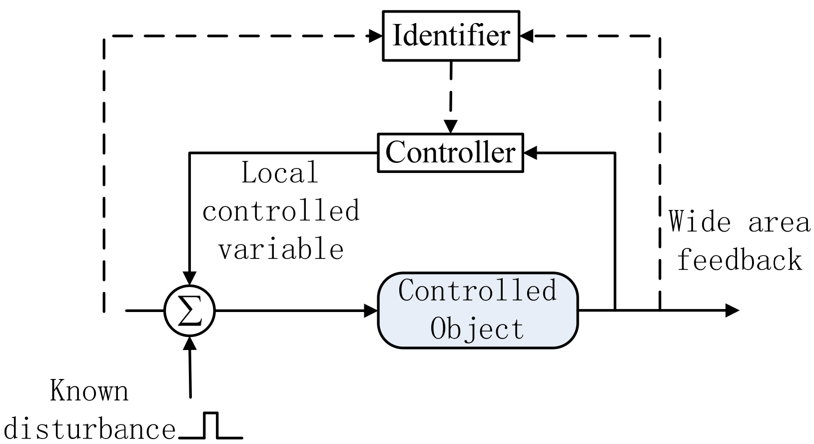

Fig. 5.8 Principle of the design of SVC damping controller based on system identification

Now, we will obtain the model of the controlled system through identification, and design the controller parameters according to this model. After the controller parameters are designed, the system will form a closed-loop system constructed by the additional damping control of the SVC.

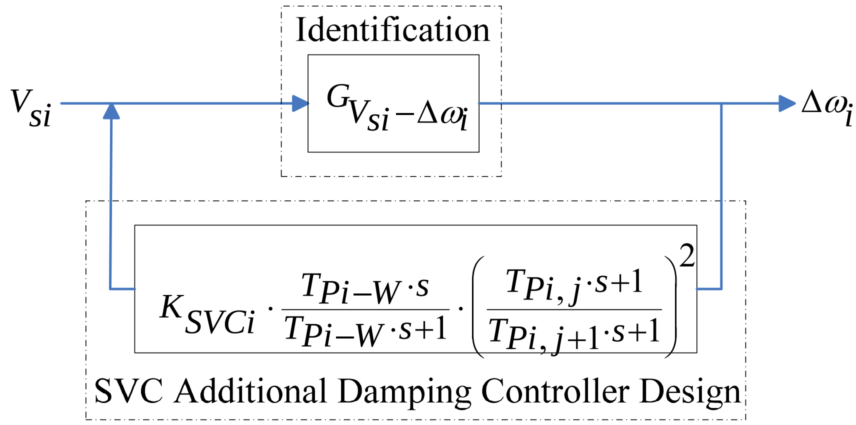

Fig. 5.9 Transfer function obtained through Prony analysis

5.3.2.4 Obtaining the Transfer Function *G*(s) of the Controlled System according to the Prony Analysis Results

The Prony analysis results (eigenvalue λ_i, residue R_i) are

$$\begin{cases}\lambda_i = \alpha_i + j\beta_i \\ R_i = m_i + jn_i\end{cases} \tag{5.58}$$

Where $R_i, m_i, n_i \in R^{M\times 1}, i = 1,2..., p$

To obtain transfer function G(s), we have

$$G(s)=\sum_{i=1}^{p}\frac{R_i}{s-\lambda_i}=\sum_{i}^{\frac{p}{2}}\frac{2m_i s-(2\alpha_i m_i+2\beta n_i)}{s^2-2\alpha_i s+(\alpha_i^2+\beta_i^2)} \tag{5.59}$$

Prony analysis yields the transfer function G(s) of open-loop controlled system, shown in Fig. 5.10, and the SVC performs closed-loop control with it:

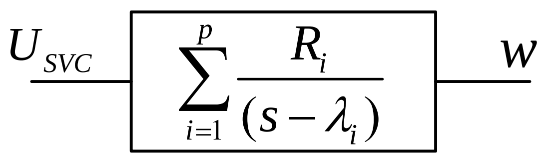

Fig. 5.10 Output of closed-loop SVC control after Prony analysis yields the transfer function

As mentioned, the transfer function of the controlled system $G(s)$ can be got by Prony identification, the input of which is voltage of the SVC(U_{SVC}) and the output of which is the speed deviation of the different generators w. Getting the $G(s)$ SVC controller parameters can be tuned accordingly. If the parameters of U_{SVC}, T_w, T_1, T_2, T_3 are properly tuned, then the SVC design work can be done.

5.3.3 Simulation Platform and Data of SVC Damping Control

(1) Brief Introduction of PSCAD Simulation Software

PSCAD / EMTDC was initially developed by Dennis Woodford in Canada Manitoba Hydroelectric Power Bureau in 1976. After 30 years of development, PSCAD / EMTDC has surmounted EMTP, the prevalent transient simulation program of power system ever, in the ways of models and functions, and become the most advanced software of power system electromagnetic transient simulation worldwide. So far, more than 1000 organizations are using this software.

The basic functions of the PSCAD/EMTDC program are power system electromagnetic transient simulations and calculations, and the typical applications are to forecast the law of how the variables of interest change over time after a certain disturbance occurs, such as a switch operation or a fault. Besides, PSCAD/EMTDC can also be used as a powerful tool for harmonic analysis of the power system, and, meanwhile, for simulation calculations of power electronics area.

PSCAD/EMTDC describes and solves the complete differential equations of power system and its control (including electromagnetic and electromechanical systems). Such simulations tools are different from those to solve for flow. The latter describe the circuits (i.e. electromagnetic process) with steady solutions by solving the dynamic mechanical (i.e. rotating inertia) differential equations.

The measurements of practical systems can be achieved in many ways. The programs to solve for flow are represented by the steady equations, and they can only solve for the amplitudes and phases of fundamental-frequency sections. But the simulation results of PSCAD can display all the states of the power system, and the only limits lie in the time steps that the users themselves choose. Such time steps may range from microseconds to seconds.

(2) The IEEE 30-bus system is selected as the simulation system.

The IEEE 30 Bus Test Case represents a portion of the American Electric Power System (in the Midwestern US) as of December, 1961.

5.3.4 Simulation Results and Analyses

Fault settings: at the instant of 2s, a three-phase grounding fault at bus No.9, duration: 0.3s.

Principle of compensation location consideration: Analysis of the system shows that bus 14 is far from the power sources and is shortage of reactive power compensation. We consider installing the SVC at bus 14, with a compensation capacity of 210Mvar.

The difference of the rotation speeds of machine 3 and machine 4 connecting bus 14 is selected as the feedback signal.

The analyses of results are performed with the result review software of TSAT (Transient Security Assessment Tool), a new tool for transient security evaluations developed jointly by State Grid Nanjing Automation Research Institute and Canada Powertech Company. The powerful calculation capability of TSAT provides fast quantitative solutions for transient security evaluation problems, and TSAT is capable of providing precise and reliable stability evaluations for the systems with fast changing operation conditions.

5.3.4.1 Time Domain Analysis of Additional Damping Control of the SVC

The following Fig. 5.11 shows the time domain damping effect when applying the additional control strategy compared with traditional SVC compensation.

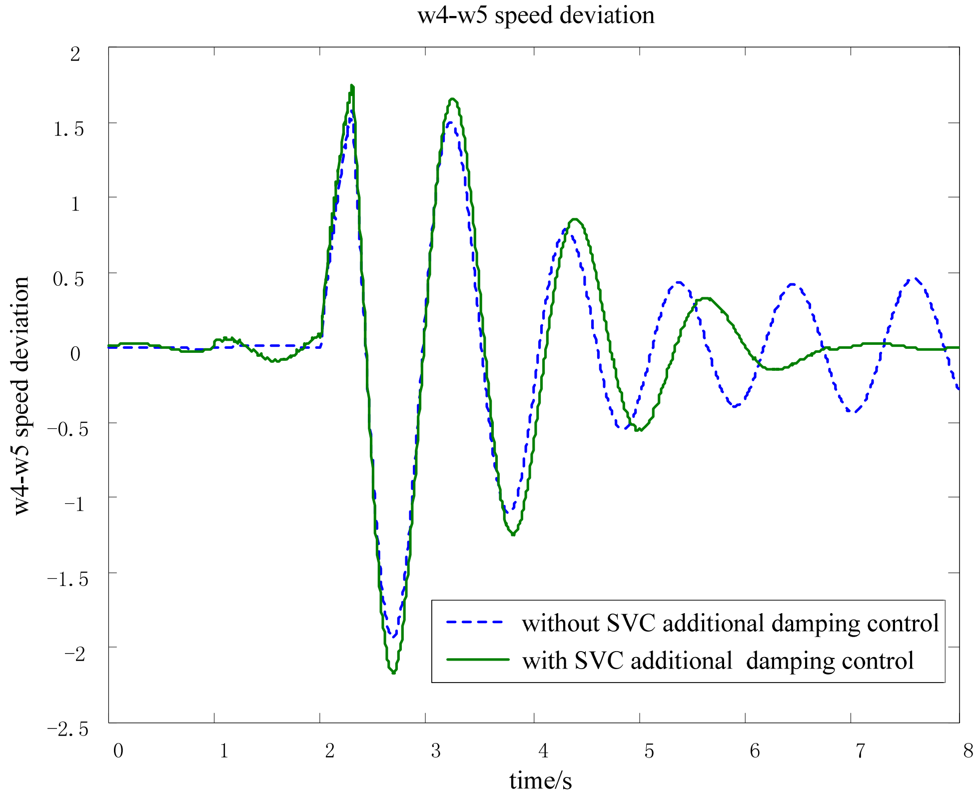

Fig. 5.11 Time domain damping effect comparison

The reactive power output is shown in Fig.5.12. The original signal output of the SVC in voltage regulation mode is the steady component, the value is at around 60Mvar, and the modulation output signal is add upon the steady component.

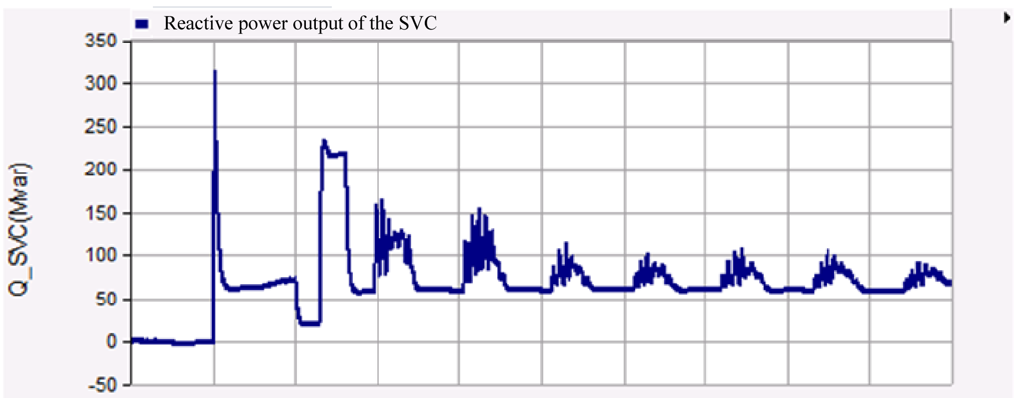

Fig. 5.12 SVC reactive power output.

The line voltage output at the installation node is shown in Fig.5.13. The original signal output of the SVC in voltage regulation mode is the steady component the value is at around 35kV, and the modulation output signal is add upon the steady component.

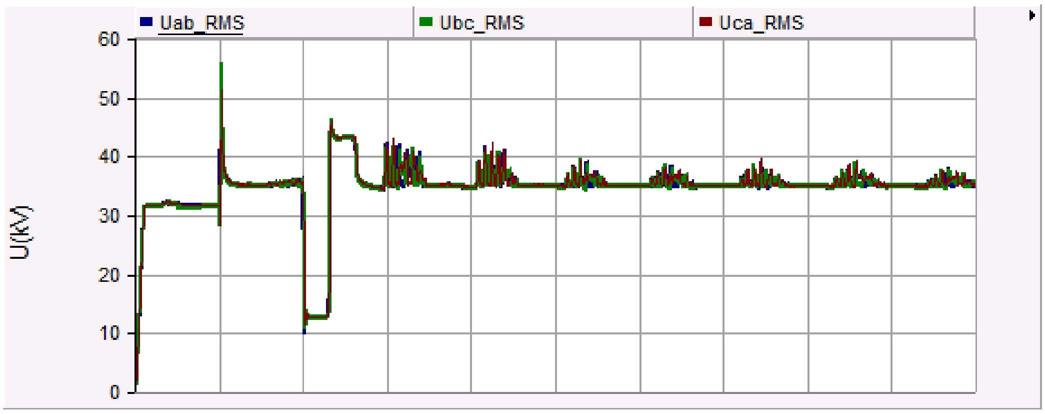

Fig. 5.13 The line voltage output at the installation node

5.3.4.2 Frequency Domain Analysis of Additional Damping Control of the SVC

(1) Main Oscillation Patterns without Damping Control of SVC

TSAT Prony Analysis Results

No	Magnitude	Phase (deg)	Frequency (Hz)	Damping (%)	Real (1/s)	Imaginary (rad/s)
1*	**3.8384**	**86.899**	**0.938**	**4.272**	**-0.2521**	**5.896**
2	1.2642	43.619	1.207	66.974	-6.8371	7.581
3 *	**0.9251**	**94.165**	**1.060**	**6.930**	**-0.4628**	**6.662**
4 *	**0.8527**	**-111.836**	**0.775**	**3.044**	**-0.1484**	**4.873**
5	0.8440	-99.049	1.712	42.144	-4.9989	10.757
6	0.1680	180.000	0.000	100.000	-2.4027	0.000
7	0.0285	13.557	2.722	5.897	-1.0103	17.102
8	0.0236	-25.346	7.619	56.252	-32.5707	47.872
9	0.0141	-57.772	2.443	5.761	-0.8858	15.350
10	0.0101	-30.608	1.853	5.435	-0.6337	11.642
11	0.0015	130.776	3.249	8.215	-1.6826	20.414
12	0.0013	-20.899	3.943	10.912	-2.7196	24.775
13	0.0012	-92.498	19.095	0.804	-0.9649	119.979
14	0.0011	-12.176	5.038	13.223	-4.2226	31.652
15	0.0010	-148.420	19.331	4.957	-6.0284	121.463
16	0.0009	-0.725	22.222	3.007	-4.1998	139.627
17	0.0009	-28.016	28.001	6.655	-11.7348	175.934
18	0.0008	-111.944	7.661	8.174	-3.9478	48.137
19	0.0006	80.231	21.024	0.602	-0.7957	132.096
20	0.0005	-101.823	6.704	7.133	-3.0126	42.125

* It can be seen that patterns 1,3 and 4 have large energy while showing weak dampings, and are the dominant patterns of system low-frequency oscillations.

The parameters and diagrams of the main patterns are shown as follows:

Mode1. Magnitude: 3.8384, Phase: 86.899°, Frequency: 0.938Hz, Damping: 4.272%, λ_1=-0.2521+j5.896

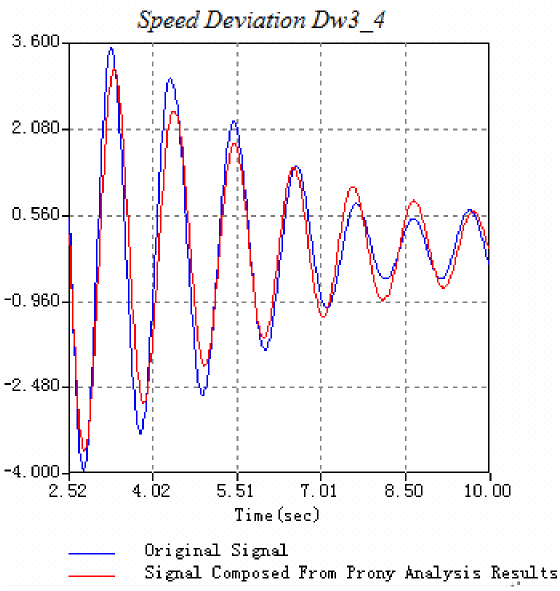

Fig. 5.14 Deviations of rotation speeds of the original signal and Prony analysis

Mode3. Magnitude: 0.9251, Phase: 94.165°, Frequency: 1.060Hz, Damping: 6.930% λ_3=-0.4628+j6.662

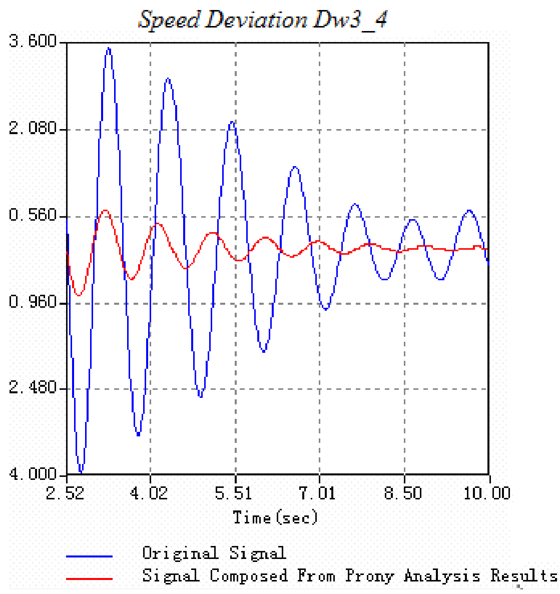

Fig. 5.15 Deviations of rotation speeds of the original signal and Prony analysis
(without SVC, pattern 3)

Mode4.   Magnitude: 0.8527, Phase: 111.836°, Frequency: 0.775Hz, Damping: 3.044%, λ_4 =-0.1484+j4.873

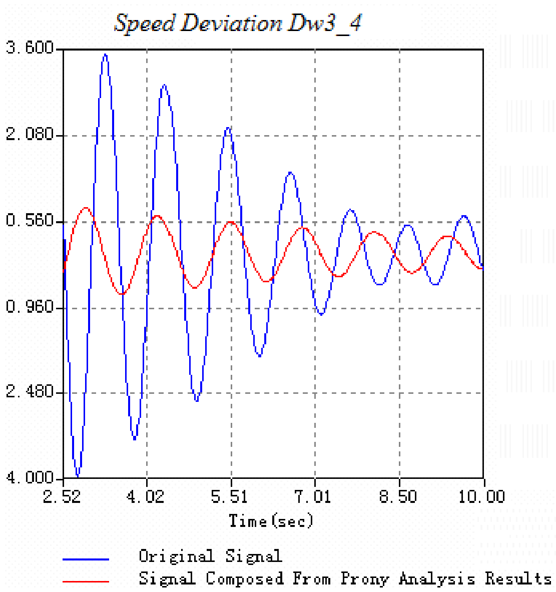

Fig. 5.16 Deviations of rotation speeds of the original signal and Prony analysis (without SVC, pattern 4)

(2) Frequency Domain Analysis with Additional Damping Control of SVC

TSAT Prony Analysis Results

No	Magnitude	Phase (deg)	Frequency (Hz)	Damping (%)	Real (1/s)	Imaginary (rad/s)
1*	**2.2146**	**100.185**	**0.915**	**14.455**	**-0.8403**	**5.752**
2*	**0.6760**	**-177.300**	**0.758**	**5.465**	**-0.2607**	**4.763**
3	0.1068	0.000	0.000	100.000	-4.0789	0.000
4	0.0979	101.042	17.954	18.844	-21.6451	112.808
5*	**0.0938**	**143.160**	**1.654**	**13.012**	**-1.3636**	**10.390**
6	0.0661	-42.629	17.327	5.136	-5.5987	108.871
7	0.0251	179.837	7.696	36.157	-18.7522	48.354
8	0.0098	-124.390	12.848	2.423	-1.9566	80.729
9	0.0088	-135.067	3.278	9.491	-1.9638	20.598
10	0.0076	-135.064	12.169	1.961	-1.4995	76.463
11	0.0073	-162.666	16.165	0.719	-0.7304	101.569
12	0.0072	-83.014	14.255	0.891	-0.7981	89.567
13	0.0067	175.064	15.743	0.592	-0.5858	98.915
14	0.0066	-66.595	2.731	4.394	-0.7547	17.158
15	0.0049	102.870	11.762	2.014	-1.4885	73.900
16	0.0048	-150.920	15.302	0.243	-0.2339	96.146
17	0.0045	175.645	17.279	0.586	-0.6365	108.564
18	0.0045	-154.437	16.568	0.620	-0.6452	104.101

19	0.0038	180.000	24.725	2.527	-3.9274	155.350
20	0.0035	-75.226	2.136	2.929	-0.3934	13.424

The parameters and diagrams of the main patterns are shown as follows:

Mode1. Magnitude: 2.2146, Phase: 100.185°, Frequency: 0.915Hz, Damping: 14.455%, $\lambda_1 = -0.8403 + j5.752$

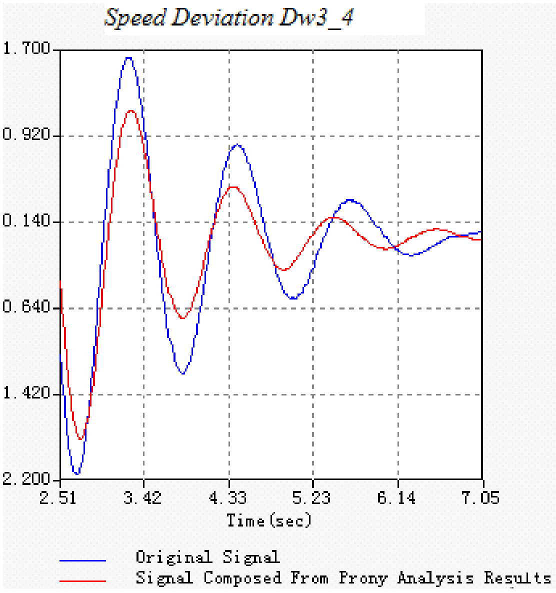

Fig. 5.17 Deviations of rotation speeds of the original signal and Prony analysis (with SVC in operation, pattern 1)

Mode2. Magnitude: 0.6760, Phase: 177.300°, Frequency: 0.758Hz, Damping: 5.465%, $\lambda_2 = -0.2607 + j4.763$

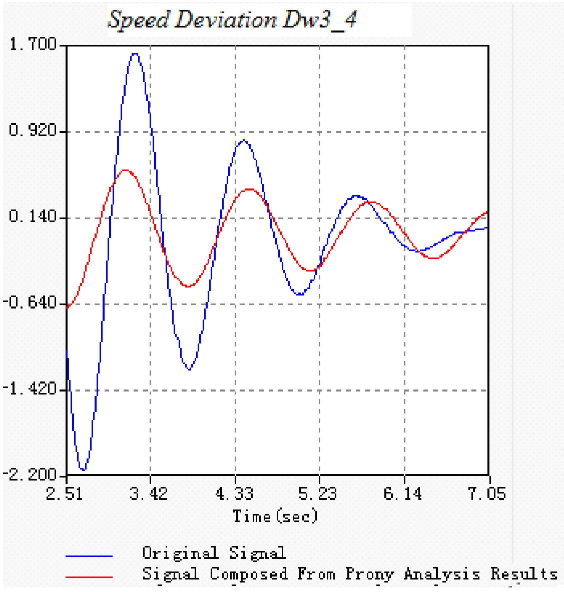

Fig. 5.18 Deviations of rotation speeds of the original signal and Prony analysis (with SVC in operation, pattern 2)

Mode5. Magnitude: 0.0938, Phase: 143.160°, Frequency: 1.654Hz, Damping: 13.012%, λ_5=-1.3636+j10.390

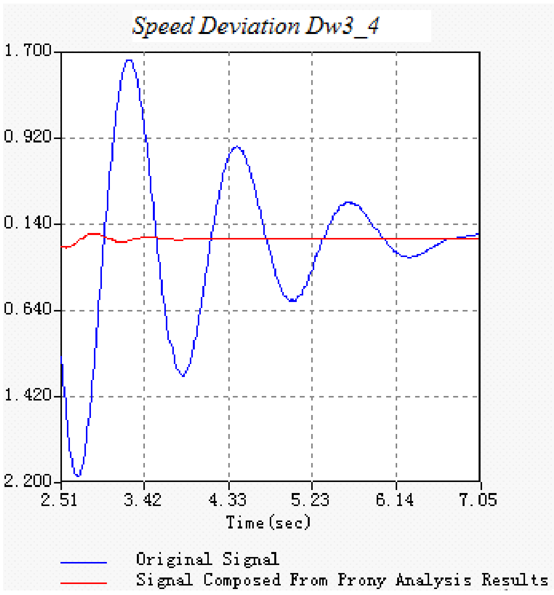

Fig. 5.19 Deviations of rotation speeds of the original signal and Prony analysis (with SVC in operation, pattern 5)

The main oscillation modes of the system without SVC installation by Prony Analysis results as in Table 5.1.

Table 5.1 TSAT without PRONY analysis results

Magnitude	Phase (deg)	Frequency (Hz)	Damping (%)	Real (1/s)	Imaginary (rad/s)
3.8384	86.899	0.938	4.272	-0.2521	5.896
1.2642	43.619	1.207	66.974	-6.8371	7.581
0.9251	94.165	1.060	6.930	-0.4628	6.662
0.8527	-111.836	0.755	3.044	-0.1484	4.873
0.8440	-99.049	1.712	42.144	-4.9989	10.757

The main oscillation modes of the system with SVC installation by Prony Analysis results as in Table 5.2.

Table 5.2 TSAT with PRONY analysis results

Magnitude	Phase (deg)	Frequency (Hz)	Damping (%)	Real (1/s)	Imaginary (rad/s)
2.2146	100.185	0.915	14.455	-0.8403	5.572
0.6760	-177.300	0.758	5.465	-0.2607	4.763
0.1068	0.000	0.000	100.000	-4.0789	0.000
0.0979	101.042	17.954	18.844	-21.6451	112.808
0.0938	143.160	1.654	13.012	-1.3636	10.390

The dominant eigenvalues of the SVC before and after the additional damping control is applied are distributed as shown in Fig.5.20.

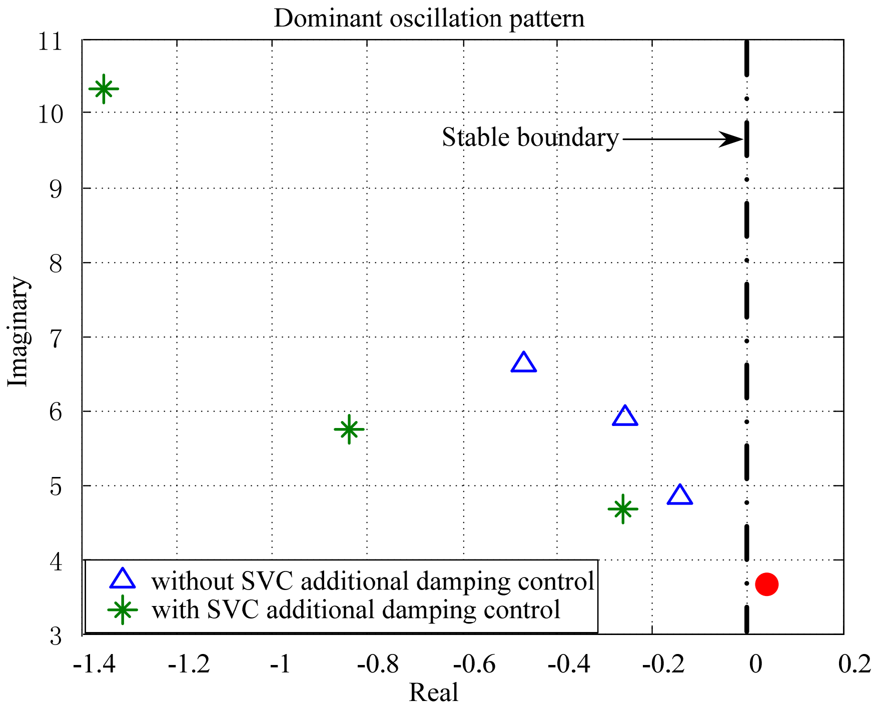

Fig.5.20 Dominant eigenvalues of the SVC before and after the additional damping control

It's obvious that the dominant eigenvalues of the SVC could be shifted leftwards on the complex plane.

5.3.5 Coordinated Damping Control of Multiple SVCs

Multiple FACTS devices are needed to be installed in China Southern Power Grid, and these devices will be controlled in a coordinated way so the the holistic performance can be optimized. It is imperative to study the coordinated control strategies for multiple SVCs.

The principle of coordinated control for multiple SVCs is shown in Fig. 5.21.

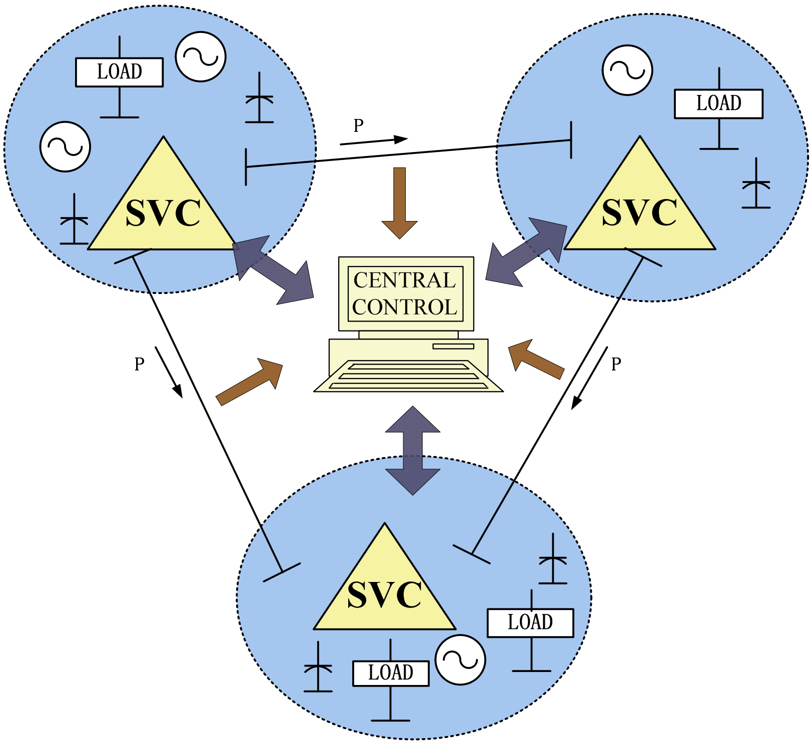

Fig. 5.21 Schematic diagram for the principle of coordinated control for multiple SVCs

After obtaining the wide-area feedback signals, the control center controls multiple SVC installations in a coordinated way to optimize the control results. The feedback signals usually include such signals reflecting the interregional oscillations as rotation speed difference $\Delta\omega$, angle difference $\Delta\delta$ and power oscillation signal ΔP, and the control signal still takes the SVC output voltage U_{SVC}. The SVC forms a closed-loop control for the system. There are two ways to design the SVC controller parameters:

After knowing the identified or order-reduced linear system model

$$\begin{cases} \dot{X}(t) = AX(t) + BU(t) \\ Y(t) = CX(t) \end{cases} \tag{5.60}$$

We can complete the coordinated settings of parameters of the controller for multiple SVCs in the ways of nonlinear optimization of

This approach requires a uniformly coordinated controller to control the outputs of multiple SVCs simultaneously.

And a novel approach to controlling two sets of parallel SVCs will be mentioned at the end of this dissertation. The two sets of SVCs, installed in Chuxiong Commutation Station, the sending end of the Chuxiong-Huizhou ±800kV ultrahigh-voltage DC power transmission lines, were the pioneer worldwide to be controlled totally independently and automatically with identical control quantities and control objectives. That is, the two sets of SVCs achieved distributed independent control without a more advanced uniform controller, greatly enhancing the reliability, expandability and flexibility.

5.3.5.1 Nonlinear Optimization Design

Scholars have introduced mathematical nonlinear constrained optimization theory into controller design, and design parameters with the generally accepted numerical operation methods.

The general form of optimization models is

$$\min_{x} z = f(x),\ s.t.\ g(x) \le 0 \tag{5.61}$$

where s.t. is the abbreviation form of "subject to" in English; x and $g(x)$ both can take the vector forms, i.e. solve multi-parameter questions with multiple constraints. When one of $f(x)$ and $g(x)$ is a nonlinear function, the optimization problem is referred to as a nonlinear constrained optimization. And there has been a mathematical branch to solve such questions, there are such mature and reliable algorithms as feasible direction method, penalty function method, gradient projection method, sequential quadratic programming method, and so on, and there are various software packages. For example, MATLAB provides a special tool kit for constrained optimization problems.

The design of SVC controller parameters can be transformed into am optimization problem by abstraction, when x is the respective parameters to be determined, z is a scalar with explicit concept and general significance, the minimum of which means the optimal control results of the SVC controller, and $g(x)$ is the total of the constrains that x is subject to. Thus, the problem of SVC controller design is transformed into a problem to find proper z and $g(x)$.

(1) Objective function

The objective function should be directly relevant to the damping effect of closed-loop system $G(s)$ with additional damping control feedback loop on low-frequency oscillations.

(2) Constraints

Constraints of parameter ranges

Stability constraint

Robustness constraint

Other constraints

5.3.5.2 Decentralized Coordinated Optimal Control

The linear optimal objective function is

$$\min J = \int_0^\infty [X^T(t)QX(t) + U^T(t)RU(t)]dt \tag{5.62}$$

where P and Q are weight matrices.

By evaluating the Levine-Athans equation

$$\begin{cases} B^T PVC^T + RKCVC^T = 0 \\ (A+BKC)V + V(A+BKC)^T + I = 0 \\ (A+BKC)^T P + P(A+BKC) + Q + C^T K^T RKC = 0 \end{cases} \tag{5.63}$$

We get the control feedback law:

$$U(t) = KY(t) \tag{5.64}$$

5.4 Summary

1. This chapter makes a detailed overview of the power system low-frequency oscillation problem and its analytical methods.

2. This chapter makes theoretical analysis of SVC additional damping control.

3. This chapter designs the SVC additional damping controller on the basis of Prony Identification.

(1) Conducts Prony analysis to find the dominant eigenvalues of the system with TSAT software

(2) Conducts simulation calculations of the SVC damping low-frequency oscillations in accordance with the IEEE 30-bus system with PSCAD software

1) Time domain analysis shows that after 210Mvar SVC with additional damping control is installed at bus 14, the three-phase instantaneous grounding short-circuit fault can calm down oscillations in 4.5s after the fault occurs.

2) Frequency analysis shows that after of SVC additional damping control is installed, the dominant eigenvalues of the SVC could be shifted leftwards on the complex plane such that the system can be stabilized and the power transmission margins can be improved, where the rightmost eigenvalue moves leftwards by 0.1 unit, and the three dominant eigenvalues move leftwards by o.5 unit on average. That means that the SVC additional damping control achieves good results in attenuating oscillations and enhancing dynamic stability.

CHAPTER 6 ENGINEERING EXAMPLES AND SIMULATIONS OF SVCs IN POWER SYSTEMS

6.1 PSCAD/EMTDC Simulations

6.1.1 Introduction of Simulation Models

(1) The system models include:

1) Single-machine infinite system model with the following parameters: rated short-circuit current at the 35kV side: 40kA; rated short-circuit capacity at the 500kV side: 15000MVA. The rated capacity of the SVC is 210Mvar. The SVC is connected to the middle of the 500kV power transmission lines through a step-down transformer, and the model is mainly used to test the steady operation characteristics of the system.

2) IEEE 30-bus model. The generators are synchronous machines with excitation regulating systems. This model is mainly used to test the dynamic operation characteristics of the system.

(2) The model of the SVC in Wuzhou substation is as follows:

TCR capacity: 210Mvar;

Minimum firing angle of the thyristors: 116 degrees;

Maximum firing angle of the thyristors: 165 degrees;

Firing angle of the thyristors at a half load: 130.9 degrees;

One bank of parallel capacitors of 60Mvar with a series reactance rate of 12%;

One bank of filtering capacitors of 45Mvar with a resonance frequency of 250Hz;

One bank of filtering capacitors of 60Mvar with a resonance frequency of 350Hz;

One bank of filtering capacitors of 45Mvar with a resonance frequency of 550Hz;

Designed rated voltage of the SVC installation: 36.75kV;

Rated voltage of actual operating system: 35kV.

6.1.2 Simulations of Steady Operation Characteristics

When the system is in its steady operation, the control system of the SVC works in the fixed output control manner based on the voltage deviations and with slope rectifications.

In the voltage control manner, the SVC installation shall meet the requirements of the response time in the following steps:

The response time is defined as the time that it takes the SVC to improve its output to 90% of the expectation after step signals are inputted that enables the SVC to output 75% of inductive reactive power to 75% of capacitive reactive power. In this process, the SVC output shall meet the following requirements: a response time of no more than 100ms, and a overshoot voltage of no more than 20% of the settings. And the stability time before the SVC reaches 95% of the expected voltage shall be less than 300ms.

When the system is in its steady operation, put the TCR into operation at the instant of 1.5s, and the filers at the instant of 1s. Fig. 6.1 shows the curve of the total reactive power outputted by the SVC, Fig. 6.2 shows the curve of the voltage at the 500kV bus where the SVC is installed, and Fig. 6.3 shows the curve of firing angle α of the TCRs.

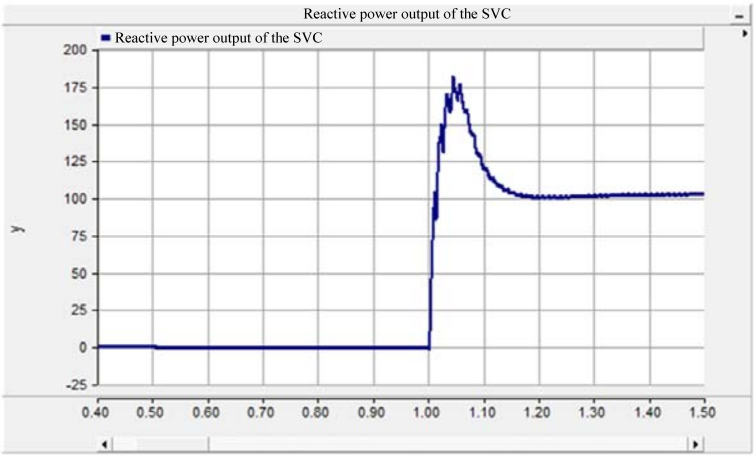

Fig. 6.1 Reactive power output of the SVC (Mvar) when the system is in steady operation

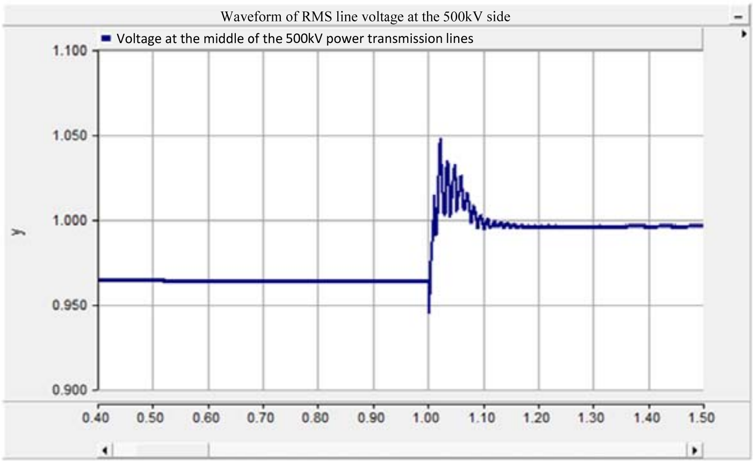

Fig. 6.2 Voltage at the middle of the 500kV power transmission lines when the system is in steady operation

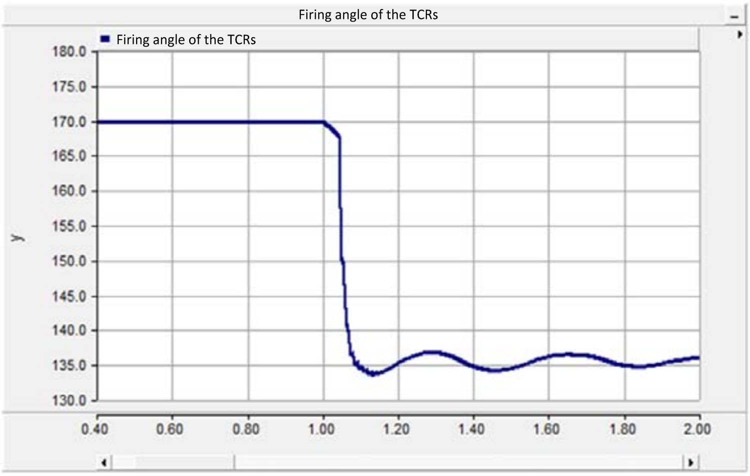

Fig. 6.3 Firing angle of the TCRs when the system is in steady operation

As can be seen from these three figures, when the system is in steady operation, the SVC bus voltage is about 0.97p.u., and when the TCRs are put into operation at the instant of 0.5s, the firing angle is 170 degrees, and the SVC reactive power output is nearly zero. When the filters are put into operation at the instant of 1s, the system produces an overshoot voltage of about 0.03pu, and the TCR operates immediately to adjust the firing angle to about 135 degrees and to stabilize the voltage at 0.996p.u.. The SVC outputs 102Mvar reactive power output with a response time of about 70ms and a maximum overshoot voltage of only 3% of the settings. And the stability time when the voltage reaches 95% of the expectation is less than 200ms.

In Fig. 6.2, the SVC voltage at the 500kV side finally stabilizes at 0.996pu other than 1pu mainly because of two reasons: one is that a variable admittance control strategy is added into the controller, which can enable the SVC to have at least 50% of spare reactive power when the system is in steady operation; the other is that a slow admittance control strategy is added into the controller, which can enable the SVC to switch on/off the surrounding capacitors and inductors, and to have at least 50% of spare reactive power when there are small disturbances in the system.

6.1.2.1 When the capacitors are put into operation

Taking the voltage at the 500kV high-voltage side of the transformer as the monitoring object, and putting the 45 Mvar capacitor bank into operation at the instant of 2s, we get the total reactive power output, the firing angle of the TCRs and the bus voltage where the SVC is installed as shown in Fig.6.4, Fig.6.5 and Fig. 6.6.

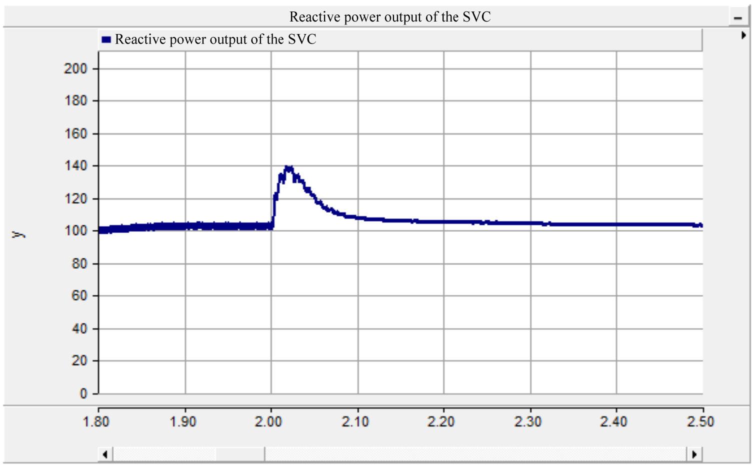

Fig. 6.4 Reactive power output of the SVC (Mvar) when a 45Mvar capacitor bank is put into operation

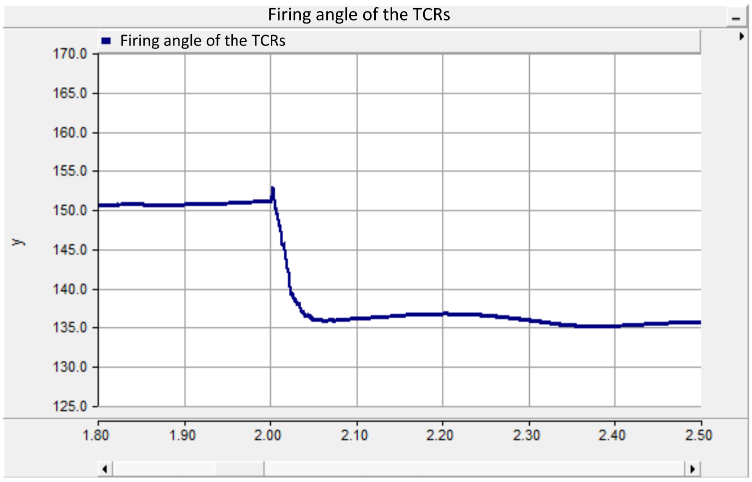

Fig. 6.5 Firing angle of TCRs when a 45Mvar capacitor bank is put into operation

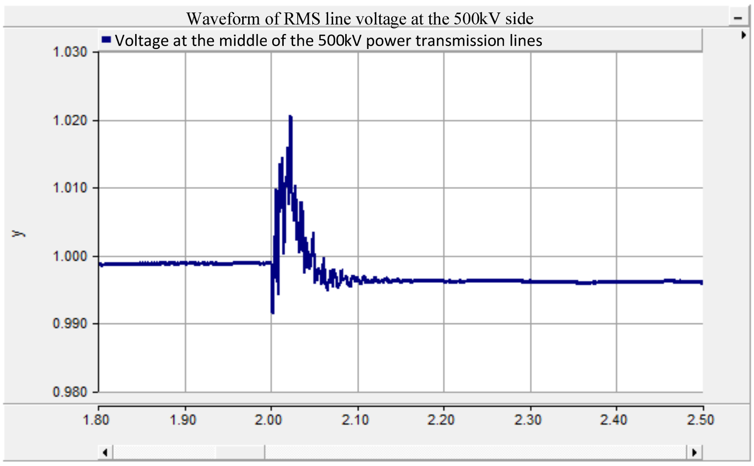

Fig. 6.6 Line voltage (RMS) at the 500kV side of the SVC when a 45Mvar capacitor bank is put into operation

Taking the voltage at the 500kV high-voltage side of the transformer as the monitoring object, and putting the 60 Mvar capacitor bank into operation at the instant of 2s, we get the total reactive power output, the firing angle of the TCRs and the bus voltage where the SVC is installed as shown in Fig.6.7, Fig.6.8 and Fig. 6.9.

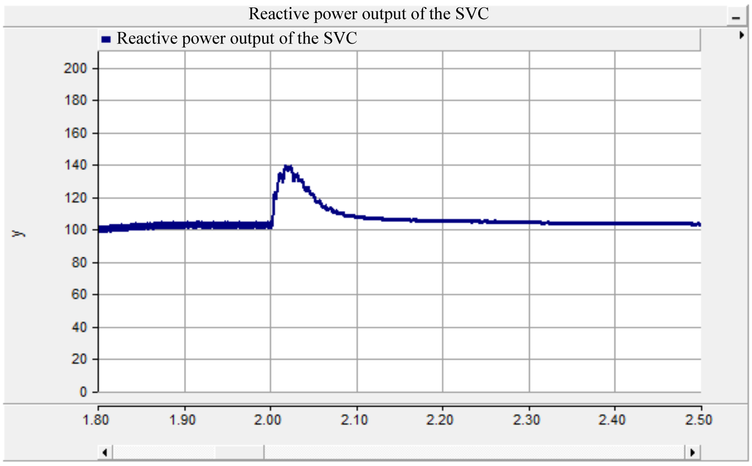

Fig. 6.7 Reactive power output of the SVC (Mvar) when a 60Mvar capacitor bank is put into operation

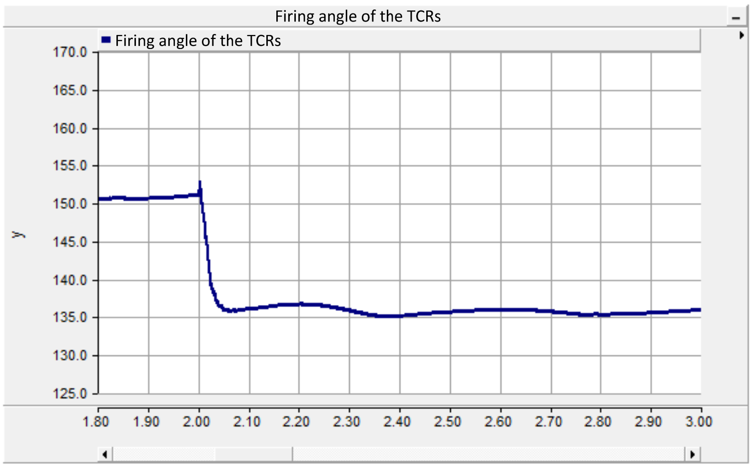

Fig. 6.8 Firing angle of TCRs when a 60Mvar capacitor bank is put into operation

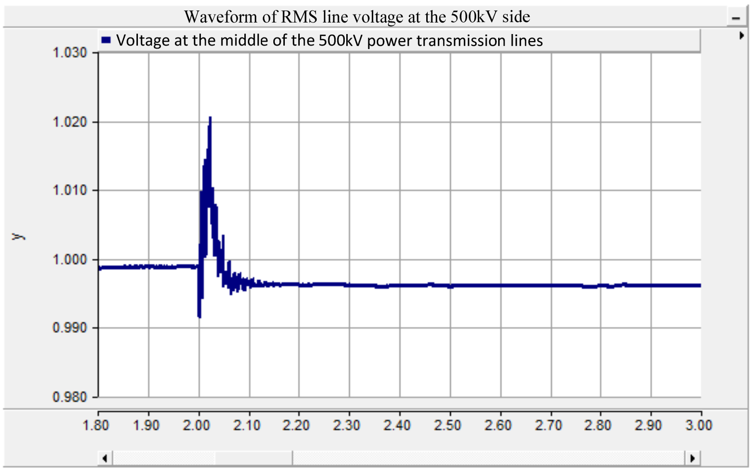

Fig. 6.9 RMS line voltage at the 500kV side of the SVC when a 60Mvar capacitor bank is put into operation

6.1.2.2 When the capacitors are tripped

Taking the voltage at the 500kV high-voltage side of the transformer as the monitoring object, and tripping the 45 Mvar capacitor bank at the instant of 2s, we get the total reactive power output, the firing angle of the TCRs and the bus voltage where the SVC is installed as shown in Fig.6.10, Fig.6.11 and Fig. 6.12.

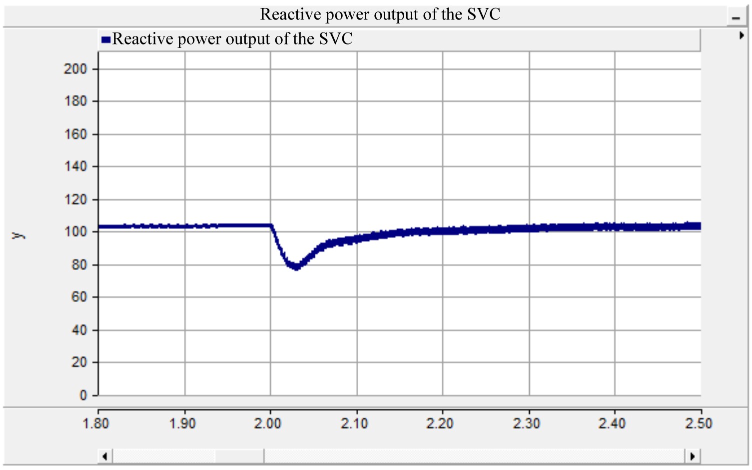

Fig. 6.10 Reactive power output of the SVC (Mvar) when a 45Mvar capacitor bank is tripped

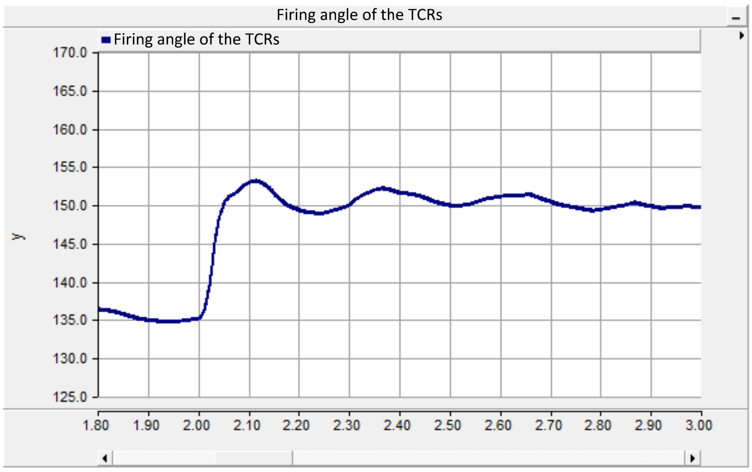

Fig. 6.11 Firing angle of TCRs when a 45Mvar capacitor bank is tripped

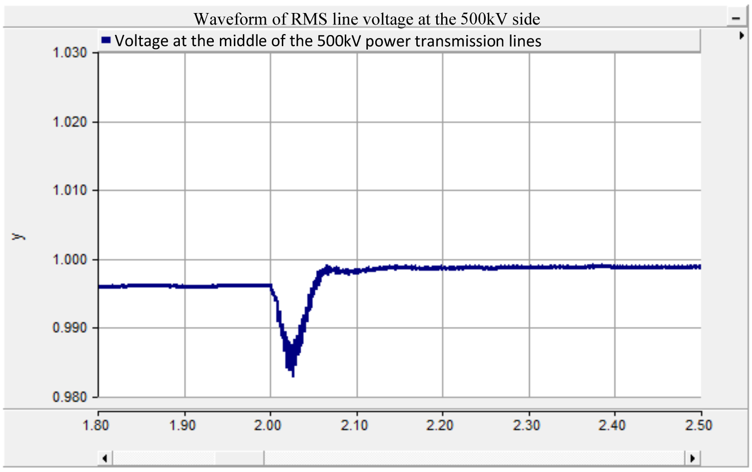

Fig. 6.12 Line voltage (RMS) at the 500kV side of the SVC when a 45Mvar capacitor bank is tripped

Taking the voltage at the 500kV high-voltage side of the transformer as the monitoring object, and tripping the 60 Mvar capacitor bank at the instant of 2s, we get the total reactive power output, the firing angle of the TCRs and the bus voltage where the SVC is installed as shown in Fig.6.13, Fig.6.14 and Fig. 6.15.

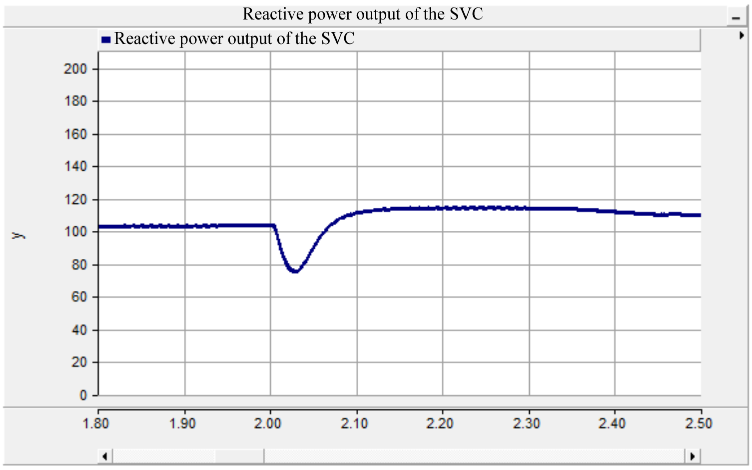

Fig. 6.13 Reactive power output of the SVC (Mvar) when a 60Mvar capacitor bank is tripped

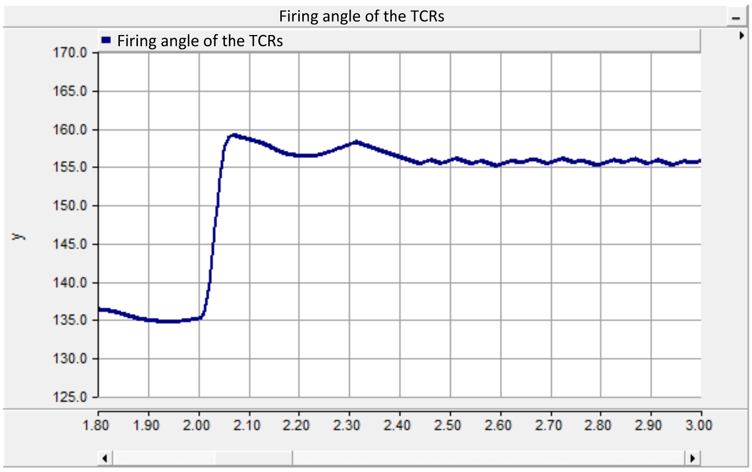

Fig. 6.14 Firing angle of TCRs when a 60Mvar capacitor bank is tripped

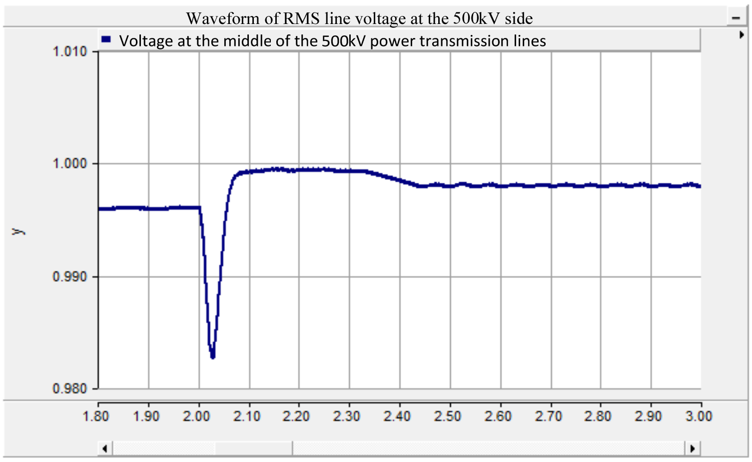

Fig. 6.15 Line voltage (RMS) at the 500kV side of the SVC when a 60Mvar capacitor bank is tripped

6.1.3 Simulations of Transient Operation Characteristics

6.1.3.1 Three-phase fault near the earth

Fault description: A three-phase grounding fault occurs near the earth at the instant of 2s, and is cleared in 0.1s.

Fig. 6.16 shows the curve of the total reactive power output of the SVC, Fig.6.17 shows the curve of the voltage at the 500kV bus where the SVC is installed, and Fig. 6.18 shows the curve of the firing angle $\alpha$of the TCRs in the SVC.

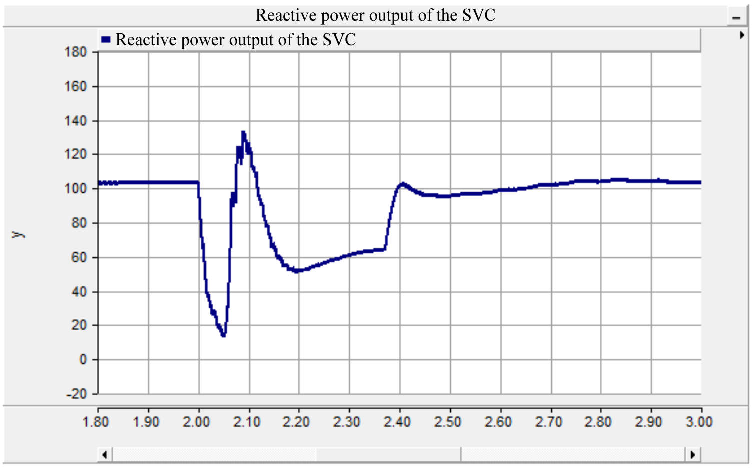

Fig. 6.16 Total reactive power output of the SVC in time of a three-phase grounding fault near the earth

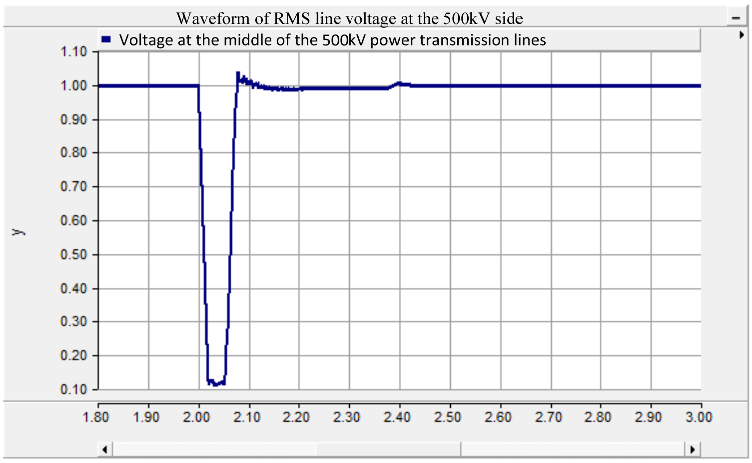

Fig. 6.17 Voltage at the 500kV side of the SVC in time of a three-phase grounding fault near the earth

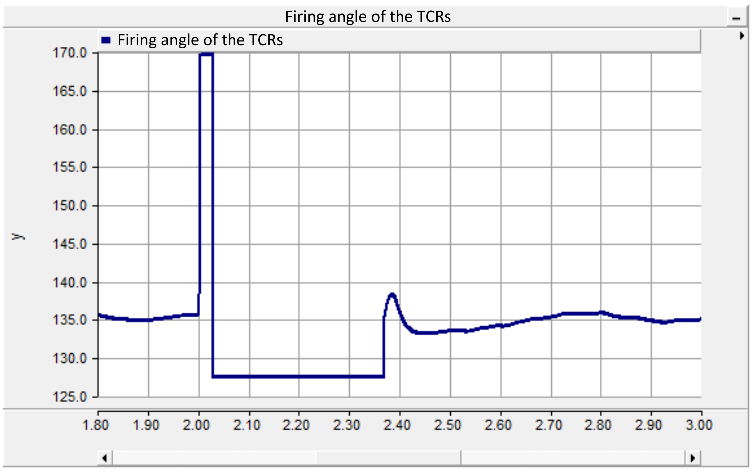

Fig. 6.18 Firing angle of the TCRs in time of a three-phase grounding fault near the earth

As shown in Fig.6.16, after a three-phase grounding fault occurs, the reactive power output of the SVC first drops to nearly 0, then increases to 130Mvar immediately, drops again to about 50Mvar, lasting for about 0.3s, and then recovers to 102Mvar. Fig.6.17 shows that, after a three-phase grounding fault occurs, the voltage at the 500kV side drops rapidly, and, after the fault is cleared, the voltage recovers to 0.988pu, lasting for 0.3s, and recovers to 0.996pu. Fig. 6.18 shows that, after a three-phase grounding fault occurs, the firing angle of the TCRs is 170 degrees, lasting for 0.02s, becomes 127.6 degrees, lasting for 0.3s, and then changes again to stabilize at about 135 degrees.

The reason for the above conditions is the low-voltage control strategy added into the controller. When a three-phase grounding fault occurs and the SVC detects an average three-phase voltage that is less than 0.6pu and lasts for 0.02s, the low-voltage strategy is launched; when the average three-phase voltage is above 0.7pu and lasts for 0.3s, the low-voltage strategy exits. The low-voltage strategy ensures that no serious system overvoltage will arise when the SVC is put into operation after the three-phase grounding fault is cleared.

If there is no low-voltage control strategy, when the voltage last low, the SVC controller would demand a mass of capacitive reactive power output till the maximum, i.e. the controller comes into saturation. And then if the grounding fault is cleared and the voltage is restored, the response of the SVC controller would be lag since it would cost time to quit deep saturation and the SVC would still be deeply capacitive at the moment, therefore the overvoltage would occur.

When the low-voltage control strategy is launched, the admittance of TCR branch is adjusted to half of the upper limit so that the SVC controller output is not in deep saturation. When the voltage is restored while the fault is cleared, the SVC controller would respond immediately and the SVC could quit capacitive status quickly to avoid the overvoltage.

6.1.3.2 Three-phase grounding fault via resistors

Fault description: A three-phase grounding fault occurs via resistors at the instant of 2s, and is cleared in 0.1s. The simulation results are as follows.

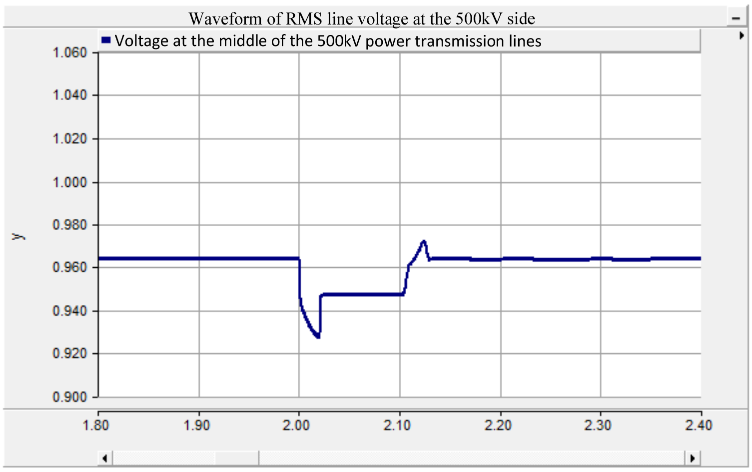

Fig. 6.19 Voltage at the 500kV side in time of a three-phase grounding fault via resistors far from the earth when the SVC is out of operation

Fig.6.19 shows how the RMS voltage at the 500kV side changes over time when the SVC is out of operation and a three-phase grounding fault via resistors occurs at a point far from the earth.

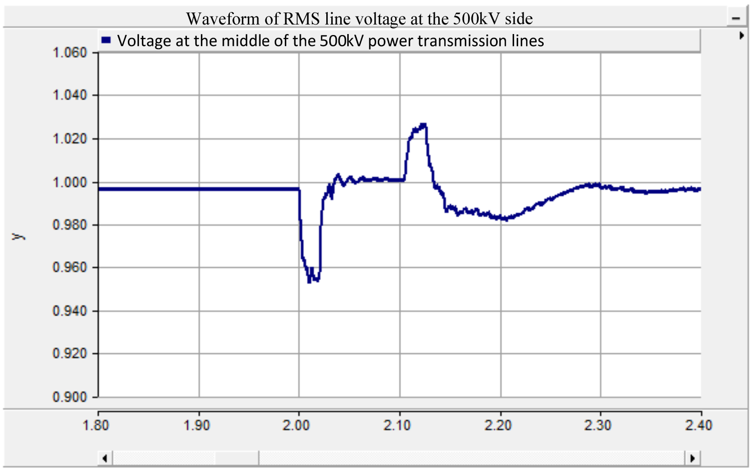

Fig. 6.20 Voltage at the 500kV side in time of a three-phase grounding fault via resistors far from the earth when the SVC is in operation

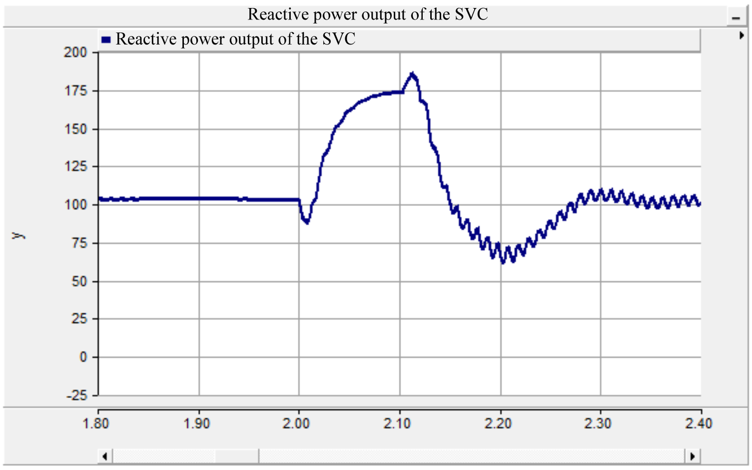

Fig. 6.21 Reactive power output of the SVC in time of a three-phase grounding fault via resistors far from the earth when the SVC is in operation (Mvar)

Fig.6.20 shows the curve of the RMS voltage at the 500kV side over time when the SVC is in operation and a three-phase grounding fault via resistors occurs at a point far from the earth, where, after the fault occurs at the instant of 2s, the voltage drops to 0.96pu rapidly, the TCRs quickly operates such that the voltage is regulated and restored to 1.0pu again in 20ms until the fault is cleared. After that, the voltage moves up to 1.03pu because the TCRs are still triggered at the pre-fault angle. Then the TCRs operate quickly to regulate the firing angle so that the voltage can be reduced in 20ms, and the system voltage enters a dynamic process with fluctuations of small amplitudes until it stabilizes at the pre-fault level at 2.3s. The whole dynamic process lasts for about 200ms.

Fig.6.21 shows the curve of the reactive power output of the SVC over time when the SVC is in operation and a three-phase grounding fault via resistors occurs at a point far from the earth. The reactive power output of the SVC stabilizes at 102Mvar before the fault. Then, the fault occurs at 2s, and the firing angle of the TCRs increases the reactive power output of the SVC continuously to realize the strong dynamic compensation of reactive power. After the fault is cleared, the reactive power of the SVC recovers to 102Mvar in 200ms.

Fig.6.20 and Fig.6.21 deal well with the functions of the SVC for strong compensation of reactive power to boost the system recovery.

6.1.3.3 Single-phase grounding fault

Fault description: A single-phase grounding fault occurs at phase A at the instant of 2s, and is cleared in 0.1s. The simulation results are as follows.

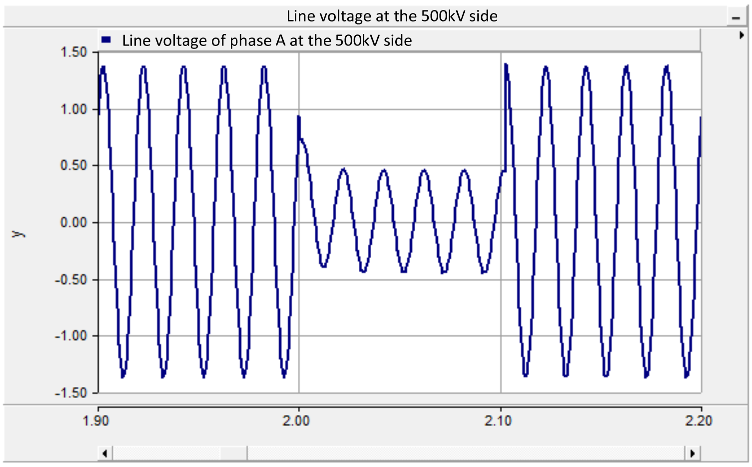

Fig. 6.22 Voltage at the 500kV side in time of a single-phase grounding fault at phase A when the SVC is out of operation

Fig.6.22 shows the line voltage of phase A at the 500kV side of the main transformer when the SVC is out of operation and a single-phase phase grounding fault occurs at phase A at 2s and is cleared in 0.1s. Before the fault, the peak value of the line voltage reaches 1.36pu, and the rated peak voltage is 1.414pu. At the instant of the fault, the amplitude of the voltage drops to 0.45pu. After the fault is cleared, the voltage recovers to 1.39pu and then to 1.36pu.

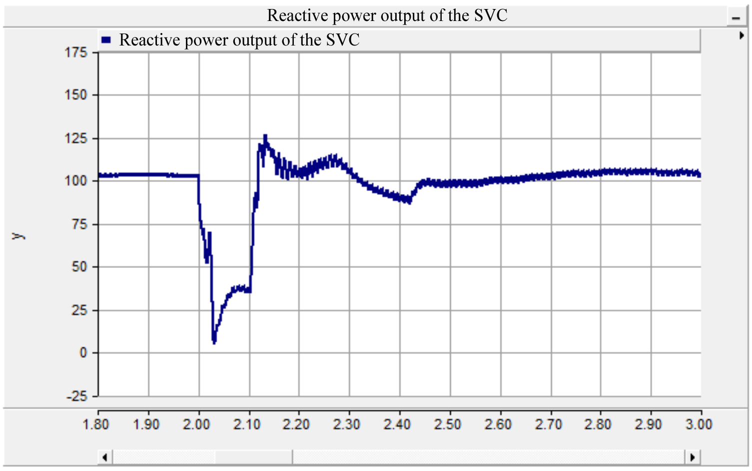

Fig. 6.23 Reactive power output of the SVC in time of a single-phase grounding fault at phase A

Fig.6.23 shows the curve of the reactive power output of the SVC when the SVC is in operation, and a single-phase grounding fault occurs at phase A at 2s and is cleared in 0.1s. At the instant of the fault, the reactive power output of the SVC drops to about 25Mvar. After the fault is cleared, the voltage increases but, owing to the response time of the SVC, the reactive power output of the SVC remains at a high level. Then the firing angles of the thyristors are regulated such that the reactive power output of the SVC remains at the pre-fault level, i.e. 102Mvar.

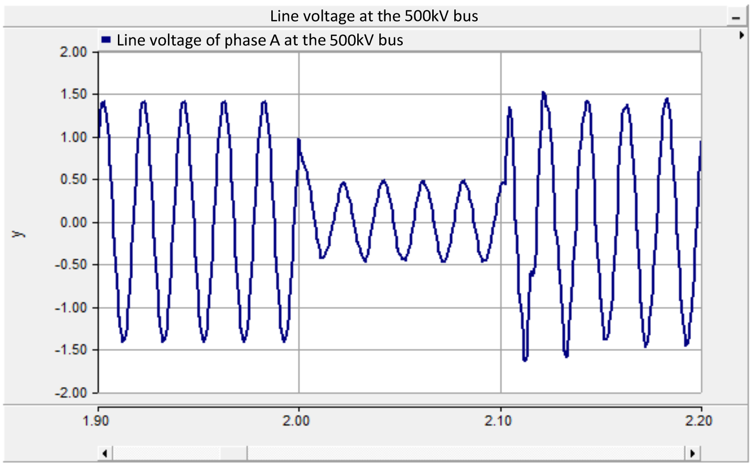

Fig. 6.24 Line voltage of phase A at the 500kV bus of the SVC in time of a single-phase grounding fault at phase A

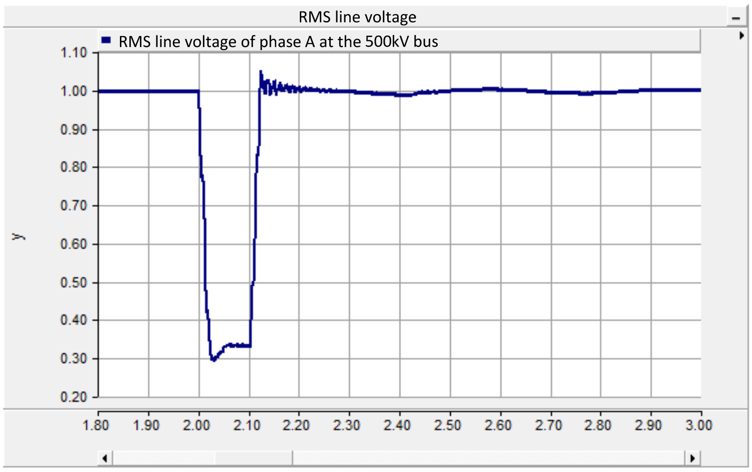

Fig. 6.25 RMS line voltage of phase A at the 500kV bus of the SVC in time of a single-phase grounding fault at phase A

Fig.6.24 and Fig.6.25 show the curves of how line voltage and RMS line voltage of phase A at the 500kV bus of the SVC change over time when the SVC is in operation, and a single-phase phase grounding fault occurs at phase A at 2s and is cleared in 0.1s respectively. Before the fault, the peak value of the line voltage reaches

1.405pu, and the rated peak line voltage is 0.996pu. At the instant of the fault, the amplitude of the voltage drops to 0.5pu and the RMS voltage drops to 0.33pu. After the fault is cleared, owing to the response time of the SVC, the reactive power output of the SVC remains at a high level, and the voltage amplitude and RMS voltage move up to 1.6pu and 1.05pu respectively. Then the firing angles of the thyristors are regulated such that the voltage amplitude stabilizes at 1.405pu and the RMS voltage at 0.996 p.u.

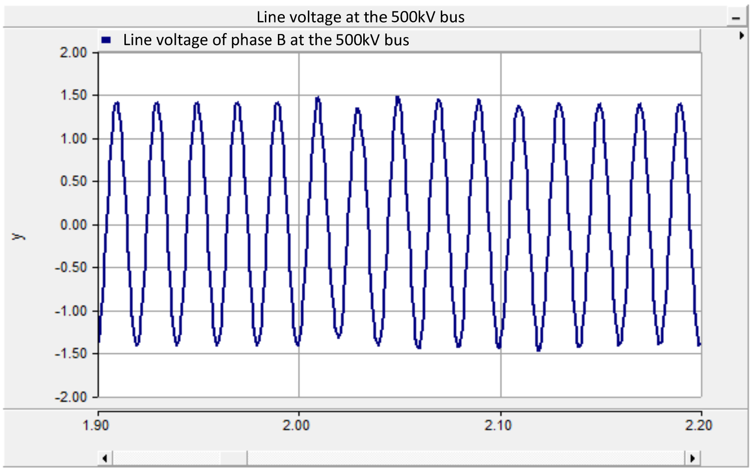

Fig. 6.26 Line voltage of phase B at the 500kV bus of the SVC in time of a single-phase grounding fault at phase A

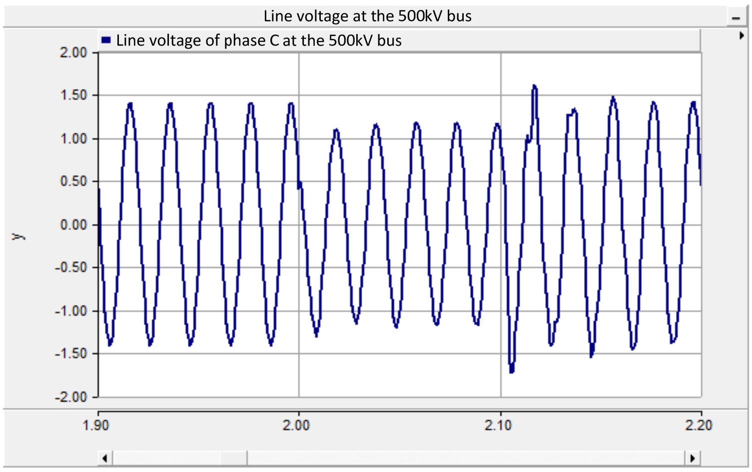

Fig. 6.27 Line voltage of phase C at the 500kV bus of the SVC in time of a single-phase grounding fault at phase A

Fig.6.26 and Fig.6.27 show the waveforms of voltages of phases B and C at the 500kV bus of the SVC before and after the fault. As can be seen from the two figures, voltages of phases B and C change little in time of a single-phase grounding fault at phase A. And this is because of the phase adjustment manner of the controller.

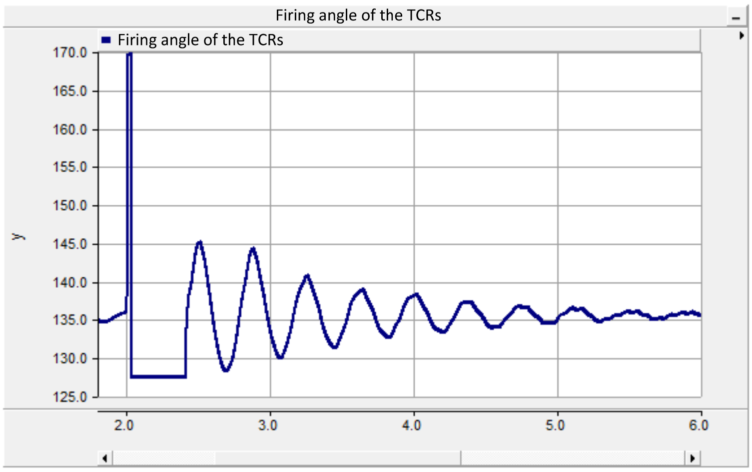

Fig. 6.28 Firing angle of the TCRs of phase A in time of a single-phase grounding fault at phase A

Fig.6.28 shows how the curve of the firing angle of the TCRs between phases A and B changes over time when the SVC is in operation, and a single-phase phase grounding fault occurs at phase A at 2s and is cleared in 0.1s. Before the fault occurs, the firing angle stabilizes at 135 degrees, making the voltage at the 500kV side approximate to 1.0pu. At the time of the fault, the fault is set to last for 0.02s until the TCRs operate to launch the low-voltage strategy such that the firing angle is maintained at 127.5 degrees and lasts for 0.3s. Then the low-voltage strategy is cancelled, the firing angle continues to change until it stabilizes at 135 degrees, and the voltage at the 500kV side stabilizes at 0.996 p.u..

6.1.3.4 Double-phase grounding fault

Fault description: A double-phase short-circuit fault occurs between phases A and B at the instant of 2s, and is cleared in 0.1s.

Fig.6.29 and Fig.6.30 show the curves of how the line voltages of phases A and B vary over time when the SVC is out of operation, and a double-phase short-circuit fault occurs between phases A and B at the instant of 2s, and is cleared in 0.1s. At the time of the fault, the line voltages of both phases A and B drop at different degrees, and after the fault is cleared, the voltages recover to the pre-fault levels.

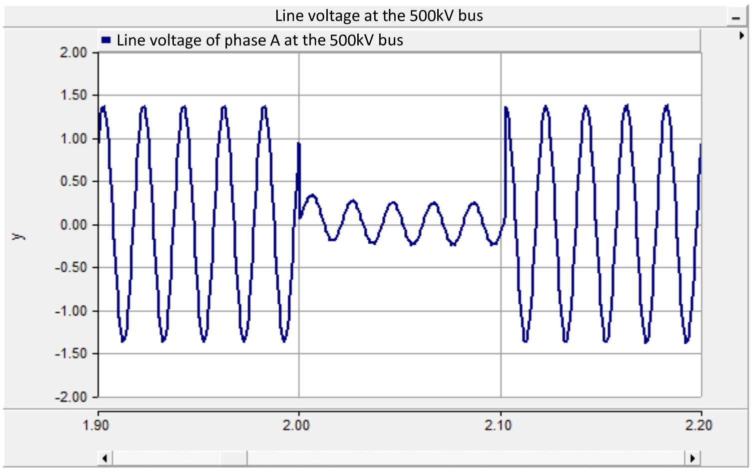

Fig. 6.29 Line voltages of phase A at the 500kV bus of the SVC when the SVC is out of operation, and a double-phase short-circuit fault occurs between phases A and B

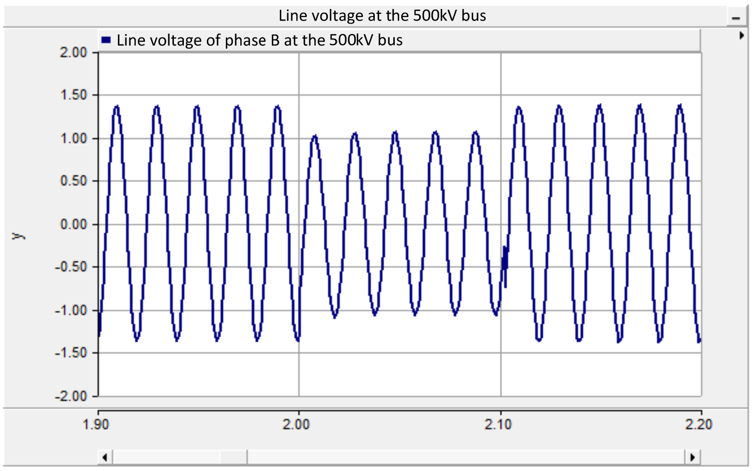

Fig. 6.30 Line voltages of phase B at the 500kV bus of the SVC when the SVC is out of operation, and a double-phase short-circuit fault occurs between phases A and B

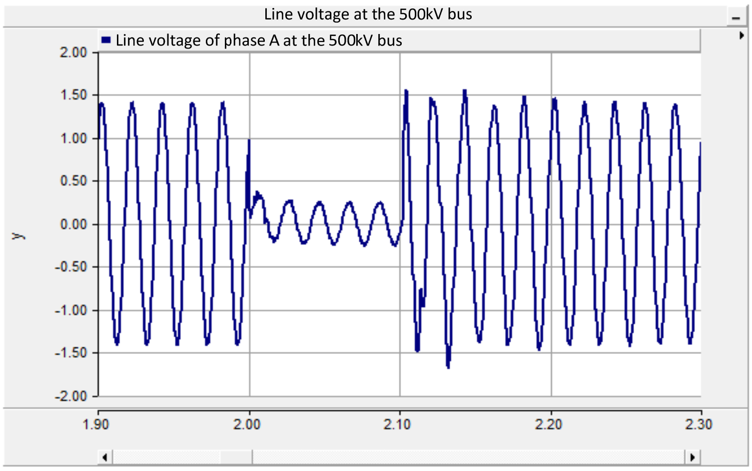

Fig. 6.31 Line voltages of phase A at the 500kV bus of the SVC when the SVC is in operation, and a double-phase short-circuit fault occurs between phases A and B

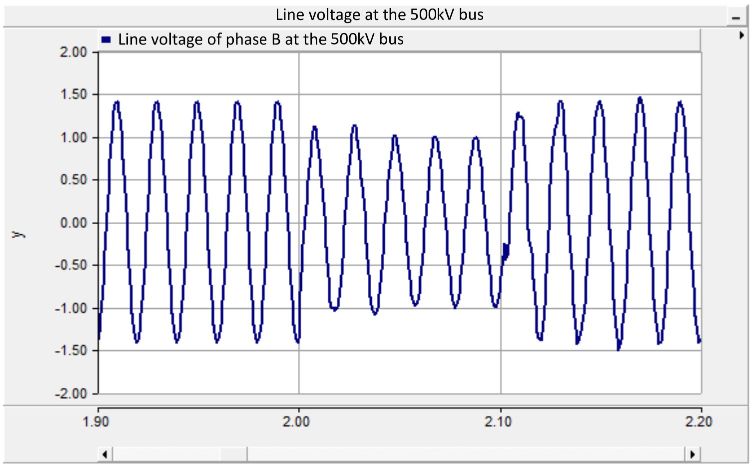

Fig. 6.32 Line voltages of phase B at the 500kV bus of the SVC when the SVC is in operation, and a double-phase short-circuit fault occurs between phases A and B

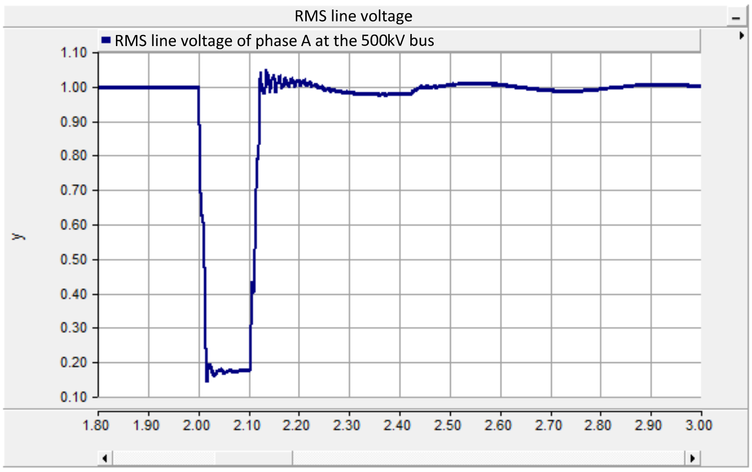

Fig. 6.33 RMS line voltages of phase A at the 500kV bus of the SVC when the SVC is in operation, and a double-phase short-circuit fault occurs between phases A and B

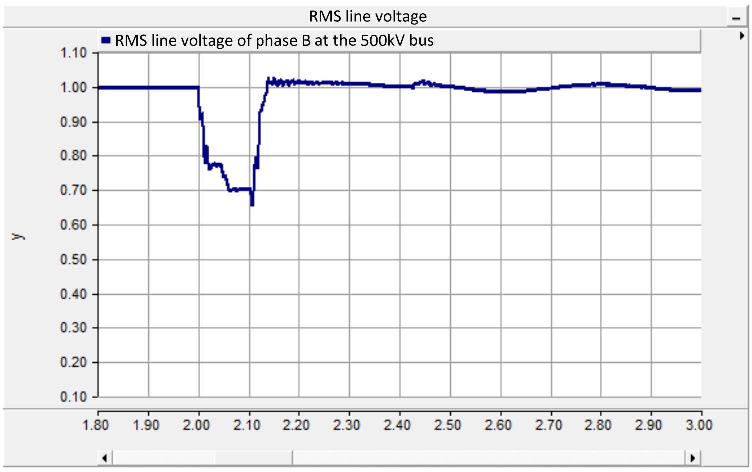

Fig. 6.34 RMS line voltages of phase B at the 500kV bus of the SVC when the SVC is in operation, and a double-phase short-circuit fault occurs between phases A and B

Fig.6.31 and Fig. 6.32 show the curves of the line voltages of phases A and B varying over time when the SVC is in operation, and a double-phase grounding fault occurs between phases A and B at 2s and is cleared in 0.1s. Fig.6.33 and Fig. 6.34 show the curves of the RMS line voltages of phases A and B varying over. At the time of the fault, the voltages of both phases A and B drop at different degrees. After the fault, the firing angle is regulated such that the voltages quickly recover to the pre-fault levels.

Fig. 6.35 shows the curve of the reactive power output of the SVC changing over time when the SVC is in operation, and a double-phase grounding fault occurs between phases A and B at 2s and is cleared in 0.1s. Before the fault occurs, the reactive power output of the SVC remains at 102Mvar. At the time of the fault, the SVC output drops to 0 in 0.1s, and the low-voltage strategy operates, bringing about small fluctuations in the reactive power output of the SVC until the output remains at 67.8Mvar. The whole process lasts for 0.3s until the low-voltage strategy is cancelled and the reactive power output of the SVC recovers to 102Mvar.

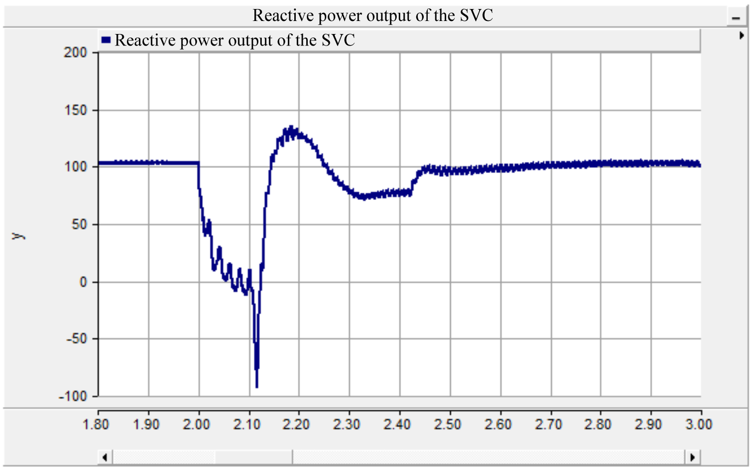

Fig.6.35 Reactive power output of the SVC at the time of a double-phase short-circuit fault between phases A and B (Mvar)

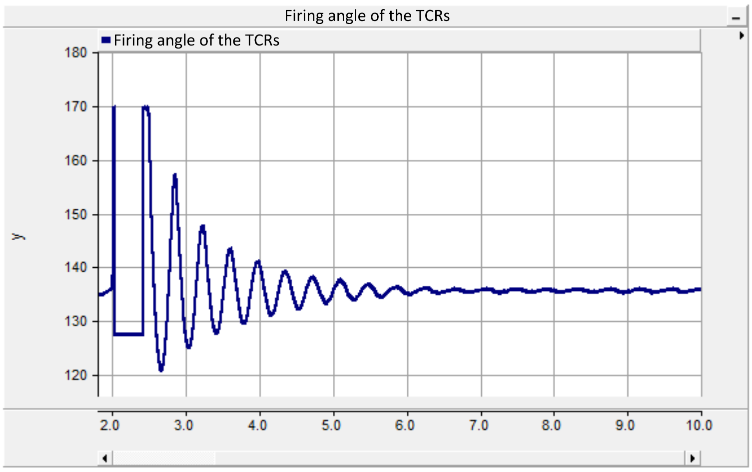

Fig.6.36 Firing angle of the TCRs at the time of a double-phase short-circuit fault between phases A and B (Mvar)

Fig.6.36 shows the curve of the firing angle of the TCRs changing over time when the SVC is in operation, and a double-phase grounding fault occurs between phases A and B at 2s and is cleared in 0.1s. Before the fault occurs, the firing angle is 135 degrees. At the time of the fault, the low-voltage strategy is launched, and the firing angle of the TCRs becomes 127.5 degrees. After the fault is cleared, the firing angle is quickly regulated such that is stabilizes at the pre-fault level of 135 degrees.

6.1.4 Simulations of Dynamic Operation Characteristics

To test the functions of the control strategies to suppress oscillations, we conduct flow calculation in accordance with the IEEE 30-bus system. The generators are synchronous machines with excitation regulating systems. This model is mainly used to test the dynamic operation characteristics of the system. The rated voltage of the power transmission lines is 500kV.

The simulation parameters are set up as follows:

SVC capacity: 210Mvar;

Minimum firing angle of the thyristors: 116 degrees;

Maximum firing angle of the thyristors: 165 degrees;

Firing angle of the thyristors at a half load: 130.9 degrees;

One bank of parallel capacitors of 60Mvar with a series reactance rate of 12%;

One bank of filtering capacitors of 45Mvar with a resonance frequency of 250Hz;

One bank of filtering capacitors of 60Mvar with a resonance frequency of 350Hz;

One bank of filtering capacitors of 45Mvar with a resonance frequency of 550Hz;

Designed rated voltage of the SVC installation: 36.75kV;

Rated voltage of actual operating system: 35kV.

According to the checking computations, the voltage of bus 14 is rather low, posing the greatest impact on the system stability. So, the 210 Mvar SVC is connected to bus 14 via a transformer. To make the system produce oscillations, we set up a three-phase grounding fault to occur at bus 9 at 2s, and to be cleared in 0.1s. And the deviations between the rotation speeds of generators 4 and 5 are studied for generators 4 and 5 installed at buses 6 and 8 are connected to bus 14 through power transmission lines.

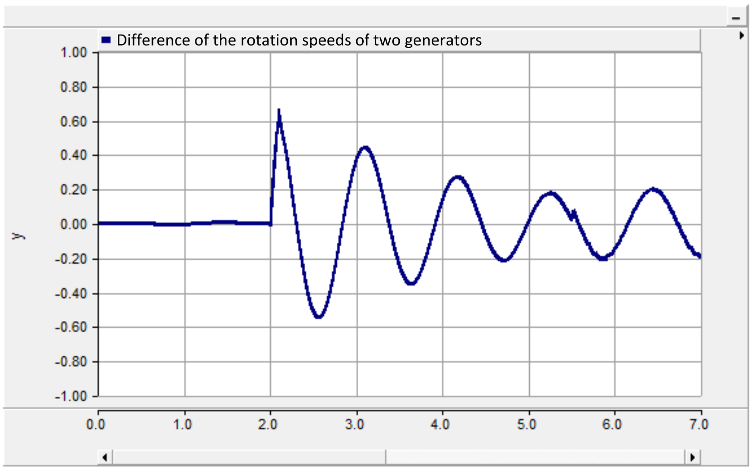

Fig. 6.37 Difference of the rotation speeds of two generators without SVC installed

Fig.6.37 shows the curve for the difference of the rotation speeds of generators 4 and 5 when the SVC is not installed, and a three-phase grounding fault occurs at bus 9 at 2s and is cleared in 0.1s. As can be seen from the figure, before the fault occurs at 2s, the difference of the rotation speeds remain at about zero; when the fault occurs at 2s, the difference of the rotation speeds increases dramatically; after the fault is cleared, the difference of the rotation speeds drops, accompanied by fluctuations with amplitudes of about 0.2rad. According to the computation results, the oscillation frequency is about 1Hz, meaning that there are 1Hz oscillations in the system.

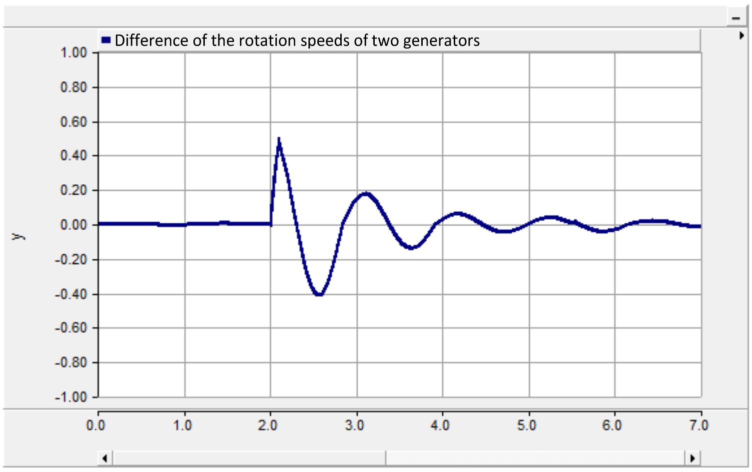

Fig. 6.38 Difference of the rotation speeds of two generators with the SVC in operation

Fig.6.38 shows the curve for the difference of the rotation speeds of generators 4 and 5 when the SVC is in operation, and a three-phase grounding fault occurs at bus 9 at 2s and is cleared in 0.1s. As can be seen from the figure, when the fault occurs at 2s, the difference of the rotation speeds increases dramatically; after the fault is cleared, the difference of the rotation speeds drops gradually, and recovers to the before-fault state in about 7 seconds. By comparing Fig. 6.37 with Fig. 6.38, we can see that the SVC plays a role in suppressing power oscillations.

6.2 RTDS Simulations

6.2.1 Introduction of Simulation Models

(1) The system models include:

1) Single-machine infinite system model with the following parameters: rated short-circuit current at the 35kV side: 40kA; rated short-circuit capacity at the 500kV side: 15000MVA. The rated capacity of the SVC is 210Mvar. The SVC is connected to the middle of the 500kV power transmission lines, and the model is mainly used to test the steady operation characteristics of the system.

2) Six-machine system model with the following parameters: rated voltage at the generator sides: 35kV; short-circuit current at the 35kV side: 40kA; rated short-circuit

capacity at the 220kV side: 8500MVA; rated short-circuit capacity at the 500kV side: 15000MVA. The rated capacity of the SVC is 210Mvar. The SVC is connected to the middle of the 500kV power transmission lines via a step-down transformer, and the model is mainly used to test the dynamic operation characteristics of the system.

(2) The model of the SVC in Wuzhou substation is as follows:

TCR capacity: 210Mvar;

Minimum firing angle of the thyristors: 116 degrees;

Maximum firing angle of the thyristors: 165 degrees;

Firing angle of the thyristors at a half load: 130.9 degrees;

One bank of parallel capacitors of 60Mvar with a series reactance rate of 12%;

One bank of filtering capacitors of 45Mvar with a resonance frequency of 250Hz;

One bank of filtering capacitors of 60Mvar with a resonance frequency of 350Hz;

One bank of filtering capacitors of 45Mvar with a resonance frequency of 550Hz;

Designed rated voltage of the SVC installation: 36.75kV;

Rated voltage of actual operating system: 35kV.

The SVC parameters are entered into the real SVC controller as settings, the current and voltage signals used to simulate the China Southern Power Grid system by the RTDS simulator are transformed and outputted to the sampling boards of the SVC controller, and the SVC control signals are transformed into the 0~5V level signals and outputted into the RTDS device, i.e. the real SVC controller is connected to the simulated actual power grid and the RTDS simulator connecting the primary electrical system of the SVC through the i/o interfaces of the RTDS, so that the dynamic characteristics of the real SVC controller in the grid can be tested.

6.2.2 Simulations of Steady Operation Characteristics

When the system is in its steady operation, the control system of the SVC works in the fixed output control manner based on the voltage deviations and with slope rectifications. And the voltage deviations are to be determined by the reference voltage settings and the actual voltage of the bus to be controlled by the SVC.

When the system is in steady operation, put the TCR into operation at the instant of 1s, and put the parallel capacitor banks and the filtering capacitor banks into operation at the instant of 2s.

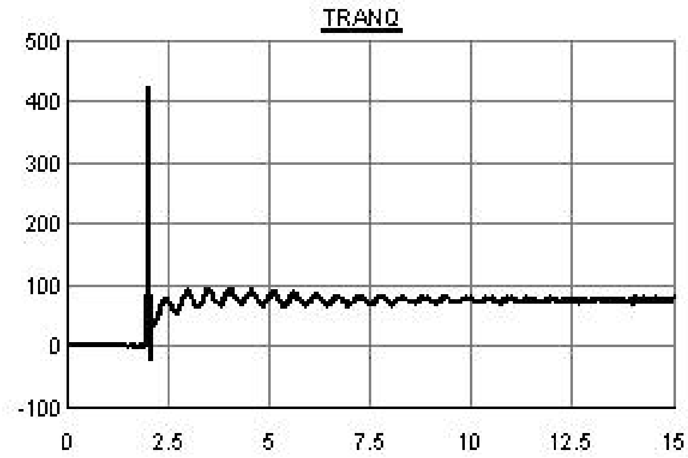

Fig. 6.39 Reactive power output of the SVC (Mvar) when the system is in steady operation

Fig.6.39 shows the curve of the reactive power output of the SVC changing over time when the system is in steady operation, the TCRs are put into operation at 1s, and the parallel capacitor banks and the filtering capacitor banks are put into operation at 2s. When the TCRs are put into operation at 1s, the SVC sends out no reactive power. When the parallel and filtering capacitor banks are put into operation at 2s, they generate a large amount of reactive power instantly, and then the reactive power stabilizes at 80Mvar quickly (in about 70ms), when the SVC maintains a reactive power reserve of 130Mvar.

Fig.6.40 shows the curves of the firing angles of the thyristors changing over time when the system is in steady operation, the TCRs are put into operation at 1s, and the parallel capacitor banks and the filtering capacitor banks are put into operation at 2s. When the TCRs are put into operation at 1s, the firing angles of the TCRs are 170 degrees, causing the SVC outputs no inductive reactive power to the system and the system voltages to drop. When the parallel and filtering capacitor banks are put into operation at 2s, the firing angles of the TCRs operate quickly such that the angles stabilize at 130 degrees.

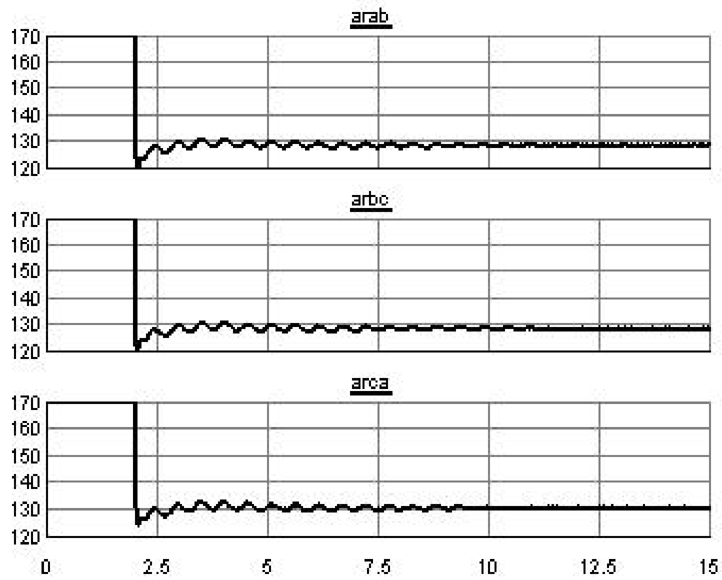

Fig. 6.40 Firing angle of the TCRs when the system is in steady operation

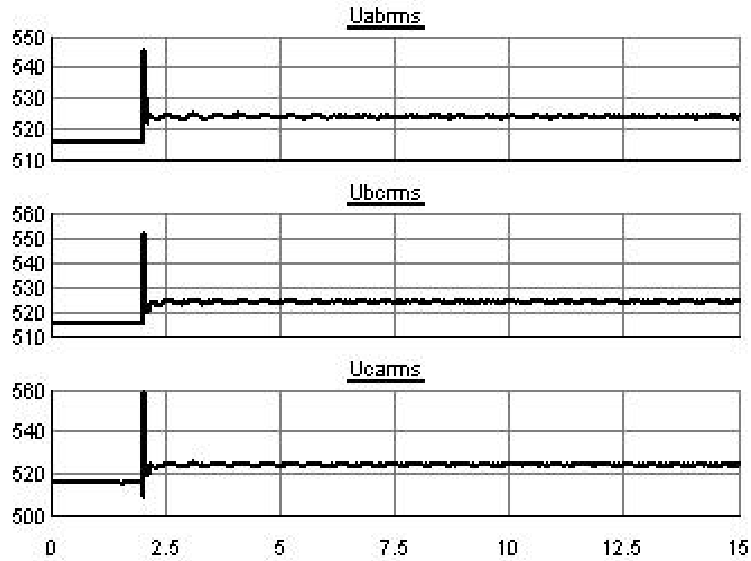

Fig. 6.41 Voltages at the 500kV side of the SVC when the system is in steady operation

Fig.6.41shows the curves of the RMS line voltages at the 500kV side of the SVC changing over time when the system is in steady operation, the TCRs are put into operation at 1s, and the parallel capacitor banks and the filtering capacitor banks are put into operation at 2s. When the TCRs are put into operation at 1s, the voltages remain unchanged at 517kV. When the parallel and filtering capacitor banks are put into operation at 2s, the voltages move up to 552kV instantly, and then stabilizes at

524kV quickly (in less than 70ms).

In Fig.6.41, the voltages at the 500kV side finally stabilize at 524kV other than at 525kV mainly because of two reasons: one reason is that the variable admittance control strategies added into the controller may enable the SVC to maintain a reactive power reserve of at least 50% when the system is in steady operation; the other is the slow admittance control strategies added into the controller enable the SVC to switch on/off the surrounding capacitors and inductors when there are small disturbances in the system, and to have at least 50% of spare reactive power when there are small disturbances in the system.

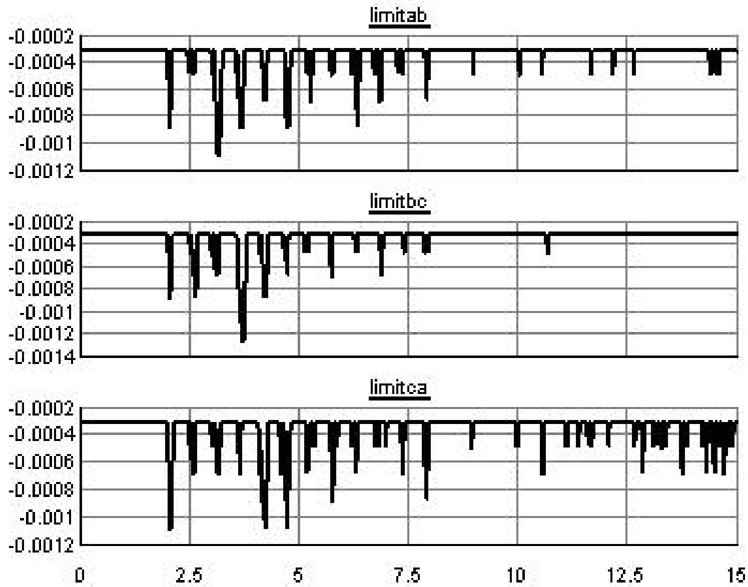

Fig. 6.42 Amplitudes of changing when the system is in steady operation

6.2.2.1 When the capacitors are switched on

Taking the voltage at the 500kV high-voltage side of the transformer as the monitoring object, and switching on a 45 Mvar capacitor bank at the instant of 1s, we get the total reactive power output, the firing angle of the TCRs and the bus voltage where the SVC is installed as shown in Fig.6.43, Fig.6.44 and Fig. 6.45.

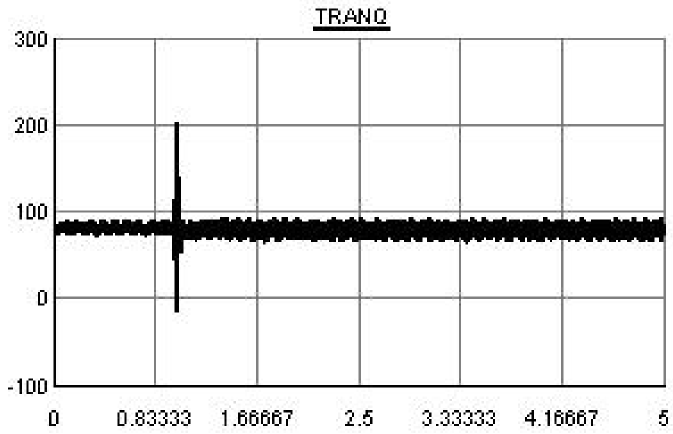

Fig. 6.43 Reactive power output of the SVC (Mvar) when a 45Mvar capacitor bank is switched on

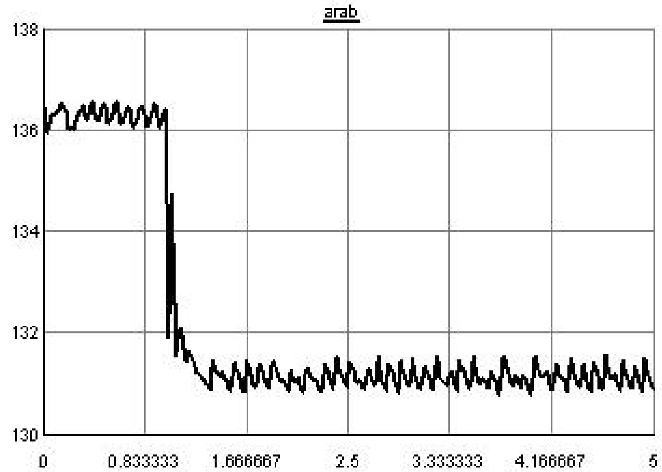

Fig. 6.44 Firing angle of TCRs when a 45Mvar capacitor bank is switched on

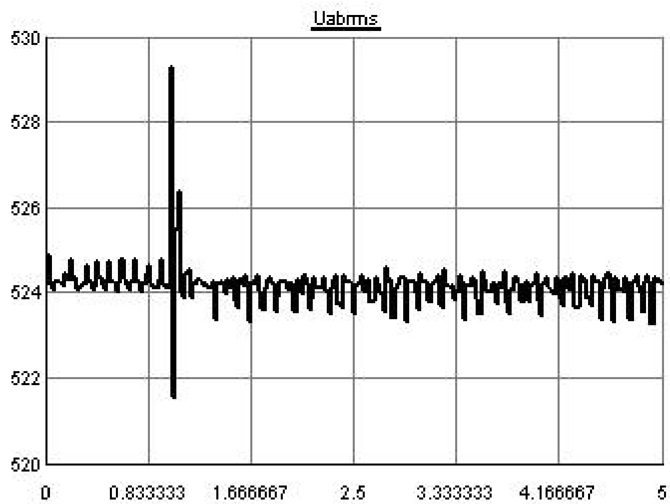

Fig. 6.45 RMS line voltage at the 500kV side of the SVC when a 45Mvar capacitor bank is switched on

Taking the voltage at the 500kV high-voltage side of the transformer as the monitoring object, and putting the 60 Mvar capacitor bank into operation at the instant of 2s, we get the total reactive power output, the firing angle of the TCRs and the bus voltage where the SVC is installed as shown in Fig.6.46, Fig.6.47 and Fig. 6.48.

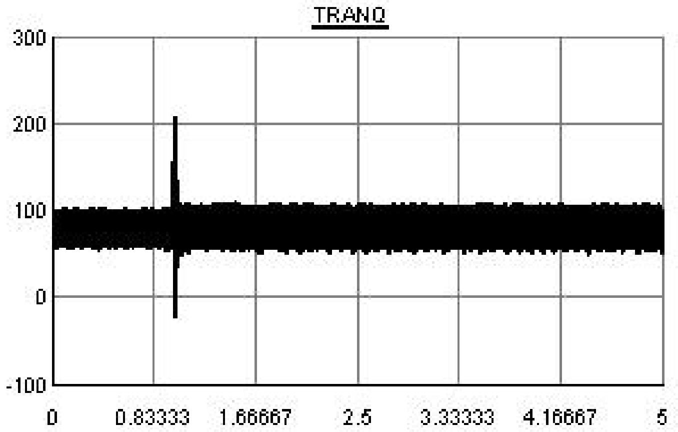

Fig. 6.46 Reactive power output of the SVC (Mvar) when a 60Mvar capacitor bank is switched on

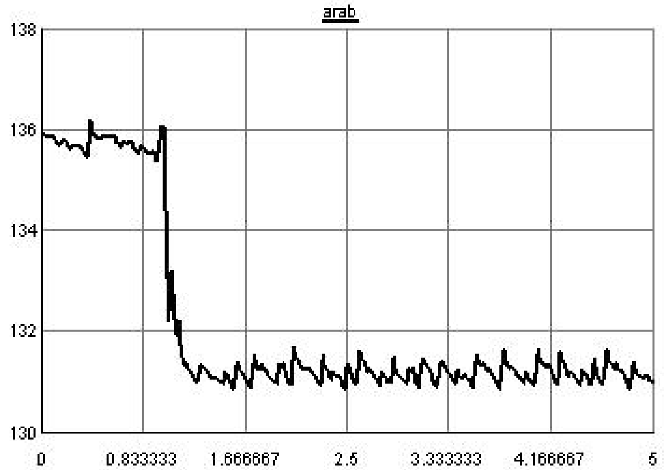

Fig. 6.47 Firing angle of TCRs when a 60Mvar capacitor bank is switched on

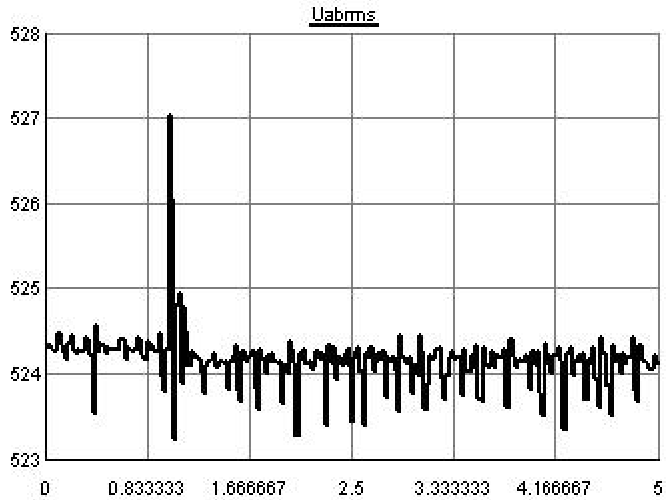

Fig. 6.48 RMS line voltage at the 500kV side of the SVC when a 60Mvar capacitor bank is switched on

6.2.2.2 When the capacitors are switched off

Taking the voltage at the 500kV high-voltage side of the transformer as the monitoring object, and switching off a 45 Mvar capacitor bank at the instant of 2s, we get the total reactive power output, the firing angle of the TCRs and the bus voltage where the SVC is installed as shown in Fig.6.49, Fig.6.50 and Fig. 6.51.

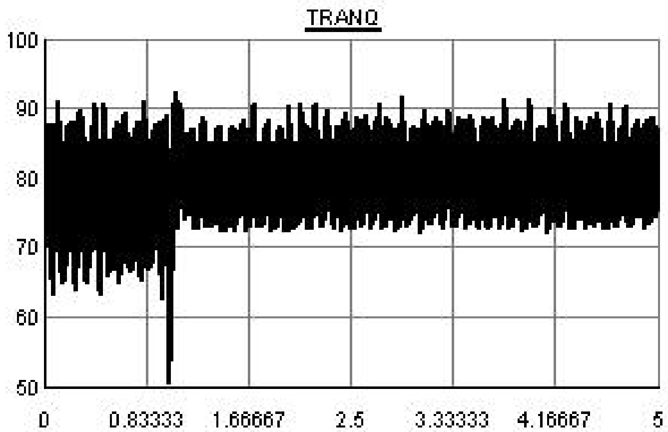

Fig. 6.49 Reactive power output of the SVC (Mvar) when a 45Mvar capacitor bank is switched off

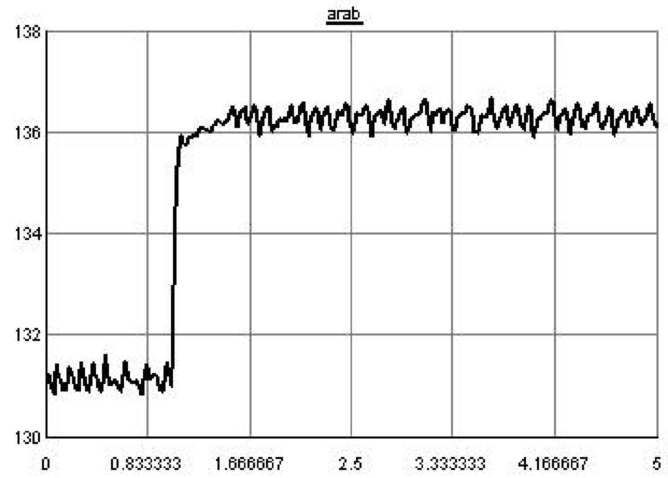

Fig. 6.50 Firing angle of TCRs when a 45Mvar capacitor bank is switched off

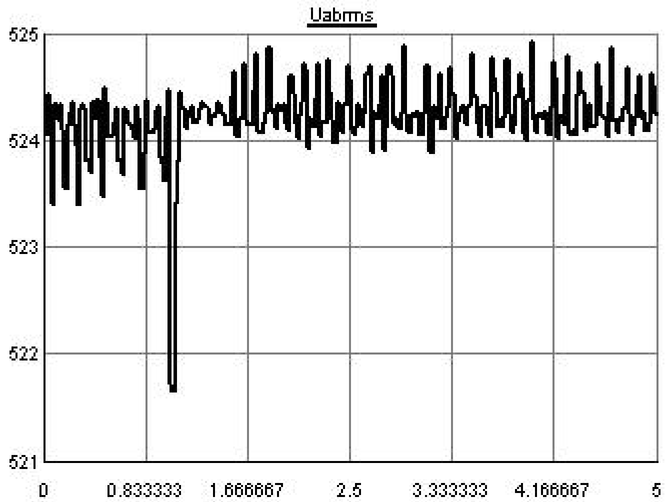

Fig. 6.51 Line voltage (RMS) at the 500kV side of the SVC when a 45Mvar capacitor bank is switched off

Taking the voltage at the 500kV high-voltage side of the transformer as the monitoring object, and tripping a 60 Mvar capacitor bank at the instant of 2s, we get the total reactive power output, the firing angle of the TCRs and the bus voltage where the SVC is installed as shown in Fig.6.52, Fig.6.53 and Fig. 6.54.

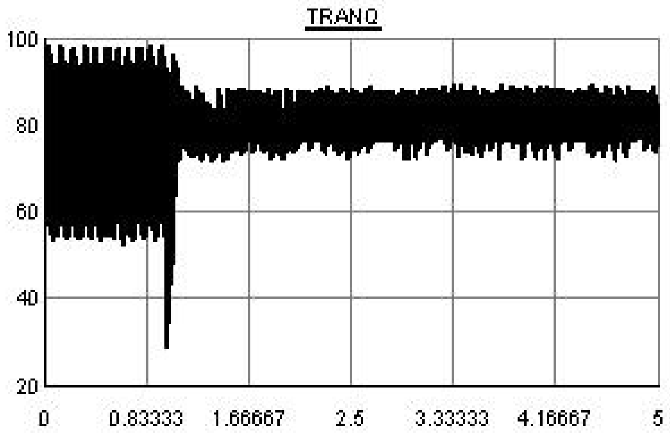

Fig. 6.52 Reactive power output of the SVC (Mvar) when a 60Mvar capacitor bank is switched off

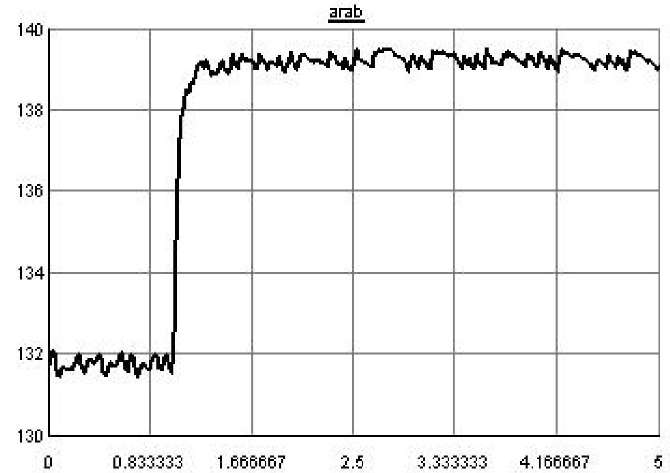

Fig. 6.53 Firing angle of TCRs when a 60Mvar capacitor bank is switched off

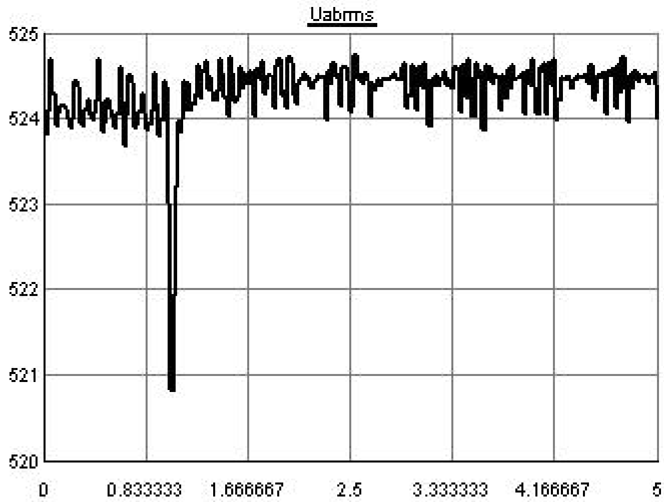

Fig. 6.54 Line voltage (RMS) at the 500kV side of the SVC when a 60Mvar capacitor bank is switched off

6.2.3 Simulations of Transient Operation Characteristics

Assume that a fault occurs at 1.5s and is cleared in 0.1s when the system is in transient-state operation and the SVC is in operation all along.

6.2.3.1 3-phase fault near the earth at the 500kV side

Fault description: A three-phase grounding fault occurs near the earth at the 500kV side at the instant of 2s, and is cleared in 0.1s.

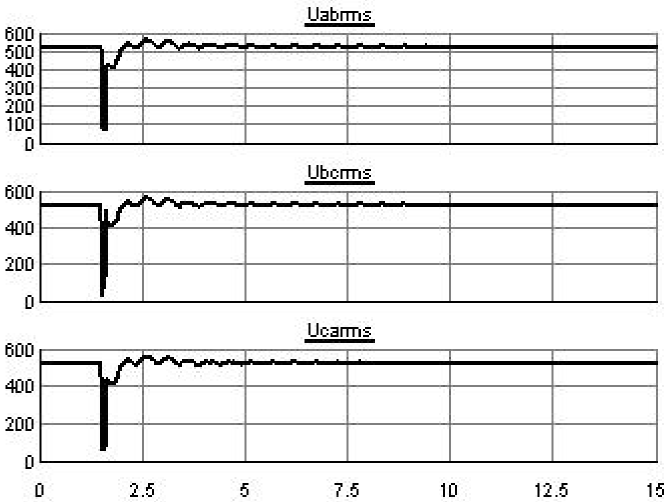

Fig. 6.55 Voltages at the 500kV side of the SVC in time of a three-phase grounding fault near the earth at the 500kV side

Fig. 6.55 shows the curves of the voltages at the 500kV side changing over time when a three-phase grounding fault occurs near the earth at the 500kV side at the instant of 1.5s, and is cleared in 0.1s. Before the fault occurs at 1.5s, the system is in steady operation, and the voltages remain at 524kV. When the three-phase short-circuit fault occurs at 1.5s, the voltages drop quickly to below 100kV until the fault is cleared in 0.1s and the voltages move up to the original state without the SVC. And the voltages increase again in 0.3s until they stabilize at the pre-fault level, i.e. 534kV.

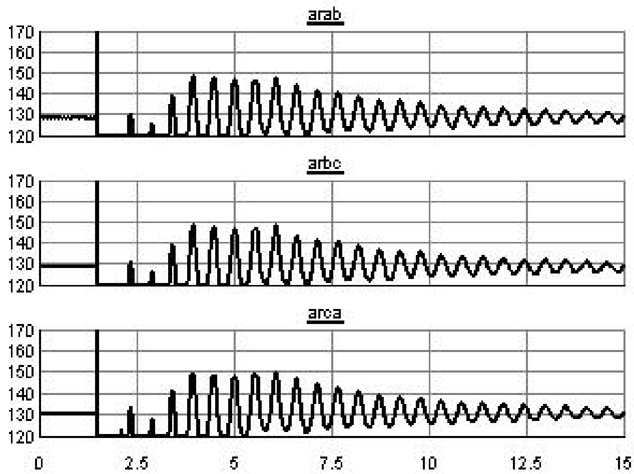

Fig. 6.56 Firing angles of the TCRs in time of a three-phase grounding fault near the earth at the 500kV side

Fig. 6.56 shows the curves of the firing angles of the TCRs changing over time when a three-phase grounding fault occurs near the earth at the 500kV side at the instant of 1.5s, and is cleared in 0.1s. Before the fault occurs at 1.5s, the system is in steady operation, and the firing angles of the TCRs are 130 degrees. When the three-phase short-circuit fault occurs at 1.5s, the firing angles of the TCRs become 170 degrees quickly, lasting for 0.02s, become 120 degrees, lasting for 0.03s, and change again until they finally stabilize at the pre-fault degree, i.e. 130 degrees.

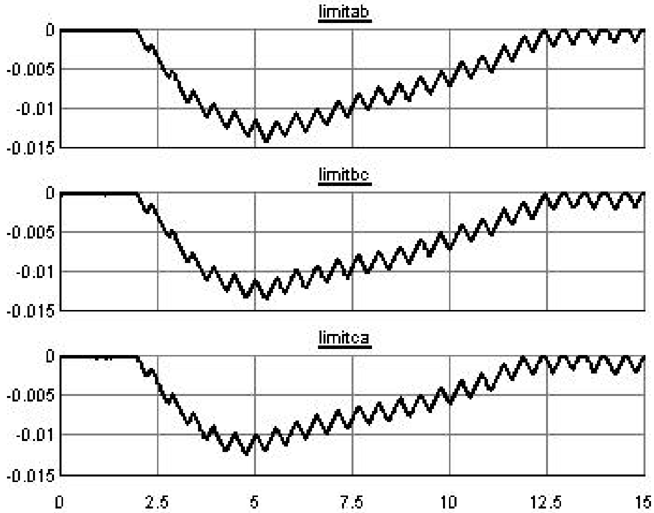

Fig. 6.57 Amplitudes of changing admittance limits in time of a three-phase grounding fault near the earth at the 500kV side

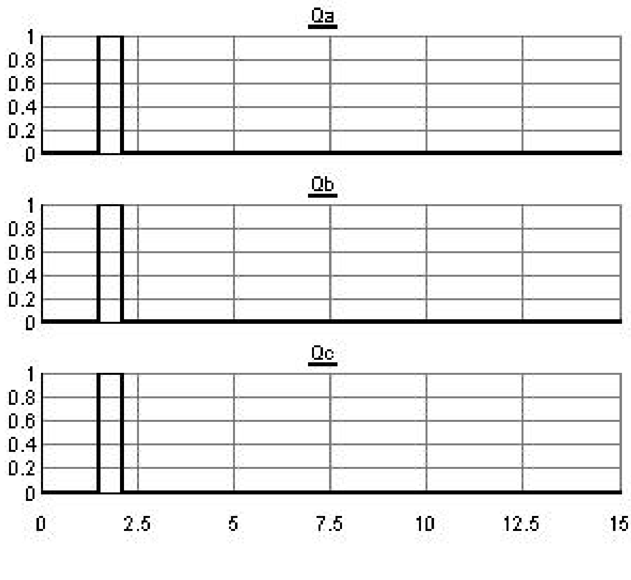

Fig. 6.58 Low-voltage protection in time of a three-phase grounding fault near the earth

As can be seen from the curves of the SVC admittance limits changing over time shown in Fig.6.57, the post-fault admittance limits first drop and then recover to the normal values slowly. The reason for this phenomenon is the low-voltage strategies added to the controller. When the three-phase grounding fault occurs and the SVC detects the voltages of three phases that are below 0.6pu in average and last for 0.02s, the low-voltage strategies are launched. When the voltages of three phases are higher than 0.7pu in average and last for 0.03s, the low-voltage strategies exit. The low-voltage strategies ensure that it will not result in excessive overvoltage in the system to put the SVC into operation after the three-phase grounding fault is cleared.

The low-voltage protection enabling signals are shown in Fig.6.58, where the high levels arise at 1.52s, and, after the fault is cleared, the high levels recover to low levels in 0.3s, i.e. at 1.9, and the low-voltage protection strategies are cancelled.

6.2.3.2 Three-phase fault far from the earth at the 500kV side

Assume that three-phase grounding fault occurs far from the earth at the instant of 1.5s, and is cleared in 0.1s.

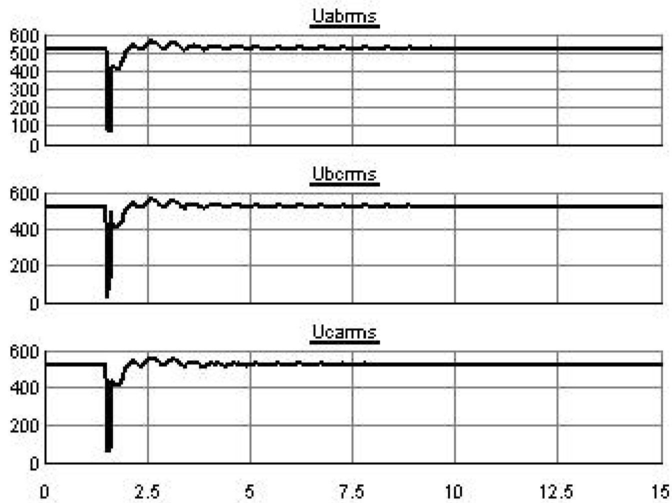

Fig. 6.59 Voltages at the 500kV side of the SVC in time of a three-phase grounding fault far from the earth

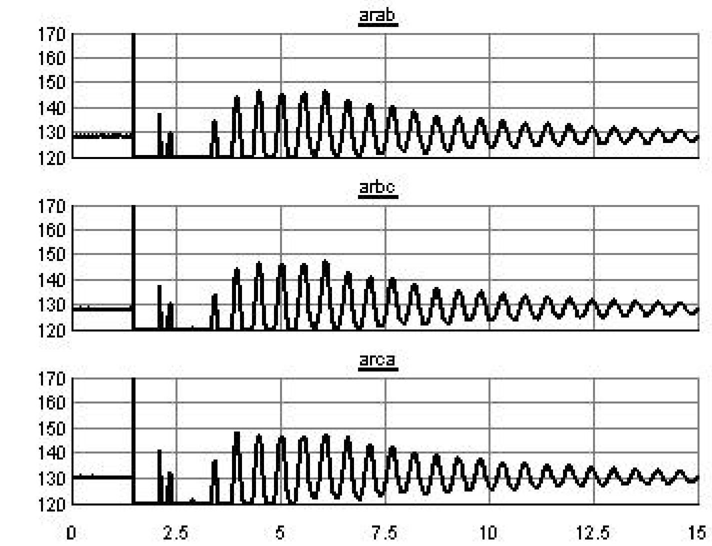

Fig. 6.60 Firing angles of the TCRs in time of a three-phase grounding fault far from the earth at the 500kV side

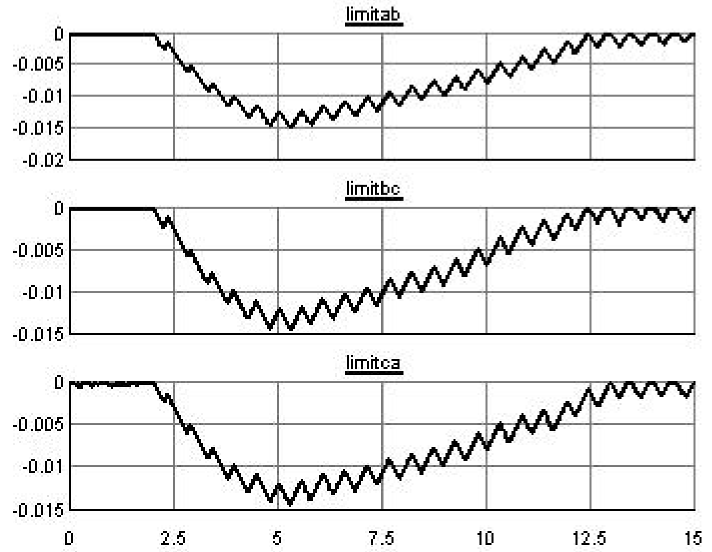

Fig. 6.61 Amplitudes of changing admittance limits in time of a three-phase grounding fault far from the earth at the 500kV side

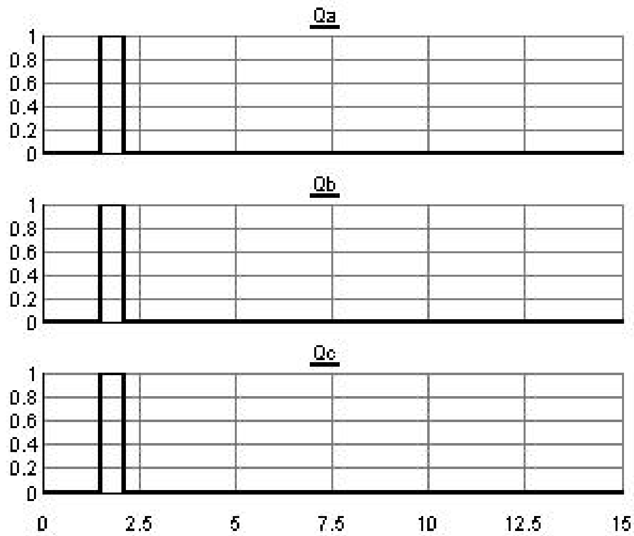

Fig. 6.62 Low-voltage protection in time of a three-phase grounding fault far from the earth at the 500kV side

As can be seen from the above figure, the low-voltage protection strategies of the SVC successfully suppress the overvoltage that may usually arise when the faults are tripped.

6.2.3.3 Three-phase fault far from the earth at the 220kV side

Fault description: A three-phase grounding fault occurs far from the earth at the 220kV side at the instant of 1.5s, and is cleared in 0.1s.

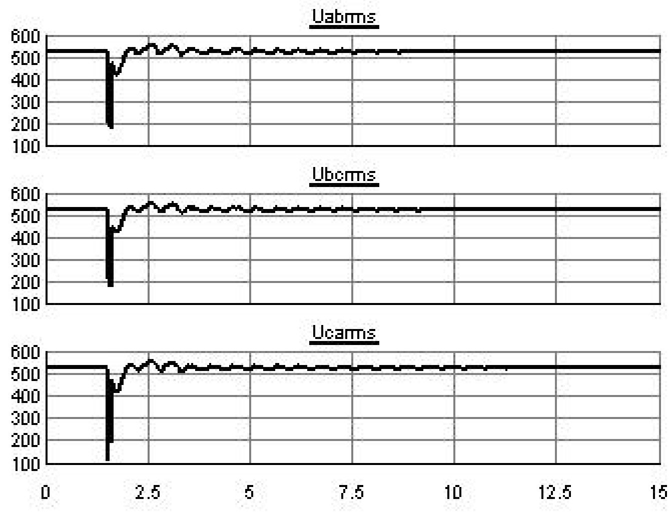

Fig. 6.63 Voltages at the 5000kV side of the SVC in time of a three-phase grounding fault far from the earth

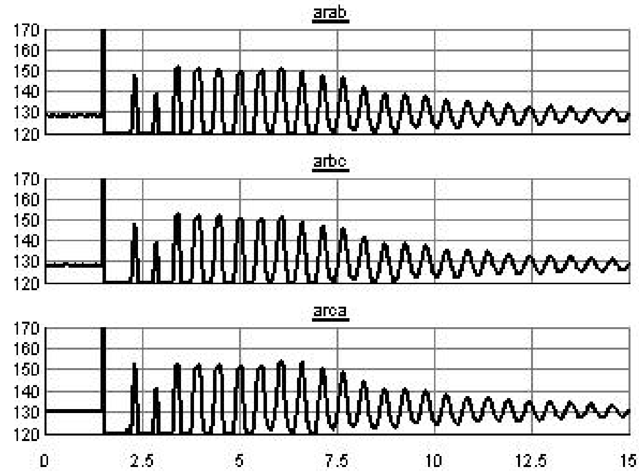

Fig. 6.64 Firing angles of the TCRs in time of a three-phase grounding fault far from the earth at the 220kV side

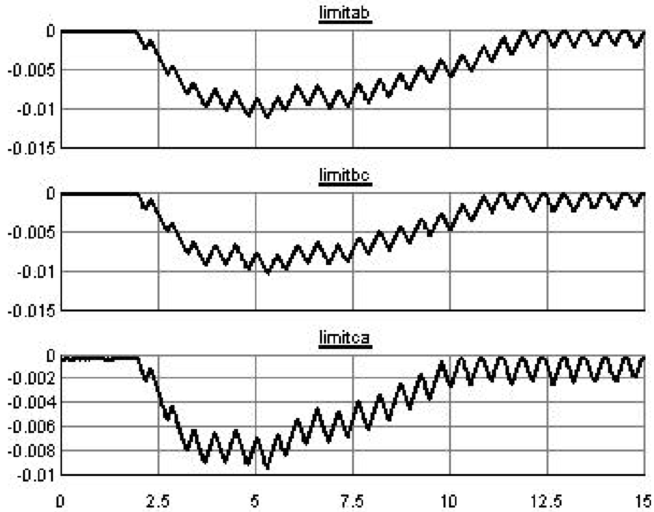

Fig. 6.65 Amplitudes of changing admittance limits in time of a three-phase grounding fault far from the earth at the 220kV side

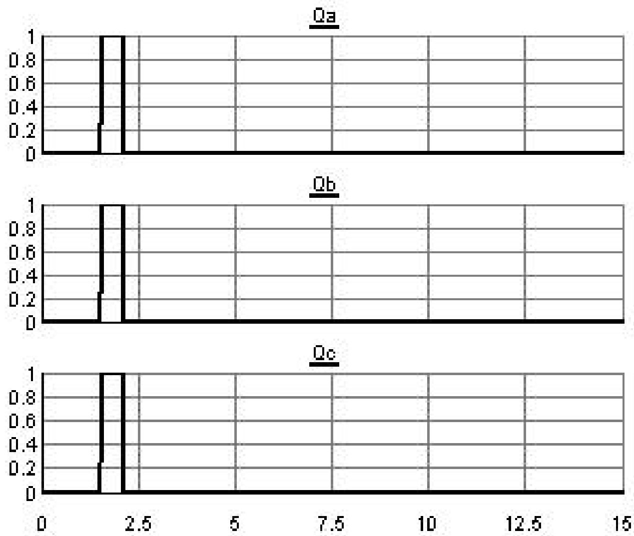

Fig. 6.66 Low-voltage protection in time of a three-phase grounding fault far from the earth at the 220kV side

As can be seen from the above figure, the low-voltage protection strategies of the SVC successfully suppress the overvoltage that may usually arise when the faults are tripped.

6.2.3.4 Three-phase fault near the earth at the 220kV side

Fault description: A three-phase grounding fault occurs near the earth at the 220kV side at the instant of 1.5s, and is cleared in 0.1s.

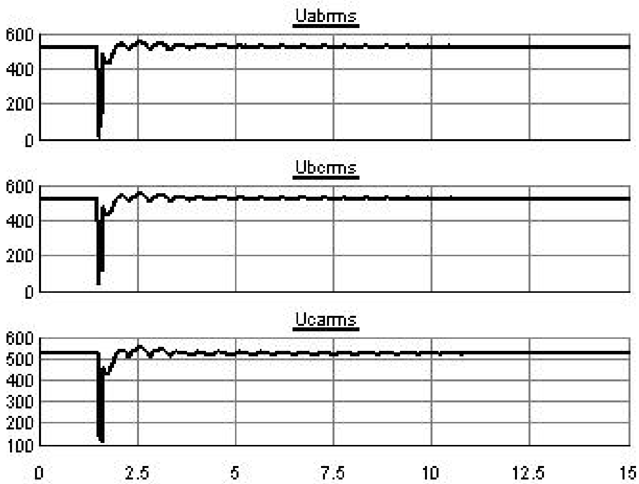

Fig. 6.67 Voltages at the 5000kV side of the SVC in time of a three-phase grounding fault near the earth at the 220kV side

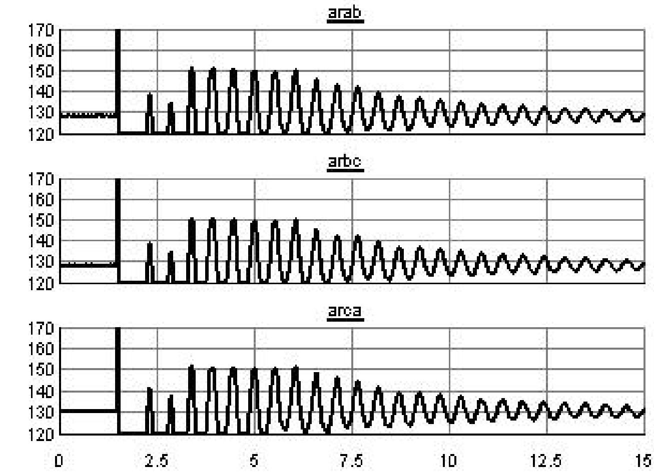

Fig. 6.68 Firing angle of the TCRs at the time of a three-phase short-circuit fault near the earth at the 220kV side

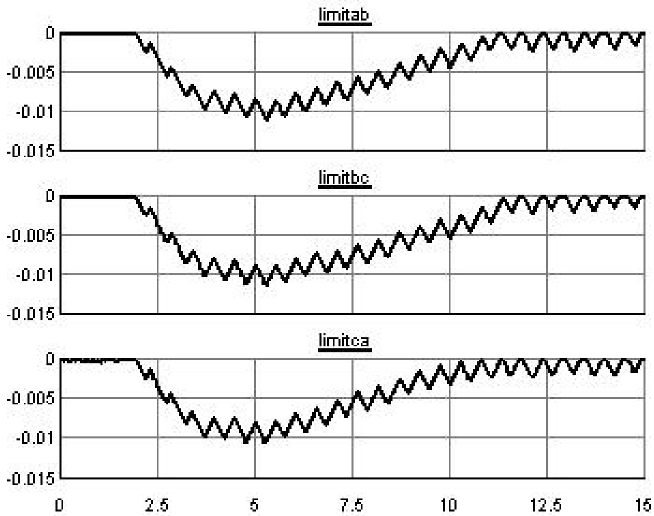

Fig. 6.69 Amplitudes of changing admittance limits in time of a three-phase grounding fault near the earth at the 220kV side

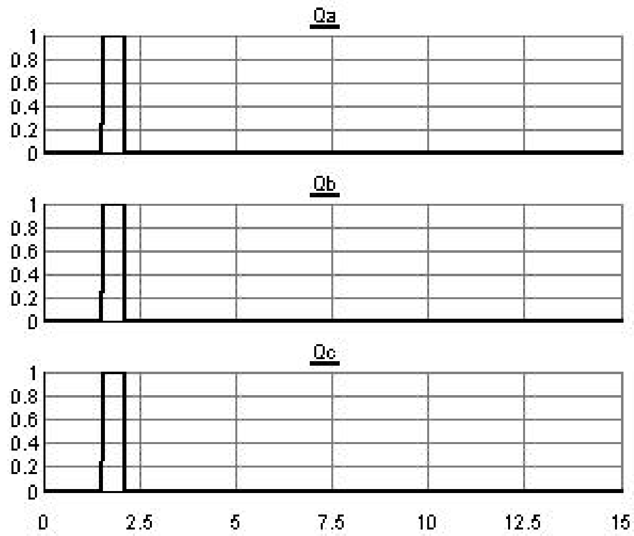

Fig. 6.70 Low-voltage protection in time of a three-phase grounding fault near the earth at the 220kV side

6.2.3.5 Single-phase fault near the earth at the 500kV side

Fault description: A single-phase grounding fault occurs near the earth at phase A at the 500kV side at the instant of 2s, and is cleared in 0.1s.

Fig. 6.71 shows the curves of the line voltages at the 500kV side changing over time when a single-phase grounding fault occurs near the earth at phase A at the 500kV side at the instant of 1.5s, and is cleared in 0.1s. Before the fault occurs at 1.5s, the system is in steady operation, and the voltages remain at 524kV. When the three-phase short-circuit fault occurs at 1.5s, the voltages drop quickly to below 100kV until the fault is cleared in 0.1s. Then there are voltage overshoots, and, in a short time (about 200ms), the voltages stabilize at 524kV, with fluctuations of 500V. And the voltage fluctuations are analyzed to result from the low-frequency oscillations of the system.

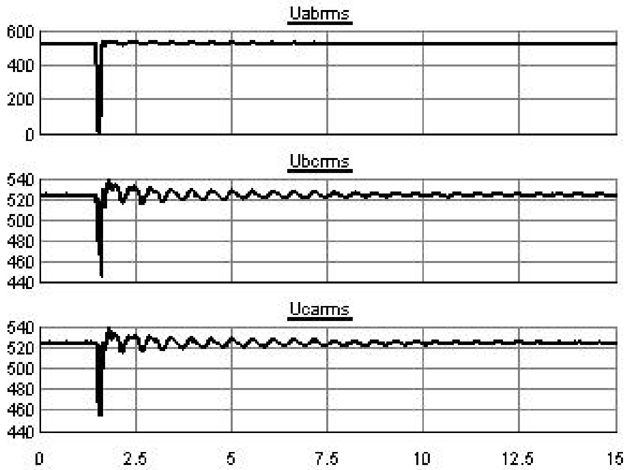

Fig. 6.71 Voltages at the 500kV side of the SVC in time of a single-phase grounding fault near the earth at the 500kV side

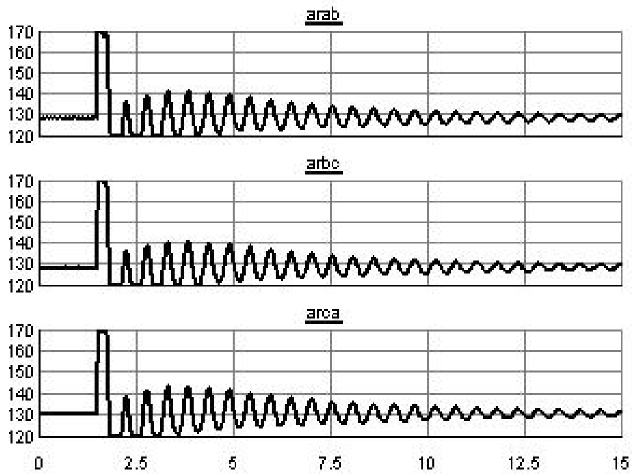

Fig. 6.72 Firing angles of the TCRs in time of a single-phase grounding fault near the earth at the 500kV side

Fig. 6.72 shows the curves of the firing angles of the TCRs changing over time when a single-phase grounding fault occurs near the earth at phase A at the 500kV side at the instant of 1.5s, and is cleared in 0.1s. Before the fault occurs at 1.5s, the system is in steady operation, and the firing angles of the TCRs are 130 degrees. When the singe-phase short-circuit fault at phase A occurs at 1.5s, the firing angles of the TCRs become 170 degrees quickly, proving the largest amount of reactive power for the system. After the fault is tripped, the firing angles change continuously to stabilize the voltages quickly until the firing angles finally stabilize at 130 degrees.

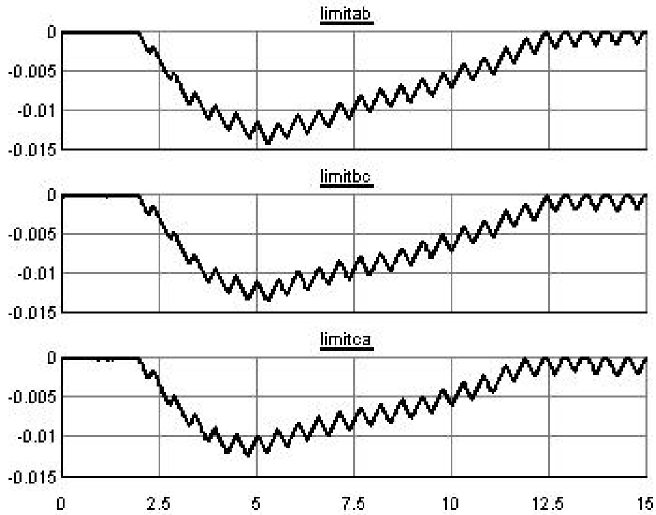

Fig. 6.73 Amplitudes of changing admittance limits in time of a single-phase grounding fault near the earth at the 500kV side

Fig. 6.73 shows the curves of amplitudes of changing admittance limits changing over time when a single-phase grounding fault occurs near the earth at phase A at the 500kV side at the instant of 1.5s, and is cleared in 0.1s. When the fault occurs, the admittance limits increase such that the SVC provides more reactive power for the system. After the fault is cleared, the admittance limits recover gradually.

6.2.3.6 Single-phase fault far from the earth at the 500kV side

Fault description: A single-phase grounding fault occurs far from the earth at phase A at the 500kV side at the instant of 1.5s, and is cleared in 0.1s.

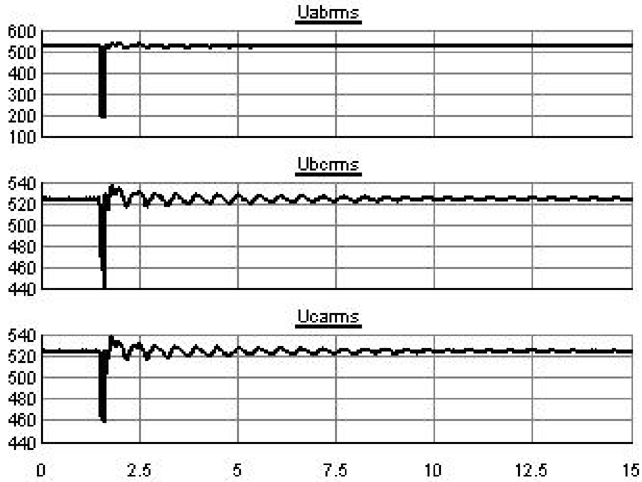

Fig. 6.74 Voltages at the 500kV side of the SVC in time of a single-phase grounding fault far from the earth

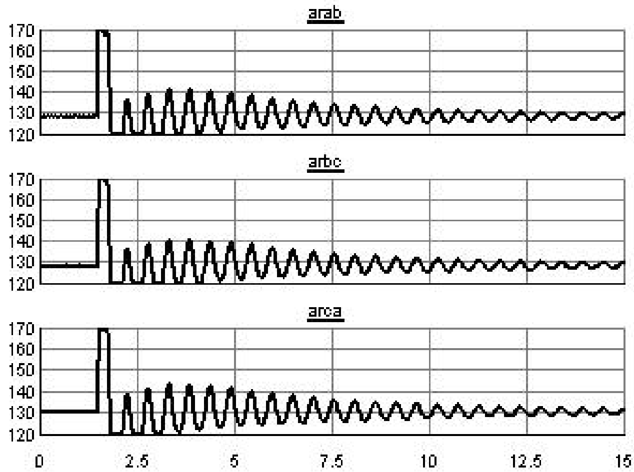

Fig. 6.75 Firing angles of the TCRs in time of a single-phase grounding fault far from the earth at the 500kV side

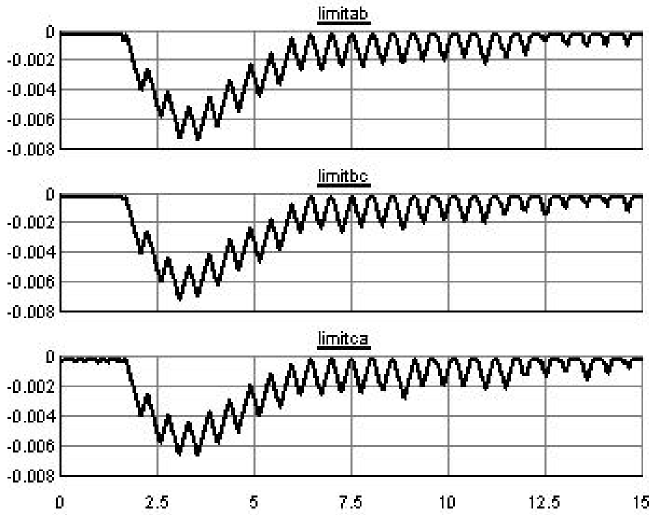

Fig. 6.76 Amplitudes of changing admittance limits in time of a single-phase grounding fault far from the earth at the 500kV side

6.2.3.7 Single-phase fault far from the earth at the 220kV side

Fault description: A single-phase grounding fault occurs far from the earth at phase A at the 220kV side at the instant of 1.5s, and is cleared in 0.1s.

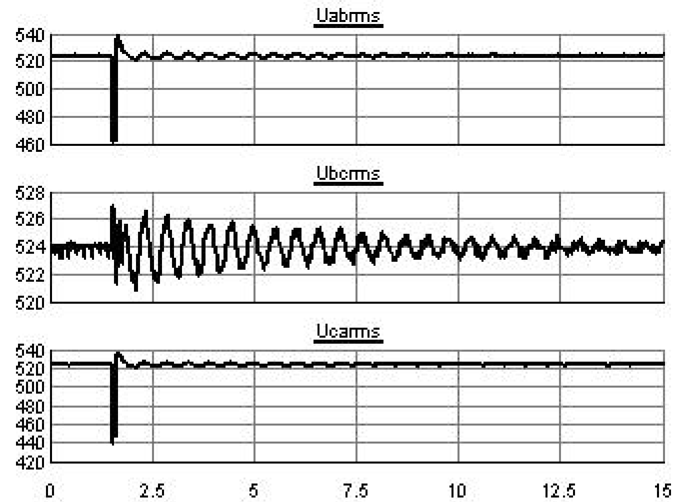

Fig. 6.77 Voltages at the 500kV side of the SVC in time of a single-phase grounding fault far from the earth at the 220kV side

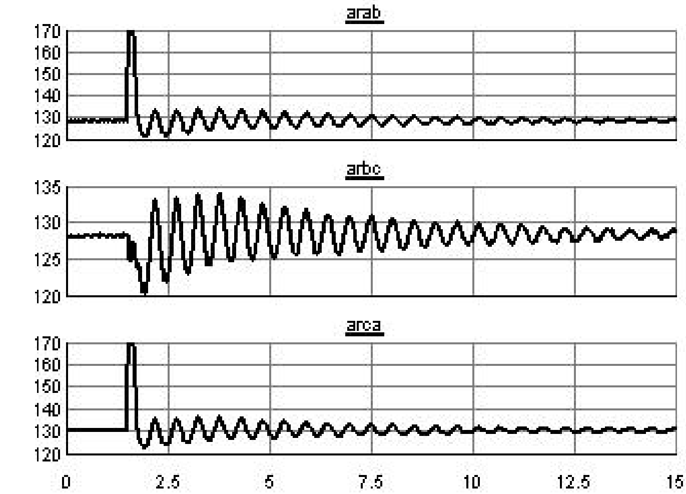

Fig. 6.78 Firing angles of the TCRs in time of a single-phase grounding fault far from the earth at the 220kV side

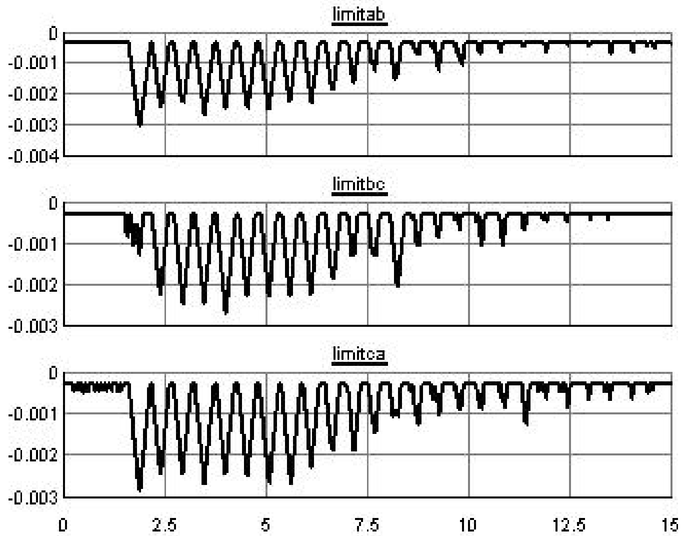

Fig. 6.79 Amplitudes of changing admittance limits in time of a single-phase grounding fault far from the earth at the 220kV side

6.2.3.8 Single-phase fault near the earth at the 220kV side

Fault description: A single-phase grounding fault occurs at phase A at the 220kV side at the instant of 1.5s, and is cleared at 0.1s.

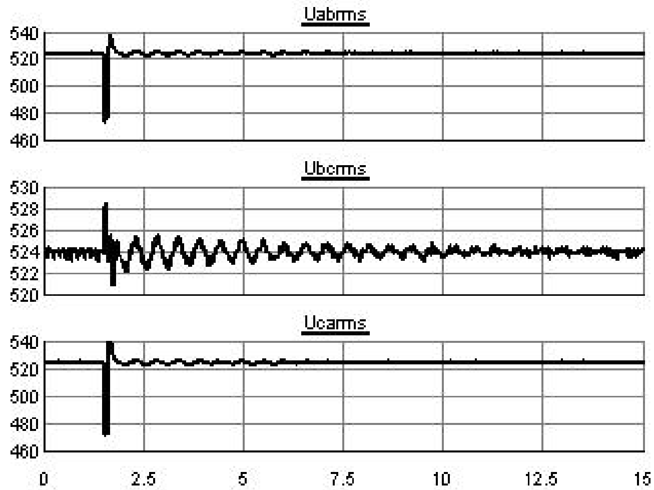

Fig. 6.80 Voltages at the 500kV side of the SVC in time of a single-phase grounding fault near the earth at the 220kV side

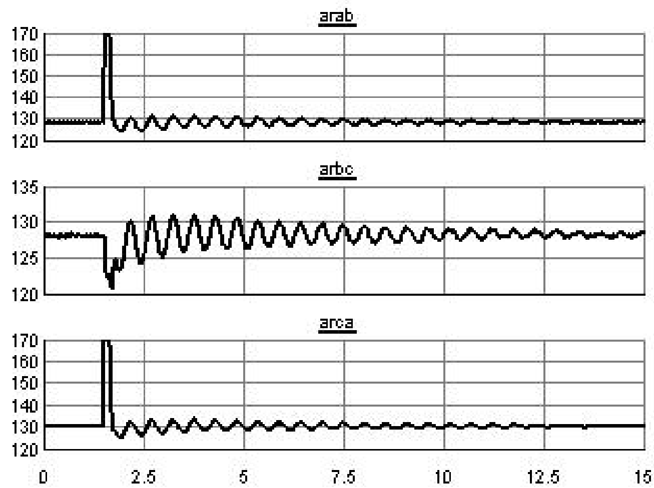

Fig. 6.81 Firing angles of the TCRs in time of a single-phase grounding fault near the earth at the 220kV side

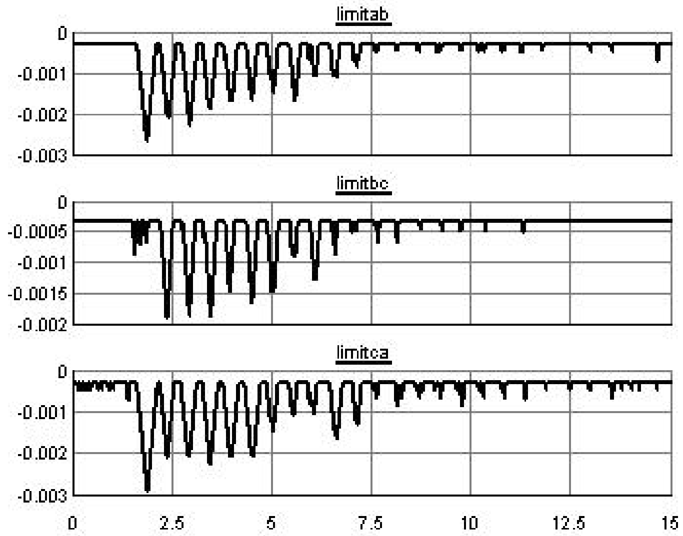

Fig.6.82 Amplitudes of changing admittance limits in time of a single-phase grounding fault near the earth at the 220kV side

6.2.3.9 N-1 fault at the 500kV side

Fault description: An N-1 fault occurs at the 500kV power transmission lines at the instant of 5s, and is cleared in 0.1s.

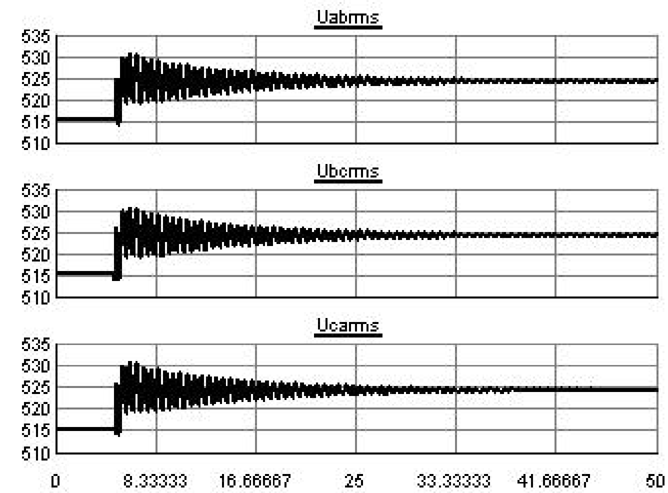

Fig. 6.83 RMS line voltages at the 500kV side when an N-1 fault occurs and the SVC is not in operation

Fig. 6.83 shows the curves of the RMS line voltages of the power transmission lines changing over time when the SVC is not in operation and an N-1 fault occurs at the 500kV power transmission lines. And it takes the voltages some time to stabilize.

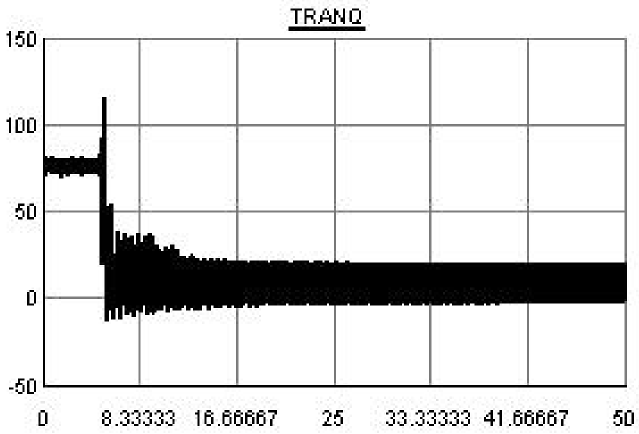

Fig. 6.84 Reactive power output of the SVC when an N-1 fault occurs at the 500kV side

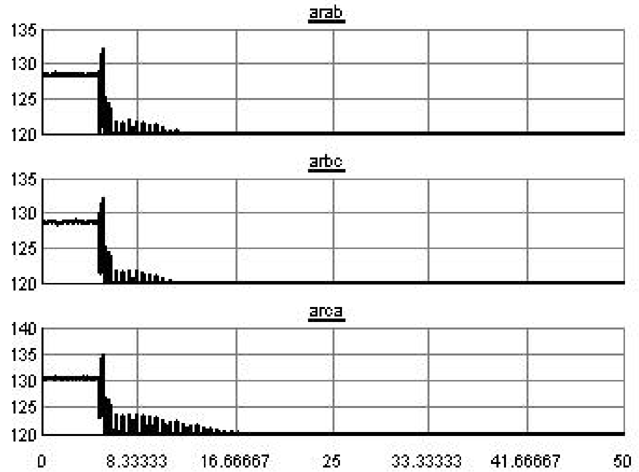

Fig. 6.85 Firing angles of the TCRs in time of an N-1 fault at the 500kV side

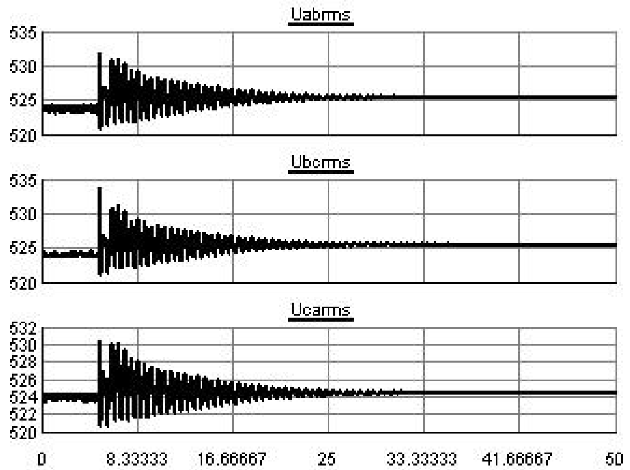

Fig. 6.86 Line voltages at the 500kV bus in time of an N-1 fault at the 500kV side

Fig. 6.84, Fig.6.85 and Fig.6.86 show the curves of the reactive power of the SVC, of the firing angles of the TCRs and of the line voltages at the 500kV bus when an N-1 fault occurs at the 500kV power transmission lines at 5s. Compared with the case that no SVC is in operation, the SVC can reduce the voltage fluctuations such that the voltages can stabilize in a short time. Compared with the SVC in steady operation, the SVC can provide more reactive power reserves in time of faults.

6.2.4 Simulations of Dynamic Operation Characteristics

Now, we will conduct flow calculations in a six-machine system and have the SVC installed in a weak voltage point. The SVC models have been introduced before. A three-phase grounding fault occurs at the 500kV side, and is cleared in 0.1s. We will study the rotation speeds of the two generators that contribute most to the flow at the installation point of the SVC.

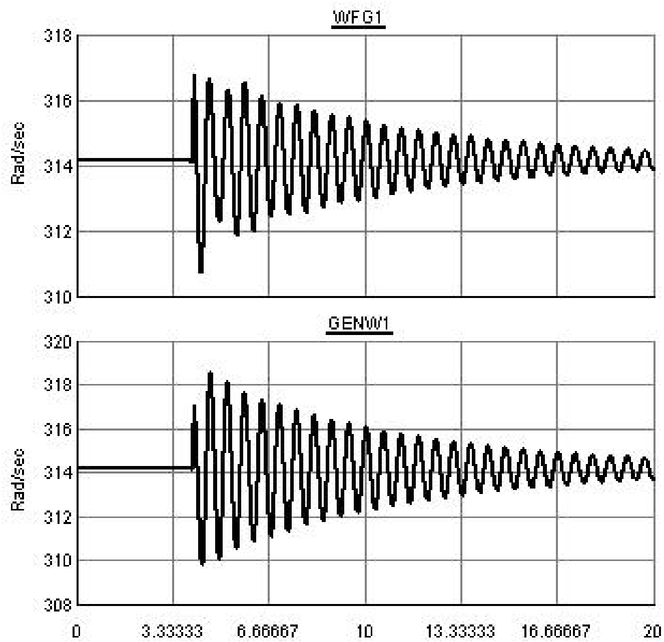

Fig. 6.87 Rotation speeds of the two generators when no SVC is in operation

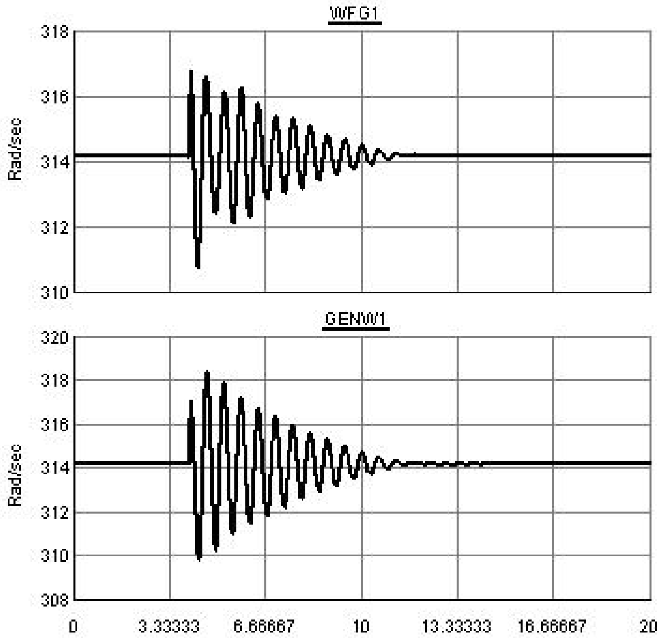

Fig. 6.88 Rotation speeds of the two generators when an SVC is in operation

According to the computations, the oscillation frequency is 1.7Hz. Fig. 6.87 shows that the rotation speeds of the two generators have not yet stabilized in 20 seconds starting from the fault occurrence when no SVC is in operation. Fig. 6.88 shows that the rotation speeds of the two generators have yet stabilized in 6 to 8 seconds starting from the fault occurrence when an SVC is in operation. This means that this control strategy can enhance the system damping and suppress oscillations.

6.3 Summary

Steady and transient simulation analyses in accordance with the single-machine infinite system and dynamic simulation analysis in accordance with the IEEE 30-bus system with PSCAD/EMTDC, and steady and transient simulation analyses in accordance with the single-machine infinite system and dynamic simulation analysis in accordance with the 6-machine system with RTDS (Real-time Digital Simulator) indicate that the control strategies can stabilize voltages and improve the rates of qualified voltages when the system is in steady states; the control strategies can help the SVC provide strong reactive power compensation and promote the system recovery when the system is in transient states; the control strategies can help the SVC increase dampings and suppress oscillations when the system is in dynamic states; the SVC is equipped with the functions of voltage control, admittance control, suppression of angle oscillation, low-frequency oscillation and subsynchronous resonance/oscillation, and deicing, fully capable of meeting the requirements of the SVC to be installed in Wuzhou.

So far, the SVC with the additional damping controller designed on the basis of Prony Identification has been in operation in Wuzhou Substations for more than two years, fully meeting the requirements of the expected technical indices of design and contributing a lot to improving the voltage stability and suppressing low-frequency oscillations in China Southern Power Grid.

CHAPTER 7 ALGORITHM IMPLEMENTATION AND ENGINEERING PRACTICE OF SUPPRESSING SUBSYNCHONOUS OSCILLATIONS WITH SVC

Dynamic voltage support and reactive power compensation have been generally accepted as a way to strengthen the power system performance. The main goal to install the SVC is to maintain the system voltage within a predefined range; the SVC can also improve the transient stability of the grid by providing dynamic support for the voltages of the key buses, and enhance the steady stability of the grid by increasing the system damping. One big advantage that distinguishes the SVC from other reactive power compensation devices lies in its rapid changes of reactive power output. So, by controlling the SVC properly, we can change the transmission characteristics of the system rapidly to increase the system damping effectively.

7.1 Introduction of the Subsynchronous Oscillation Phenomena in Guohua Jinjie Power Plant

The continuous application of such measures as series compensator compensation and HVDC in the power system has brought about tremendous economic benefit as well as stability problems for the power systems, and the subsynchronous resonance/oscillation is one of the main stability problems.

As early as in 1937, experts and scholars have proposed the subsynchronous resonance (SSR) problem, but the problem of the torsional oscillation of shafting has been overlooked all along. In 1970's, the generator shafts were damaged twice by the subsynchronous resonances in the Mohave Substation in the US, resulting in an upsurge of SSR research worldwide.

Research of SSR started late in our country. With the continuous increase of the capacity of the "Transmission of the West Power to the East" project, it is necessary to install series compensation capacitors in the long-distance AC power transmission lines, but this also brings about the SSR problems that are urgent to be solved. For example, there are SSR problems in the Guohua Jinjie Power Plant when series compensation capacitors are applied in the outward power transmission project.

Guohua Jinjie Power Plant is one of the key items of the "Transmission of the West Power to the East" project. There are 4×60MVA generators in Jinjie Power plant, a double-circuit power transmission lines between Jinjie and Xinzhou, and three-circuit lines between Xinzhou and Shijiazhuang for power transmission. If all of the four generators operate in full outputs, then the outward transmission capabilities are insufficient. So, fixed series capacitor compensators are installed in the double-circuit power transmission lines between Jinjie and Xinzhou and the three-circuit lines between Xinzhou and Shijiazhuang to alleviate the power transmission pressure. The series compensation degree is high, and theoretical calculation indicates that the series compensators installed in the above power transmission lines will result in subsynchronous resonance/oscillation in the shaftings of the generators.

In 1979, filtering and damping means were listed as one of the measures to alleviate the SSR problems. It has been applauded by experts from home and abroad to suppress subsynchronous resonance/oscillations with the FACTS devices, and has made great process both theoretically and in practice. As the most prevalent and stable equipment of the FACTS family, the SVC has been widely applied in the compensations of loads and power transmission lines. T. H. Putman and D. G. Ramey first proposed attenuating SSR with the SVC, i.e. connecting the thyristor-controlled reactors (TCRs), important parts of the SVC, to the terminal bus of the generator to be protected in parallel, and dampening the SSR by regulating the currents in the TCRs [7.1].

The research of subsynchronous resonance/oscillation started late in our country, and most scholars attach their importance to such FACTS devices as HVDC and TCSC. And the research of suppressing SSR with the SVC was almost blank before, and the research of the SVC mainly concentrated on the functions of voltage regulation.

It was just in this context that Shenhua Group decided to study how to suppress the subsynchronous resonance/oscillations of the generators in Jinjie Power Plant with the TCR+FC type of SVC. Four sets of SVCs have been installed at the terminal buses of the thermal power generator in Jinjie Power Plant and have been used to suppress subsynchronous resonance successfully. This was the first time the SVCs were used to suppress subsynchronous resonance/oscillation continuously.

The typical connection manner that has been applied abroad is to connect the TCRs to the 20kV bus at the generator terminal via a devoted transformer without power filters (FC), and this kind of devoted transformer offsets the major high-order harmonic currents through the special wiring manner of the multiple windings. This installation is also referred to as dynamic stabilizer. Analyses and research indicate that the SVC (TCR + FC) connects the 500kV bus in the power plant via a 500kV/35kV step-down transformer in a new connection manner, which only takes the unit shafting as the regulation and control signal of the TCRs and, in the coordination of appropriate parameters of the power filters, has good capability of suppressing subsynchronous resonance/osillation between the generators and the grid. The SVCs designed in this way have been put into operation in Jinjie Power Plant, and the results of field tests indicate that, the SVCs can suppress the subsynchronous resonance/oscillation as expected without having any bad impact on the grid.

7.2 Control Theory and Algorithm Implementation of Suppressing Subsynchronous Resonance with the SVC

7.2.1 Principle of Suppressing Subsynchronous Resonance with the SVC

As a kind of parallel compensator, the SVC has been widely used for dynamic compensation of reactive power to provide voltage support, enhance transient stability and ameliorate the oscillation damping characteristics.

The basic principle for the TCR part of the SVC is show in Fig. 7.1, where the susceptance of the compensation reactor is related to the conduction angle δ of the reactor, i.e. δ =2 π -2 α . After the rated inductance of the reactors is determined, the conduction angle of the thyristor controlled reactors can change the equivalent susceptance of the reactors in the circuit. The relationship between the equivalent susceptance and the firing angle of the compensation reactors is as follows:

$$Br = \frac{2\pi - 2\alpha + \sin 2\alpha}{\pi \omega L} \tag{7.1}$$

where

α is the firing angle of the reactors, and

L is the rated inductance of the reactors.

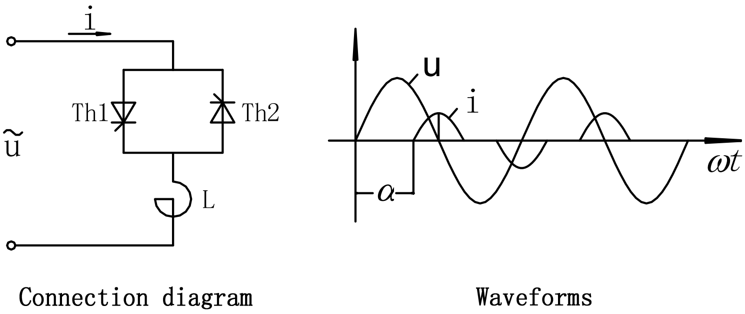

Fig. 7.1 Diagrams for the principle of the TCR

The total output of fundamental-frequency and subsynchronous-frequency currents of the SVC can be expressed by

$$i_{SVC} = u_1 \bullet B_1 + \sum_{k=1}^{N} u_k \bullet B_{1k} + i_{else} \tag{7.2}$$

where

u_1 is the fundamental-frequency voltage,

B_1 is the fundamental-frequency admittance of the SVC,

u_k is the subsynchronous-frequency voltage,

B_{1k} is the subsynchronous-frequency susceptance, and

i_{else} is the other negligible current components.

The fundamental-frequency susceptance of the SVC can be taken as the output of the fundamental value B_{ref1} of the input reference susceptance via an inertia link [7.2, 7.3]:

$$B_1 = B_{ref} \bullet \frac{e^{-sT_d}}{1 + sT_s} \tag{7.3}$$

where T_d is the lagging time constant of the thyristor loops, and T_s is the equivalent inertia time constant of the pulse control.

When subsynchronous resonance occurs, there may be subsynchronous-frequency voltage components in the bus voltage, and the subsynchronous-frequency voltage components will result in subsynchronous-frequency current components when imposed on the SVC. It is notable that the subsynchronous-frequency voltage components are far less than the power-frequency voltages in the grid, meaning that the subsynchronous-frequency current components resulting from subsynchronous-frequency voltage components are far less than the power-frequency currents, and that it is hard for the subsynchronous-frequency current components to change the subsynchronous-frequency characteristics of the grid. However, it requires to output currents that are reverse to the subsynchronous-frequency currents in direction to the generators to suppress the SSR with the SVC, which means introducing the subsynchronous-frequency components into the fundamental-frequency susceptance regulation process by regulating the susceptance of the SVC actively so that the required subsynchronous-frequency currents can be generated. The concrete approach is to add subsynchronous-frequency components to the fundamental-frequency reference susceptance of the SVC controller,

$$B_{1ref} = B_{10ref} + \sum_{k=1}^{N} B_{1kref}(t) \bullet \cos(\omega_k t + \phi_{kref}) \tag{7.4}$$

where

B_{1ref} is the new composite fundamental-frequency susceptance of the original fundamental-frequency reference susceptance and the subsynchronous-frequency components,

B_{10ref} is the DC current of the fundamental-frequency susceptance,

B_{1kref} is the fundamental-frequency components,

ω_k is the subsynchronous modal angular frequency of the shafting,

k is the number of subsynchronous modes of the shafting,

ϕ_{kref} is the initial phase of the subsynchronous-frequency components.

Since the susceptance finally outputted by the SVC controller is mainly dependent on the reference susceptance, we have

$$B_1 \approx B_{1ref} \tag{7.5}$$

Denote $u_1 = u_1(t) \bullet \cos \omega_1 t$, where ω_1 is the fundamental frequency.

Substituting the above equation into Equation (7.2), we get

$$u_1 \bullet B_1 \approx u_1(t) \bullet B_{10} \cos \omega_1 t + \frac{1}{2} \sum_{k=1}^{N} u_1(t) B_{1kref}(t) \bullet \cos \left[(\omega_1 \pm \omega_k) \bullet t \pm \phi_{kref} \right] \quad (7.6)$$

There are super-synchronous components at the right side of Equation (7.6), but these components are far away from the subsynchronous resonance frequency, and will not cause subsynchronous resonances. For facility of research, we ignore their impact, and field measurements also prove that such impact is negligible.

So, Equation (7.2) can also be expressed by

$$i_{SVC} = i_1 + i_{\omega_1 - \omega_k} + i_{else} \quad (7.7)$$

where

i_1 is the fundamental-frequency current, and

$i_{\omega_1 - \omega_k}$ is the subsynchronous-frequency currents.

As can be seen from the above derivation process, if various modal frequencies are added to the fundamental-frequency susceptance regulation process of the SVC, then the output currents will include subsynchronous-frequency current components of frequencies $\omega_1 - \omega_k$. These current components will enter the stator windings of the generator and generate subsynchronous torques of frequencies ω_k to suppress the SSR. By controlling the amplitudes and initial phases of the modulation signals, we can regulate the subsynchronous-frequency currents and the amplitudes and phases of corresponding subsynchronous torques so as to suppress the SSR. Field tests also verify that this method is effective.

The basic unit of the SVC used to suppress SSR is the TCR, but the TCRs can only provide inductive reactive power. To make the SVC generate capacitive reactive power, we need to connect capacitors in parallel to the bus of the TCRs. So we need to connect the main parts of the SVC, the TCRs and the FCs (the FCs are used to filter the harmonics of the TCR units and provide capacitive reactive power support), in parallel to the bus at the terminal of the protected generator or to the power transmission lines via a step-up transformer, and the SVC will attenuate the SSR by regulating the currents in the TCRs.

It is notable that there are four generators in Jinjie Power Plant, and the generators are connected to the two segments of power transmission buses via step-up transformers. To eliminate the oscillations among the generators, we need to connect the SVCs to the high-voltage power transmission buses, other than to the buses at the terminals of the protected generators as described in some past references. Such a parallel structure can make one set of SVC detect the subsynchronous resonance/oscillation signals generated by multiple generators that are connected to a bus segment in parallel simultaneously, and suppress the subsynchronous resonance/oscillations. Thus the subsynchronous resonance/oscillations generated by multiple generators that are connected to a bus segment in parallel can be eliminated, and these generators can be synchronized in the power transmission lines. The schematic diagram of single-phase structure of the SSR-DS system in Jinjie Power Plant is shown in Fig. 7.2.

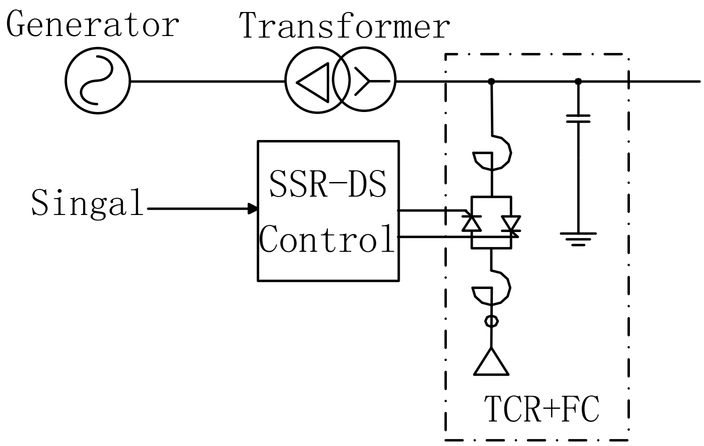

Fig. 7.2 Schematic diagram of single-phase structure of the SSR-DS system in Jinjie Power Plant

The SVC used to suppress the SSR can amplify the currents in time of resonance. We can select the testing quantities containing the modal components of torsional oscillation of the prime motors as the input signals of the controller, control the firing angles of the thyristors accordingly to change the angles of flow of the TCRs and the currents flowing through the branches, and further fine-tune the power output of the generators so that the generators can produce the damping torques to suppress the SSR. When there are no torsional oscillations in the shaftings of the generators, the SVC can be regarded as a stable and continuous reactive power load.

Such signals as the differences of the rotation speeds of the generators, the output power, and the differences of the speeds of high-voltage cylinders all contain the modal components of torsional oscillations. Experiments indicate that the latter two kinds of signals are more sensitive to the phase shift of the controller. So we choose the differences of the rotation speeds as the input signals of the controller, which can enhance the testing precision and are easy for engineering implementation, so as to enhance the control results of the SVC.

When the differences of the rotation speeds are taken as the input signals of the controller, the reactive currents in the TCRs need to be regulated such that the currents and the differences of the rotation speeds of the generators are in reverse directions, i.e. they have a phase shift of 180 degrees. Thus, when the generator rotor speeds increase, the inductive currents in the TCRs decrease, i.e. the reactive power absorbed by the TCRs drops. Then, both the voltages at the terminals of the generators and the electromagnetic power output increase, and, as a result, the power outputs of the generators are increased. But for the constant mechanical input, the increase of electromagnetic power will result in the decrease of the kinetic energy of the rotors, and in the drop of the rotor speeds finally. Conversely, the decreases of speeds will lead to the increases of the inductive currents in the TCRs, the decrease of the electromagnetic power output of the generators, and the acceleration of the rotors of the generators. On the basis of the fast response characteristics of the TCRs, the goal of suppressing subsynchronous resonance/oscillations can be achieved. The structure diagram of this system is shown in Fig.7.3, and the block diagram for the principle of the controller is shown in Fig. 7.4.

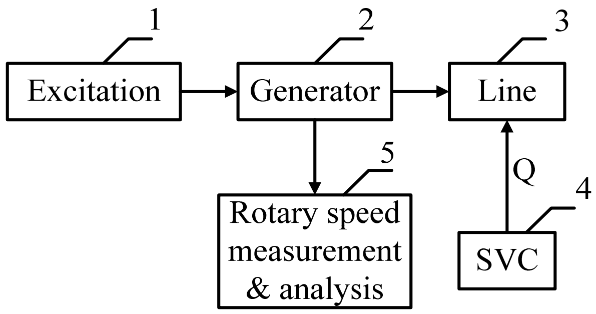

Fig. 7.3 Diagram of the SSR-DS structure

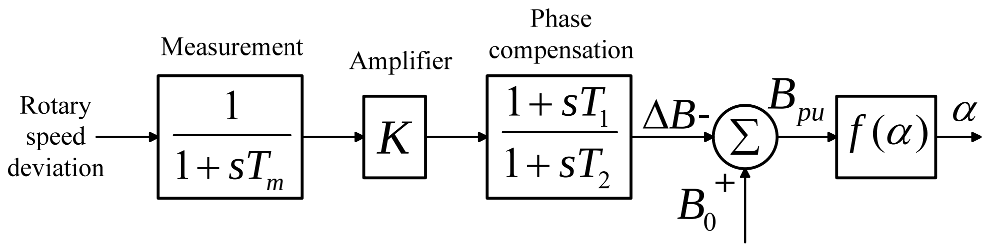

Fig. 7.4 Block diagram of the SSR-DS system control principle

7.2.2 Research and Implementation of the Algorithm of Suppressing Subsynchronous Resonance with the SVC in Jinjie Power Plant

As the principle described above indicates, the TCR+FC type of SVCs that are widely applied in the grids currently can suppress the subsynchronous resonance/oscillations, but the above research still stay in theoretical research of simulation research stage. We have made concrete method of engineering implementation, and this was the first actual engineering practice.

The controller of the SVC used to suppress the subsynchronous resonance/oscillations in Jinjie Power Plant applies the proportion control strategy, taking the differences of the rotation speeds of the generators as the input signals of the controller. The differences of the rotation speeds produce the subsynchronous rotation speed components corresponding to various frequencies after the filtering link, and the components are summated after passing through the phase compensation link and the proportional link such that the reactive currents of the TCRs and the differences of the rotation speeds are reverse in the phases, and the SSR is suppressed.

When the system is in stable operation, the TCRs operate stably at a certain fixed angle of flow, equivalent to a stable and continuous reactive power load.

According to the theoretical calculations and field measurements, the three central frequencies of the subsynchronous resonance/oscillation frequencies of the four generators in Jinjie Power Plan are 13.02Hz, 22.77Hz and 28.16Hz respectively. Since the generators are from the same manufacturer and share basically the same central frequencies, they can apply the same pattern in the control algorithm with the same operation parameters.

After the three central frequencies are determined, we will determine the core control algorithm of the control system in three links: filtering link, proportional phase-shift link, and weighted summation link. The concrete control algorithm is shown in Fig.7.5.

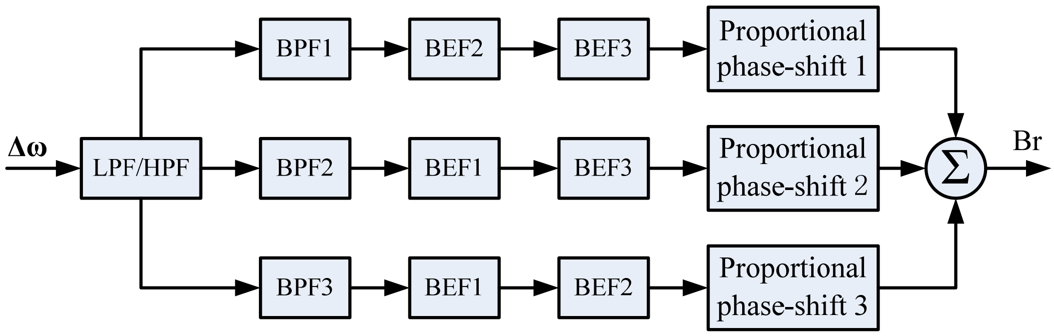

Fig. 7.5 Block diagram of the control algorithm

All the links shown in Fig.7.5 accomplish the testing and processing of the signals together, where

(1) The functions of the low-pass and high-pass filters are to filter out the signals that are above 50Hz or below 10Hz, such that the central subsynchronous frequencies can remain in the output signals.

(2) Band-pass filters 1, 2 and 3 mainly perform filtering for the three subsynchronous central frequencies, and to ensure the real-time properties of the control system, we choose the orders of the filters to be fairly low and rely on the band-stop filters for precise processing.

(3) Band-stop filters 1, 2 and 3 are corresponding to the three central subsynchronous frequencies. For example, for central frequency 1, band-stop filters 2 and 3 are used to further filter out the other two central frequencies, only leaving the subsynchronous signals of central frequency 1 in the final output signals. The other two central frequencies can be processed in the same manner.

(4) Proportional phase shifts 1, 2 and 3 are used to compensate for the changes of gains and phases such that the final output and the input signals of rotation speeds are basically reverse in the phases, and to summate the output signals in a weighted way to

yield the signal of the equivalent admittance Br corresponding to the TCRs. Then the control system processes the equivalent admittance and sends out triggering pulses such that the SVC can generate the currents or reactive power necessary for the suppression of subsynchronous resonance/oscillations and the subsynchronous resonance/oscillations are suppressed by the currents or reactive power flowing through the bus that the SVC is connected to.

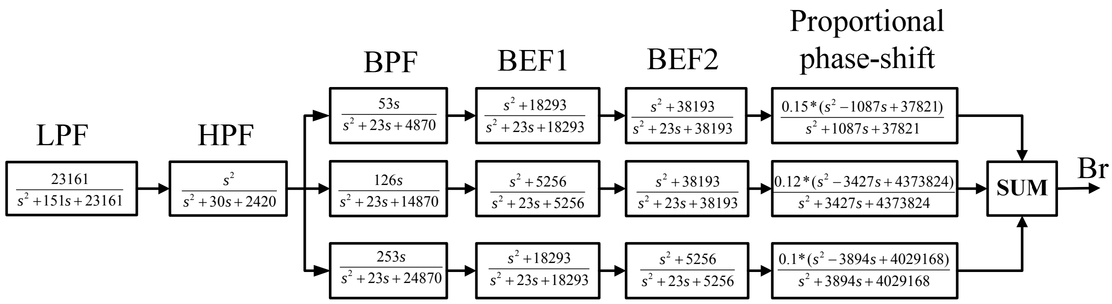

Fig. 7.6 Transfer function of the SSR-DS

Fig.7.6 shows the transfer function adopted by the SSR-DS. And the simulation results of the suppression of subsynchronous resonance in Jinjie Power Plant are shown in Fig.7.7.

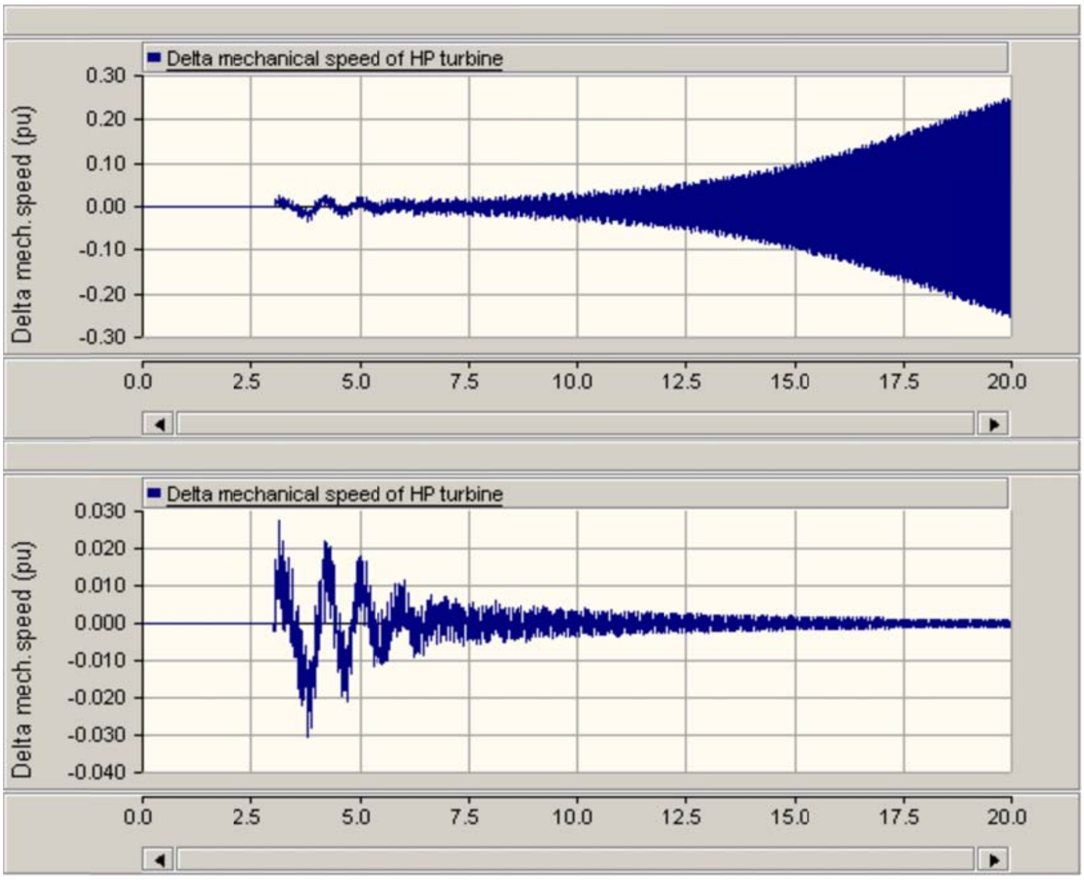

Fig. 7.7 Deviations of the rotation speeds of No.1 generator (upper: without SSR-DS; lower: with SSR-DS)

In accordance with the four generators in Jinjie Power Plant that are connected to the two segments of high-voltage power transmission buses via step-up transformers, we conducted theoretical analysis and simulation, modified the connection manner described by the IEEE that the SVCs must be connected to the terminal buses boldly, divided the four sets of SVCs into two combinations, with two SVCs in each combination, and connected the two combinations of SVCs to the two segments of high-voltage power transmission lines. The schematic diagram for the final system structure is shown in Fig.7.8.

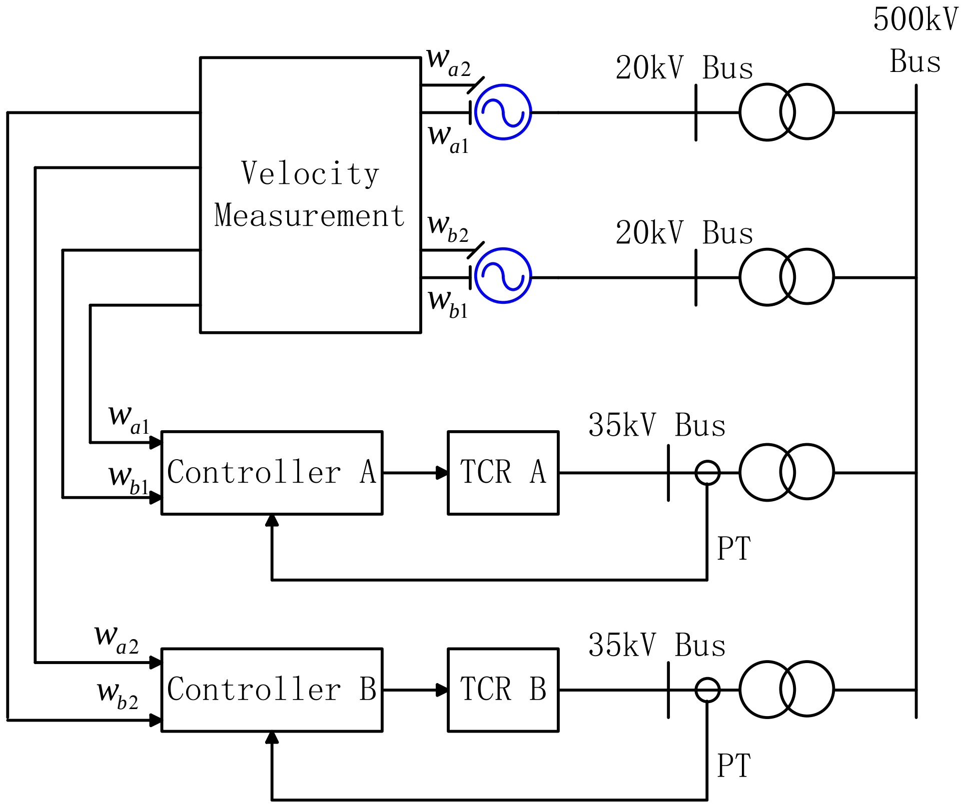

Fig. 7.8 Schematic diagram of the system structure (half of the whole project)

Fig. 7.8 shows the schematic diagram of the system structure of half the whole project, and the diagram of the other half is virtually identical. The two controllers of the two SVCs connected to each bus segment are mutually spare for both generators, and one controller can enable the SVCs to suppress the subsynchronous resonance/oscillations of the two generators connected to the same 500kV bus segment.

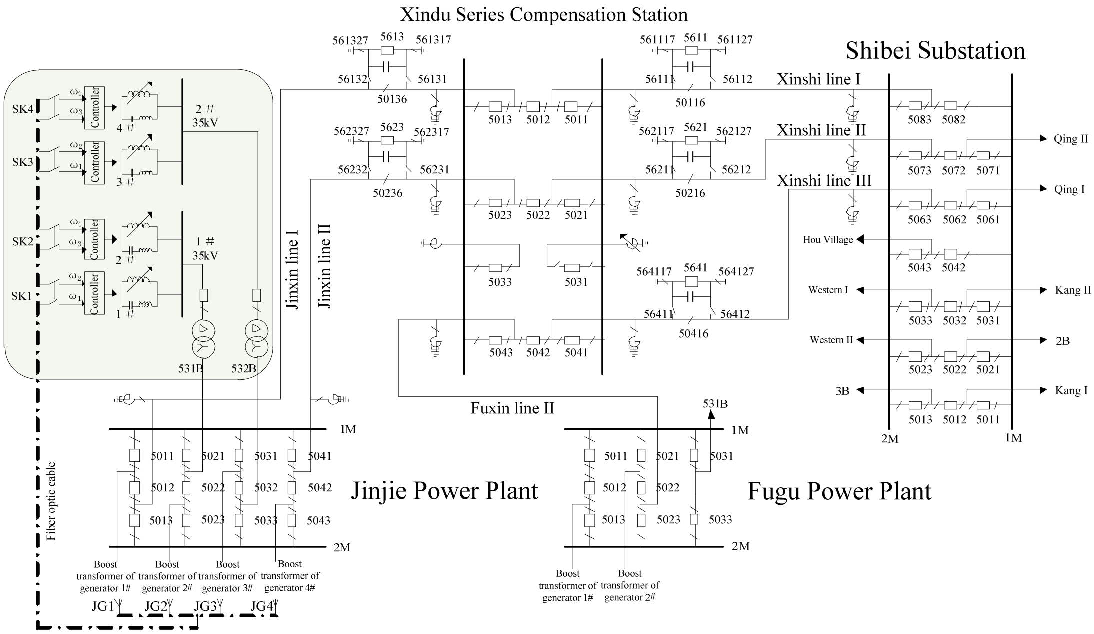

Fig. 7.9 Diagram of power transmission lines in Jinjie Power Plant (Provided by Jinjie Power Plant)

Fig.7.9 shows the diagram of power transmission lines in Jinjie Power Plant, where the four sets of SVCs are connected to two segments of high-voltage buses as are shown at the top left of the diagram.

7.3 Dynamic Simulation Experiments of Subsynchronous Resonance Suppression in Jinjie Power Plant

7.3.1 General

Dynamic simulation experiments of SSR suppression by the SSR-DS were conducted with the SVC controllers, silicon-controlled valve banks, reactors, speed measuring sensors, testing devices as well as the unit platform (ABB VFD, variable-frequency speed-regulating three-phase asynchronous motors, three-phase synchronous generators, excitation power sources) in the State Key Laboratory of

Power System in Tsinghua University to test the principle of suppressing the SSR by the SSR-DS and the effectiveness of the SSR-DS controller.

Experiments were done to activate and suppress the SSR with the SSR-DS in the three working conditions (generators connected to the grid directly, generators connected to the grid via series reactors, and generators loaded and not connected to the grid) on the generation unit platform, and to test the impact of phase correction parameters and proportional gain parameters on the SSR suppression. Analysis of the experiment data indicated that the results of SSR-DS on SSR activation and suppression are different under the three working conditions, with the results being the best, the medium and the worst under the conditions that the generators are loaded and not connected to the grid, are connected to the grid via series reactors, and are connected to the grid directly. The SSR-DS mainly generates the third-, fifth- and seventh-order harmonics with little impact on the system voltages and with a response time of below 300ms. The results of SSR suppression by the SSR-DS are shown by the experiment data tabulated in Table 7.1.

Table 7.1 Main data of dynamic simulation experiments of SSR-DS

No.	Operation manner of generators		SSR amplitude (rad/s)	Suppression results
1	directly connected to the grid	superimposition of 13.02Hz subsynchronous signals	0.035	No results
		superimposition of 13.02Hz subsynchronous signals + SSR-DS in compensatory operation (suppression)	0.036	
		superimposition of 22.77Hz subsynchronous signals	0.017	No results
		superimposition of 22.77Hz subsynchronous signals + SSR-DS in compensatory operation (suppression)	0.018	
		superimposition of 28.16Hz subsynchronous signals	0.01	No results
		superimposition of 28.16Hz subsynchronous signals + SSR-DS in compensatory operation (suppression)	0.013	
2	connected to the grid via series reactors	superimposition of 13.02Hz subsynchronous signals	0.033	**27.3%**
		superimposition of 13.02Hz subsynchronous signals + SSR-DS in compensatory operation (suppression)	0.024	
		superimposition of 22.77Hz subsynchronous signals	0.0092	**62%**
		superimposition of 22.77Hz subsynchronous signals + SSR-DS in compensatory operation (suppression)	0.0035	
		superimposition of 28.16Hz subsynchronous signals	0.006	**56.7%**
		superimposition of 28.16Hz subsynchronous signals + SSR-DS in compensatory operation (suppression)	0.0026	
3	loaded and not connected to the grid	superimposition of 13.02Hz subsynchronous signals	0.045	**64.4%**
		superimposition of 13.02Hz subsynchronous signals + SSR-DS in compensatory operation (suppression)	0.016	
		superimposition of 22.77Hz subsynchronous signals	0.052	**65.4**
		superimposition of 22.77Hz subsynchronous signals + SSR-DS in compensatory operation (suppression)	0.018	
		superimposition of 28.16Hz subsynchronous signals	0.0075	**86.7%**
		superimposition of 28.16Hz subsynchronous signals + SSR-DS in compensatory operation (suppression)	0.001	

The conclusions are:

(1) The design of the rotation speed testers interfaced with the SSR-DS meets the design requirements in terms of precision.

(2) The design of the various modal filtering links of the rotation speed signals of the SSR-DS meets the design requirements in terms of precision.

(3) The holistic phase-delaying method of the rotation speed correcting sensors and rotation testers, the processing and operation link of the rotation speed signals, and the SSR-DS triggering link is correct.

(4) Theoretical analysis of the impact of the coefficients in the phase correction links on the suppression of SSR by the SSR-DS tallies with the practice.

(5) Theoretical analysis of the impact of the coefficients in the gain links on the suppression of SSR by the SSR-DS tallies with the practice.

(6) The rotation speed testers and the SSR-DS controllers meet the design requirements in terms of holistic performance.

(7) The actual output signals of the SSR-DS tally with the theoretical analysis.

(8) Experiments show that the SSR-DS can suppress the SSR effectively.

For the concrete contents of experiments, please refer to the following section in this chapter.

7.3.2 Contents of Dynamic Simulation Experiments

7.3.2.1 Items and Curves of Experiments

First, the variable frequency drives by ABB drove the three-phase asynchronous motors, and the motors continued to drive the synchronous generators to generate electricity (generators connected to the grid directly, generators connected to the grid via series reactors, and generators loaded and not connected to the grid). Then, the rotation speeds of the synchronous generators were measured, and if no constant subsynchronous rotation speed signals could be detected out of the rotation speed signals, then the SSR-DS system would be integrated into system to provide fixed-frequency (13.02Hz, 22.72Hz, 28.16Hz) subsynchronous compensation. After that, the rotation speeds of the synchronous generators were measured again, and if constant subsynchronous rotation speed signals could be detected out of the rotation speed signals, the experiment of activating the SSR by SSR-DS was successful.

Next, the variable frequency drives by ABB was rebooted to start the three-phase asynchronous motors in a constant-torque and closed-loop way, and the motors drove the synchronous generators to generate electricity (generators connected to the grid directly, generators connected to the grid via series reactors, and generators loaded and not connected to the grid). After that, the rotation speeds of the synchronous generators were measured, and if any constant subsynchronous rotation speed signals could be detected out of the rotation speed signals, then the SSR-DS would be integrated into the system. Later, the rotation speeds of the synchronous generators were measured again, and if the subsynchronous rotation speed signals could be detected to be weaker, then the experiment of suppressing the SSR by SSR-DS was successful.

Table 7.2 Experiment items and records

No.	Operation manner of generators		SSR amplitude (rad/s)	Remarks
1	directly connected to the grid	generators in sole operation	0.001	Fig.7.10
		13.02Hz subsynchronous torsional oscillations aroused by SSR-DS	0.009	Fig.7.10
		22.72Hz subsynchronous torsional oscillations aroused by SSR-DS	0.0038	Fig.7.11
		28.16Hz subsynchronous torsional oscillations aroused by SSR-DS	0.007	Fig.7.12
		superimposition of 13.02Hz subsynchronous signals	0.035	Fig.7.13
		superimposition of 13.02Hz subsynchronous signals + SSR-DS in compensatory operation	0.036	Fig.7.13
		superimposition of 22.77Hz subsynchronous signals	0.017	Fig.7.14
		superimposition of 22.77Hz subsynchronous signals + SSR-DS in compensatory operation	0.018	Fig.7.14
		superimposition of 28.16Hz subsynchronous signals	0.01	Fig.7.15
		superimposition of 28.16Hz subsynchronous signals + SSR-DS in compensatory operation	0.013	Fig.7.15
2	connected to the grid via series reactors	generators in sole operation	0	Fig.7.16
		13.02Hz subsynchronous torsional oscillations aroused by SSR-DS	0.01	Fig.7.16
		22.77Hz subsynchronous torsional oscillations aroused by SSR-DS	0.012	Fig.7.17
		28.16Hz subsynchronous torsional oscillations aroused by SSR-DS	0.013	Fig.7.18
		superimposition of 13.02Hz subsynchronous signals	0.033	Fig.7.19
		superimposition of 13.02Hz subsynchronous signals + SSR-DS in compensatory operation	0.024	Fig.7.19
		superimposition of 22.77Hz subsynchronous signals	0.0092	Fig.7.20
		superimposition of 22.77Hz subsynchronous signals + SSR-DS in compensatory operation	0.0035	Fig.7.20
		superimposition of 28.16Hz subsynchronous signals	0.006	Fig.7.21
		superimposition of 28.16Hz subsynchronous signals + SSR-DS in compensatory operation	0.0026	Fig.7.21

3	loaded and not connected to the grid	generators in sole operation	0	Fig.7.22
		13.02Hz subsynchronous torsional oscillations aroused by SSR-DS	0.014	Fig.7.22
		22.72Hz subsynchronous torsional oscillations aroused by SSR-DS	0.006	Fig.7.23
		28.16Hz subsynchronous torsional oscillations aroused by SSR-DS	0.011	Fig.7.24
		superimposition of 13.02Hz subsynchronous signals	0.045	Fig.7.25
		superimposition of 13.02Hz subsynchronous signals + SSR-DS in compensatory operation	0.016	Fig.7.25
		superimposition of 22.77Hz subsynchronous signals	0.052	Fig.7.26
		superimposition of 22.77Hz subsynchronous signals + SSR-DS in compensatory operation	0.018	Fig.7.26
		superimposition of 28.16Hz subsynchronous signals	0.0075	Fig.7.27
		superimposition of 28.16Hz subsynchronous signals + SSR-DS in compensatory operation	0.001	Fig.7.27
4	connected to the grid via series reactors, with a phase shift	superimposition of 13.02Hz subsynchronous signals	0.045	Fig.7.28
		superimposition of 13.02Hz subsynchronous signals + SSR-DS in compensatory operation + a phase shift of 0°	0.036	Fig.7.28
		superimposition of 13.02Hz subsynchronous signals + SSR-DS in compensatory operation + a phase shift of -30°	0.041	Fig.7.29
		superimposition of 13.02Hz subsynchronous signals + SSR-DS in compensatory operation + a phase shift of -20°	0.041	Fig.7.30
		superimposition of 13.02Hz subsynchronous signals + SSR-DS in compensatory operation + a phase shift of -10°	0.038	Fig.7.31
		superimposition of 13.02Hz subsynchronous signals + SSR-DS in compensatory operation + a phase shift of +10°	0.038	Fig.7.32
		superimposition of 13.02Hz subsynchronous signals + SSR-DS in compensatory operation + a phase shift of +20°	0.041	Fig.7.33
		superimposition of 13.02Hz subsynchronous signals + SSR-DS in compensatory operation + a phase shift of +30°	0.043	Fig.7.34
5	connected to the grid via series reactors, with a gain proportion	superimposition of 13.02Hz subsynchronous signals	0.011	Fig.7.35
		superimposition of 13.02Hz subsynchronous signals + SSR-DS in compensatory operation + a gain proportion of 100％	0.0045	Fig.7.35
		superimposition of 13.02Hz subsynchronous signals + SSR-DS in compensatory operation + a gain proportion of 75％	0.005	Fig.7.36
		superimposition of 13.02Hz subsynchronous signals + SSR-DS in compensatory operation + a gain proportion of 50％	0.006	Fig.7.37
		superimposition of 13.02Hz subsynchronous signals + SSR-DS in compensatory operation + a gain proportion of 25％	0.008	Fig.7.38

The recorded figures of the experiments are as follows:

(NOTE: In each of the following relative figures (Fig. 7-10 to 7-38), the top curve is the rotational speed signal, the middle curve is Fourier analysis for rotational speed signal with SVC installed, and the bottom curve is Fourier analysis for rotational speed signal without SVC.)

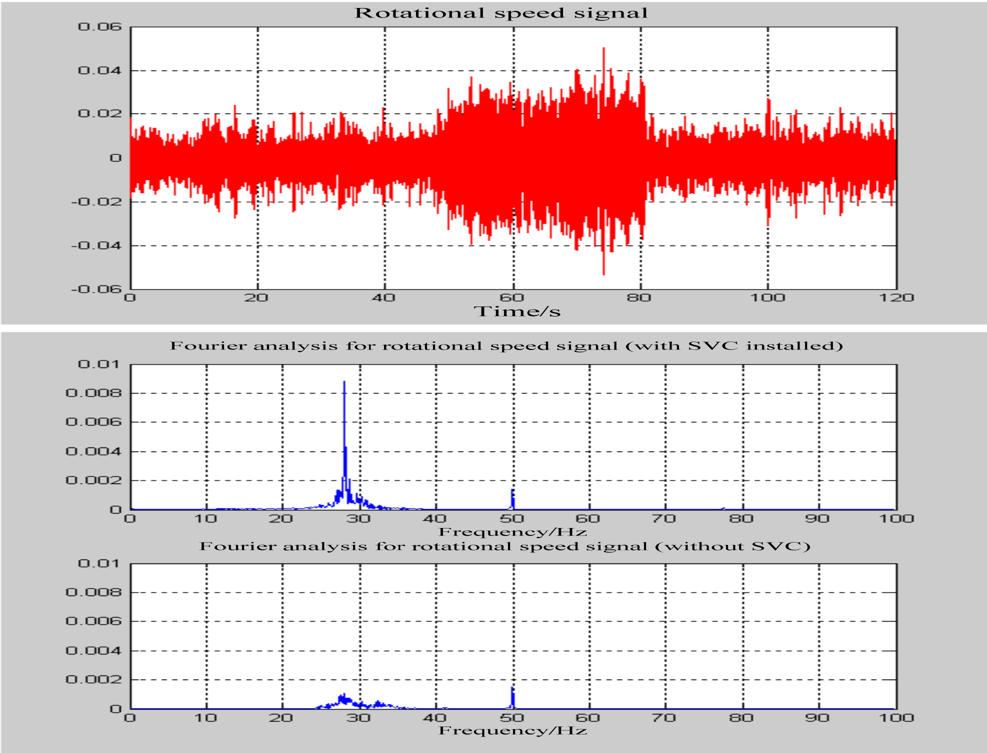

Fig. 7.10 Generators directly connected to the grid + 13.02Hz subsynchronous torsional oscillations aroused by SSR-DS

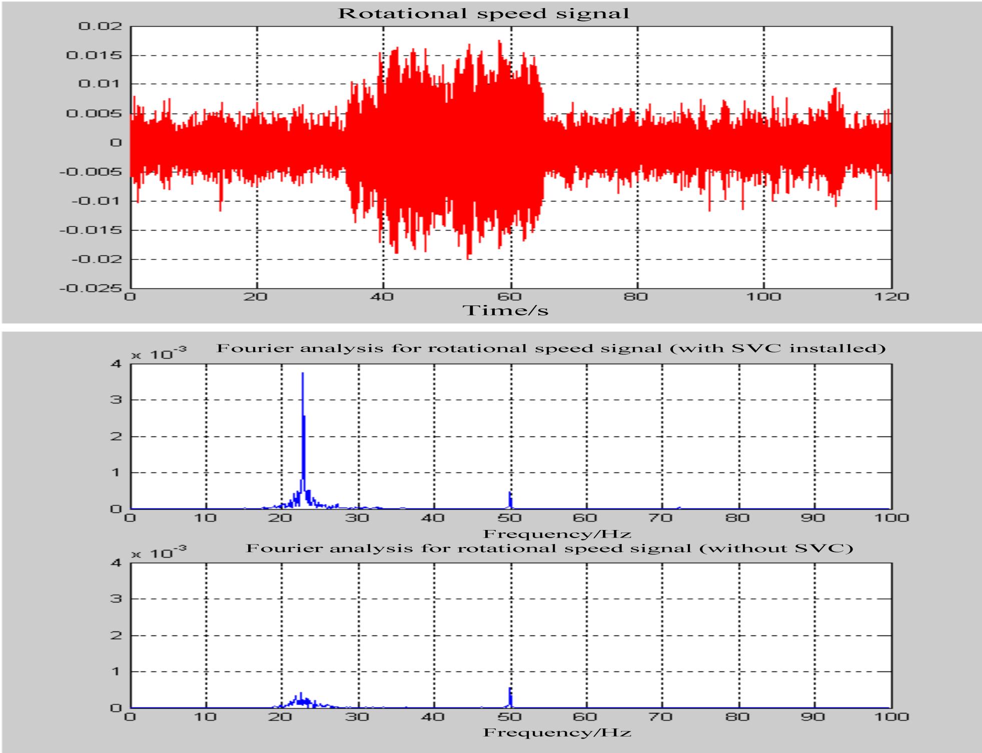

Fig. 7.11 Generators directly connected to the grid + 22.77Hz subsynchronous torsional oscillations aroused by SSR-DS

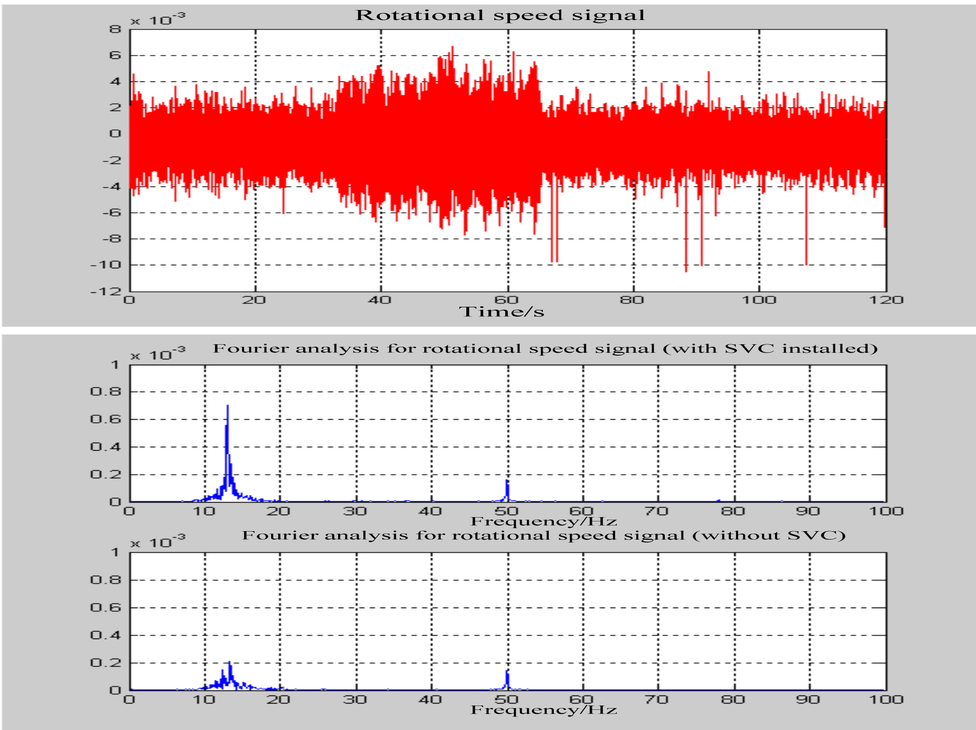

Fig. 7.12 Generators directly connected to the grid + 28.16Hz subsynchronous torsional oscillations aroused by SSR-DS

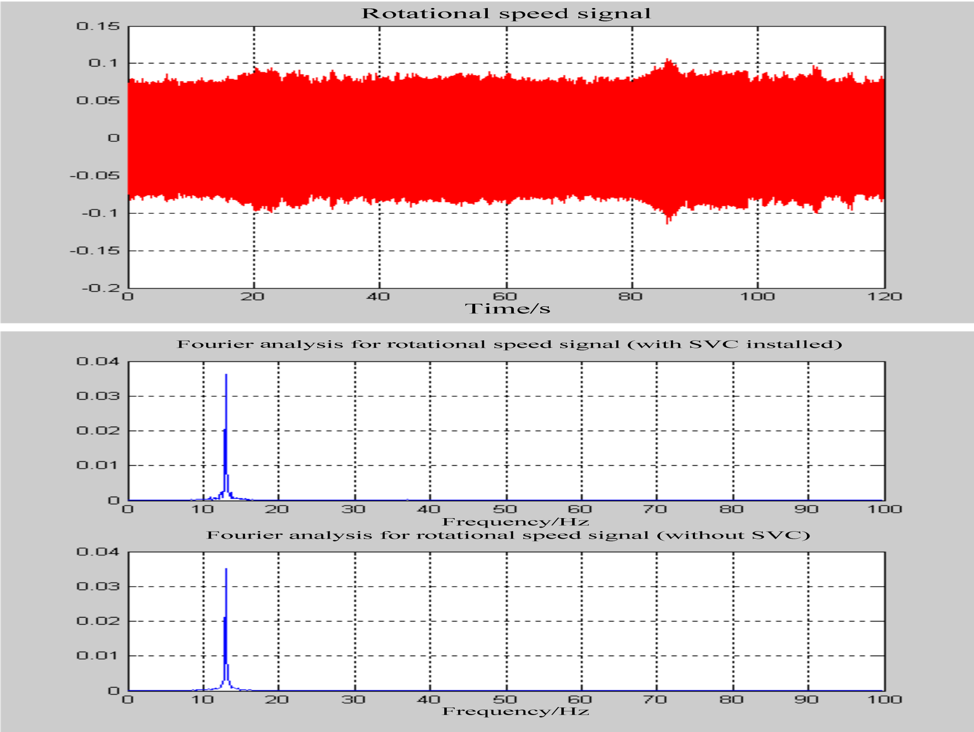

Fig. 7.13 Generators directly connected to the grid + superimposition of 13.02Hz subsynchronous signals + SSR-DS in compensatory operation

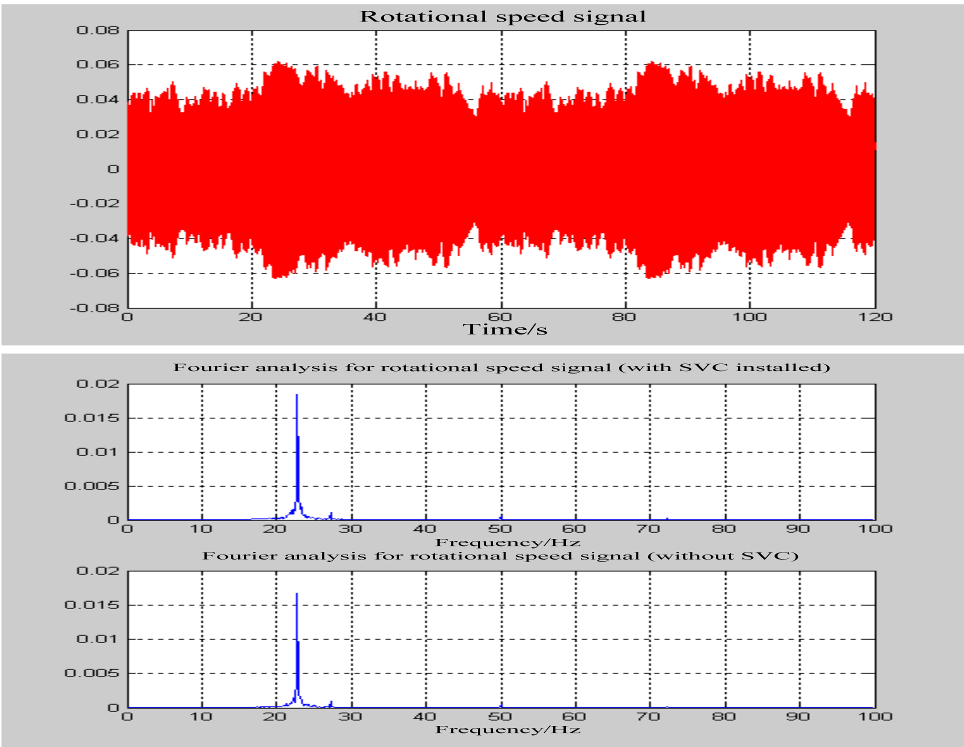

Fig. 7.14 Generators directly connected to the grid + superimposition of 22.77Hz subsynchronous signals + SSR-DS in compensatory operation

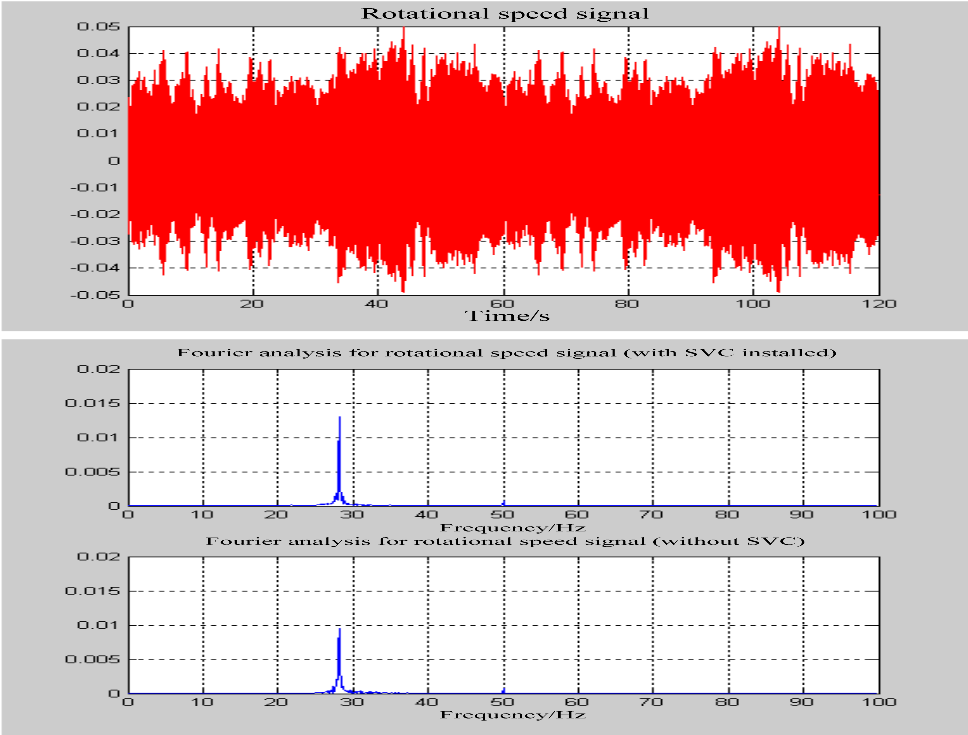

Fig. 7.15 Generators directly connected to the grid + superimposition of 28.16Hz subsynchronous signals + SSR-DS in compensatory operation

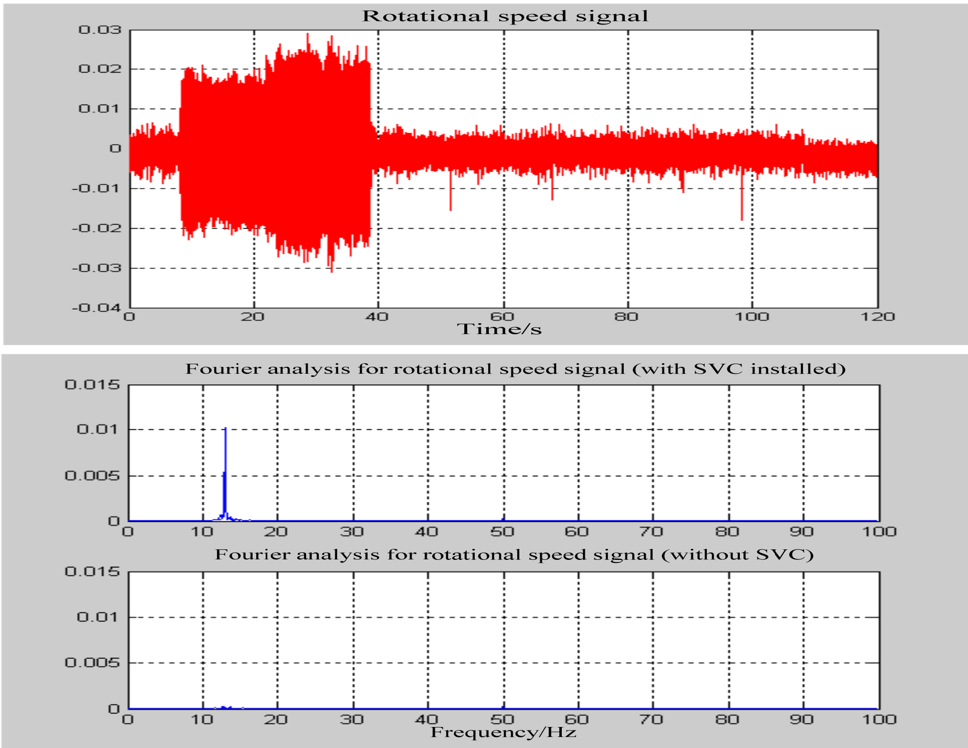

Fig. 7.16 Generators connected to the grid via series reactors + 13.02Hz subsynchronous torsional oscillations aroused by SSR-DS

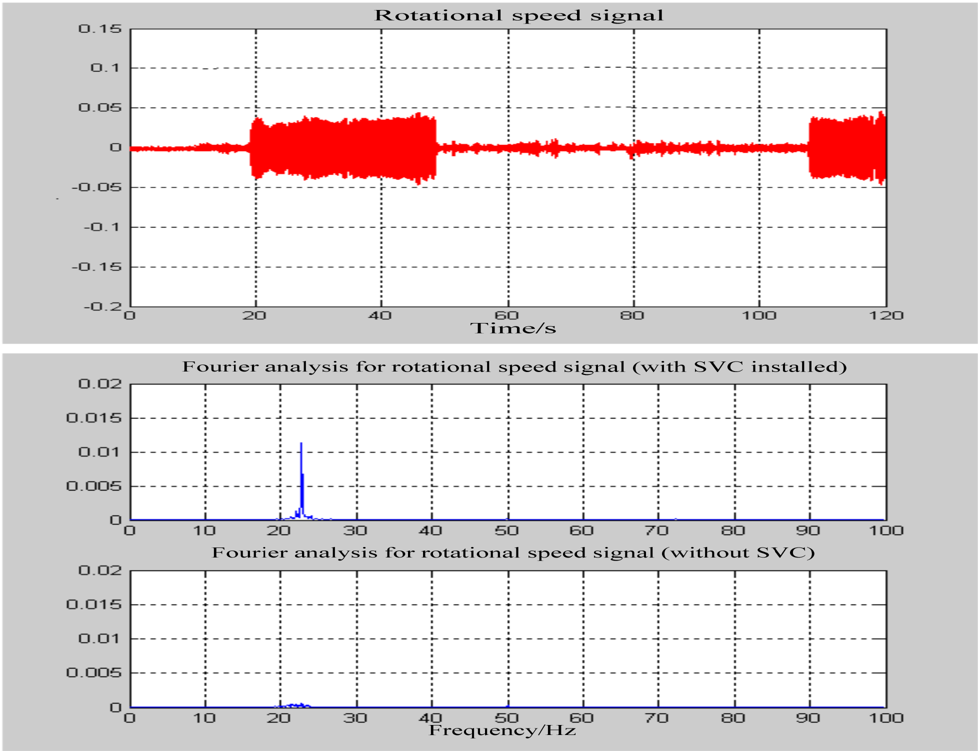

Fig. 7.17 Generators connected to the grid via series reactors + 22.77Hz subsynchronous torsional oscillations aroused by SSR-DS

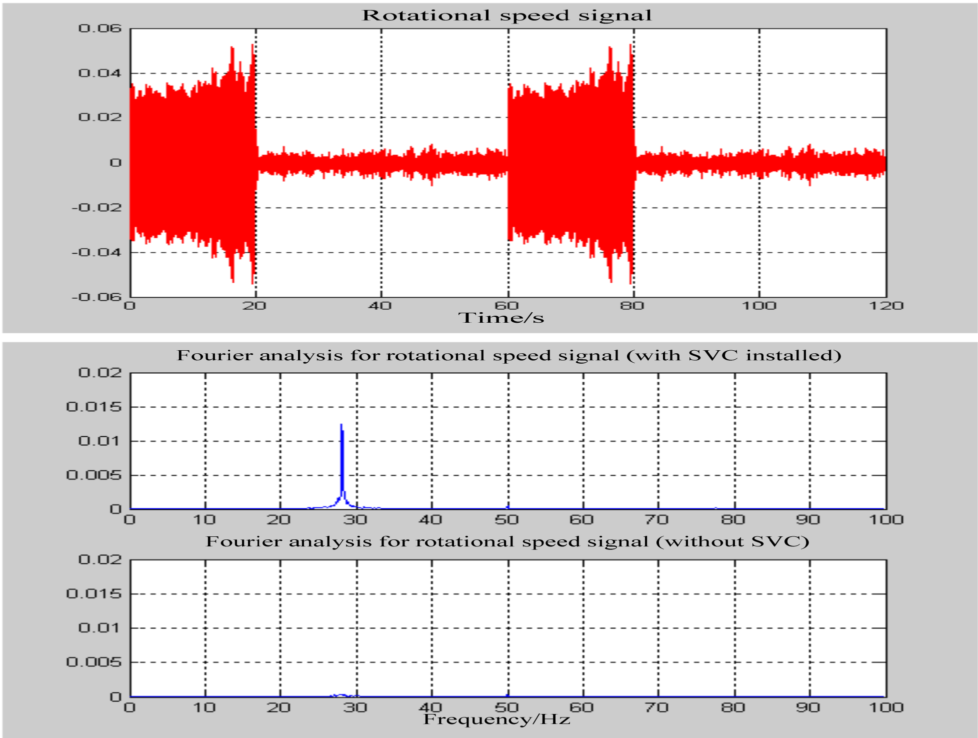

Fig. 7.18 Generators connected to the grid via series reactors + 28.16Hz subsynchronous torsional oscillations aroused by SSR-DS

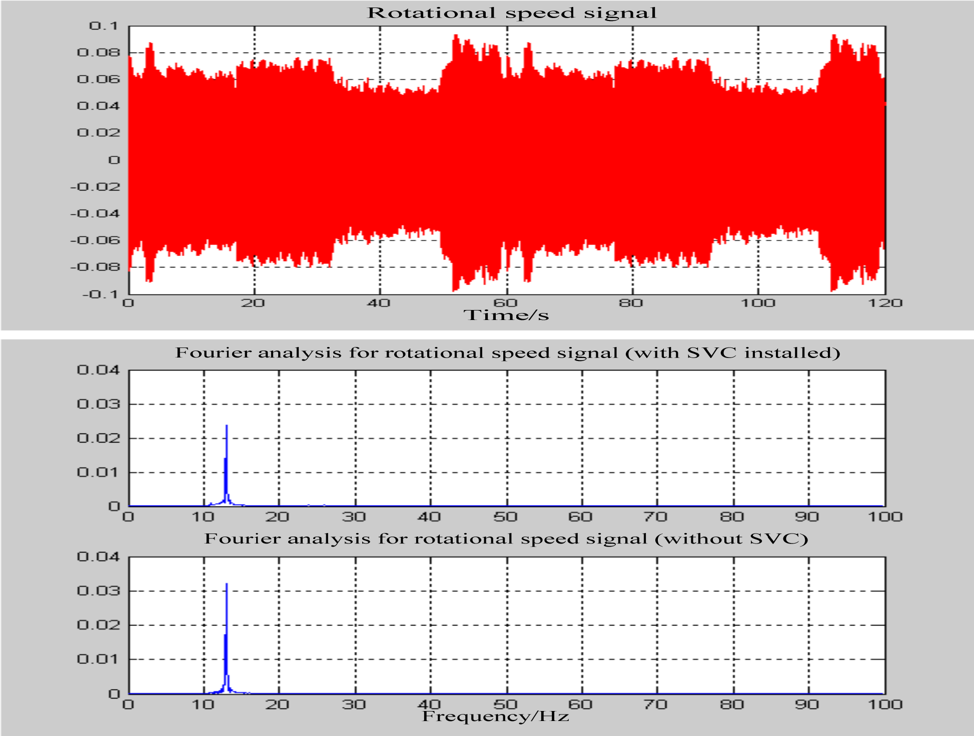

Fig. 7.19 Generators connected to the grid via series reactors + superimposition of 13.02Hz subsynchronous signals + SSR-DS in compensatory operation

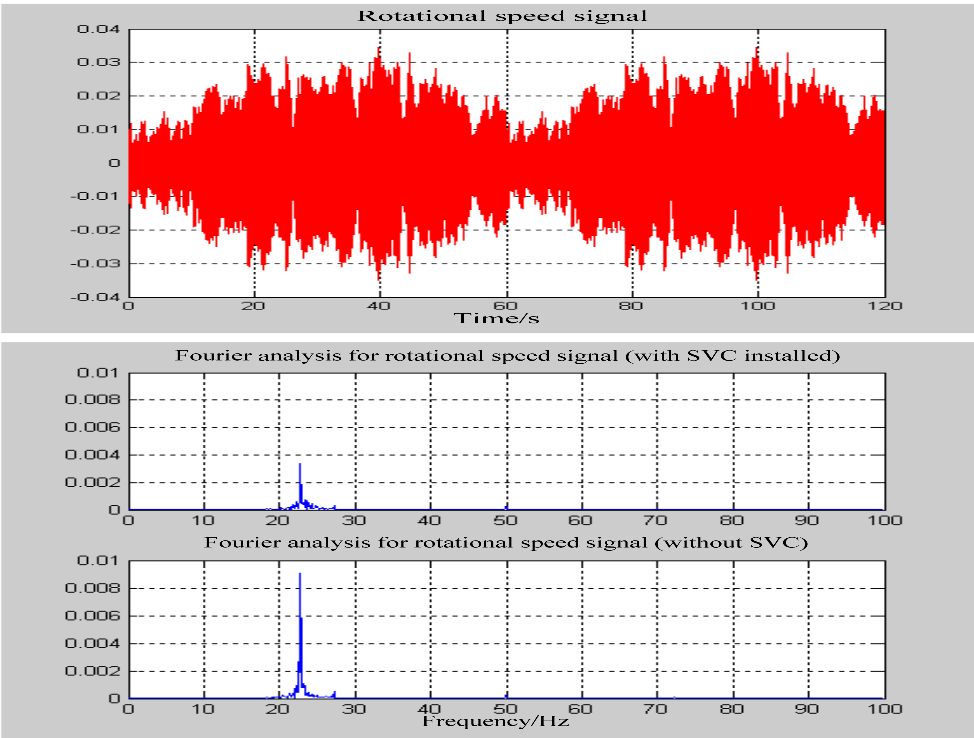

Fig. 7.20 Generators connected to the grid via series reactors + superimposition of 22.77Hz subsynchronous signals + SSR-DS in compensatory operation

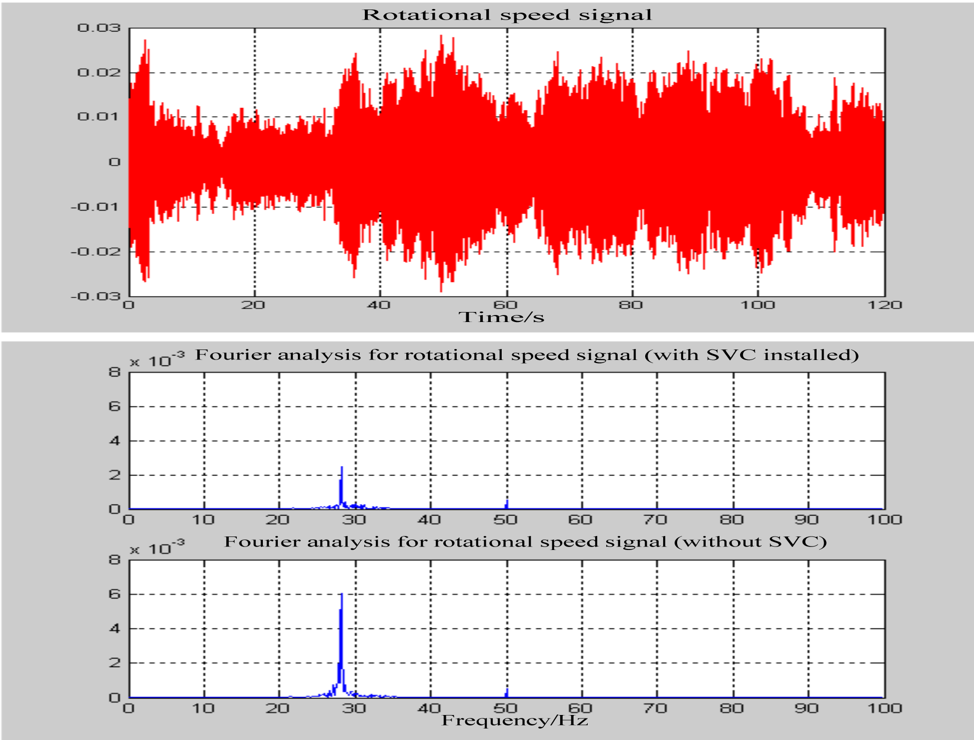

Fig. 7.21 Generators connected to the grid via series reactors + superimposition of 28.16Hz subsynchronous signals + SSR-DS in compensatory operation

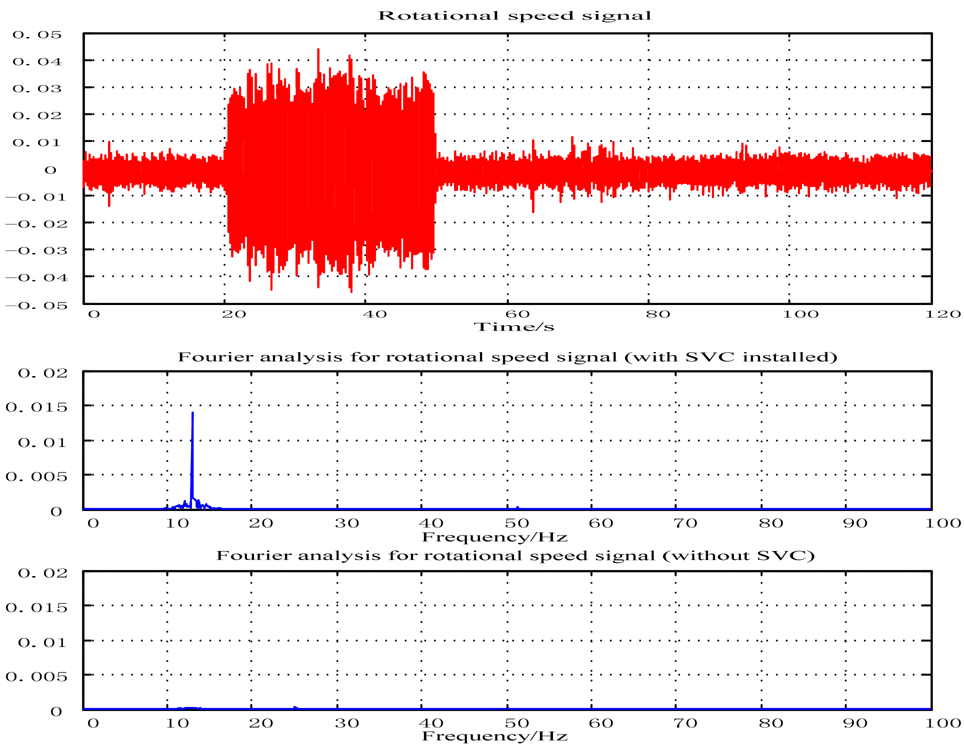

Fig. 7.22 Generators loaded and not connected to the grid + 13.02Hz subsynchronous torsional oscillations aroused by SSR-DS

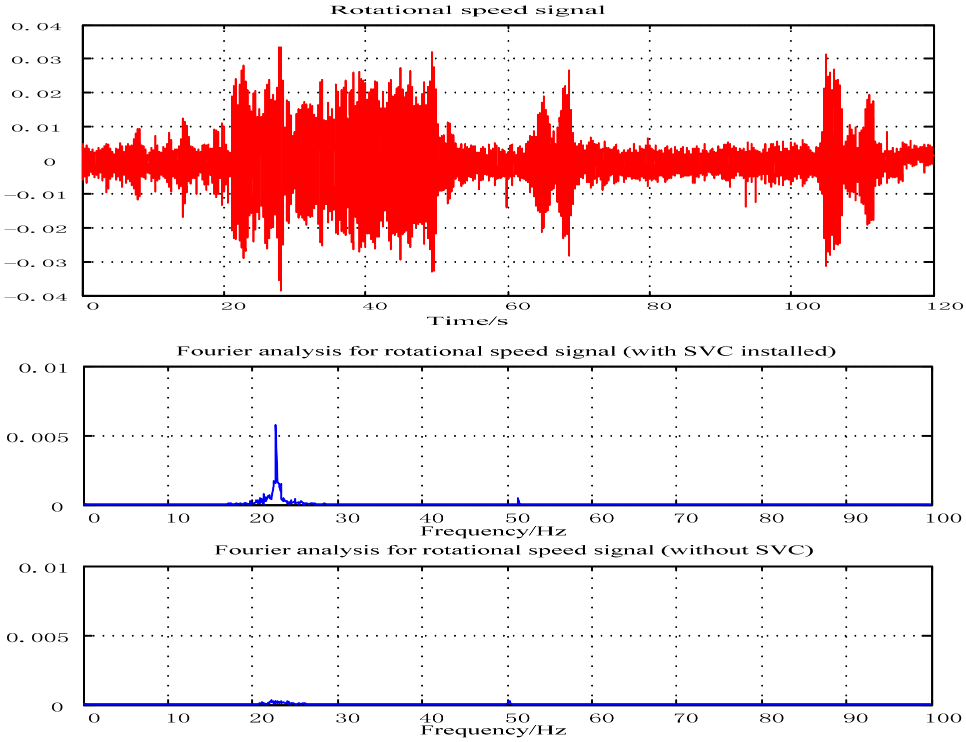

Fig. 7.23 Generators loaded and not connected to the grid + 22.77Hz subsynchronous torsional oscillations aroused by SSR-DS

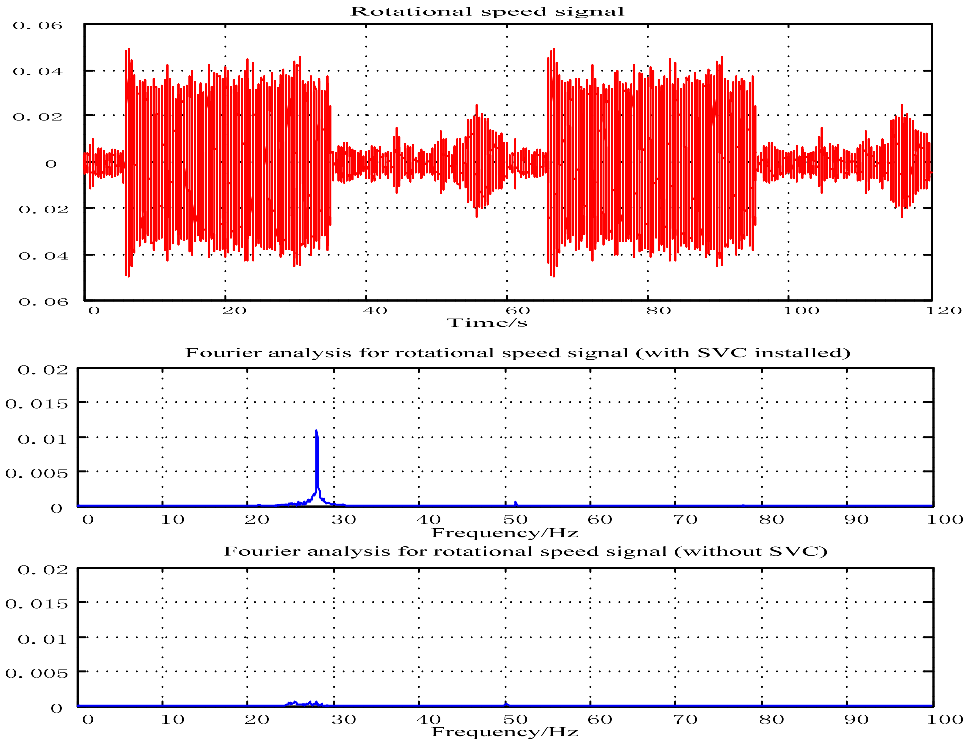

Fig. 7.24 Generators loaded and not connected to the grid + 28.16Hz subsynchronous torsional oscillations aroused by SSR-DS

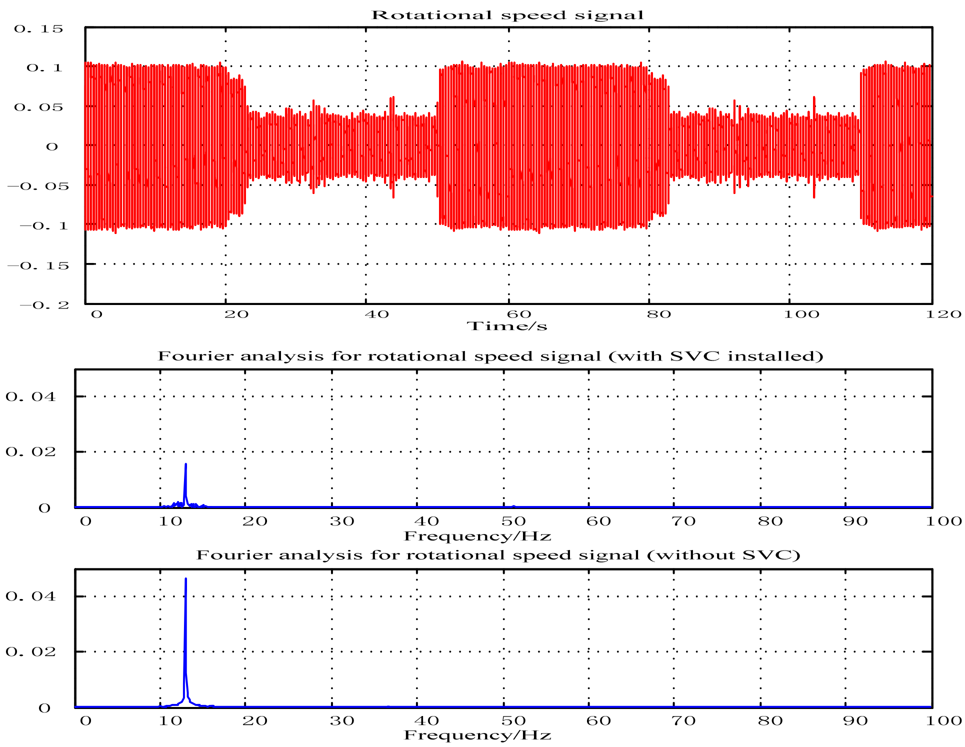

Fig. 7.25 Generators loaded and not connected to the grid + superimposition of 13.02Hz subsynchronous signals + SSR-DS in compensatory operation

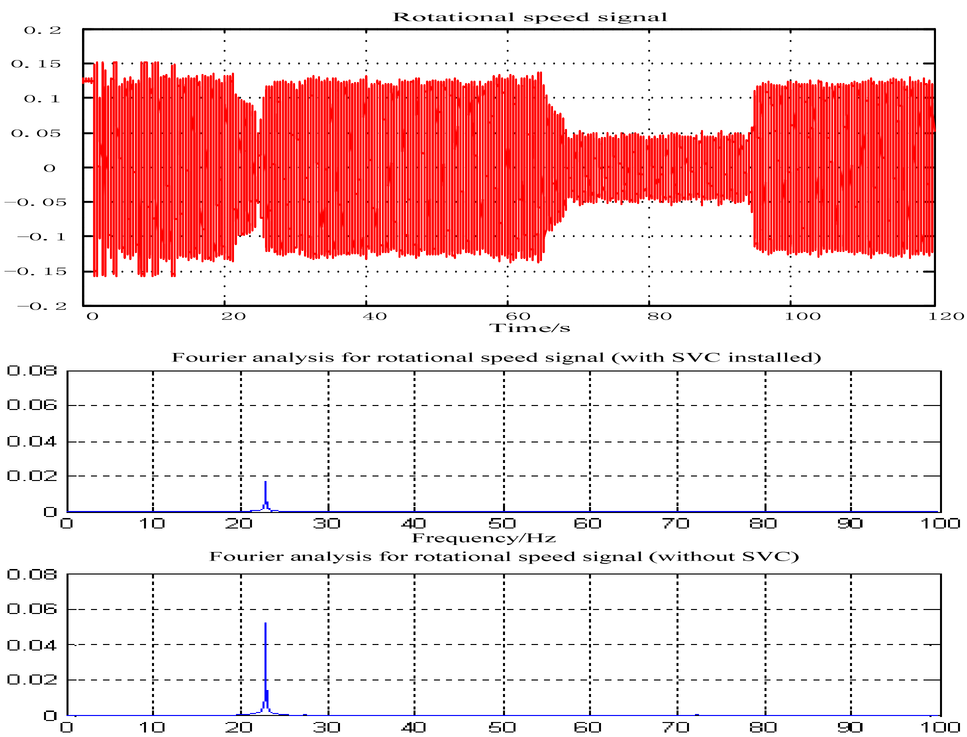

Fig. 7.26 Generators loaded and not connected to the grid + superimposition of 22.77Hz subsynchronous signals + SSR-DS in compensatory operation

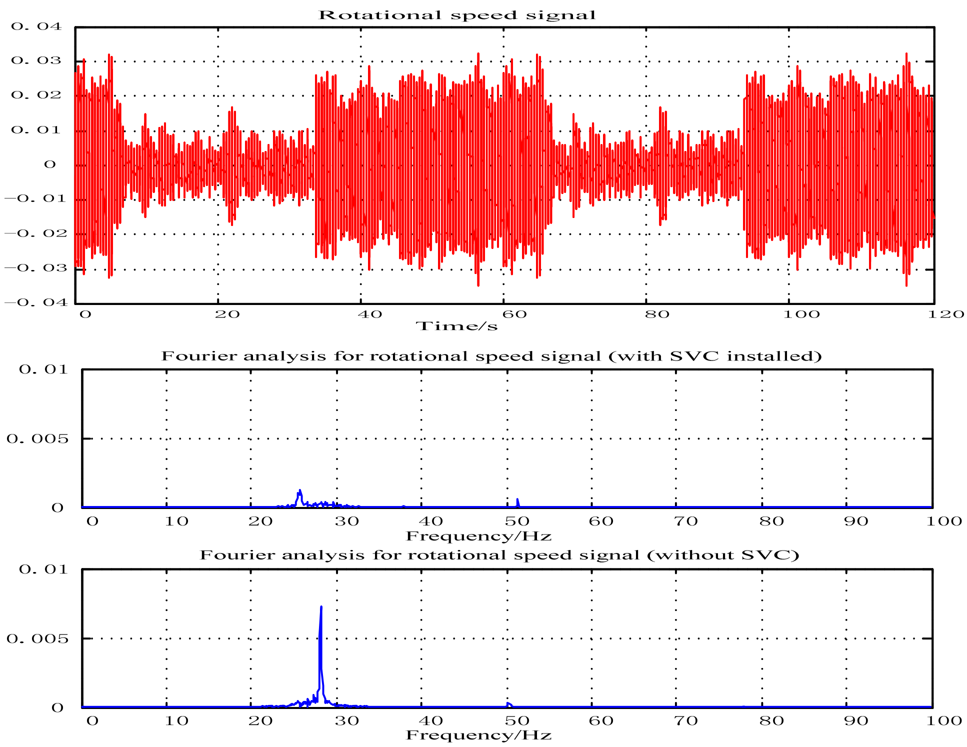

Fig. 7.27 Generators loaded and not connected to the grid + superimposition of 28.16Hz subsynchronous signals + SSR-DS in compensatory operation

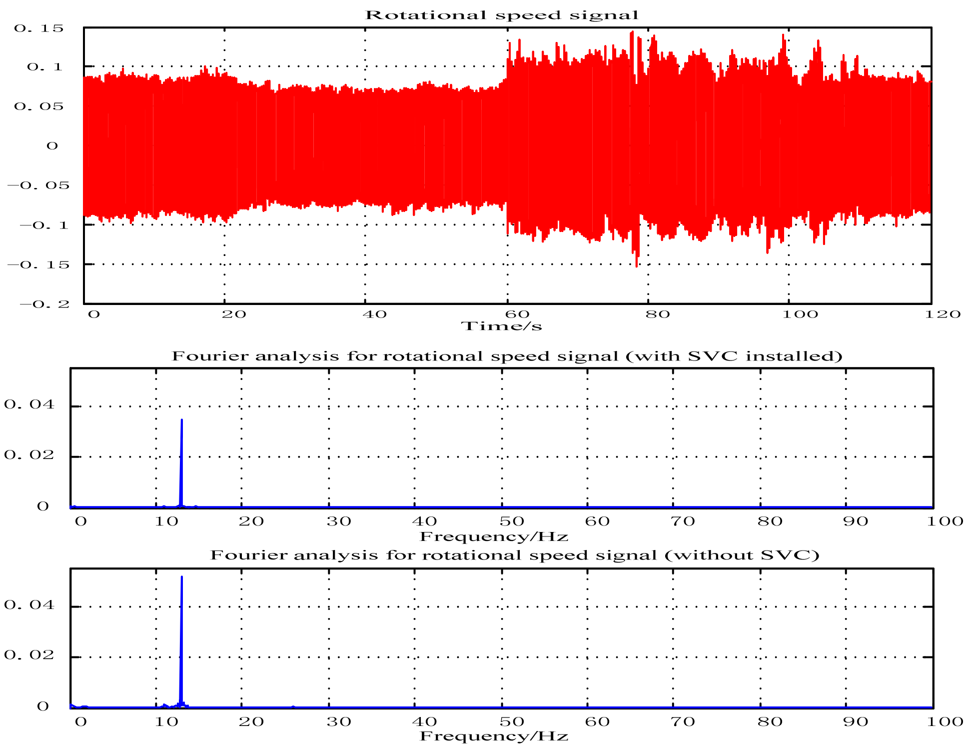

Fig. 7.28 Generators connected to the grid via series reactors + superimposition of 13.02Hz subsynchronous signals + SSR-DS in compensatory operation + phase shift 0°

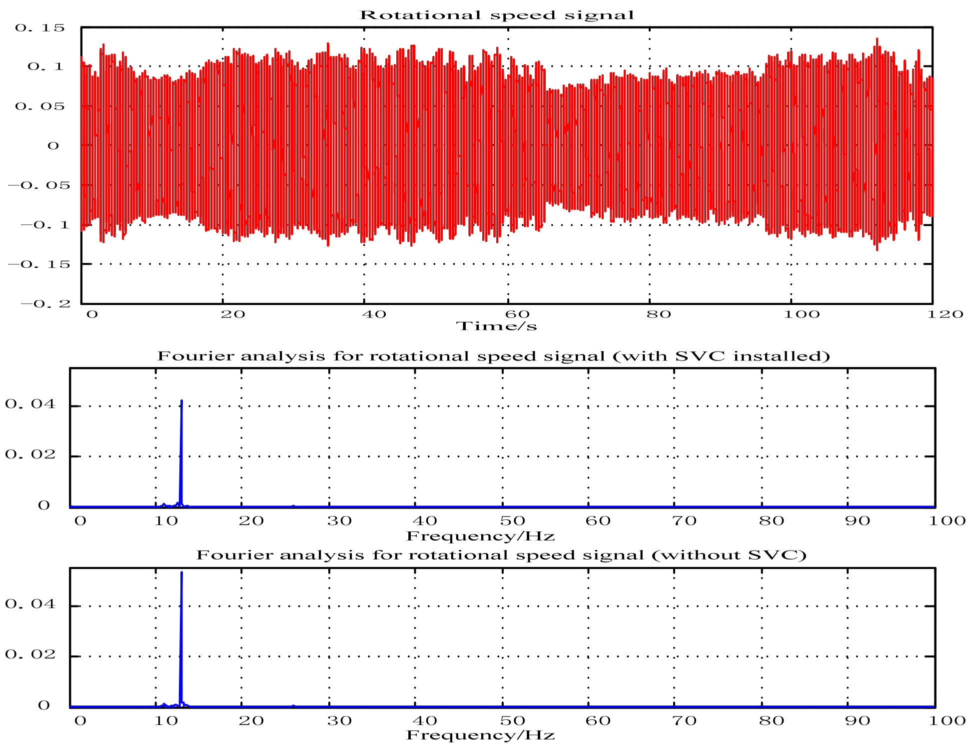

Fig. 7.29 Generators connected to the grid via series reactors + superimposition of 13.02Hz subsynchronous signals + SSR-DS in compensatory operation + phase shift -30°

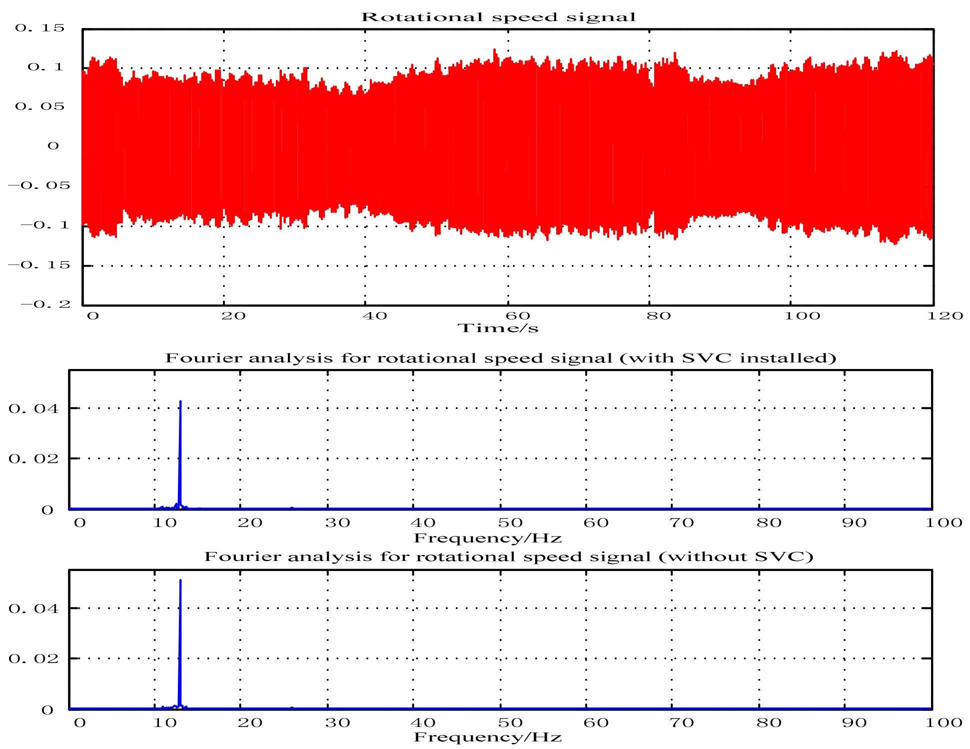

Fig. 7.30 Generators connected to the grid via series reactors + superimposition of 13.02Hz subsynchronous signals + SSR-DS in compensatory operation + phase shift -20°

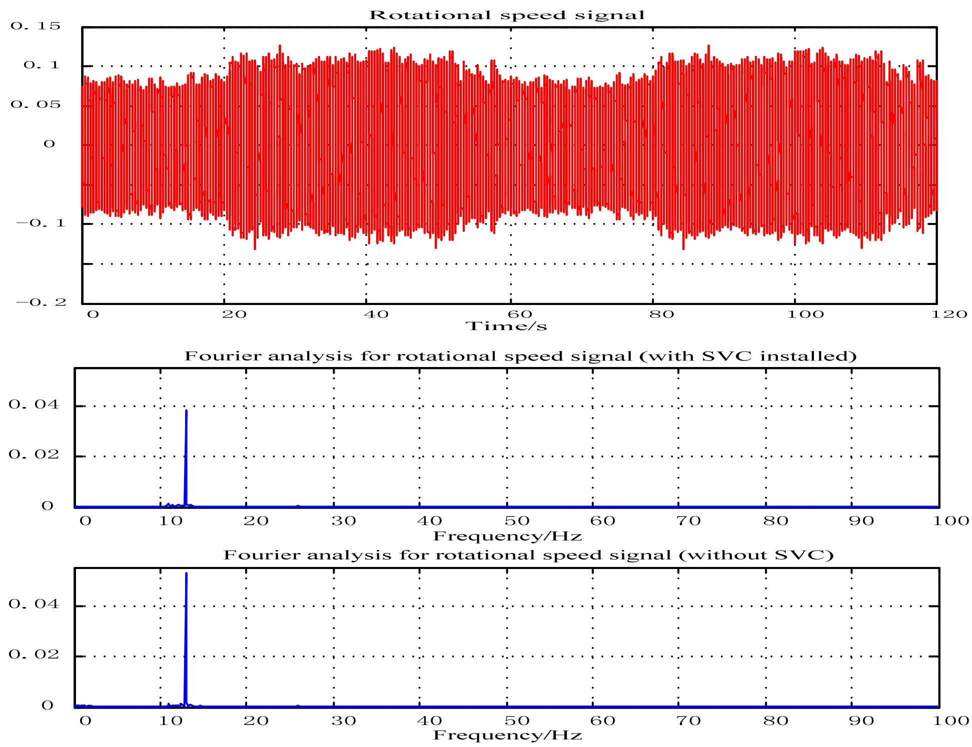

Fig. 7.31 Generators connected to the grid via series reactors + superimposition of 13.02Hz subsynchronous signals + SSR-DS in compensatory operation + phase shift -10°

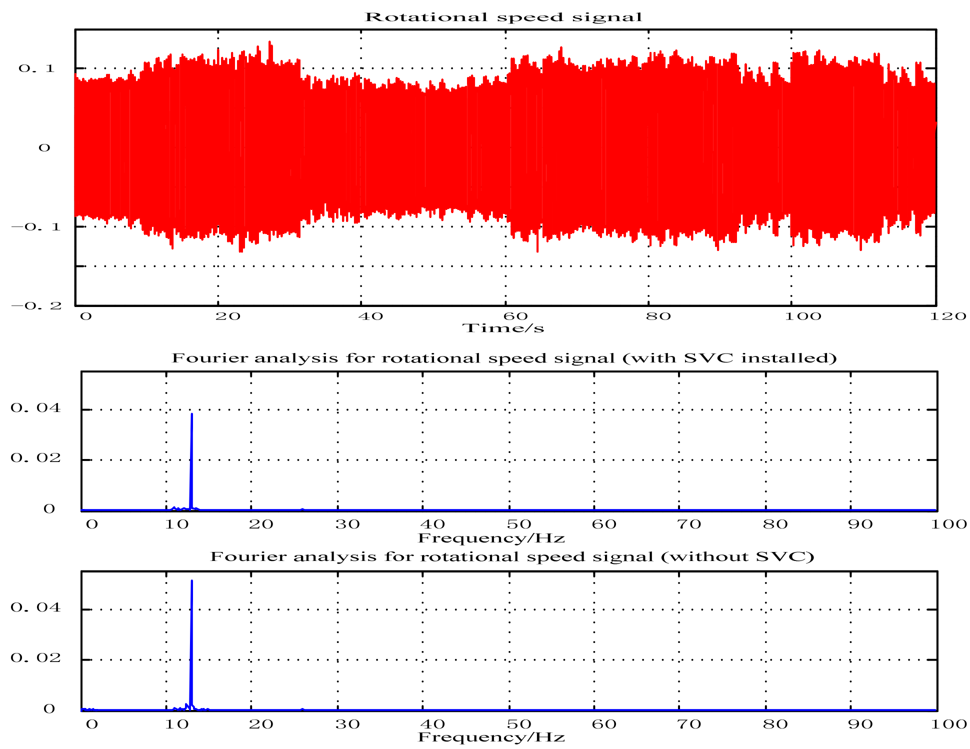

Fig. 7.32 Generators connected to the grid via series reactors + superimposition of 13.02Hz subsynchronous signals + SSR-DS in compensatory operation + phase shift +10°

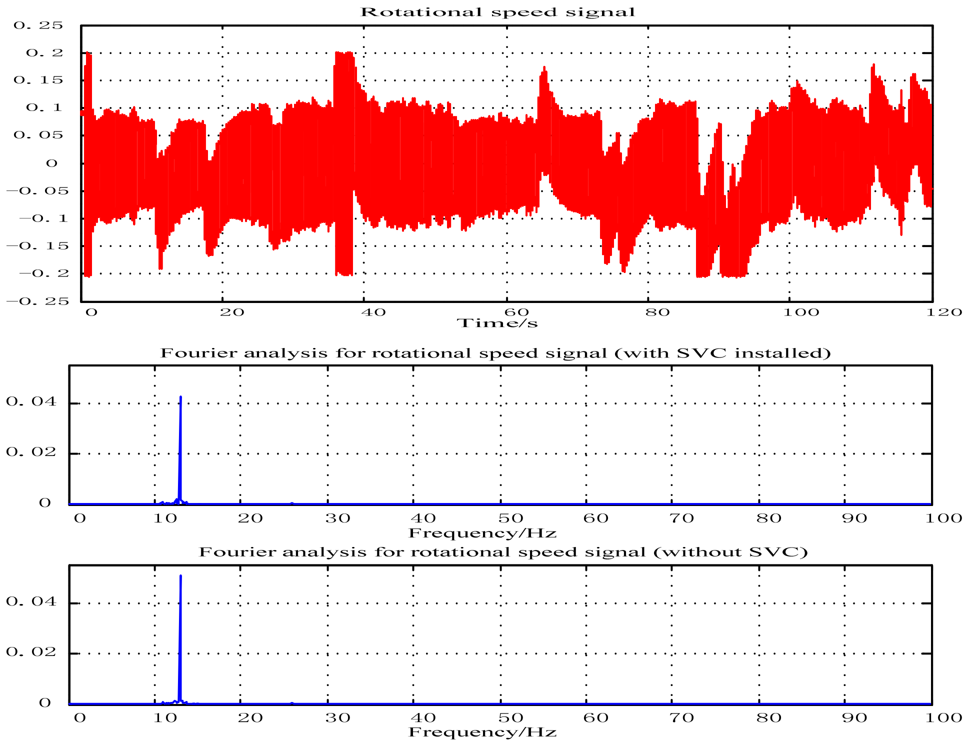

Fig. 7.33 Generators connected to the grid via series reactors + superimposition of 13.02Hz subsynchronous signals + SSR-DS in compensatory operation + phase shift +20°

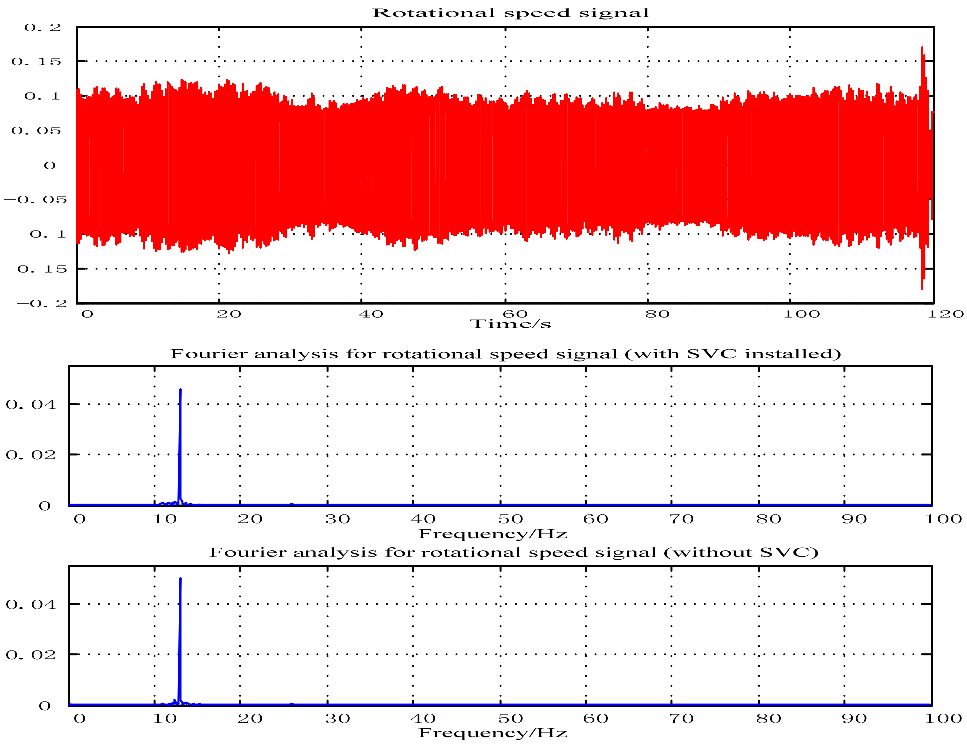

Fig. 7.34 Generators connected to the grid via series reactors + superimposition of 13.02Hz subsynchronous signals + SSR-DS in compensatory operation + phase shift +30°

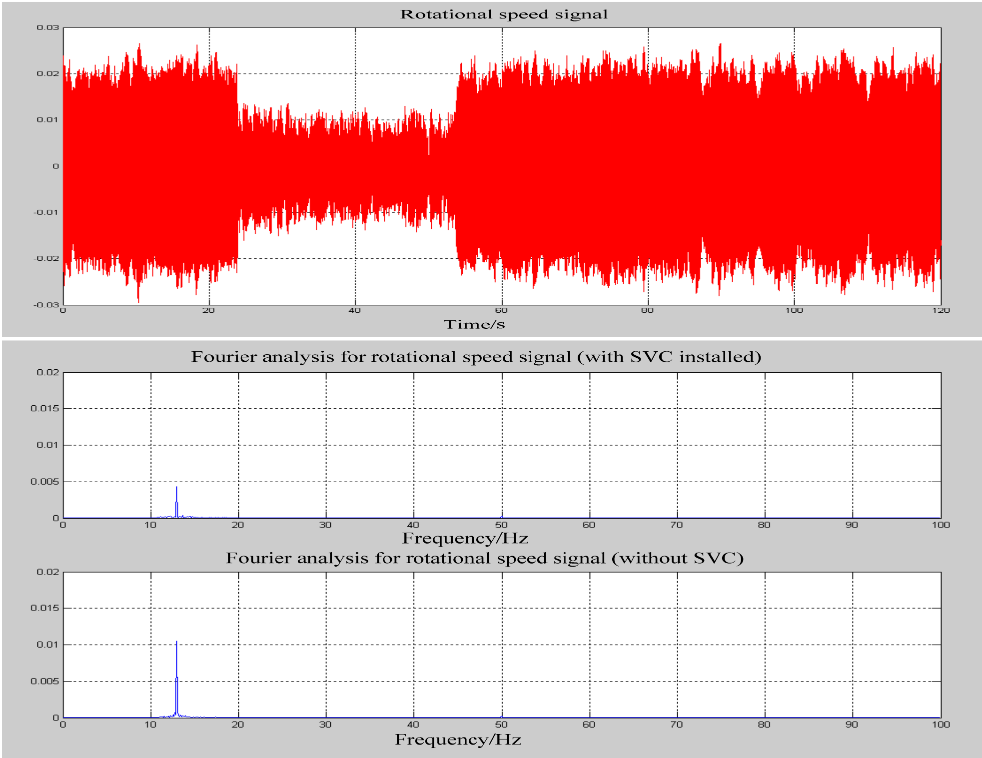

Fig. 7.35 Generators connected to the grid via series reactors + superimposition of 13.02Hz subsynchronous signals + SSR-DS in compensatory operation + gain proportion 100%

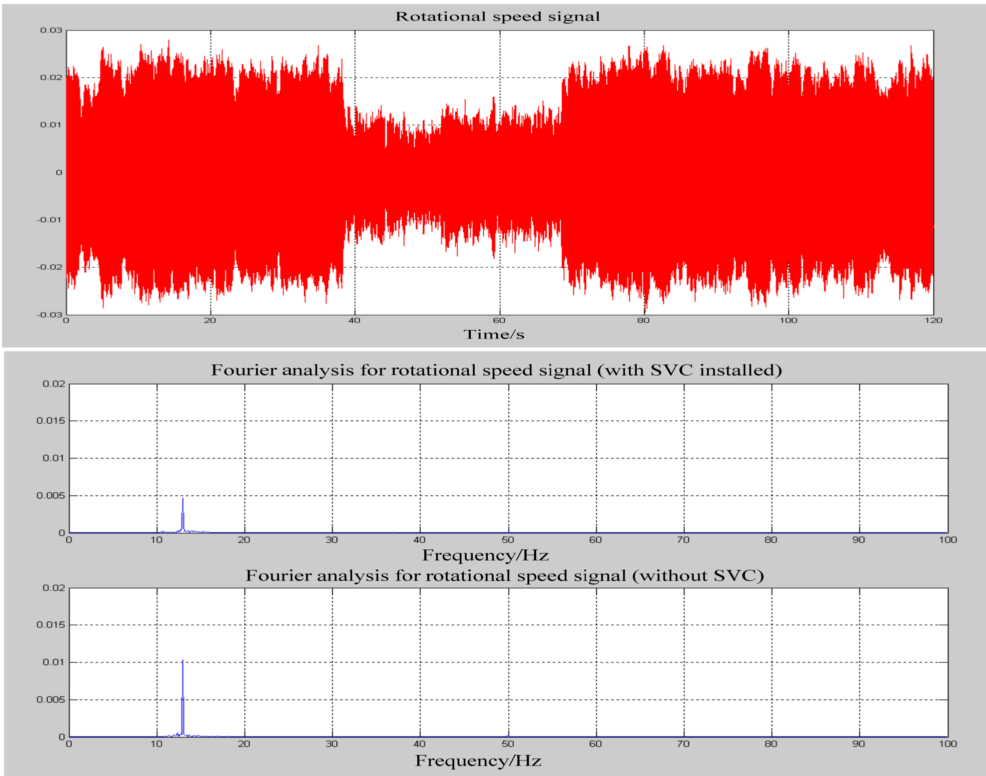

Fig. 7.36 Generators connected to the grid via series reactors + superimposition of 13.02Hz subsynchronous signals + SSR-DS in compensatory operation + gain proportion 75%

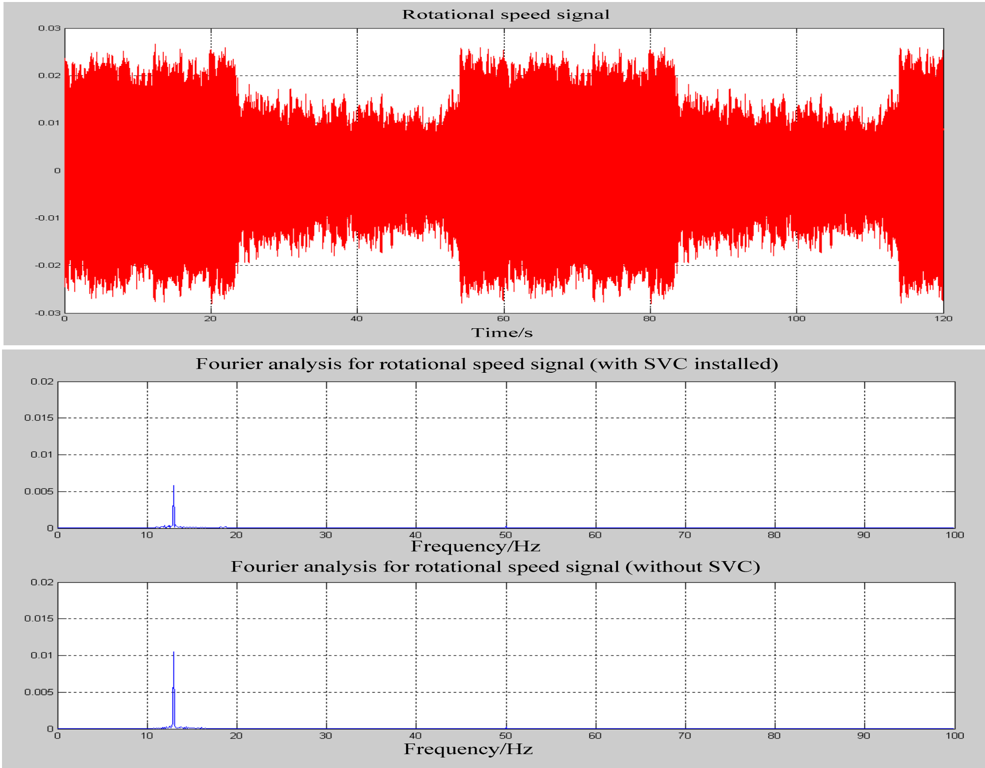

Fig. 7.37 Generators connected to the grid via series reactors + superimposition of 13.02Hz subsynchronous signals + SSR-DS in compensatory operation + gain proportion 50%

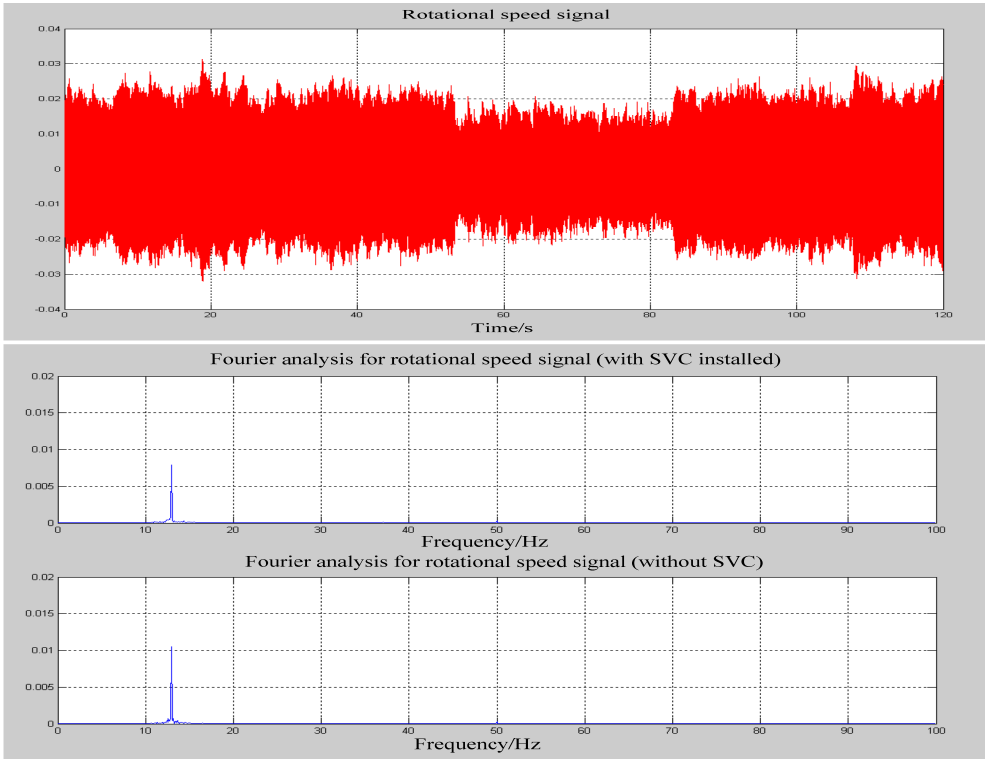

Fig. 7.38 Generators connected to the grid via series reactors + superimposition of 13.02Hz subsynchronous signals + SSR-DS in compensatory operation + gain proportion 25%

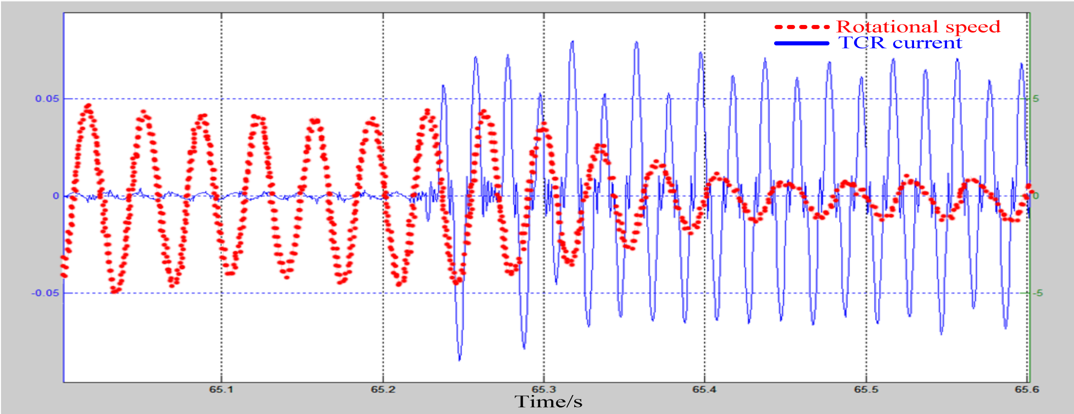

Fig. 7.39 Response curves with generators connected to the grid via series reactors + superimposition of 13.02Hz subsynchronous signals + SSR-DS put into compensatory operation

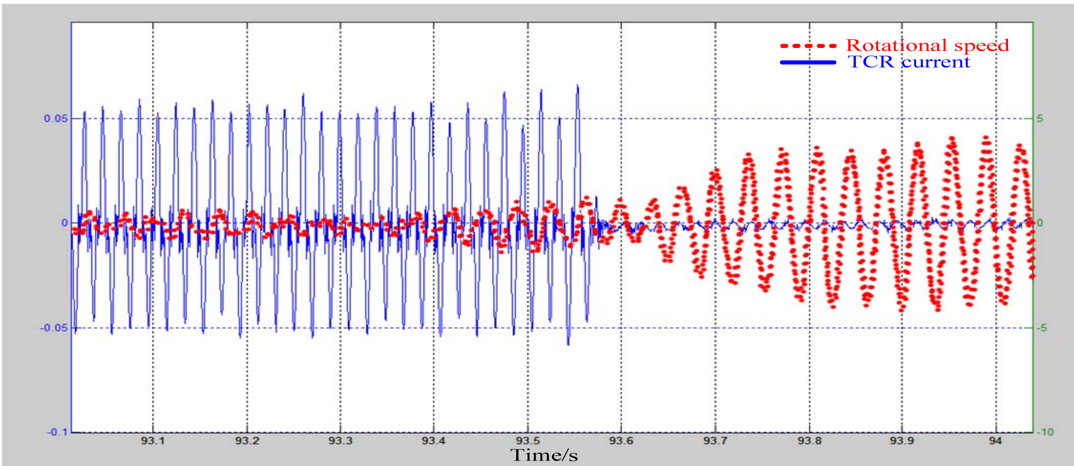

Fig. 7.40 Response curves with generators connected to the grid via series reactors + superimposition of 13.02Hz subsynchronous signals + SSR-DS tripped out of compensatory operation

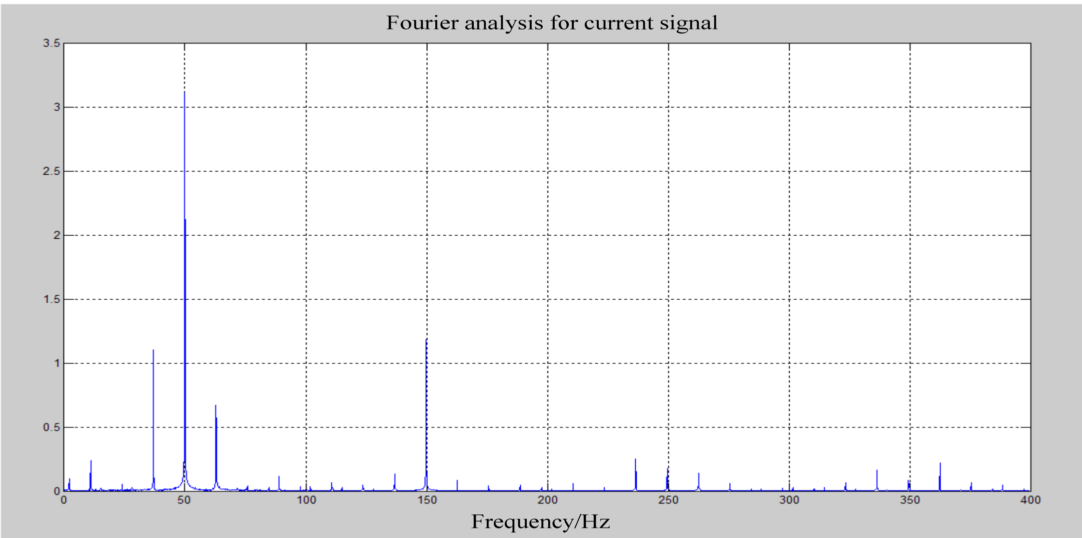

Fig. 7.41 Curves of TCR current with generators connected to the grid via series reactors + superimposition of 13.02Hz subsynchronous signals + SSR-DS in compensatory operation

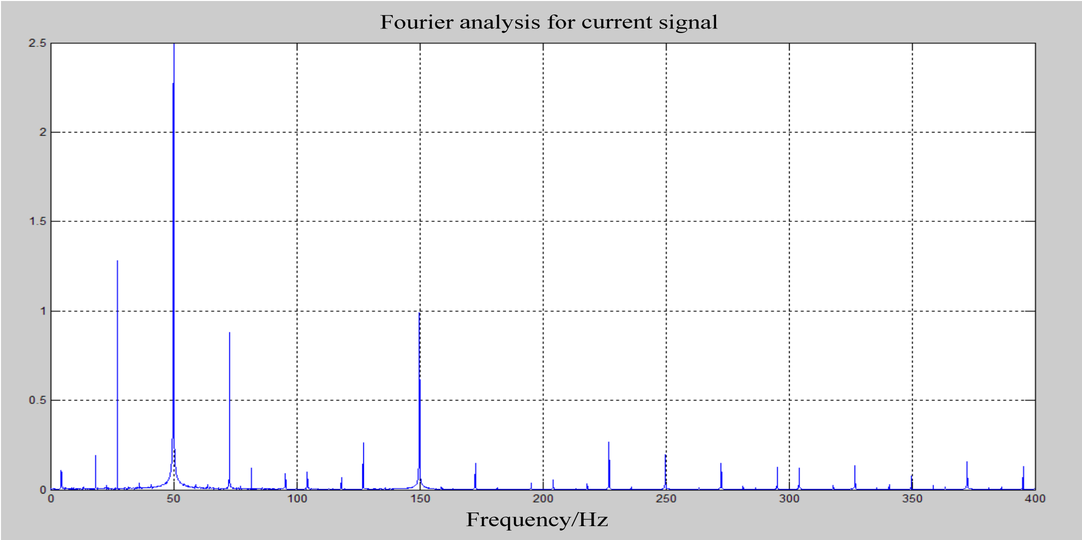

Fig. 7.42 Curves of TCR current with generators connected to the grid via series reactors + superimposition of 22.77Hz subsynchronous signals + SSR-DS in compensatory operation

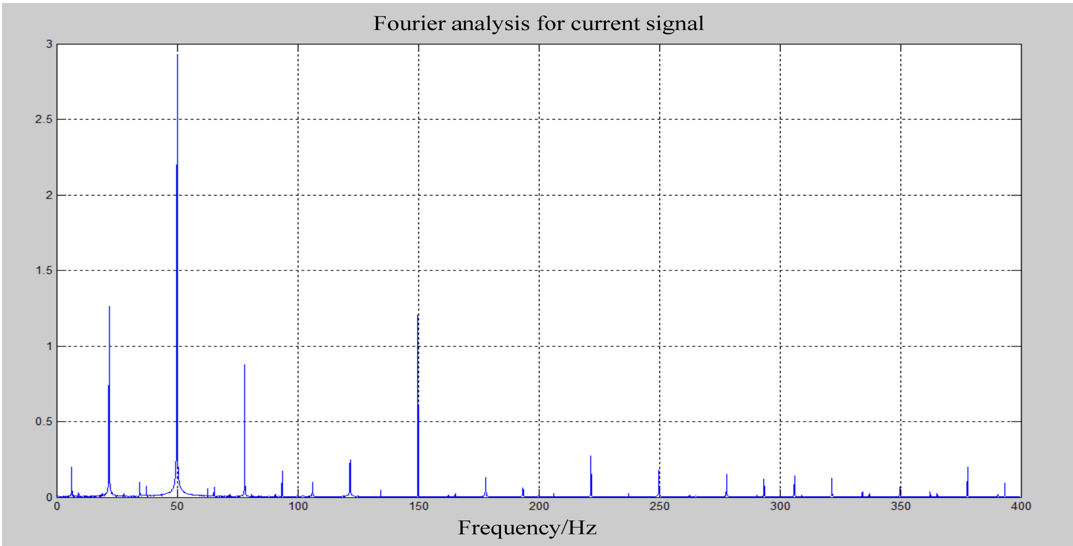

Fig. 7.43 Curves of TCR current with generators connected to the grid via series reactors + superimposition of 28.16Hz subsynchronous signals + SSR-DS in compensatory operation

7.3.2.2 Data Analysis and Conclusions

(1) When the generators were directly connected to the grid, owing to the large short-circuit capacity and small impedance at the 380V power supply system as well as the large equivalent impedance of the generators, most of the currents generated by the SSR-DS flowed into the system, with only small currents flowing into the generators, so the results of suppressing the subsynchronous resonance/oscillations of

the generators by the SSR-DS were not obvious.

(2) When the generators were connected to the grid via series reactors, before the SSR-DS was put into operation, the amplitudes of subsynchronous resonance/oscillations (13.02Hz, 22.77Hz and 28.16Hz) of the generators were 0.033, 0.0092 and 0.006 respectively; after the SSR-DS was put into operation for automatic closed-loop compensation of rotation speeds, the amplitudes of subsynchronous resonance/oscillations (13.02Hz, 22.77Hz and 28.16Hz) of the generators were 0.024, 0.0035 and 0.0026 respectively. These data indicates that the results of the SSR-DS in suppressing the shafting torsional oscillations are obvious, proving that the SSR-DS can suppress the shafting torsional oscillations of the generators.

(3) When the generators were loaded and not connected to the grid, before the SSR-DS was put into operation, the amplitudes of subsynchronous resonance/oscillations (13.02Hz, 22.77Hz and 28.16Hz) of the generators were 0.045, 0.052 and 0.0075 respectively; after the SSR-DS was put into operation for automatic closed-loop compensation of rotation speeds, the amplitudes of subsynchronous resonance/oscillations (13.02Hz, 22.77Hz and 28.16Hz) of the generators were 0.016, 0.018 and 0.001 respectively. These data indicates that the results of the SSR-DS on suppressing the shafting torsional oscillations are obvious (suppression proportions at 13.02Hz, 22.77Hz and 28.16Hz were 64.4%, 65.4% and 86.7% respectively), proving that the SSR-DS can suppress the shafting torsional oscillations of the generators.

(4) When the generators were connected to the grid via series reactors + superimposition of 13.02Hz subsynchronous signals + phase shift, before the SSR-DS was put into operation, the amplitude of subsynchronous resonance/oscillations of the generators was 0.045; after the SSR-DS was put into operation for automatic closed-loop compensation of rotation speeds, the amplitudes of subsynchronous resonance/oscillations of the generators at phase shift angles 0°, -30°, -20°, -10°, +10°, +20° and +30° were 0.036, 0.041, 0.041, 0.038, 0.038, 0.041, 0.043 respectively. These data indicate that the effect of the SSR-DS in suppressing the shafting torsional oscillations of the generators is directly related to the phase shift angle settings, and either leftward shift or rightward shift of the phase shift angle may impact the results of the SSR-DS in suppressing the subsynchronous torsional oscillations of the

generators.

(5) When the generators were connected to the grid via series reactors + superimposition of 13.02Hz subsynchronous signals + gain proportion, before the SSR-DS was put into operation, the amplitude of subsynchronous resonance/oscillations of the generators was 0.011; after the SSR-DS was put into operation for automatic closed-loop compensation of rotation speeds, the amplitudes of subsynchronous resonance/oscillations of the generators at gain proportions 100%, 75%, 50%, and 25% were 0.0045, 0.005, 0.006, and 0.008 respectively. These data indicate that the effect of the SSR-DS in suppressing the shafting torsional oscillations of the generators is directly related to the gain proportion parameter settings, and for the system of these experiments, the smaller the gain proportion, the smaller the output of the SSR-DS, and the worse the results of the SSR-DS in suppressing the subsynchronous resonance/oscillations of the generators.

(6) When the generators were connected to the grid via series reactors + superimposition of 13.02Hz subsynchronous signals, the response times of the system when the SSR-DS compensation system was put in/out of operation, i.e. the time differences since the SSR-DS was put in/out of operation until the SSR stabilized, were measured, and both measurements were below 300ms, verifying the rapidity of the responses of the SSR-DS system. The response times includes the total time delays of the rotation speed testers, triggering digital filtering link, the phase correction link, and the triggering link (refer to Fig.7.39 and Fig.7.40).

(7) When the generators were connected to the grid via series reactors with the superimpositions of 13.02Hz, 22.77Hz and 28.16Hz subsynchronous signals, the output currents of the SSR-DS were measured respectively. The measurements indicate that the harmonic components of the output currents of the SSR-DS are mainly frequency multipliers $f_{nm} = nf_0$, $n = 1,3,5,7,...$ and sub-harmonics $f_{nm} = nf_0 \pm f_{m1}$, $n = 1,3,5,7,...$ When the system was connected in delta, the triple harmonics mainly circulated within the TCRs, with only a small amount flowing into the grid, and this agrees with the theoretical analyses.

7.4 Records of Field Tests

The three central frequencies of the subsynchronous resonance/oscillations of the four generators in Jinjie Power Plant are 13.02Hz, 22.77Hz and 28.16Hz respectively. Filtering and calculations are performed in accordance with these three central frequencies in the control algorithms, and recordings were conducted in accordance with these three frequencies at the outward output end of the control system during field tests, such that the whole system was being tested in a real-time way during the final tests. And we can see the results of the control system in suppressing subsynchronous resonance/oscillations from the real-time curves of the three central frequencies.

The field test results of the SSR-DS in Jinjie Power Plant agreed well with the dynamic simulation test results. Owing to the limits of length, only part of field test waveforms will be shown.

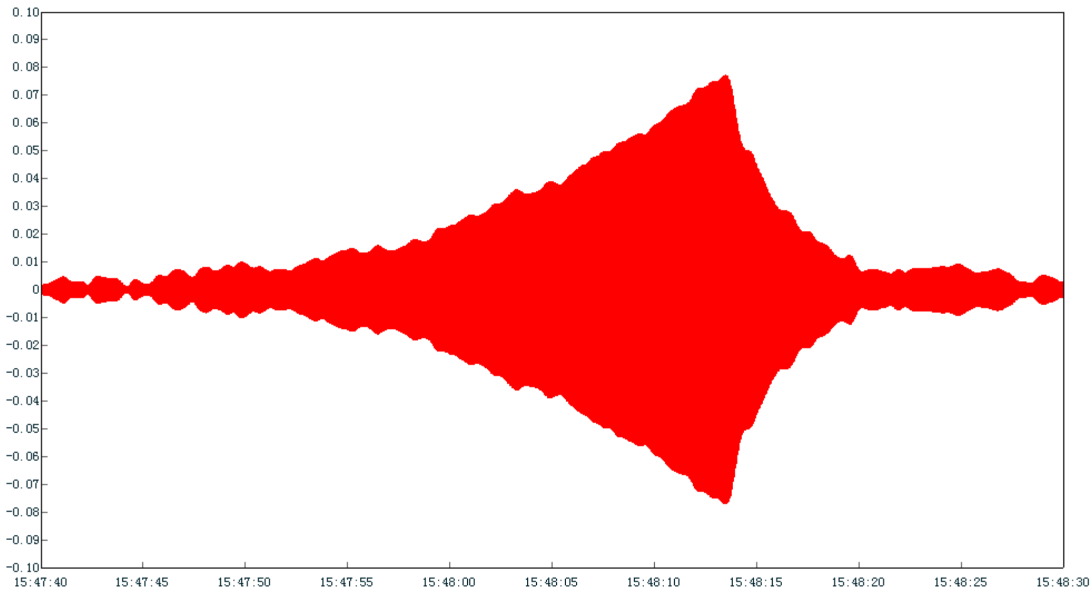

Fig. 7.44a Amplitude of modal frequency 28.16Hz diverges when the SSR-DS is out of operation, and converges when the SSR-DS is put into operation when the series compensators are in operation

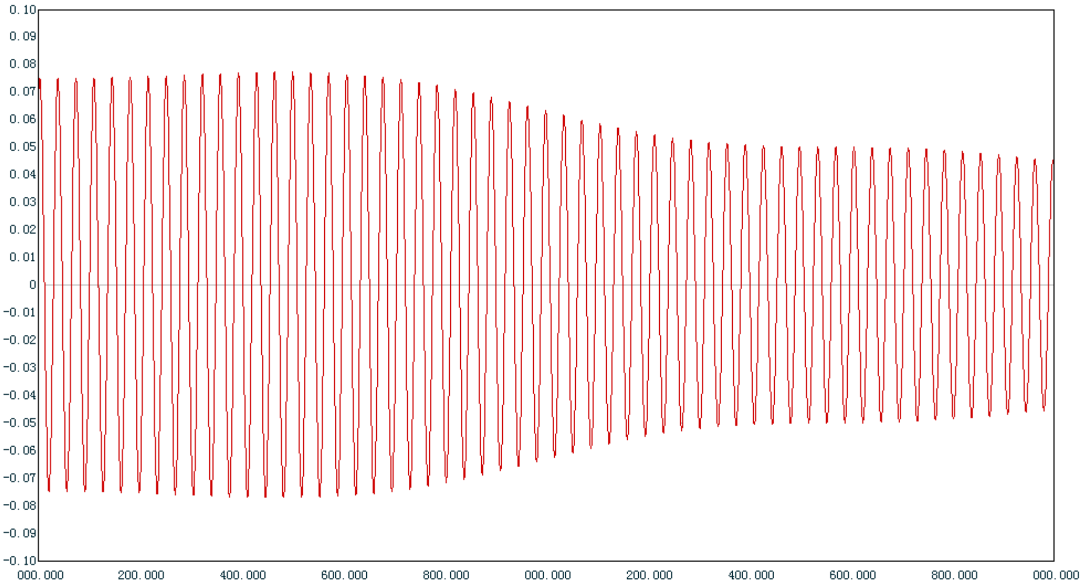

Fig. 7.44b Transient-state waveform recorded when the SSR-DS is put into operation

As shown in Fig. 7.44a, when the series compensators are in operation and the SSR-DS is out of operation for suppression, the amplitude of the modal frequency diverges, and when the SSR-DS is put into operation for suppression, the amplitude of the modal frequency converges rapidly. Fig.7.44b shows the transient-state waveform recorded when the SSR-DS was put into operation.

The following are the field measured waveforms of the amplitudes of subsynchronous resonance/oscillations at the three central frequencies when a short-circuit fault occurs in the Xinzhou-Shijiazhuang series compensation lines II.

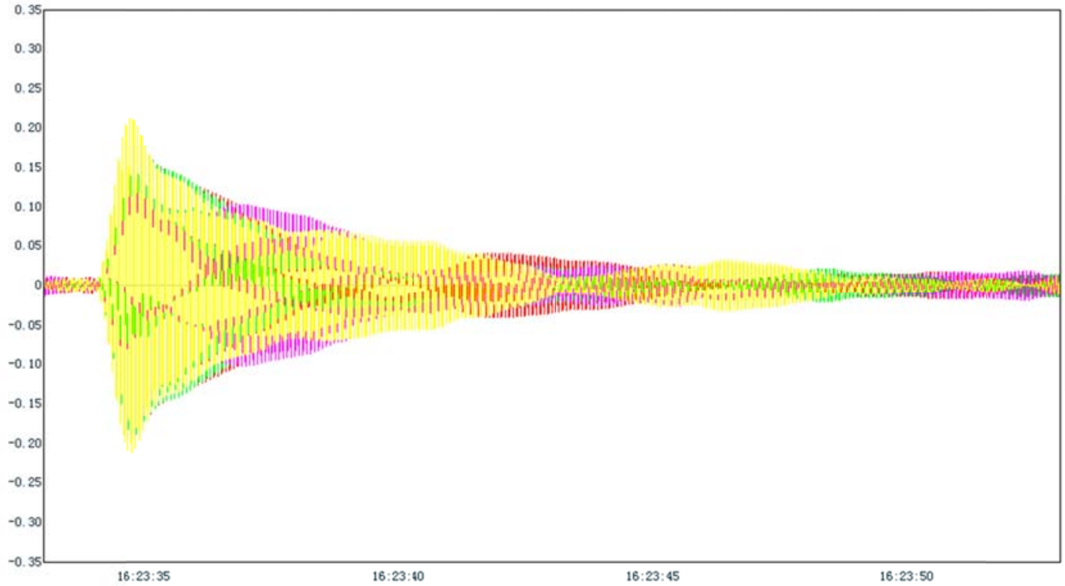

Fig. 7.45a Waveforms of three-phase currents when a short-circuit fault occurred, and the SSR-DS was put into operation to suppress 13Hz SSR

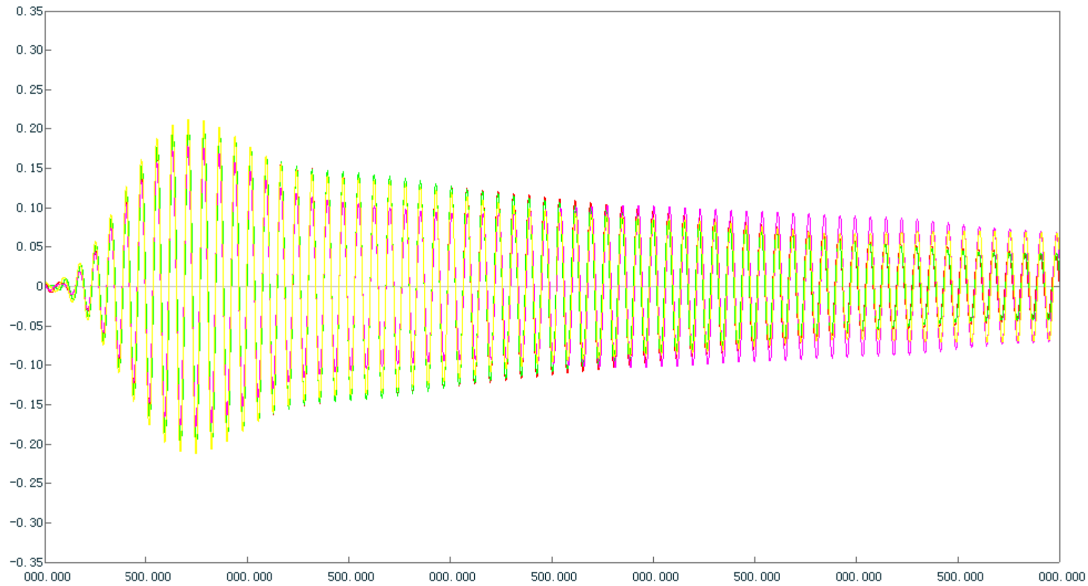

Fig. 7.45b Transient-state waveforms of three-phase currents when the SSR-DS was put into operation (1)

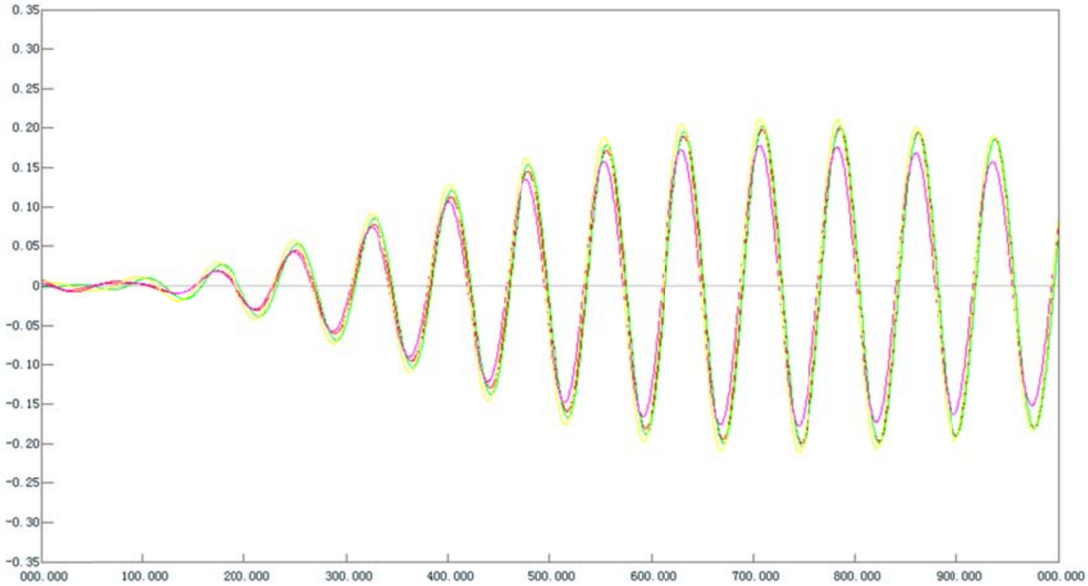

Fig. 7.45c Transient-state waveforms of three-phase currents when the SSR-DS was put into operation (2)

Fig.7.45a shows the waveforms of three-phase currents when a short-circuit fault occurred in the Xinzhou-Shijiazhuang series compensation lines II, four generators were connected to the grid, and the SSR-DS was in operation to suppress the 13Hz subsynchronous resonance/oscillations, and it can be seen that the SSR-DS, after being put into operation, suppressed the subsynchronous oscillations of the generators. Fig.7.45b and Fig.7.45c show the recorded transient-state waveforms when the SSR-DS was put into operation, from which we can see that the currents decreased from the original divergence to stability rapidly.

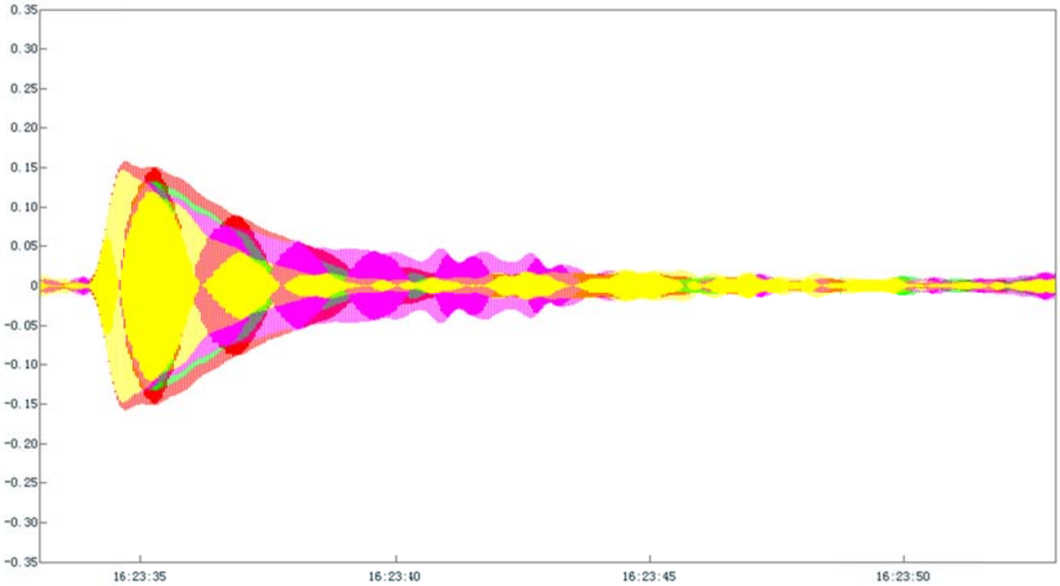

Fig. 7.46a Waveforms of three-phase currents when a short-circuit fault occurred, and the SSR-DS was put into operation to suppress 22Hz SSR

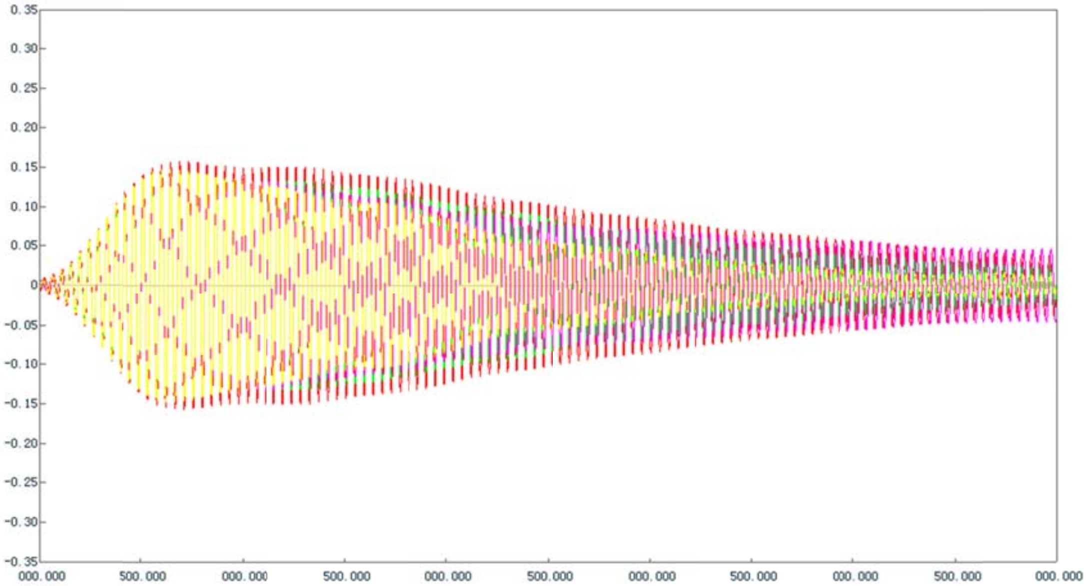

Fig. 7.46b Transient-state waveforms of three-phase currents when the SSR-DS was put into operation (1)

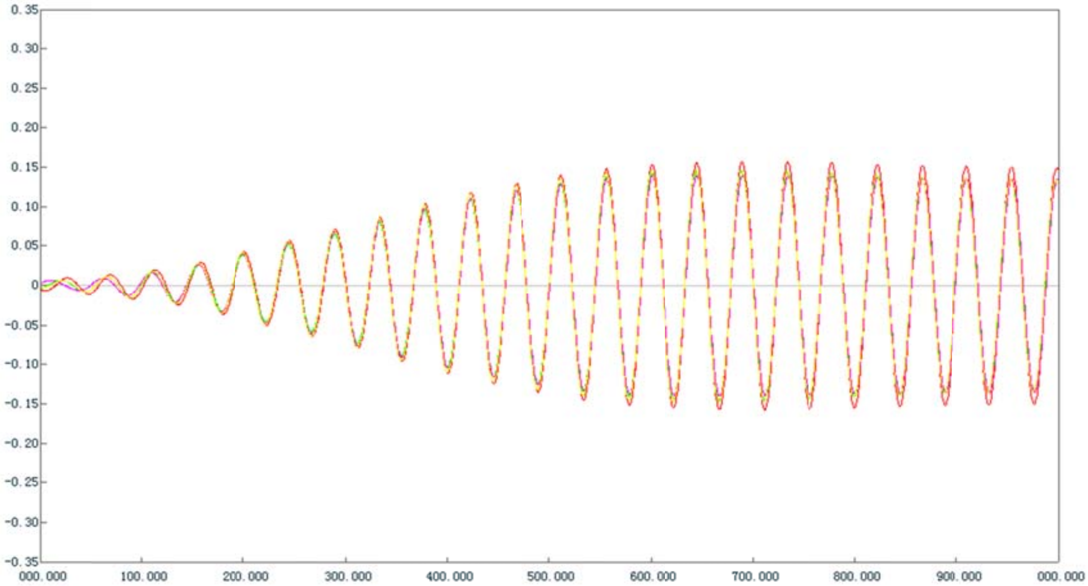

Fig. 7.46c Transient-state waveforms of three-phase currents when the SSR-DS was put into operation (2)

Fig.7.46a shows the waveforms of three-phase currents when a short-circuit fault occurred in the Xinzhou-Shijiazhuang series compensation lines II, four generators were connected to the grid, and the SSR-DS was in operation to suppress the 22Hz subsynchronous resonance/oscillations, and it can be seen that the SSR-DS, after being put into operation, suppressed the subsynchronous resonance/oscillations of the generators. Fig.7.46b and Fig.7.46c show the recorded transient-state waveforms when the SSR-DS was put into operation, from which we can see that the currents decreased from the original divergence to stability rapidly.

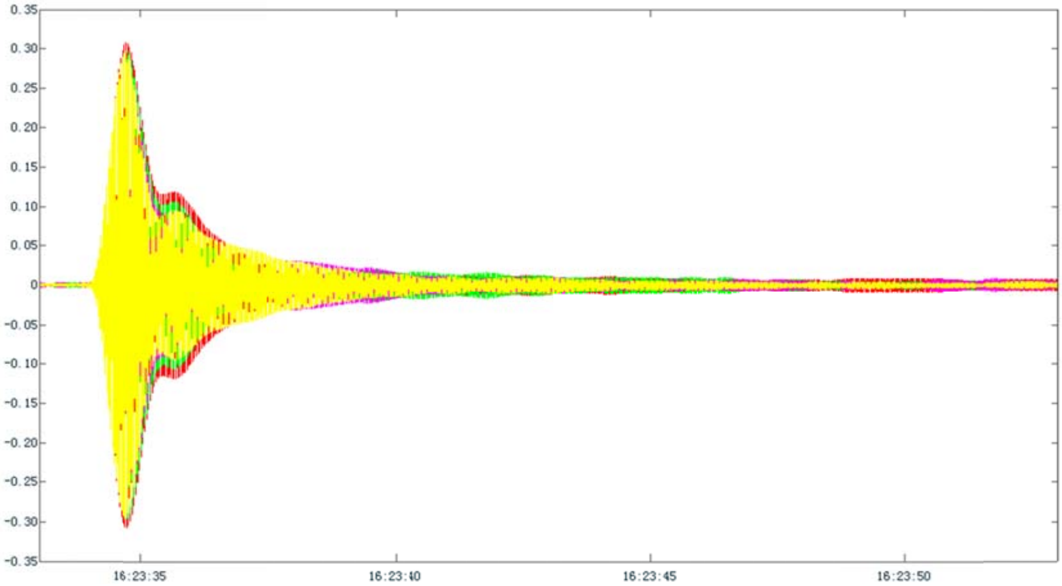

Fig. 7.47a Waveforms of three-phase currents when a short-circuit fault occurred, and the SSR-DS was put into operation to suppress 28Hz SSR

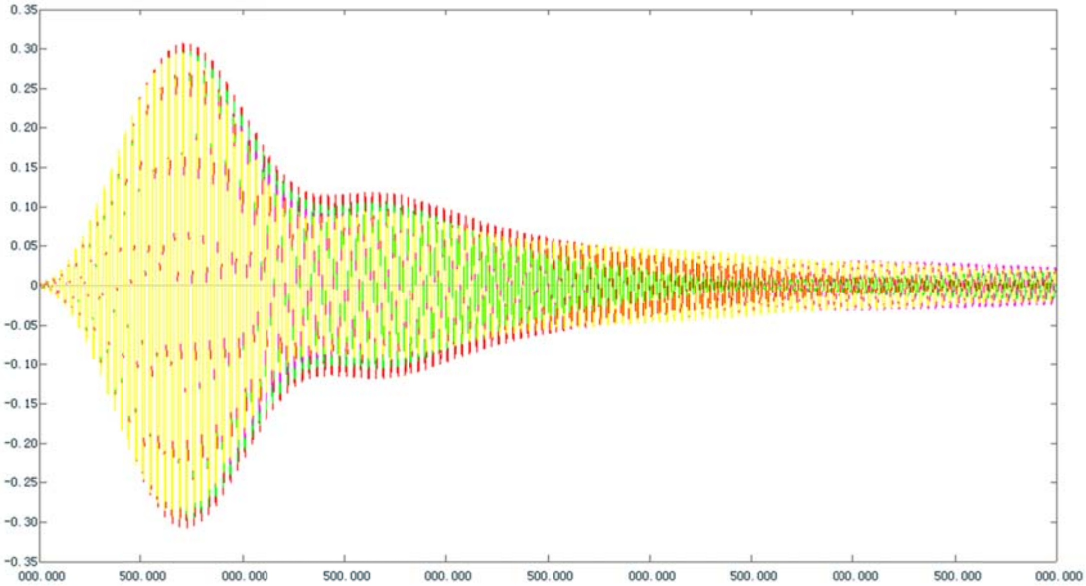

Fig. 7.47b Transient-state waveforms of three-phase currents when the SSR-DS was put into operation (1)

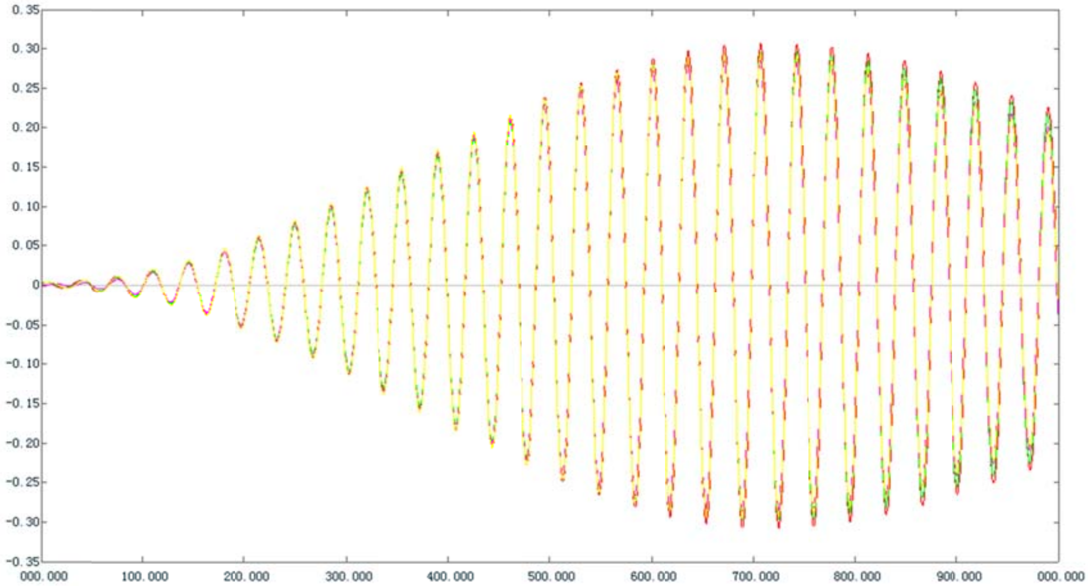

Fig. 7.47c Transient-state waveforms of three-phase currents when the SSR-DS was put into operation (2)

Fig.7.47a shows the waveforms of three-phase currents when a short-circuit fault occurred in the Xinzhou-Shijiazhuang series compensation lines II, four generators were connected to the grid, and the SSR-DS was in operation to suppress the 28Hz subsynchronous resonance/oscillations, and it can be seen that the SSR-DS, after being put into operation, suppressed the subsynchronous resonance/oscillations of the generators. Fig.7.47b and Fig.7.47c show the recorded transient-state waveforms when the SSR-DS was put into operation, from which we can see that the currents decreased from the original divergence to stability rapidly.

As can be seen from the above figures, the SSR-DS can suppress the subsynchronous resonance/oscillations of the generators well, and the four generators showed basically identical amplitudes and phases.

7.5 Summary

Simulation experiments and field operation of the subsynchronous resonance/oscillations suppression project in Jinjie Power Plant contribute the following conclusions:

The TCR + FC type of SVC is capable of suppressing the subsynchronous resonance/oscillations of the shaftings of large generators with rapid system response, high control precision and good suppression results.

A control algorithm was brought forward, proving a new approach to suppressing subsynchronous resonance/oscillations of shaftings of large generators. And the control devices designed on the basis of this algorithm have been in operation in Jinjie Power Plant with good control results, proving that this algorithm is feasible. And the devices were pioneering in our country, and in the lead worldwide.

The SVC-based SSR-DS tackles the problems of the potential damage of subsynchronous resonance/oscillations brought about by the series compensators installed in the long-distance power transmission lines. The success of this project indicates that our country has been in the lead in the way of solving the problems of subsynchronous resonance/oscillations.

CHAPTER 8 ENGINEERING EXAMLES OF SVC IN ULTRAHIGH-VOLTAGE DC POWER TRANSMISSION SYSTEM

To save the precious resources of power transmission corridors, sites of converter stations and sites of grounding poles, improve the utilization rates of power transmission resources, and enhance the technological upgrades of the grid, China Southern Power Grid built the ±800kV Yunnan-Guangdong Ultrahigh-voltage DC Power Transmission Project, the ultrahigh-voltage DC power transmission project with the highest voltage level worldwide so far.

To solve such problems of the HVDC systems as voltage stability and overvoltage in time of DC block faults, we designed two sets of SVCs, each with a capacity of 120Mvar, which were installed in Chuxiong Converter Station at the starting point of Yunnan-Guangdong Ultrahigh-voltage DC Power Transmission System. This was the first case that the SVCs were used in the ultrahigh-voltage DC power transmission system, and was also the first case that two sets of SVCs were totally independently and automatically controlled and were used to control the same objective quantity operated in parallel.

8.1 Voltage Problems in Yunnan-Guangdong UHVDC Power Transmission Lines

The Yunnan-Guangdong DC power transmission system has a capacity of 5000MW with a ±800kV voltage level, and each pole is connected in the manner of series double 12-pulse valve banks. The power transmission lines are about 1418km in length, with a sectional area of 6×630mm^2. And there are eighteen small banks of filters and capacitors in the converter station, amounting to 3366Mvar in total and 187Mvar per small bank, and the filters and capacitors are arranged in four large banks, with the capacity of the largest bank being 935Mvar (5×187MVar). So far, this system has been in operation for more than two years.

Chuxiong Converter Station at the sending end of the system is connected to the 500kV Heping Substation in the main Yunnan Grid via a double-circuit 500kV AC power transmission lines, and the Xiaowan Hydraulic power plant (with an installed capacity of 4200MW) in the west and the Jinanqiao Hydraulic power plant (with an installed capacity of 2400MW) in the northwest are both integrated into Chuxiong Converter Station via a double-circuit 500kV AC power transmission lines.

The Yunnan-Guangdong DC power transmission system has a large capacity, and the converter station at the sending end is far from power substations and near the Kunming load center in Yunnan Grid, where there are no large power sources, the system is short of reactive power support and the AC system is relatively weak. According to the results of grid stability calculations, in the parallel AC/DC operation manner, the unipolar block of Yunnan-Guanggong DC system or three-phase fault in the Chuxiong-Heping tie lines has become the most severe fault manner to restrict the stability limits of the "Transmission of West Power to the East" channels in China Southern Power Grid. In order to improve the system stability, the isolated operation manner could be adopted at Chuxiong Converter Station in the sending end of the Yunnan-Guangdong UHVDC transimission system that the tie line between Chuxiong and Heping station would quit operation and therefore the power from Xiaowan and Jinanqiao hydrolic power plants would feed the Guangdong power grid directly.

When working in the isolated manner, Chuxiong Converter Station at the sending end of the Yunnan-Guangdong DC power transmission system will also bring about some problems to the system while improving the system stability levels. For example, the AC system that the sending end of the DC system is connected to becomes weaker in strength, with the effective short-circuit ratio (ESCR)at the converter station bus being only about 1.22; the bus voltage fluctuations are large when the reactive power sources are switched, and maximum changing rates of transient voltages and steady voltages when the small banks of reactive power sources are switched in normal wiring manner may reach 4.5% and 1.9% (or even higher in the case of N-1 fault in Xiaowan station or Jinanqiao station), exceeding the limits stipulated in the specifications. Meanwhile, the bipolar block of the DC system will result in high overvoltage in the AC buses, exceeding the limits stipulated in the specifications, and measures must be taken to reduce the overvoltage levels.

8.2 Calculation Analyses and Suggestions

8.2.1 Results of the SVCs in Suppressing Voltage Fluctuations in Chuxiong Converter Station in Normal Operation Manners

According to the calculations, Fig. 8.1a through Fig. 8.1c show the transient-state curves of the bus voltages, DC firing angles, SVC outputs at the Chuxiong Converter Station when the SVCs operate with different capacities of 0Mvar, ±120Mvar, ±150MVar, ±180Mvar, ±210MVar and ±240Mvar, the outcoming lines of Xiaowan Station operate in "N-1" manner, and a 187Mvar small bank of reactive power sources are switched off. As can be seen from these figures, the fluctuations of the AC bus voltages and of the triggering angles of the converters at Chuxiong Converter Station decrease obviously.

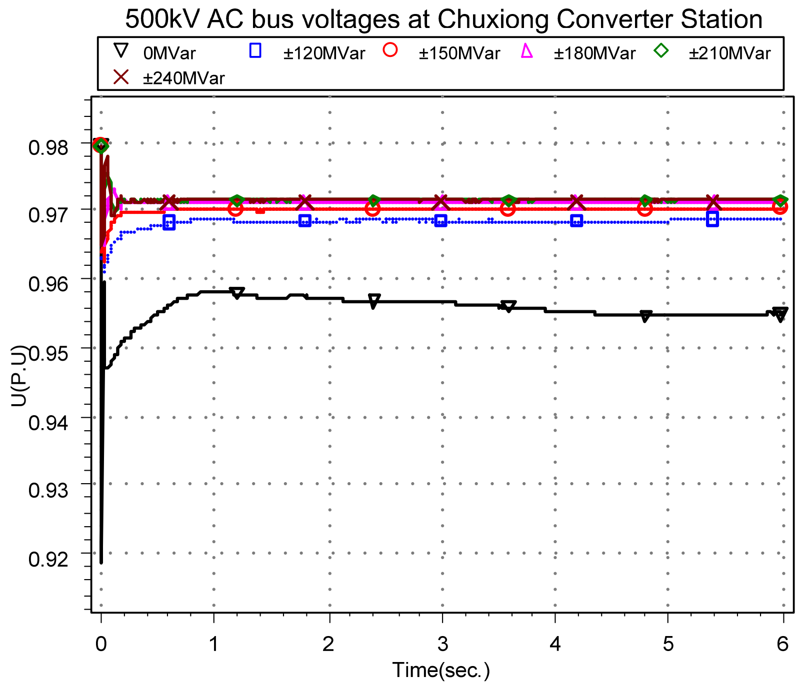

Fig. 8.1a AC bus voltages at Chuxiong Converter Station (outcoming lines of Xiaowan Station in "N-1" fault manner, and a 187Mvar small bank of reactive power sources switched off) (Calculation based on the data provided by CSG)

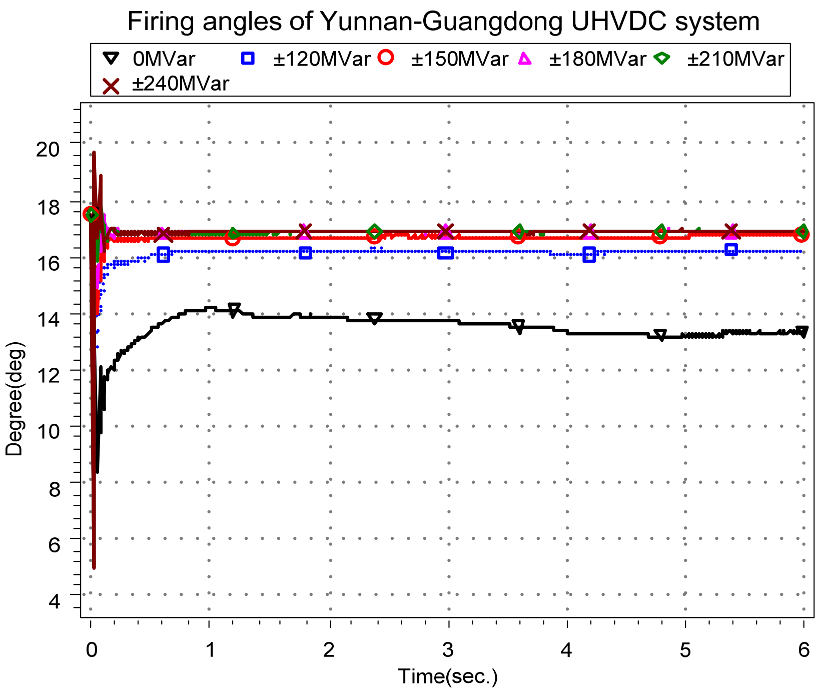

Fig. 8.1b Firing angles of Yunnan-Guangdong ultrahigh-voltage DC system (outcoming lines of Xiaowan Station in "N-1" fault manner, and a 187Mvar small bank of reactive power sources switched off) (Calculation based on the data provided by CSG)

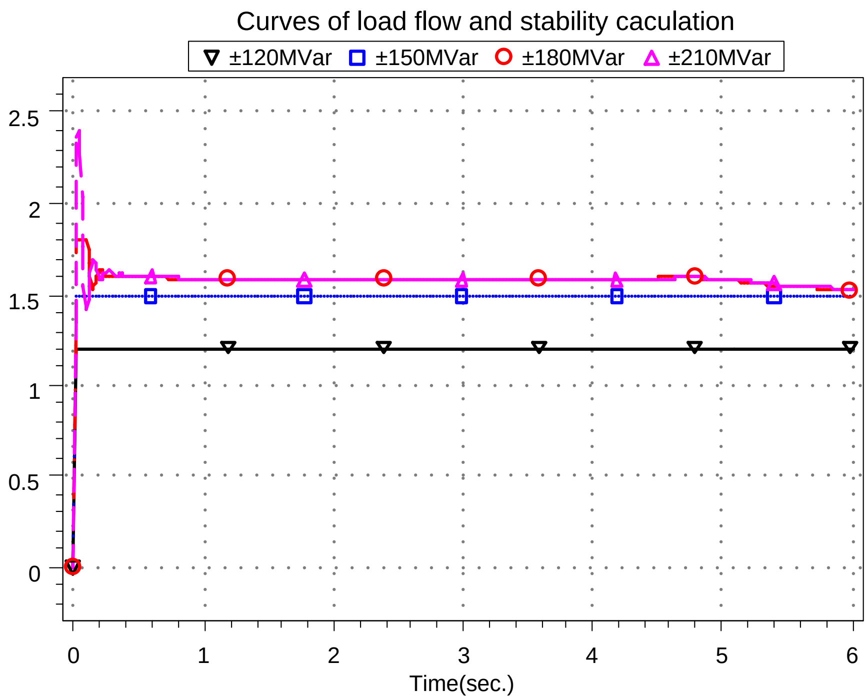

Fig. 8.1c Reactive power output of the SVCs in Chuxiong Converter Station (p.u., with 100MVA as the base) (Calculation based on the data provided by CSG)

As can be seen from the calculation results,

(1) An SVC of ±60～±90Mvar installed at the converter station can meet the requirements of voltage fluctuations suppression (1.68%~1.42% transient-state voltage fluctuations when a small bank is switched on/off) when the converter station is in normal isolated operation manner, but the SVC is incapable of meeting the requirements suppression (2.79%~2.34% transient-state voltage fluctuations when a small bank is switched on/off) when the converter station is in "N-1" isolated operation manner;

(2) The SVC of ±120Mvar installed at the converter station can basically meet the requirements of voltage fluctuations suppression when the converter station is in normal isolated operation manner and in "N-1" isolated operation manner, and the transient-state and steady-state voltage fluctuations voltage fluctuations are 1.97% and1.16% respectively when a small bank is switched on/off;

(3) The SVC of ±180Mvar installed at the converter station has more powerful capabilities of suppressing voltage fluctuations, meeting the requirements of

suppressing voltage fluctuations in normal isolated operation manner and in "N-1" isolated operation manner while maintaining fairly large margins, with the transient-state and steady-state voltage fluctuations being 1.52% and 0.87% respectively when a small bank is switched on/off;

(3) Since the capacity of a small bank of reactive power sources is 187Mvar, the SVC with a capacity above ±180Mvar will not further ameliorate the results of voltage fluctuations suppression obviously. For example, after the SVCs of ±210MVar～±240Mvar are installed at the converter station, the transient-state and steady-state voltage fluctuations are about 1.51% and 0.85% respectively when a small bank is switched on/off, basically the same case as that of the SVC of ±180Mvar;

(4) As the comparisons of the calculation results of voltage fluctuations in the context of the SVCs of different capacities indicate, an SVC of ±120 Mvar can basically meet the requirements of suppressing voltage fluctuations when a small bank is switched on/off (with the maximum transient-state voltage fluctuations being 1.97%), and the SVC with a capacity of above ±180 Mvar can meet the requirements of suppressing voltage fluctuations when a small bank is switched on/off while maintaining certain margins.

8.2.2 Effect of the SVC in Improving the Grid Stability Levels

Comparisons of the changes of the voltage fluctuations at the bus of the converter station, firing angle of the converter valves, and the DC power before and after the 240Mvar SVCs are installed at Chuxiong Converter Station are made in accordance with the stability calculation curves shown in Fig. 8.2a through Fig.8.2h, where Fig.8.2a through Fig.8.2d show the stability curves when the Yunnan Grid sends out 7065MW power at stability limits without the SVC installations in 2011, and Fig.8.2e through Fig.8.2h show the stability calculation curves when 240Mvar SVCs are installed at Chuxiong Converter Station (for the purpose of comparisons, we use the curves that are not corresponding to the stability limits while remaining the other conditions unchanged).

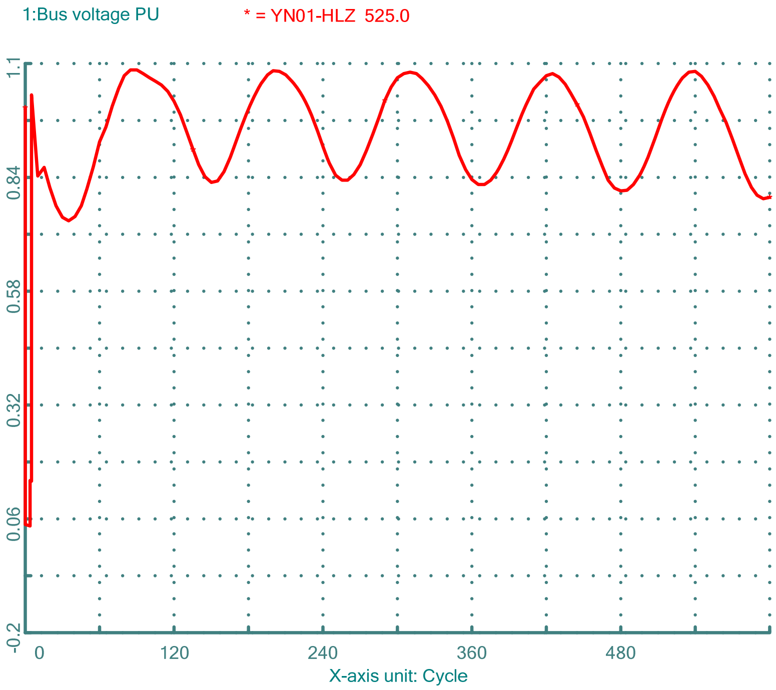

Fig. 8.2a Curve of bus voltage at Chuxiong Converter Station when a three-phase fault occurs in Chuxiong-Heping lines and no SVC is installed in 2011 (Calculation based on the data provided by CSG)

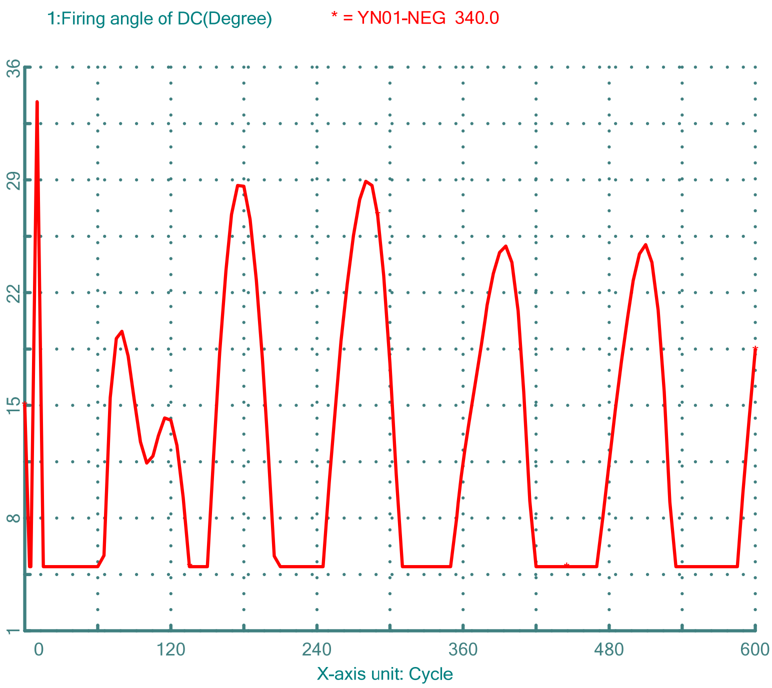

Fig. 8.2b Curve of firing angle at Chuxiong Converter Station when a three-phase fault occurs in Chuxiong-Heping lines and no SVC is installed in 2011 (Calculation based on the data provided by CSG)

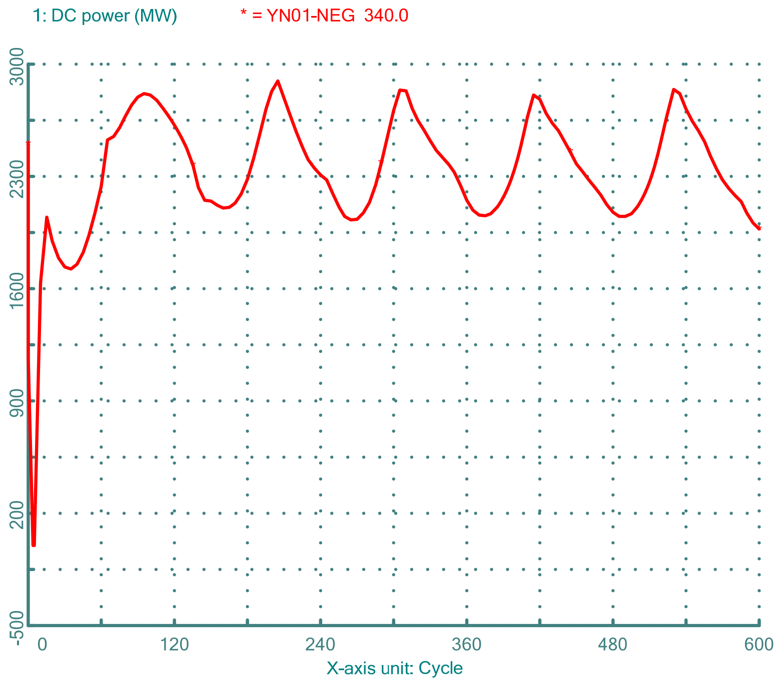

Fig. 8.2c Curve of DC power at Chuxiong Converter Station when a three-phase fault occurs in Chuxiong-Heping lines and no SVC is installed in 2011 (Calculation based on the data provided by CSG)

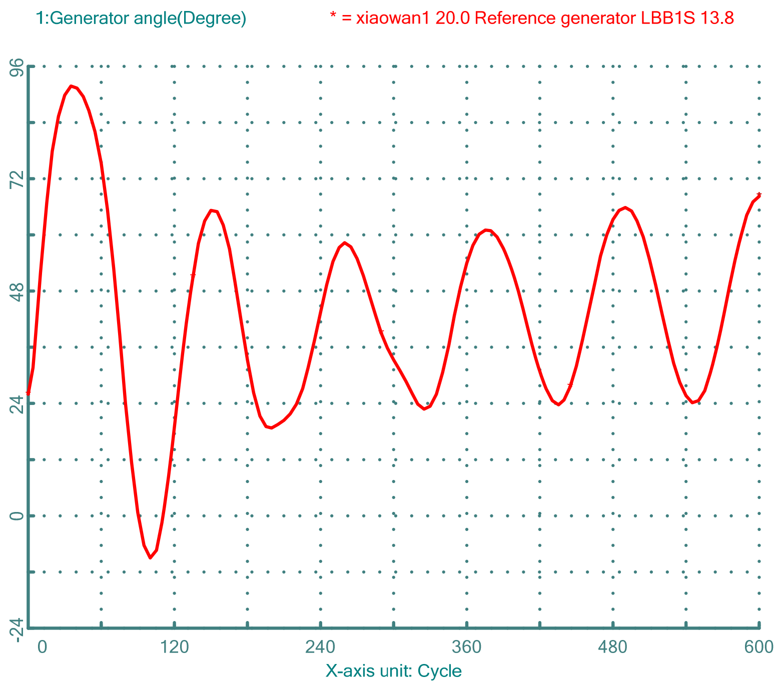

Fig. 8.2d Curve of generator angle at Xiaowan Hydraulic power plant when a three-phase fault occurs in Chuxiong-Heping lines and no SVC is installed in 2011 (Calculation based on the data provided by CSG)

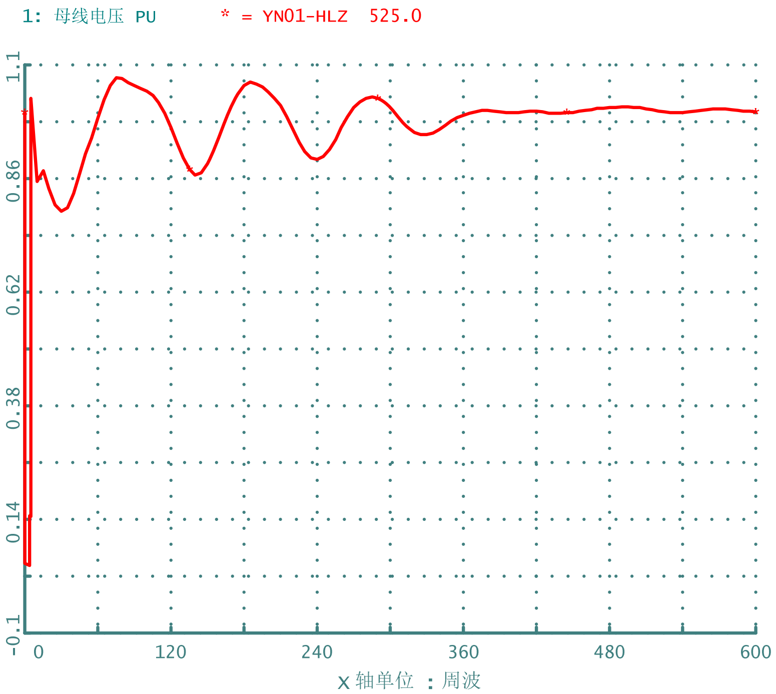

Fig. 8.2e Curve of bus voltage at Chuxiong Converter Station when a three-phase fault occurs in Chuxiong-Heping lines and the 240Mvar SVCs are installed at Chuxiong Converter Station in 2011 (Calculation based on the data provided by CSG)

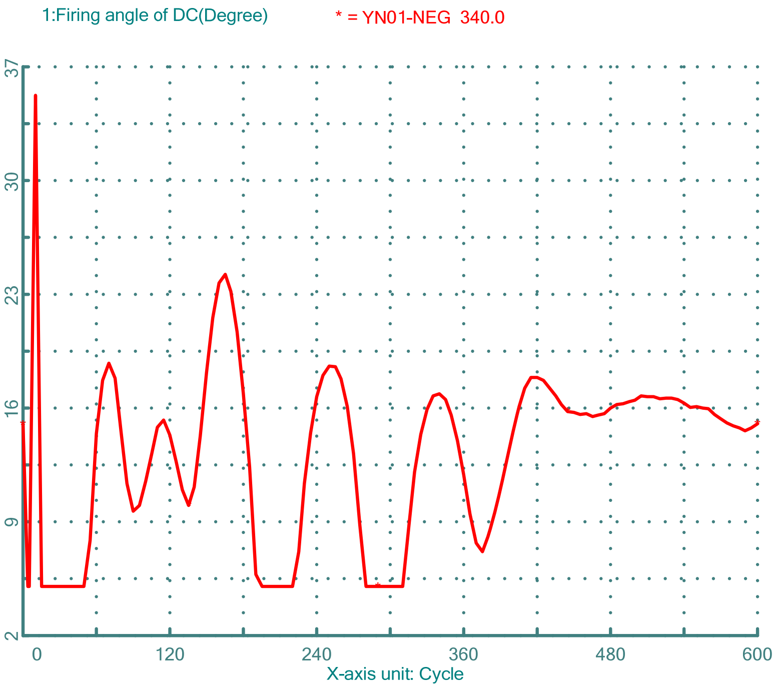

Fig. 8.2f Curve of firing angle at Chuxiong Converter Station when a three-phase fault occurs in Chuxiong-Heping lines and the 240Mvar SVCs are installed at Chuxiong Converter Station in 2011 (Calculation based on the data provided by CSG)

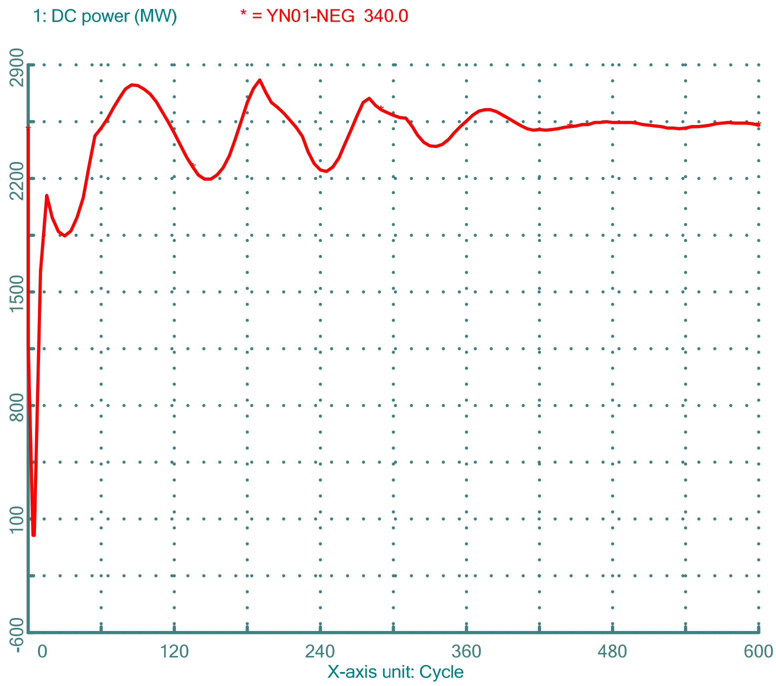

Fig. 8.2g Curve of DC power at Chuxiong Converter Station when a three-phase fault occurs in Chuxiong-Heping lines and the 240Mvar SVCs are installed at Chuxiong Converter Station in 2011 (Calculation based on the data provided by CSG)

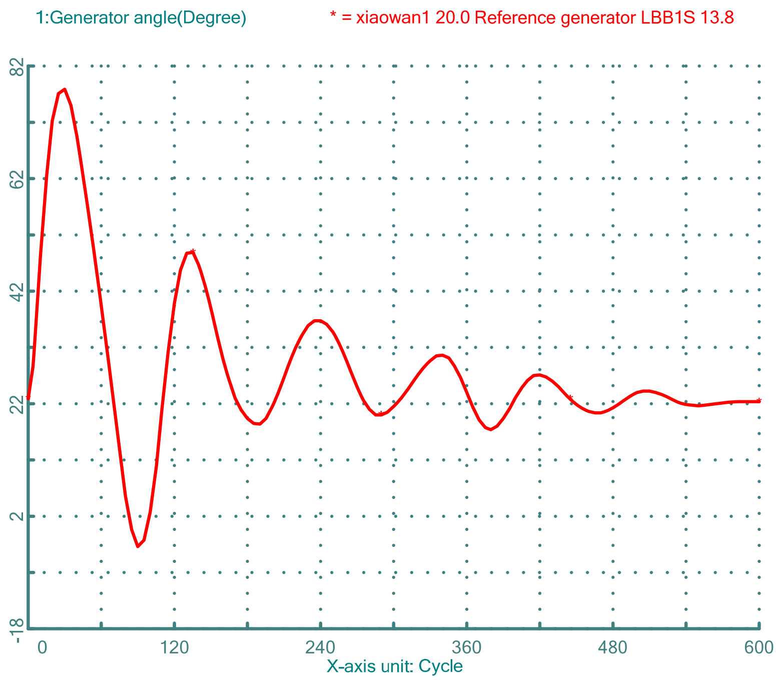

Fig. 8.2h Curve of generator angle at Xiaowan Hydraulic power plant when a three-phase fault occurs in Chuxiong-Heping lines and the 240Mvar SVCs are installed at Chuxiong Converter Station in 2011 (Calculation based on the data provided by CSG)

As the comparisons of the two groups of curves indicate, with the 240Mvar SVCs installed at Chuxiong Converter Station, when a three-phase fault occurs in Chuxiong-Heping lines, the bus voltage fluctuations at Chuxiong Converter Station decrease obviously, and the firing angle of the DC system also decrease accordingly in terms of fluctuation amplitudes and cycles. That is to say, the SVCs are helpful to the control and stability of the DC power, and therefore are beneficial to the stable operation of the AC systems.

8.3 Implementation of the First Case of Multiple Sets of Self-governed SVCs in Parallel Operation Worldwide

In recent year, with the development of large grids and ultrahigh-voltage DC power transmission systems, the SVCs have becoming increasingly large in terms of capacity. For example, the per set capacity of the SVCs at Wuzhou Substation reaches 210Mvar, close to the limits of the breaking capability of the circuit breakers. This means that, if the equipment capacities continue to increase, we can only design the multiple SVCs in parallel operation. For example the two sets of SVCs, each with a capacity of 120Mvar, operate in a parallel manner. Meanwhile, to improve reliability and flexibility, multiple sets of FACTS devices need to operate in parallel to achieve capacity expansion and flexible dispatch, and this will be one of the important directions of power electronics technology [8.1].

Among the power electronics devices, the inversion power sources have drawn a lot of attention and been researched, and is developing towards high power density, large capacity, high reliability, and intelligentization [8.2][8.3]. So far there are many control approaches to the parallel connections of the power electronics devices, among which the synchronous switching control method and the master-slave control method are easy to design and implement, but such methods can actually be regarded as one system. Since the methods are still a controller essentially, there are no redundancies in the true sense [8.4]. For the inverters, based on the droop characteristic method, there are no interconnection lines among various modules, and the reliability is high, but it is hard to realize [8.5]. It is notable that, in all these methods, the inversion power sources are taken as the research objects, the outputs are not directly connected to the large grids, the grids are not regulated or controlled, and the control feedback quantities are not from the grids, so these methods are not suitable for the multiple sets of parallel; SVCs that are used to control the grid voltages. As the needs of the SVCs of ultra-large capacities are not urgent until recent years, the past theoretical research and engineering practice of the parallel connections of large-capacity SVCs were almost blank.

The two sets of SVCs at Chuxiong Converter Station were the first case of two sets of parallel SVCs that are totally independently and automatically controlled worldwide.

The two sets of SVCs at Chuxiong Converter Station, with its new control structure, made the following breakthroughs:

(1) No special synchronization is needed between the two sets of SVCs, i.e. the synchronous switching control method or similar methods are not applied.

(2) No master-slave structures are adopted, no controller of one set of SVC controls multiple sets of devices, and the devices control themselves independently respectively.

(3) There are no interconnection lines among various modules.

(4) The SVCs share the same control objectives and may share the same feedback quantities, but they are capable of balancing their steady-state outputs and transient-state outputs without bringing about mutual oscillations back and forth.

8.3.1 Problems with Multiple Sets of Shunt self-governed SVCs with Conventional controls

The SVCs used in the grids can maintain the voltages of the integration points at certain levels, and enhance the stability of the power systems. The main control of the SVC is the closed-loop voltage feedback control, and in the context of constant reactive power control, the SVC regulates the output reactive currents to compensate for the voltage fluctuations of the systems.

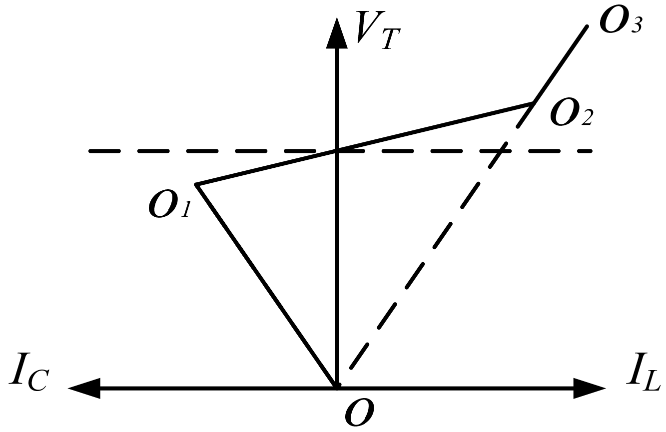

Fig. 8.3 Voltage-current characteristics of the SVC

The voltage-current characteristic curves of the TCR-based SVC are shown in Fig. 8.3, where the normal operation region of the SVC is the controllable range between O_1 and O_2 . To get the sloping voltage-current characteristic curves, we introduce additional compensatory current feedback on the basis of voltage feedback, and determine the voltage-current slopes of the SVC according to the gains of the feedback channels of the reactive compensatory currents, taking the voltage regulations as the control objective.

The two sets of SVCs at Chuxiong Converter Station were designed to operate in parallel, with the 35kV side connected to the 500kV bus via transformers, to improve the total capacity and the system reliability. Thus when the system voltage deviates from the setting, each SVC will change the reactive current outputs to regulate the system voltage to a new value. Theoretically and ideally, owing to the same settings of the voltage-current curves, each set of SVCs will share the same outputs, and no interconnected communication is needed between the two SVCs[8.6][8.7].

But actually, there may be reactive power oscillations between the two sets of SVCs for the following reasons:

(1) The voltage transformer errors result in a difference of about 1kV between the input voltage signals into the controllers of the two SVCs, making the two sets of SVCs operate at different working points, as shown in Fig. 8.4.

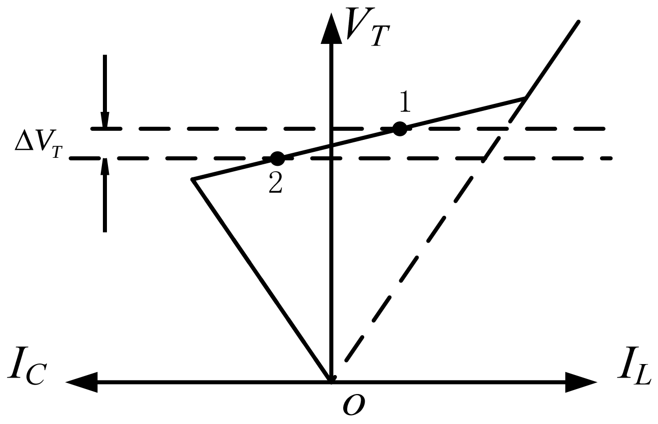

Fig. 8.4 Different currents at the working points corresponding to the same voltage in the case of deviations between the input signals of the two SVCs

(2) The ratio of the SVC capacity to the short-circuit capacity of the integrated system is small, and the SVC is only slightly capable of changing the voltage of the integration point, i.e. the slope of the voltage-current characteristic curve has a very small adjustable range. Owing to the small slope, the SVC is vulnerable to the hardware errors and disturbance signals at the proportional link of the PI controller such that the slopes of the voltage-current characteristics and the working points of the two SVCs are no longer the same. Fig.8.5 shows the case that the two sets of SVCs output capacitive and inductive reactive power respectively.

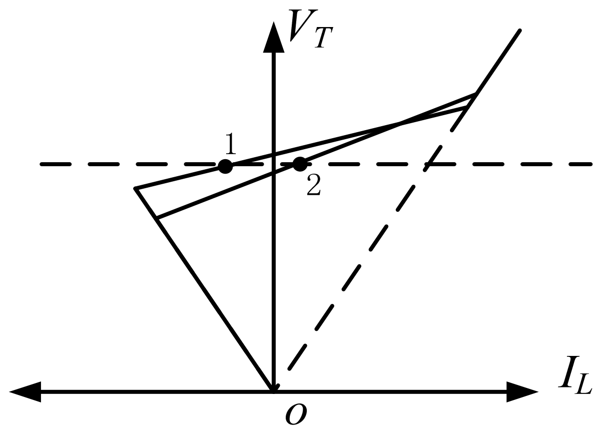

Fig. 8.5 Different working points corresponding to the same voltage when the two SVCs have different slopes of the voltage-current characteristics

If the relative magnitudes of the deviations of the feedback input signals or of the slope of the two SVCs change randomly over time owing to the disturbances, then the reactive power will necessarily be redistributed between the two SVCs, and this will bring about reactive power oscillations. Unfortunately, no one has ever considered such a practical problem that will inevitably emerge in projects.

Multiple nonideal factors may contribute to the great differences of the working points at the voltage-current characteristic curves of the two SVCs, and the capacity distribution difference resulting from the sensor errors cannot be offset by the method of increasing the slopes. In time of disturbances, when the reactive power loads are low, the reactive power may oscillate and fluctuate back and forth obviously between the two SVCs, mainly because the two SVCs are asynchronous in terms of output regulations and the SVCs are incapable of having their switching frequencies increased to more than one order of magnitude above the power frequency to eliminate the impact of the lagging responses.

RTDS experiments show that, when the two SVCs with conventional control at the Chuxiong Converter Station are independently controlled and operate in parallel, there may be the phenomena of reactive power oscillations between the SVCs sometimes. As multiple experiments indicate when two sets of SVCs are started up successively and the reactive power loads are transferred from one set of SVC to two sets of SVCs for redistribution, there may be a process of reactive power oscillations back and forth between the two sets of SVCs for reactive power redistribution.

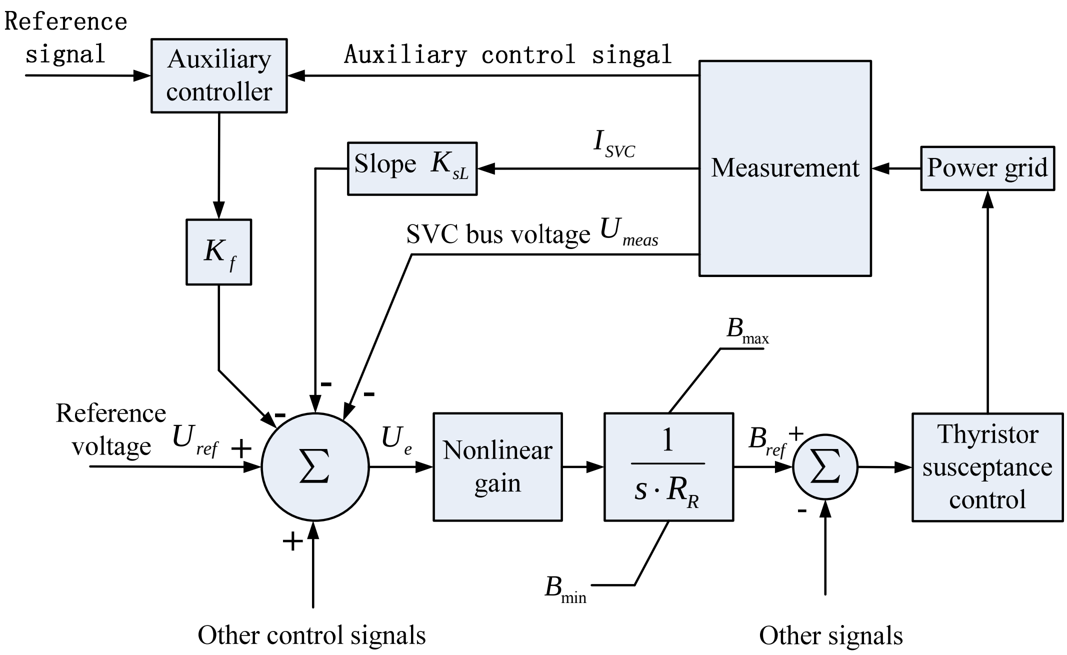

Fig. 8.6 Block diagram of original conventional control system structure

Fig.8.6 shows the block diagram of the structure of conventional SVC control systems. This structure was from the basic model 2 of SVC control system by the IEEE [8.8]. Fig.8.7a and Fig.8.7b show the basic model 2 of SVC control system by IEEE and the corresponding voltage regulator model.

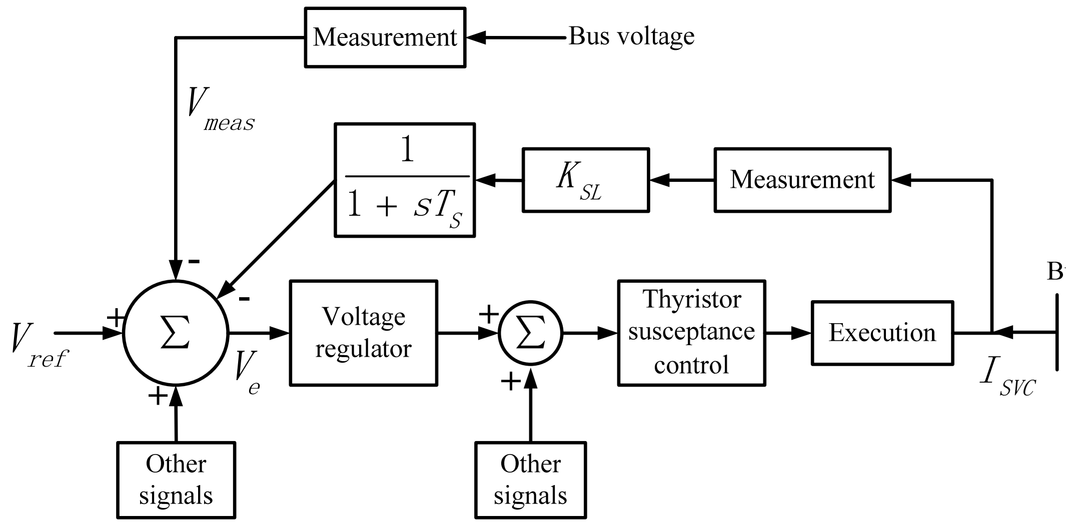

Fig. 8.7a Basic model 2 of SVC control system by IEEE

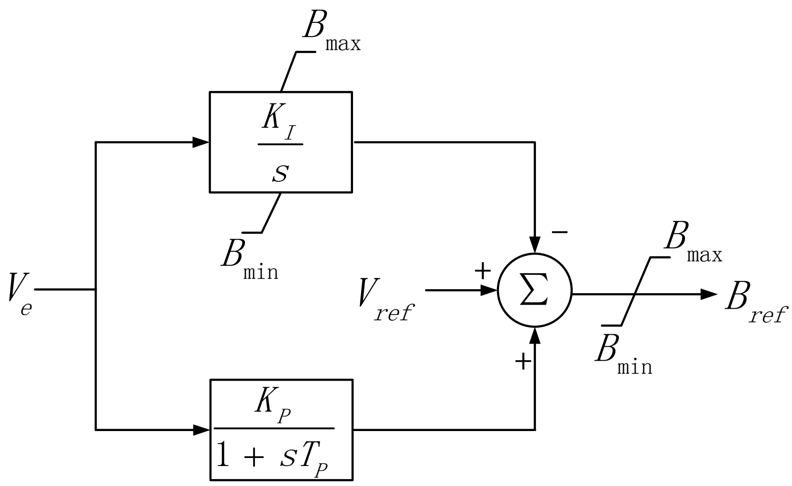

Fig. 8.7b Voltage regulator model

The equivalent of the voltage regulator in basic model 2 of SVC control system by IEEE may be

$$G(s)=\frac{K_I}{s}\left(\frac{1+sT_Q}{1+sT_P}\right) \tag{8.1}$$

where

$$T_Q = T_P + \frac{K_P}{K_Q} \tag{8.2}$$

and T_P is usually equal to 0, so the controller can be transformed into a simpler proportion-integration (PI) model.

The PID controller in the control system of the SVCs at Chuxiong Converter Station is actually a PI controller consisting of a proportion link P and an integration link I without the differentiation link D out of two considerations: the nonlinear link has taken the changing rates of errors into account and is a nonlinear PID controller essentially; the PI controller is sited in front of the control channels that contain the lagging link, and its control results may be impacted by the lagging link. And the optimal parameters of the PI links vary with the different inputs, and the parameters are hard to set up.

Many variables may impact the controller measurements, but only part of the variables are operable, where one variable must be controlled by the controller, and the other variables are defined as the disturbance variables of the control loops. In the RTDS simulation experiments, the RTDS output hardware devices can generate the random disturbances that exist permanently in practice, because these disturbances will make the control parameters deviate from the settings, and the controllers must respond to them. But, in the feedback control loops, the controllers will not act until the impact of these disturbances on the controlled variables are displayed in the measured signals, and the controllers have not even realized these disturbance before that. Thus the controllers can only try to make correct compensation according to the obtained feedback deviations, and, because the responses to the disturbances are always lagging, the oscillatory reactions of the feedback loops are the obvious consequences of such lagging response processes.

8.3.2 A Brand-new Control Structure for Multiple self-governed SVCs in Parallel Operation

When there are reactive power oscillations with the two sets of SVCs with the conventional control structure at Chuxiong Converter Station, if the oscillation frequencies are close to the inherent central frequencies of subsynchronous oscillations of the power system, the reactive power oscillations may bring about serious consequences, so measures must be taken to avoid such reactive power oscillations, and the SVC control systems needs improving.

The main objectives of improving the control systems of the two SVCs at Chuxiong Converter Station are:

(1) To ensure that the reactive power outputs of the SVCs meet the grid requirements;

(2) To coordinate the reactive power balance between the two sets of SVCs so that the two sets of SVCs can assume the reactive power outputs in equilibrium, and the rapidity and stability of the regulation responses can be achieved.

(3) To ensure that the SVCs operate securely under various operation conditions.

The crux of the two sets of self-governed SVCs in parallel operation lies in the balanced distributions of the load currents. And the two sets of SVCs must ensure the same output regulation directions even when the SVCs are not precisely synchronous; otherwise, there will be reactive power oscillations back and forth between the two sets of SVCs.

The conventional control is generally the negative-feedback control, as shown in Fig.8.8, where the regulator will not function until the controller objects are disturbed and the controlled quantities deviate from the settings, and the control actions always lag behind the disturbances. The SVC controller adopts the PI control algorithms, characterized by simple structure, easy operations, high reliability, but when the reactive power loads of the system change over a large range, owing to such factors as the large deviations, the system delay in itself and integration saturation, the PI controllers will be saturated, there will be overshoots of oscillations in the system, and the dynamic and stable performances cannot be taken into account well together.

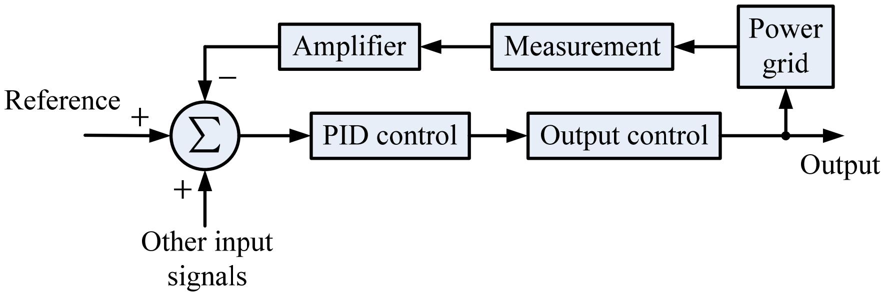

Fig. 8.8 Conventional negative feedback control structure

By studying SVC model 2 by IEEE, we can see that this model introduces current feedback to achieve the regulation difference characteristics, i.e. to modify the voltage references according to the magnitude of reactive currents, and then determine the slope of the voltage-current characteristics according to the gain of the feedback channel. Enlightened by this, we will add an input channel to the control structure, which may impact the SVC outputs and the slopes of the voltage-current characteristics.

In accordance with such drawbacks as dynamic delay and lagging inertia that exist in the system, we introduce the feedforward variables, and change the original feedback structure into a composite control structure that integrates feedback and feedforward.

According to the concept of correction in the control theory, the feedforward controller achieves the open-loop control, and does not need to take action to correct the deviations after the output variables change and produce deviations. Rather, the feedforward control functions at the same as the control functions work on the system. So, the feedforward control is timelier than the feedback control, irrelevant to the system delays. Undoubtedly, this helps to eliminate the impact of lagging links of the control channel.

When two sets of SVCs operate in parallel, the reactive power output of one set of SVC is disturbance to the control lope of the other set mutually. To reduce this disadvantageous impact, we must introduce the reactive power output of one set of SVC as the feedforward control of signals so as to optimize the system control performance. The feedforward regulations take corresponding regulatory actions according to the magnitude and directions of the disturbance, so the regulations are so rapid and timely that, theoretically speaking, they can achieve full compensations and keep the regulated quantities constant during the regulation process. Therefore, the feedforward control is indispensable for the SVC to improve the load control quality.

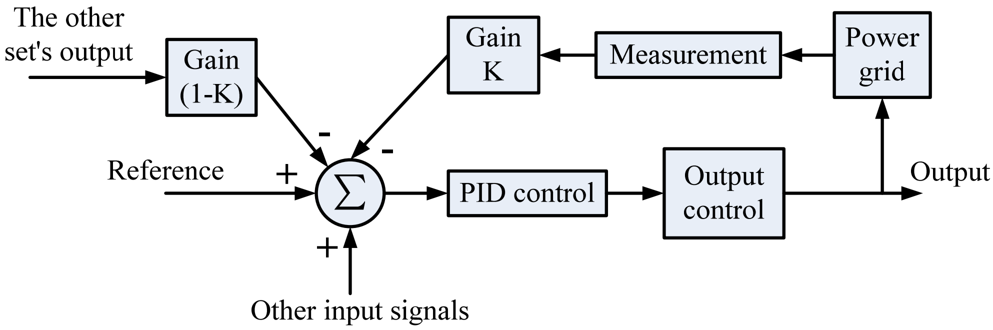

Fig. 8.9 Composite control structure integrated with the feedforward link

As shown in Fig.8.9, for one set of SVC, the currents of the other set of SVC is introduced to constitute a feedforward link. The feedforward link is essentially a pre-estimator, taking the currents of the other set of SVC as the input, and the control voltage required in the open-loop control as the output, and only when the control voltage is within the range between the maximum and minimum allowable outputs can the SVC regulate the reactive power loads assumed by the SVC to the settings with its output, where the range is positively correlated to the maximum output capability of the SVC. When the feedforward link is beyond this range, the PI controller will increase its output functions, resulting in larger fluctuations in output reactive power and worse control results. So, we should ensure that the outputs of the feedforward link are within the range of the maximum and minimum control voltages so as to facilitate so as to obtain optimal control results.

In practical projects, we may substitute half the maximum output of one set of SVC and the setting of the maximum reactive current of the other set of SVC into the control equation group to find the gain of the feedforward link pre-estimator. However, the concrete process of selecting the gain of feedforward link pre-estimator will not be addressed here.

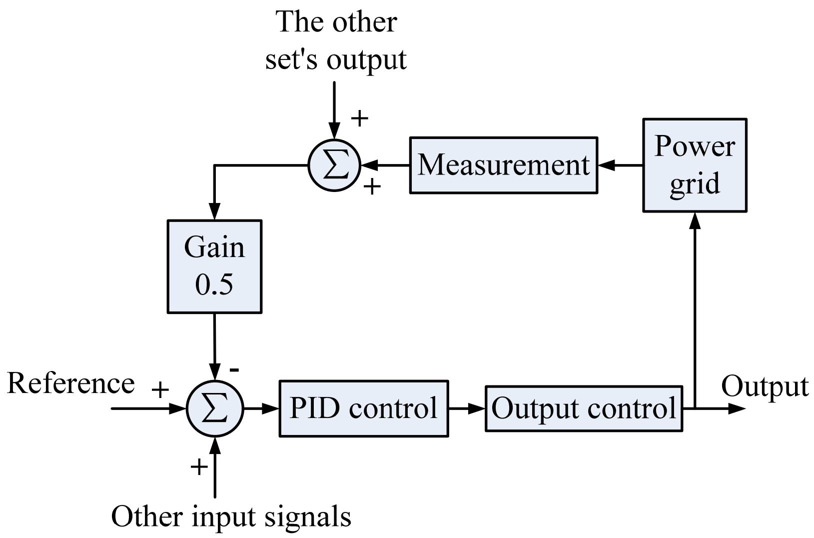

Fig. 8.10 A simplified control structure of feedforward and feedback links sharing a common input channel

In Fig.8.10, to simplify the control structure, we introduce the current of the other set of SVC, summate and average it with the current of the first set of SVC, and input the result through the channel for the current of the first set of SVC in the original control structure, i.e. the feedforward link and the current feedback link share the same channel. Taking the average of the currents of the two sets of SVCs as the input of the feedforward link, and voltage stability manner as the main closed-loop control manner, we get smoother reactive voltage output in the control loop. The voltages and output currents of the SVCs are indirectly controlled according to the magnitude of reactive power (reactive currents). The two sets of SVCs share the same input quantities in the feedforward links, and the same voltage samplings at the 500kV side as the input quantities of the main closed-loop voltage control. After the changes, the controllers of the two sets of SVCs are still mutually independent, and the calculation process of the output regulations of each set of SVC does not interact with those of the other controllers, meaning that the whole system ensures reliability and dispatching flexibility.

After studying Fig. 8.7b and Equation (8.1), in accordance with Fig.8.7a, we can see that the total gain of the current link is $-K_I \bullet K_P$.

Assume such other parameters as voltages to be constant, and then the changes of the SVC outputs are relevant only to the changes of the outputs of the current link.

Denoting the output currents of the two sets of SVCs as I_{SVC1} and I_{SVC2}, and the total gains of the current links of the two sets of SVCs as $-K_{I1} \bullet K_{P1}$ and $-K_{I2} \bullet K_{P2}$, we have

(1) In the original unrevised control structure,

The measured feedback current of the first set of SVC through the current link gain:

$$I_{SVC1} \rightarrow I_{SVC1} \bullet \left(-K_{I1} \bullet K_{P1}\right) \tag{8.3}$$

The measured feedback current of the second set of SVC through the current link gain:

$$I_{SVC2} \rightarrow I_{SVC2} \bullet \left(-K_{I2} \bullet K_{P2}\right) \tag{8.4}$$

In the unrevised control structure, we simply expect the slopes of the voltage-current characteristics of the two SVCs to be precisely identical so that they can operate at the same working point at all times, but the experiments performed when the actual controller hardware is connected to the RTDS device indicate that there are stochastic reactive power oscillations of irregular frequencies and amplitudes between the two SVCs. At this time, the two SVCs are reverse in terms of the directions of reactive current changes: when the reactive current of one SVC increases, the reactive current of the other SVC decreases, i.e., $\frac{dI_{SVC1} \bullet \left(-K_{I1} \bullet K_{P1}\right)}{dt} = \left(-K_{I1} \bullet K_{P1}\right) \bullet \frac{dI_{SVC1}}{dt}$ and $\frac{dI_{SVC2} \bullet \left(-K_{I1} \bullet K_{P1}\right)}{dt} = \left(-K_{I1} \bullet K_{P1}\right) \bullet \frac{dI_{SVC2}}{dt}$ have opposite signs.

(2) In the revised control structure,

The measured feedback current of the first set of SVC through the current link gain:

$$\frac{I_{SVC1} + I_{SVC2}}{2} \rightarrow \frac{I_{SVC1} + I_{SVC2}}{2} \bullet \left(-K_{I1} \bullet K_{P1}\right) \tag{8.5}$$

The measured feedback current of the second set of SVC through the current link gain:

$$\frac{I_{SVC1}+I_{SVC2}}{2} \to \frac{I_{SVC1}+I_{SVC2}}{2} \bullet \left(-K_{I2} \bullet K_{P2}\right) \tag{8.6}$$

Obviously, differentiating Equations (8.5) and (8.6) yields

$$\frac{d\left(\frac{I_{SVC1}+I_{SVC2}}{2} \bullet \left(-K_{I1} \bullet K_{P1}\right)\right)}{dt} = \frac{\left(-K_{I1} \bullet K_{P1}\right)}{2} \bullet \frac{d\left(I_{SVC1}+I_{SVC2}\right)}{dt} \tag{8.7}$$

and

$$\frac{d\left(\frac{I_{SVC1}+I_{SVC2}}{2} \bullet \left(-K_{I2} \bullet K_{P2}\right)\right)}{dt} = \frac{\left(-K_{I2} \bullet K_{P2}\right)}{2} \bullet \frac{d\left(I_{SVC1}+I_{SVC2}\right)}{dt} \tag{8.8}$$

Even if the measurements of current parameters are disturbed, Equations (8.7) and (8.9) are sure to have the same signs, i.e. the new control structure enables the changes of the outputs of the two SVCs to be in the same direction. And this ensures that no reactive power oscillations will occur back and forth between the two sets of SVCs.

So, introducing the output current of the other SVC as the feedforward input quantity of the very SVC enables the feedforward links to offset the impact of disturbance signals and the input quantities of the feedforward links of the two SVCs to change in the same direction. Thus, the reactive power oscillations back and forth between the two SVCs resulting from the input quantities of different phases received by the control loops of the two SVCs are avoided.

For the closed-loop control method with feedforward, the feedforward increases the response speeds of the reactive power feedback quantities, reduces the changing ranges of PI inputs, and simplifies the design of parameters. But owing to the nonlinear errors of the sensors, when the reference voltages of the two SVCs have the same phase and different amplitudes, the output reactive currents of the two sets of SVCs may be slightly different.

8.3.3 RTDS Simulation Experiments and Field Operation Performance

To test the correctness of the composite control structure, we integrated the hardware of the two self-governed controllers into the RTDS system in China Southern Power Grid for simulation experiments.

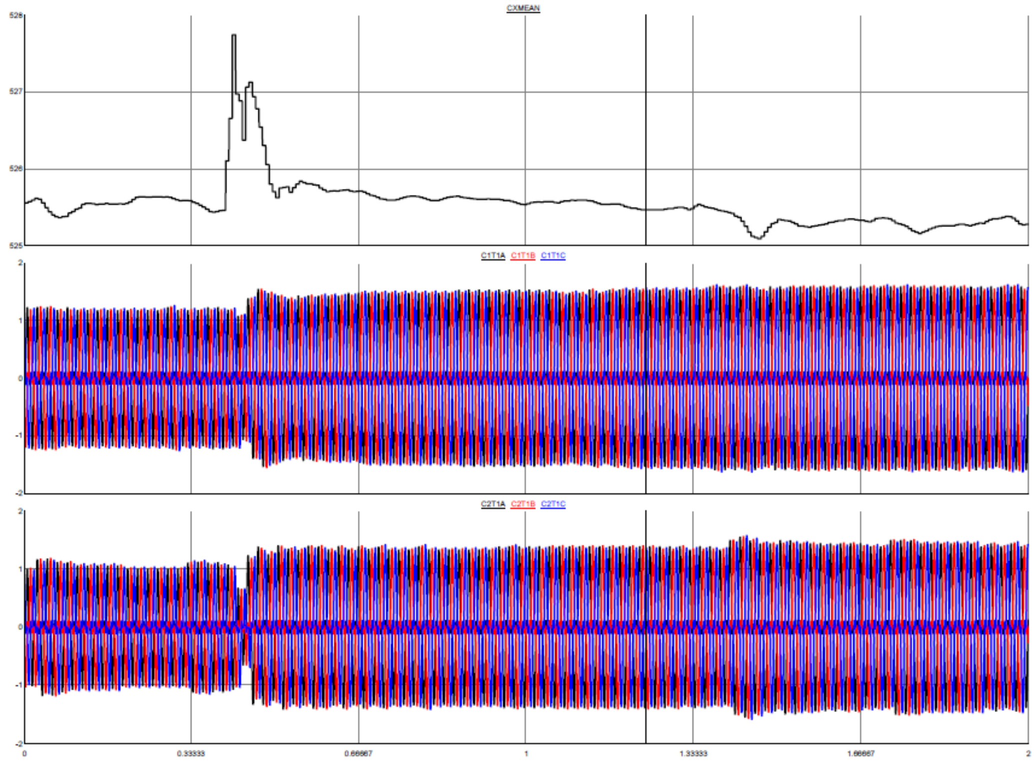

Fig. 8.11 Currents of the two SVCs when the system capacitor banks are switched on at the 500kV side (Simulation based on the data provided by CSG)

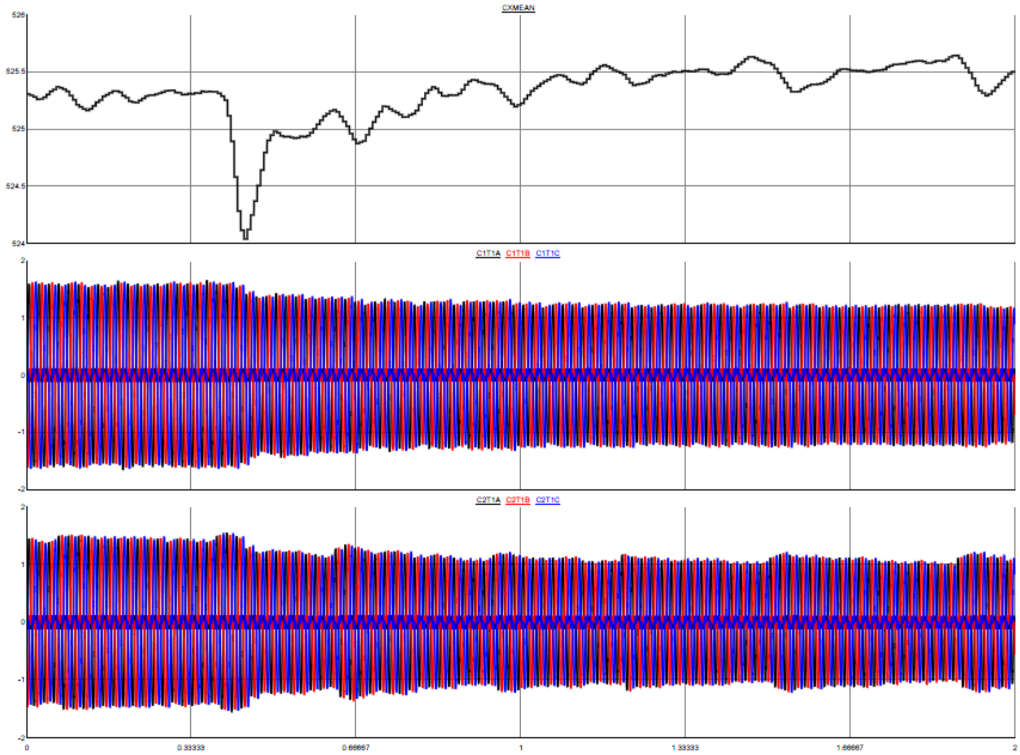

Fig. 8.12 Currents of the two SVCs when the system capacitor banks are switched off at the 500kV side (Simulation based on the data provided by CSG)

Fig.8.11 and Fig.8.12 show the changes of the currents of the two SVCs when the system capacitor banks are switched on/off at the 500kV side and the two SVCs share the same parameters. As can be seen from the two figures, the outputs of the two SVCs are basically balanced and in the same direction, and there are no reactive power oscillations back and forth between the two SVCs. Of course, the outputs of the SVCs are unlikely to be precisely average for the hardware of the two SVCs is not totally identical.

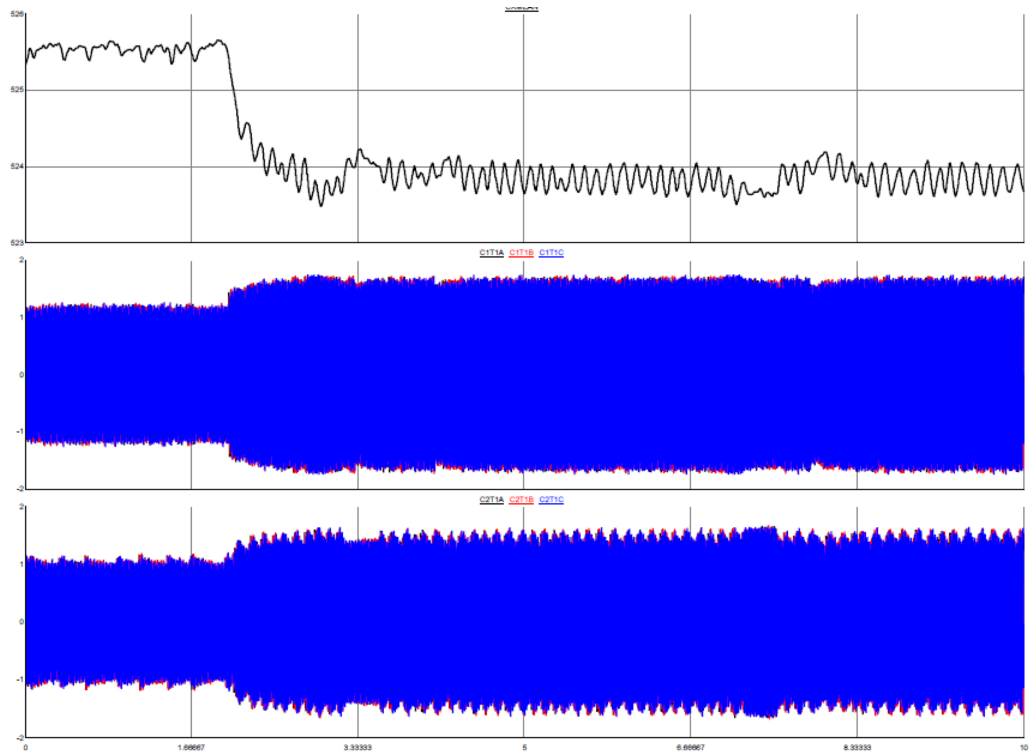

Fig. 8.13 Output currents of the two SVCs when the measurement errors of SVC2 are amplified to 1.008 times (Simulation based on the data provided by CSG)

To test the effectiveness of the new control structure in the context of unbalanced input signals between the two SVCs, we amplified the measurement errors of SVC 2 to 1.008 times artificially, and the SVCs were loaded to generate voltage fluctuations. The obtained output waveforms of the two SVCs are shown in Fig.8.13. As can be seen from this figure, the two SVCs still output in a roughly balanced way, with the regulations changing in the same direction, and the reactive power oscillations back and forth between the two SVCs are eliminated.

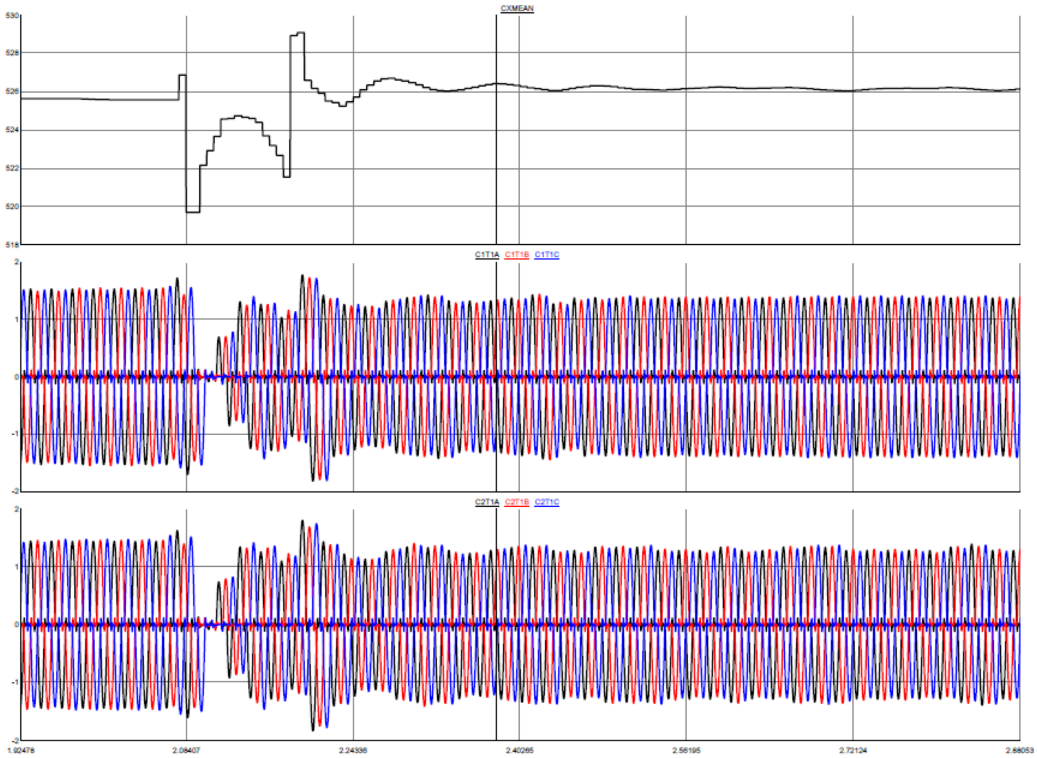

Fig. 8.14 Ooutput currents of the two SVCs in the case of a single-phase grounding fault via a 100Ω resistor for a duration of 100ms at the 500kV side (Simulation based on the data provided by CSG)

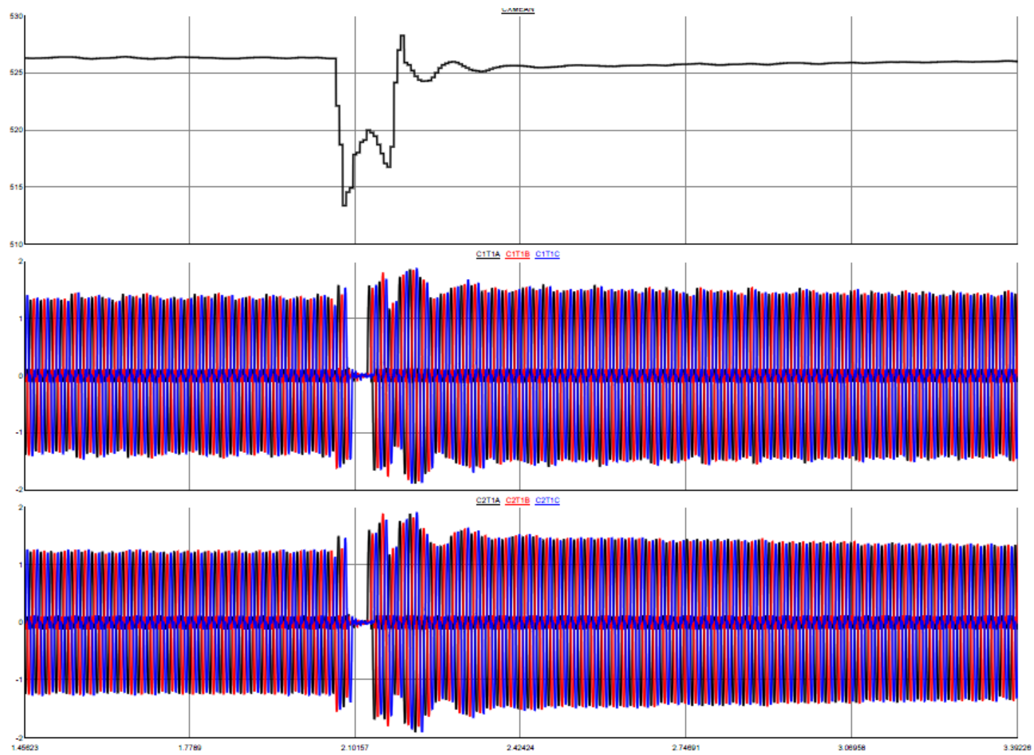

Fig. 8.15 Output currents of the two SVCs in the case of a three-phase grounding fault via 100Ω resistors for a duration of 100ms at the 500kV side (Simulation based on the data provided by CSG)

Fig.8.14 and Fig.8.15 show the output currents of the two SVCs in the case of a single-phase grounding fault via a 100Ω resistor for a duration of 100ms at the 500kV side in the case of a three-phase grounding fault via 100Ω resistors for a duration of 100ms at the 500kV side respectively. As the RTDS simulation waveforms indicate, the two SVCs output reactive power in a balanced way during the course of regulations at the instant of undergoing reactive power fluctuations without reactive power oscillations between them; then, the two SVCs also balance their reactive power output in the process towards final stability.

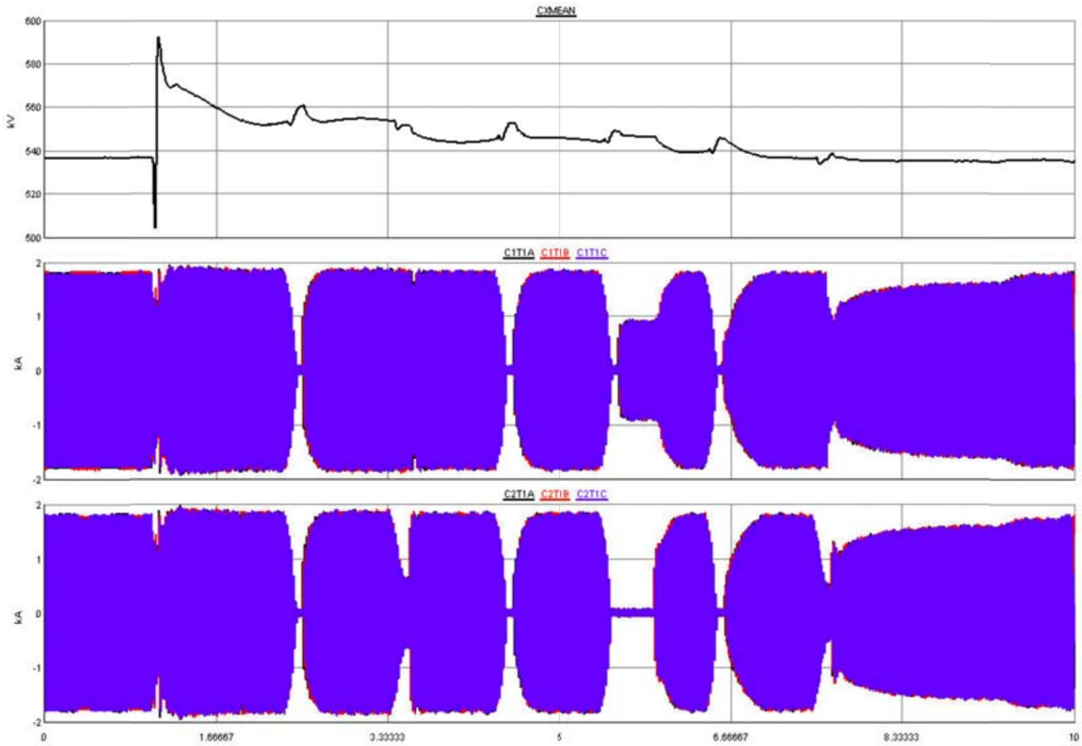

Fig. 8.16 Output currents of the two SVCs at Chuxiong Converter Station after a unipolar block fault occurs in Yunnan-Guangdong HVDC lines (Simulation based on the data provided by CSG)

Fig.8.16 shows the waveforms of the output currents of the two SVCs at Chuxiong Converter Station after a unipolar block fault occurs in Yunnan-Guangdong HVDC lines. As the figure indicates, the two SVCs basically balance their outputs and in the process of dynamic regulations after the fault occurs without reactive power oscillations, and they operate normally to stabilize the 500kV AC bus voltage within the normal range.

The two SVCs at Chuxiong Converter Station designed according to this control structure were put into operation in May 2010. Field tests and operation logs indicate that the SVCs operate well without reactive power oscillations.

8.4 Summary

(1) Disturbance signals and sensor errors may bring about reactive power oscillations between two SVCs in parallel operation.

(2) Adding a feedforward link and introducing feedforward input quantities into the two self-governed SVCs can help to avoid the reactive power oscillations resulting from the lagging responses of two sheer feedback structures to the same control objective quantity.

(3) The feedforward link is a pre-estimator essentially, and can help to improve the dynamic response characteristics of the dynamic system.

(4) After each of the two SVCs introduce the output reactive current of the other party as its own feedforward input, the controllers of the two SVCs operate independently, and this can help balance their outputs during the process of transient regulations and in stable states. The SVCs at Chuxiong Converter Station of the Yunnan-Guangdong ±800kV UHVDC power transmission project were designed based on this structure, and have been operating successfully since the commissioning in May 2010.

(5) The feedforward links endow the control systems with certain robustness to the outside disturbances and with higher precision of steady control.

(6) This new control structure can balance the outputs of the two self-governed SVCs, i.e., achieve the current averaging at the device level, and can be used to tackle the difficult problems of current-averaging in large power electronics devices. The ±200MVA STATCOMs at 500kV Dongguan Substation are based on this control structure for a large total capacity. So far, they have been in operation since August 17, 2011.

CHAPTER 9 REASERACH ON STATCOM IN PROVIDING REACTIVE POWER SUPPORT FOR THE GRID

Currently, China Southern Power Grid is the only ultrahigh-voltage, long-distance and large-capacity interconnected grid with AC/DC systems in parallel operation in our country. At the receiving-end side, Guangdong Grid, especially Zhujiang Sanjiaozhou Grid, receives a large proportion of outside electricity and is highly densely loaded, which determines that this district is in great need of reactive power compensation. There are the following problems with the China Southern Power Grid in the ways of reactive power and voltages:

(1) The dynamic reactive power compensation at the load centers is insufficient;

(2) The control manners of reactive power and voltages are limited;

(3) Such reactive power compensators as capacitors are incapable of being put into operation quickly, unable to meet the requirements of reactive power in the transient process.

So, by installing dynamic reactive power compensators in China Southern Power Grid and taking advantage of their characteristics of fast response, we can effectively improve the system voltage stability, reactive power reserve, and power receiving capability, and enhance the capability of resisting large grid faults.

In August 2011, two sets of STATCOMs amounting to 200Mvar in total were installed at 500kV Dongguan Substation in China Southern Power Grid, which apply the same system design and main control strategies as the SVCs in Chuxiong Converter Station, and will effectively tackle the problem of insufficient dynamic reactive power support at the load centers of Zhujiang Delta district and reduce the risks of voltage instability. This project integrates a 35kV system, with the

STATCOMs of the largest capacities, the highest voltage level of direct connection and the largest number of series levels.

The STATCOM can regulate the amplitudes of the voltages at the PCC by injecting reactive power into or absorbing reactive power from the PCC so as to keep the voltages constant and effectively solve the problems of voltage fluctuations and instability [9.1] [9.2] [9.3].

The STATCOM consists of the following parts:

(1) Capacitors for voltage support: their role is to provide voltage support for the devices;

(2) The voltage-sourced inverter comprising high-power power electronics components IGBTs, which controls the switching of power electronics components with the PWM theory and technology, and transforms the DV voltage of the capacitors into AC voltages with certain frequency and amplitudes.

(3) Coupling transformer and reactors, which couple the high-power converter devices with the power system, and may also filter out the high-order harmonics in the output voltages of the inverter, making the output voltages of the cascaded STATCOM close to sinusoidal waves.

9.1 Mathematical Descriptions of Cascaded STATCOM Model

The following figure shows the principle diagram of star connection of the cascaded STATCOM [9.4], and the mathematical model of STATCOM is built with the inputs and outputs:

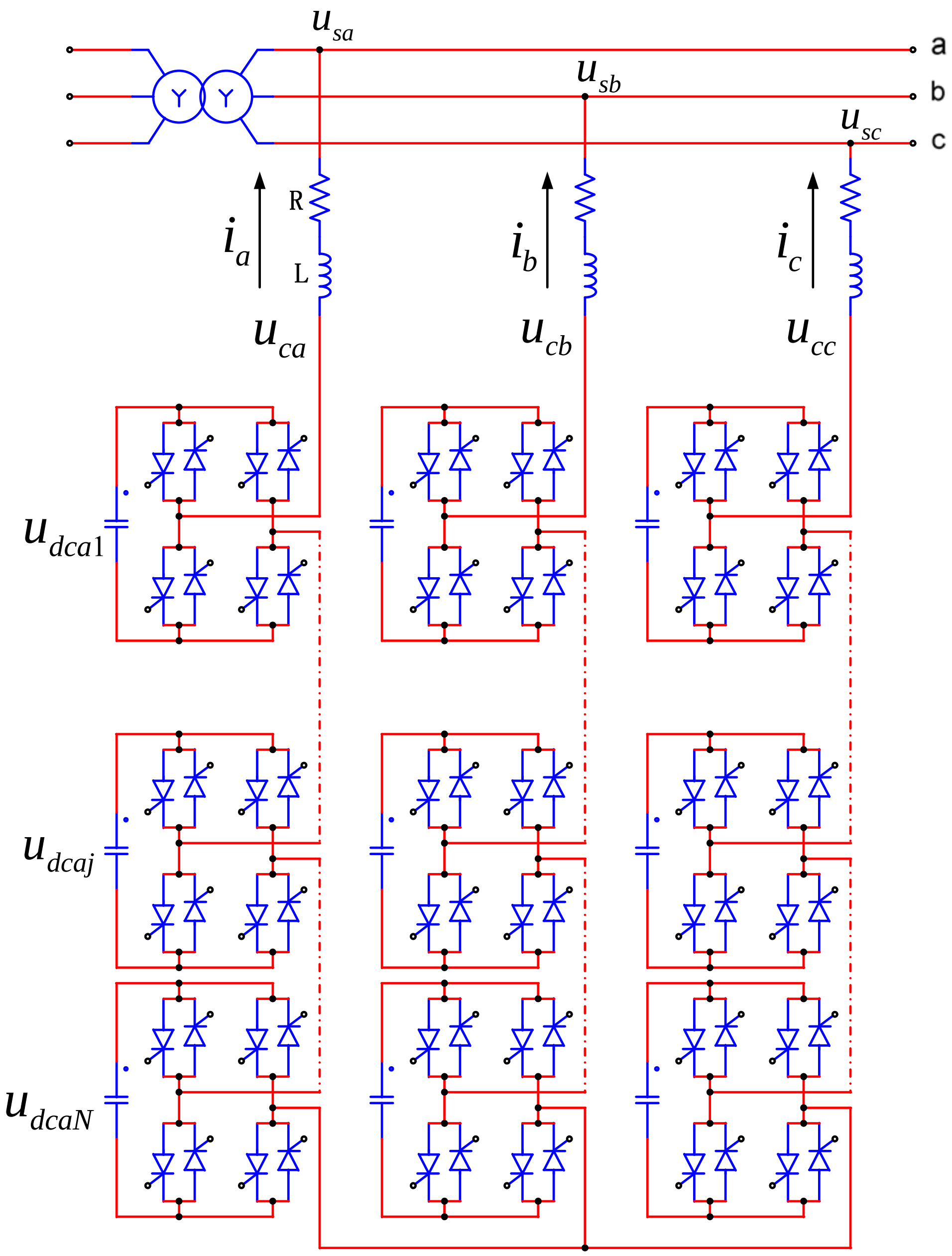

Fig. 9.1 Principle diagram of star connection of the cascaded STATCOM

According to the principle diagram of the cascaded STATCOM, the mathematical equations of phases A, B and C are

$$\begin{cases} L\dfrac{di_a(t)}{dt} = u_{ca}(t) - u_{sa}(t) - Ri_a(t) \\ L\dfrac{di_b(t)}{dt} = u_{cb}(t) - u_{sb}(t) - Ri_b(t) \\ L\dfrac{di_c(t)}{dt} = u_{cc}(t) - u_{sc}(t) - Ri_c(t) \end{cases} \tag{9.1}$$

According to the principle of constant power, the following power equations stand:

$$\begin{cases} u_{ca}i_a = -Nu_{dca}C\dfrac{du_{dca}}{dt} \\ u_{cb}i_b = -Nu_{dcb}C\dfrac{du_{dcb}}{dt} \\ u_{cc}i_c = -Nu_{dcc}C\dfrac{du_{dcc}}{dt} \end{cases} \tag{9.2}$$

where u_{dca}, u_{dcb} and u_{dcc} denote the voltages of the capacitors at the DC side of the single-phase bridges of the inverters of phases A, B and C. Since this is an ideal model, the DC components of the three-phase capacitor voltages are equal with small AC ripples when the system voltages are balances and the three phases of the STATCOM operate symmetrically. Adding up the left and right sides of the above equations to extract the expression describing the DC components, and denoting the DC component of the sum of capacitor voltages of the bridges of the inverter per phase as u_{dc}, we get the following equations describing the dynamic characteristics of the DC component:

$$\frac{3u_{dc}}{N}C\frac{du_{dc}}{dt} = -(u_{ca}i_a + u_{cb}i_b + u_{cc}i_c) \tag{9.3}$$

Substituting (V_s-amplitude of system phase voltages, *M-modulation ratio,* δ -reactive power control angle)

$$\begin{cases} u_{sa}(t) = V_s \sin \omega t \\ u_{sb}(t) = V_s \sin(\omega t - 2\pi/3) \\ u_{sc}(t) = V_s \sin(\omega t + 2\pi/3) \end{cases} \tag{9.4}$$

$$\begin{cases} u_{ca}(t) = Mu_{dc}\sin(\omega t - \delta) \\ u_{cb}(t) = Mu_{dc}\sin(\omega t - 2\pi/3 - \delta) \\ u_{cc}(t) = Mu_{dc}\sin(\omega t + 2\pi/3 - \delta) \end{cases} \tag{9.5}$$

into the three-phase mathematical equations and dynamic characteristic equations, and simplifying the results, we obtain the mathematical model of the STATCOM:

$$\begin{cases} L\dfrac{di_a(t)}{dt} = Mu_{dc}\sin(\omega t - \delta) - V_s\sin\omega t - Ri_a(t) \\ L\dfrac{di_b(t)}{dt} = Mu_{dc}\sin(\omega t - \delta - 2\pi/3) - V_s\sin(\omega t - 2\pi/3) - Ri_b(t) \\ L\dfrac{di_c(t)}{dt} = Mu_{dc}\sin(\omega t - \delta + 2\pi/3) - V_s\sin(\omega t + 2\pi/3) - Ri_c(t) \\ \dfrac{du_{dc}}{dt} = -\dfrac{NM}{3C}[\sin(\omega t - \delta)i_a + \sin(\omega t - \delta - 2\pi/3)i_b + \sin(\omega t - \delta + 2\pi/3)i_c] \end{cases} \tag{9.6}$$

This equation group consists of four unknowns and four equations. With the initial values of the currents and voltages of the STATCOM, we can find the law of the variables changing over time by evaluating this differential equations group. But the above mathematical model comprises differential equations with time-varying coefficients that are hard to evaluate, so we will transform the time-varying differential equations into constant-coefficient differential equations through linear transform, i.e. DQ0 transform. The linear transform matrix is:

$$C_{abc\to dq} = \sqrt{\frac{2}{3}}\begin{pmatrix} \cos\omega t & \cos(\omega t - \frac{2\pi}{3}) & \cos(\omega t + \frac{2\pi}{3}) \\ -\sin\omega t & -\sin(\omega t - \frac{2\pi}{3}) & -\sin(\omega t + \frac{2\pi}{3}) \\ \frac{1}{\sqrt{2}} & \frac{1}{\sqrt{2}} & \frac{1}{\sqrt{2}} \end{pmatrix} \tag{9.7}$$

Performing DQ0 transform for the currents of phases A, B and C, i.e. letting

$$\begin{bmatrix} i_d(t) \\ i_q(t) \\ i_0(t) \end{bmatrix} = C_{abc\to dq}\begin{bmatrix} i_a(t) \\ i_b(t) \\ i_c(t) \end{bmatrix} \tag{9.8}$$

we can transform the STATCOM model in the static coordinate system into the mathematical model in the rotating coordinate system:

$$L\frac{d}{dt}\begin{bmatrix} i_d \\ i_q \\ u_{dc} \end{bmatrix} = \begin{pmatrix} -R & \omega & -M\cos\delta \\ -\omega & -R & -M\sin\delta \\ \frac{NM\cos\delta}{3C} & \frac{NM\sin\delta}{3C} & 0 \end{pmatrix} \begin{bmatrix} i_d \\ i_q \\ u_{dc} \end{bmatrix} + \frac{\sqrt{3}}{\sqrt{2}}\begin{bmatrix} V_S \\ 0 \\ 0 \end{bmatrix} \quad (9.9)$$

And this is the ideal mathematical model of cascaded STATCOM. This mathematical model comprises constant-coefficient differential equations.

9.2 Steady-state Power and Currents of STATCOM

In the steady states, the currents and voltage conform to

$$\frac{di_d(t)}{dt} = \frac{di_q(t)}{dt} = \frac{du_{dc}(t)}{dt} = 0 \quad (9.10)$$

Substituting this equation into the constant-coefficient differential equations, we can find the steady-state currents and the DC side voltage as:

$$\begin{cases} i_d(\infty) = -\frac{\sqrt{3}}{\sqrt{2}} V_s \frac{\sin^2\delta}{R} \\ i_q(\infty) = \frac{\sqrt{3}}{\sqrt{2}} V_s \frac{\sin\delta\cos\delta}{R} \\ u_{dc}(\infty) = \frac{\sqrt{3}V_s}{\sqrt{2}MR}(R\cos\delta + \omega L\sin\delta) \end{cases} \quad (9.11)$$

According to the instantaneous reactive power theory, we can find the output power of the STATCOM in steady-state conditions:

$$\begin{cases} p(\infty) = \frac{\sqrt{3}}{\sqrt{2}} V_s i_d(\infty) = -\frac{3U_s^{\ 2}}{R}\sin^2\delta \\ q(\infty) = \frac{\sqrt{3}}{\sqrt{2}} V_s i_q(\infty) = \frac{3U_s^{\ 2}}{2R}\sin 2\delta \end{cases} \quad (9.12)$$

As can be seen from the analysis results, the reactive power output of the STATCOM in steady-state conditions is in direct proportion to the control quantity δ, and angle δ and K (in proportion to modulation ratio K)coordinate to maintain the stability and magnitude of the capacitor voltage. When $\delta<0$, the reactive power output is negative, and the STATCOM absorbs reactive power from the grid like inductors; when $\delta > 0$, the reactive power output is positive, and the STATCOM provides reactive power for the grid like capacitors. The negative active power of the STATCOM is because the STATCOM consumes active power.

9.3 Power Characteristics of Cascaded STATCOM in Steady Operation

The STATCOM in normal operation can be taken as an AC voltage source with controllable amplitudes and phases [9.5]. Since the three phases of the ideal model operate symmetrically, we will simplify the analysis process with a single-phase vector diagram. The equivalent single-phase circuit diagram is shown as follows:

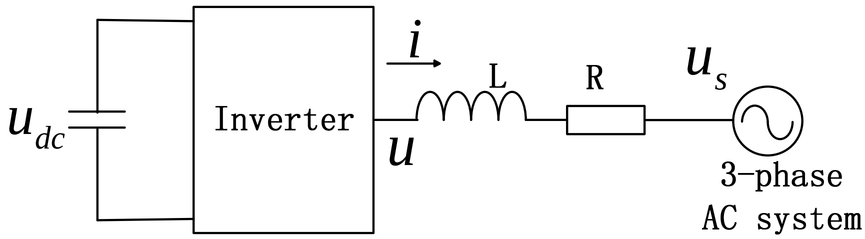

Fig. 9.2 Equivalent single-phase circuit diagram

According to the circuit diagram, we can obtain the vector diagrams of the STATCOM operating in inductive and capacitive patterns as follows:

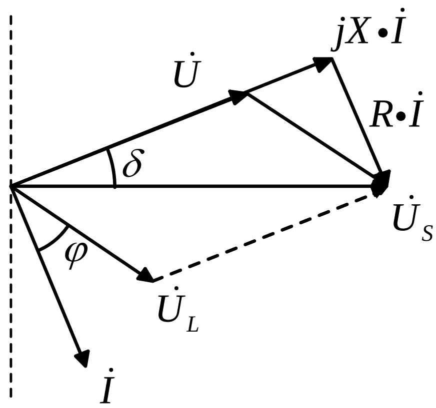

Fig. 9.3 Vector diagram of STATCOM operating in inductive pattern

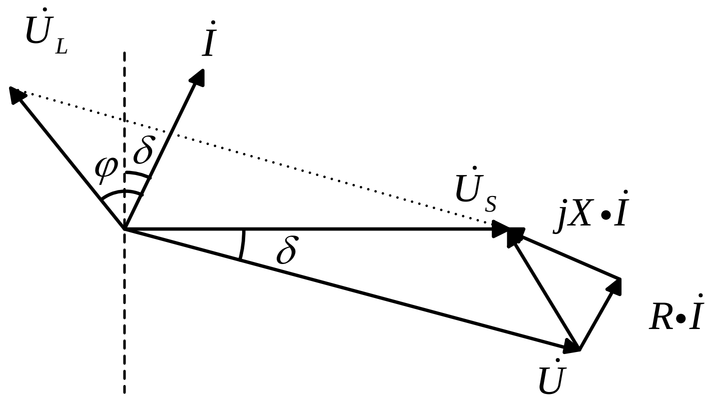

Fig. 9.4 Vector diagram of STATCOM operating in capacitive pattern

Let's take the STATCOM operating in capacitive pattern as an example to analyze the magnitude of transmission power, where the grid voltage leads the fundamental output voltage of the STATCOM by an angle δ, the voltage vector U and current vector I are perpendicular, and they meet the following equations:

$$\dot{U}_S \sin\delta = R\dot{I} \Rightarrow \dot{I} = \frac{\dot{U}_S \sin\delta}{R} \tag{9.13}$$

Decomposing the above equation yields the active current and reactive current components injecting into the grid as well as the active power and reactive power as

$$Q = \dot{U}_S\, \dot{I}\cos\delta = \dot{U}_S \frac{\dot{U}_S \sin\delta}{R}\cos\delta = \frac{\dot{U}_s^2}{2R}\sin 2\delta \tag{9.14}$$

$$P = -\dot{U}_S\, \dot{I}\sin\delta = -\dot{U}_S \frac{\dot{U}_S \sin\delta}{R}\sin\delta = -\frac{\dot{U}_s^2}{R}\sin^2\delta \tag{9.15}$$

Since the three phases of the cascaded STATCOM are symmetrical, multiplying the power by 3 yields the three-phase power in steady states, and the result is the same as that found from the equations. Likewise, the STATCOM operating in inductive pattern can also be analyzed, and the result is the same.

As can be seen from the analyses of the ideal cascaded STATCOM, the reactive power output in steady states is in direct proportion to the control quantity δ, and angle δ and K (in proportion to modulation ratio K) coordinate to maintain the stability and magnitude of the capacitor voltage. Since the STATCOM consumes active power, the active power of the STATCOM is negative.

9.4 Principle of Direct Current Decoupled Control of Cascaded DSTATCOM

For three-phase symmetrical AC systems, if only the fundamental-frequency components are considered, then the d and q components of the dq model are both DC variables in steady state, so, in the synchronously rotating coordinate system, the PI controller regulations can be used for floating regulations. On the other hand, if the initial axis reference direction of the synchronously rotating coordinate system (d,q) is properly selected, for example, d-axis overlaps grid potential vector E_{dq}, then d-axis and q-axis denote the reference axes of active currents and reactive currents respectively, and this helps the STATCOM to achieve the independent control of active and reactive components at the grid side.

In designing the control system of the cascaded STATCOM, we adopt the philosophy of double-loop control, i.e. the outside voltage loop and the inside current loop, where the role of the outside voltage loop is to control the voltage at the DC sides and to generate the current instructions for the control system at the system level, and the role of the inside current loop is control the currents according to the current instructions sent by the outside voltage loop and to track the reference currents of the outside loop.

The state equation of the STATCOM in the context of the ABC coordinates with i_a, i_b and i_c as the state variables is

$$L\frac{d}{dt}\begin{bmatrix} i_a \\ i_b \\ i_c \end{bmatrix} + R\begin{bmatrix} i_a \\ i_b \\ i_c \end{bmatrix} = \begin{bmatrix} V_{sa} - V_{ga} \\ V_{sb} - V_{gb} \\ V_{sc} - V_{gc} \end{bmatrix} \tag{9.16}$$

where L and R are the linking inductance and equivalent resistance between the converter chain and the grid, V_{sa}, V_{sb} and V_{sc} are the phase voltages of the converter chain, and V_{ga}, V_{gb} and V_{gc} are the phase voltages of the grid.

Performing $abc\text{-}dq$ coordinate transform and equivalent rotating coordinate transform for the above equation, we get the Park transform matrix

$$P = \frac{2}{3}\begin{bmatrix} \cos\theta & \cos(\theta - 2\pi/3) & \cos(\theta + 2\pi/3) \\ -\sin\theta & -\sin(\theta - 2\pi/3) & -\sin(\theta + 2\pi/3) \\ 1/2 & 1/2 & 1/2 \end{bmatrix} \tag{9.17}$$

After the park transform, we obtain the state equation in the context of the dq coordinates with i_{sd} and i_{sq} as the state variables:

$$L\frac{d}{dt}\begin{bmatrix} i_{sd} \\ i_{sq} \end{bmatrix} + \omega L\begin{bmatrix} -i_{sq} \\ i_{sd} \end{bmatrix} + R\begin{bmatrix} i_{sd} \\ i_{sq} \end{bmatrix} = \begin{bmatrix} V_{sd} - V_{gd} \\ V_{sq} - V_{gq} \end{bmatrix} \tag{9.18}$$

where ω is the fundamental-frequency angular frequency of the grid voltages, i_{sd} and i_{sq} are the d- and q-axis components of the converter chain current in the dq coordinate system, V_{gd} and V_{sd} are the d-axis components of the grid voltage and the converter chain output voltage after dq coordinate transform respectively, and, likewise, V_{gq} and V_{sq} are the q-axis components respectively.

Performing Laplace transform for the above equation yields the S-domain equation:

$$\begin{cases} (sL + R)I_{sd} - \omega L I_{sq} = V_{sd} - V_{gd} \\ (sL + R)I_{sq} + \omega L I_{sd} = V_{sq} - V_{gq} \end{cases} \tag{9.19}$$

According to the above equation, we have the equivalent block diagram of the main circuit shown in the following figure:

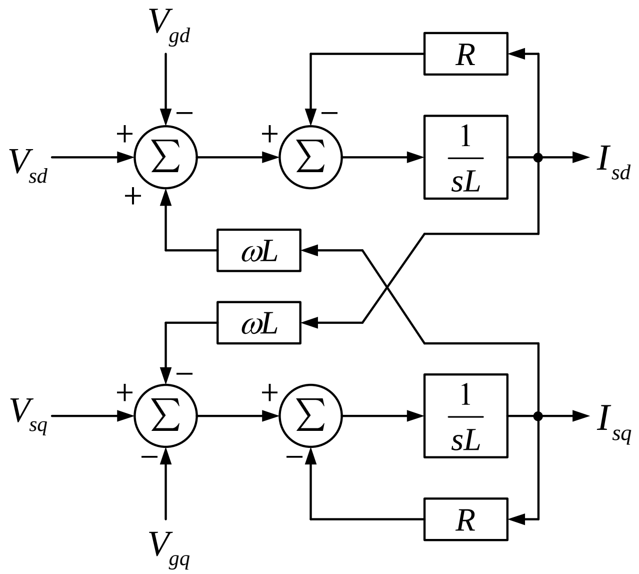

Fig. 9.5 Equivalent block diagram of the main circuit of STATCOM

9.5 Achievement of Direct Current Decoupled Control of Cascaded DSTATCOM

As can be seen from the model equations and the above figure, active current i_{sd} and reactive current i_{sq} are mutually coupled via linking reactors, the changes of active current i_{sd} will result in the changes of reactive current i_{sq}, and, likewise, the changes of reactive current i_{sq} may also lead to the changes of active current i_{sd}. The mutual coupling of the d- and q-axis variables brings about difficulties for the design of the controllers, so the decoupled feedforward control strategies are adopted. When the current controller adopts the PI controller, to achieve the decoupled current control, we design the controller in the law as shown by

$$\begin{bmatrix} v_{sd}^* \\ v_{sq}^* \end{bmatrix} = \begin{bmatrix} v_{gd} - \omega L i_{sq} + K_{p1}(i_{sd}^* - i_{sd}) + \dfrac{1}{T_{i1}}\int (i_{sd}^* - i_{sd})dt \\ v_{gq} + \omega L i_{sd} + K_{p2}(i_{sq}^* - i_{sq}) + \dfrac{1}{T_{i2}}\int (i_{sq}^* - i_{sq})dt \end{bmatrix} \tag{9.20}$$

Since the cascaded voltage-source converter can be taken as an equivalent link with a transfer function of 1, the block diagram of the direct current decoupled control of the STATCOM is shown as follows:

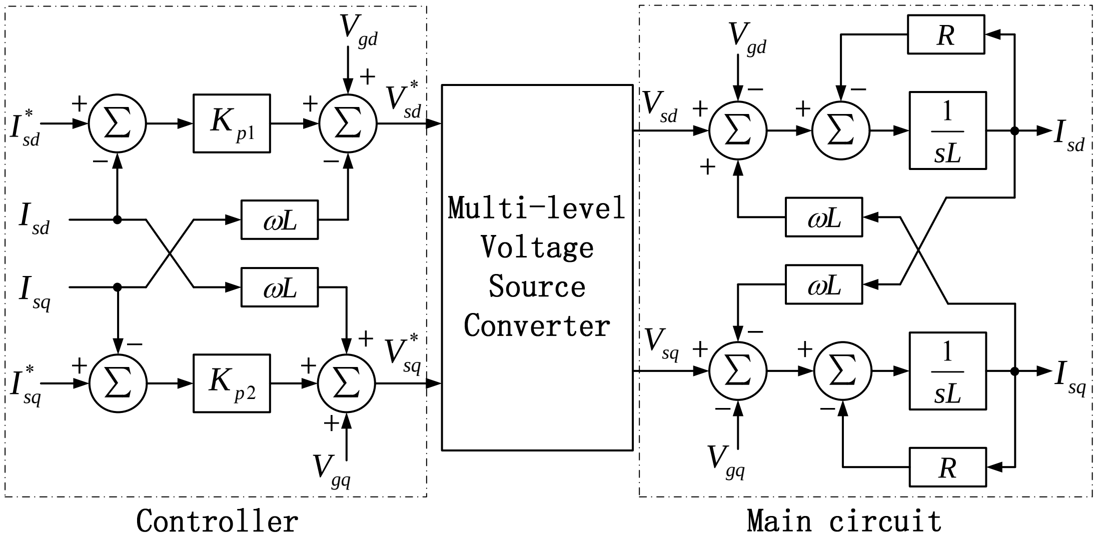

Fig. 9.6 Block diagram of the direct current decoupled control of the STATCOM

Finally we get the mathematical model of the STATCOM as

$$L\frac{d}{dt}\begin{bmatrix} i_{sd} \\ i_{sq} \end{bmatrix} + R\begin{bmatrix} i_{sd} \\ i_{sq} \end{bmatrix} + \begin{bmatrix} -K_{p1}(i_{sd}^* - i_{sd}) - \dfrac{1}{T_{i1}}\displaystyle\int (i_{sd}^* - i_{sd})dt \\ -K_{p2}(i_{sq}^* - i_{sq}) - \dfrac{1}{T_{i2}}\displaystyle\int (i_{sq}^* - i_{sq})dt \end{bmatrix} = 0 \qquad (9.21)$$

Performing Laplace transform for the above equation yields the block diagrams of the equivalent control of active current and reactive current:

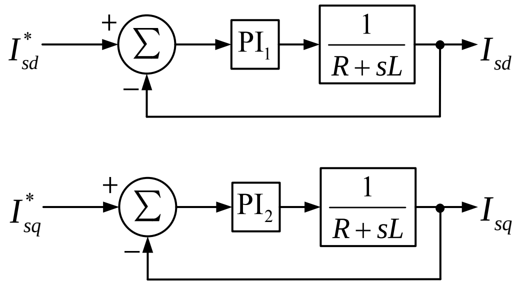

Fig. 9.7 Block diagrams of the equivalent control of currents

The controllers designed in accordance with the block diagrams of the equivalent control of currents can meet the requirements of device operation mainly in terms of such performance indices as response time, overshoots, steady-state errors and anti-disturbance capability.

The corresponding PSCAD model of decoupled feedforward controller is as

follows:

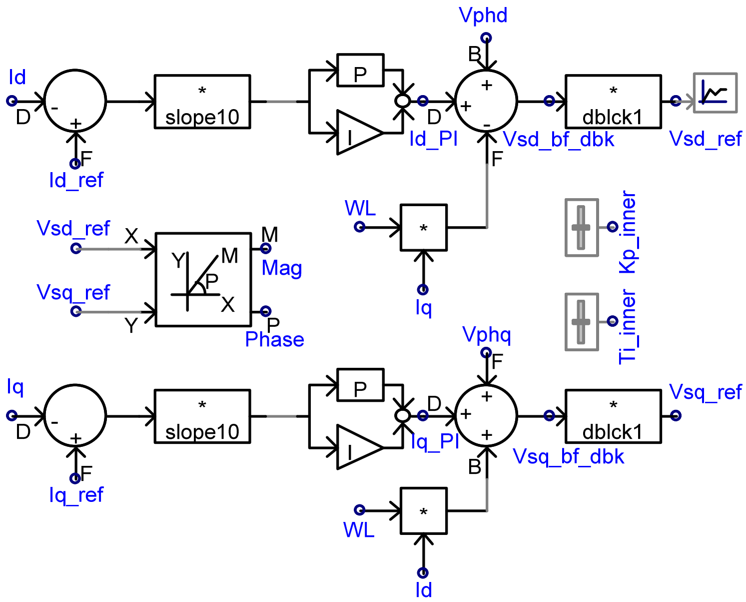

Fig. 9.8 PSCAD model of decoupled feedforward controller

9.6 Simulation Results under Normal Conditions

Under normal operation conditions, the main role of the cascaded STATCOM is to inject reactive power into or absorb reactive power from the system [9.6]. To test the operation conditions of the device, we mainly consider the three cases: reactive power output stepping from zero the capacitive maximum, reactive power output stepping from the capacitive maximum to the inductive maximum, and reactive power output stepping from the inductive maximum to the capacitive maximum, and observe the transient operation conditions of the device.

For the simulation, the STATCOM with a capacity of ±15MVA, has ten chain link inverters per phase, and the three phases are connected in a delta-connection way.

The step responses of reactive power output (reactive power output stepping from zero the capacitive maximum) of the STATCOM are shown in the following figures:

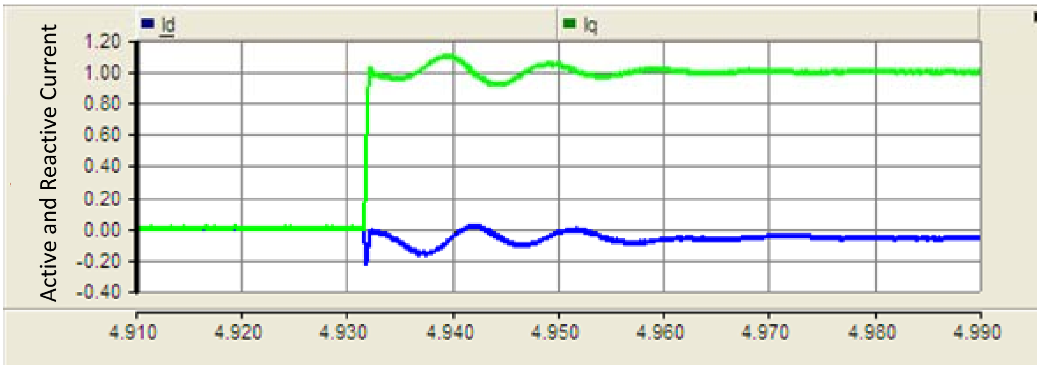

Fig. 9.9 Active current and reactive current (reactive power output stepping from zero the capacitive maximum)

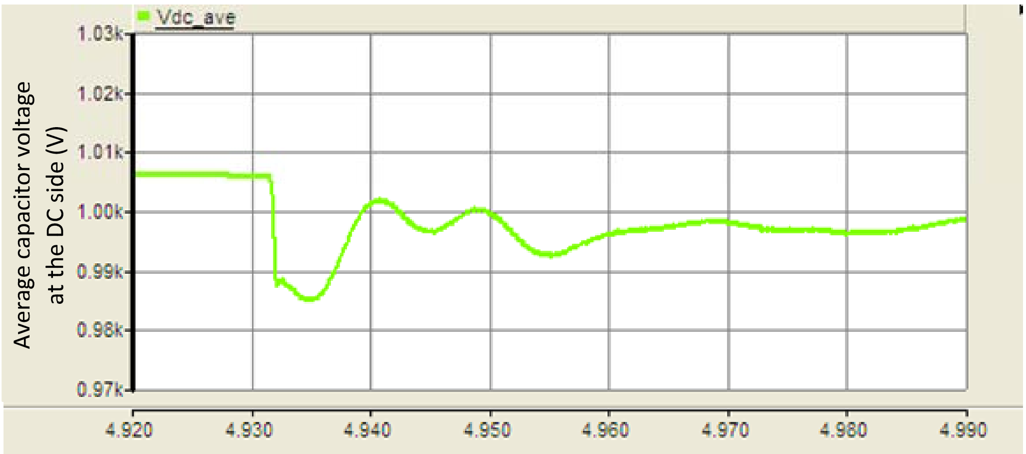

Fig. 9.10 Average capacitor voltage at the DC side (reactive power output stepping from zero the capacitive maximum)

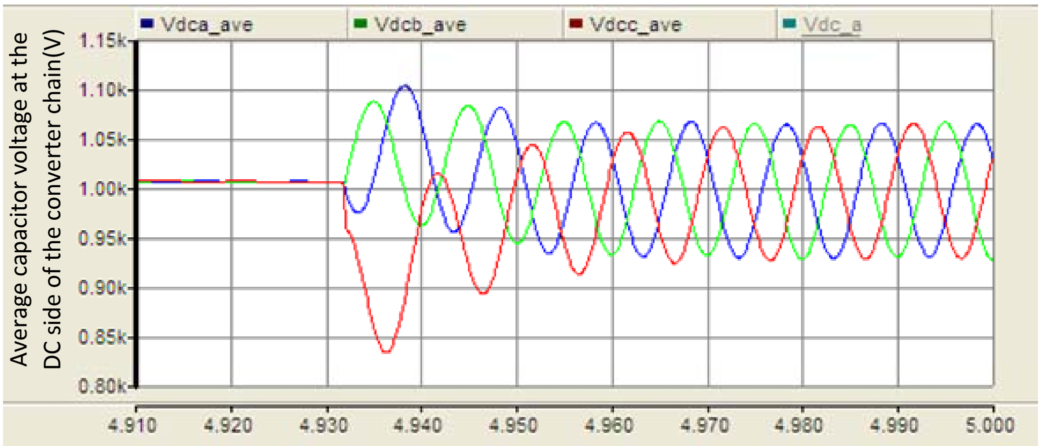

Fig. 9.11 Average capacitor voltage at the DC side of the converter chain (reactive power output stepping from zero the capacitive maximum)

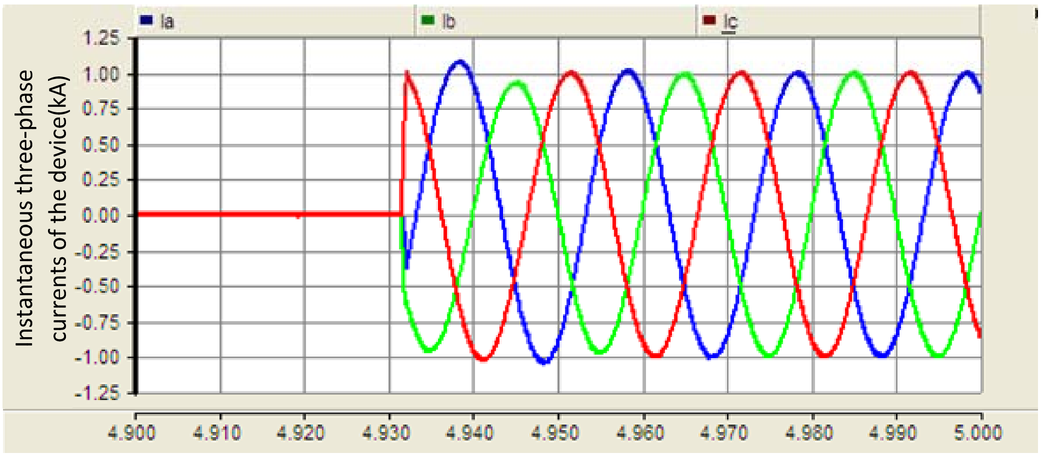

Fig. 9.12 Instantaneous three-phase currents (in kA) of the device (reactive power output stepping from zero the capacitive maximum)

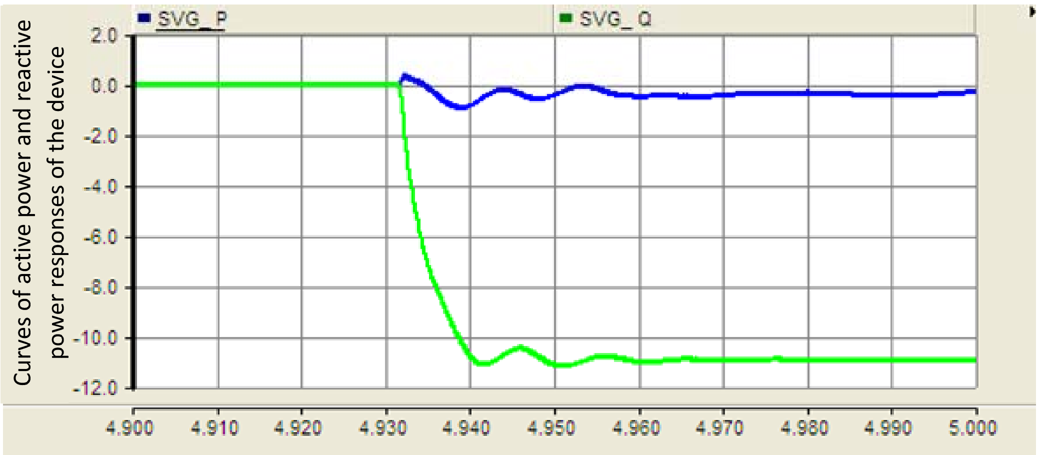

Fig. 9.13 Curves of active power and reactive power responses of the device (reactive power output stepping from zero the capacitive maximum)

The step responses of reactive power output (reactive power output stepping from the capacitive maximum to the inductive maximum) of the STATCOM are shown in the following figures:

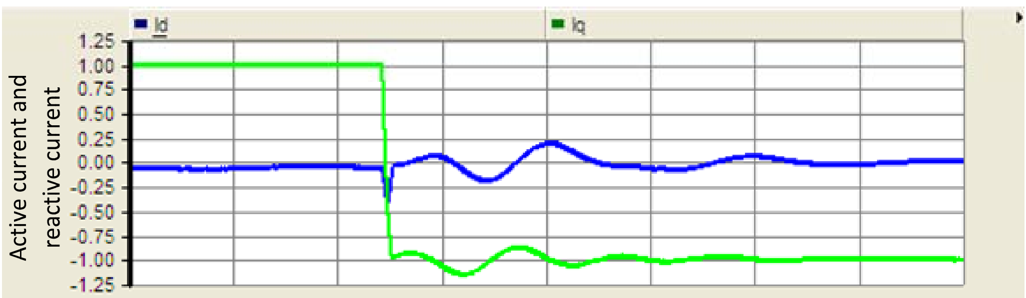

Fig. 9.14 Active current and reactive current (reactive power output stepping from the capacitive maximum to the inductive maximum)

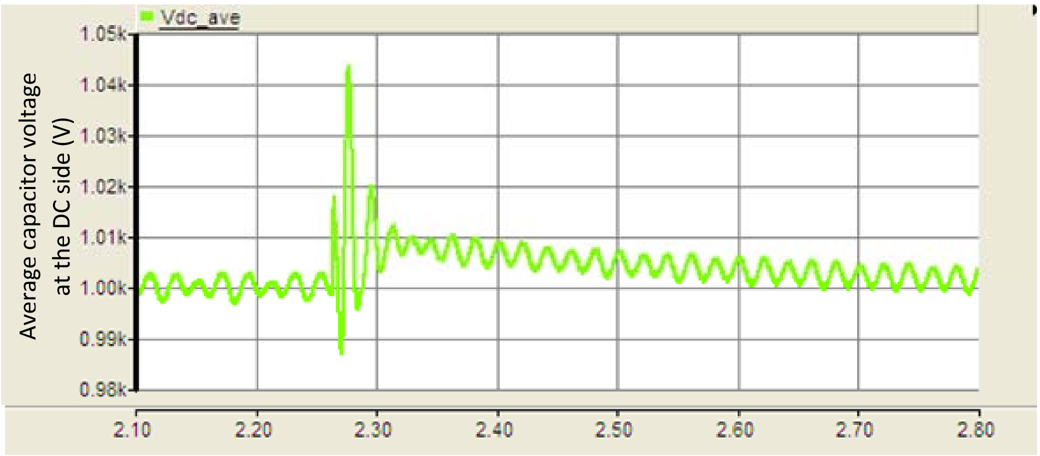

Fig. 9.15 Average capacitor voltage at the DC side (reactive power output stepping from the capacitive maximum to the inductive maximum)

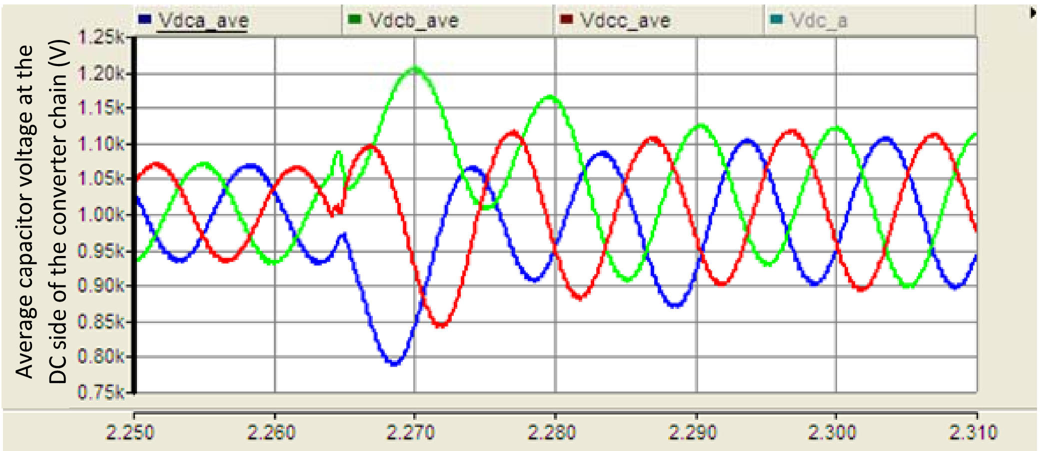

Fig. 9.16 Average capacitor voltage at the DC side of the converter chain (reactive power output stepping from the capacitive maximum to the inductive maximum)

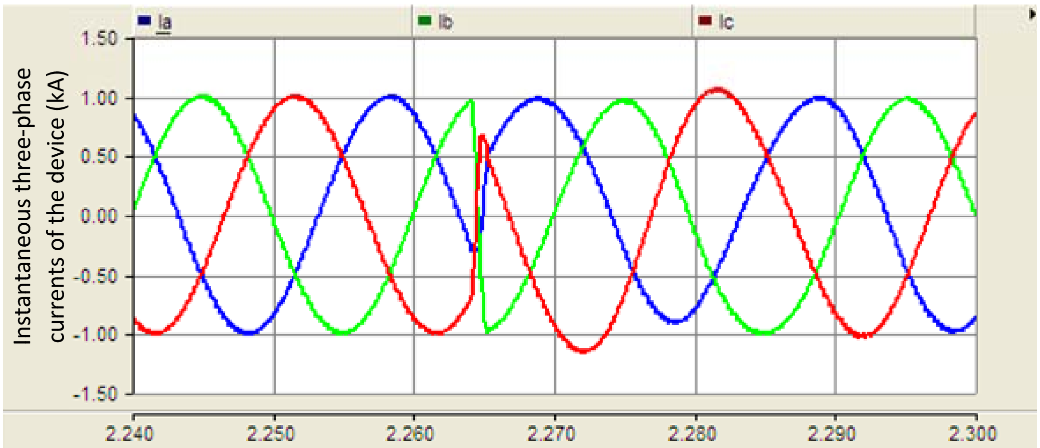

Fig. 9.17 Instantaneous three-phase currents (in kA) of the device (reactive power output stepping from the capacitive maximum to the inductive maximum)

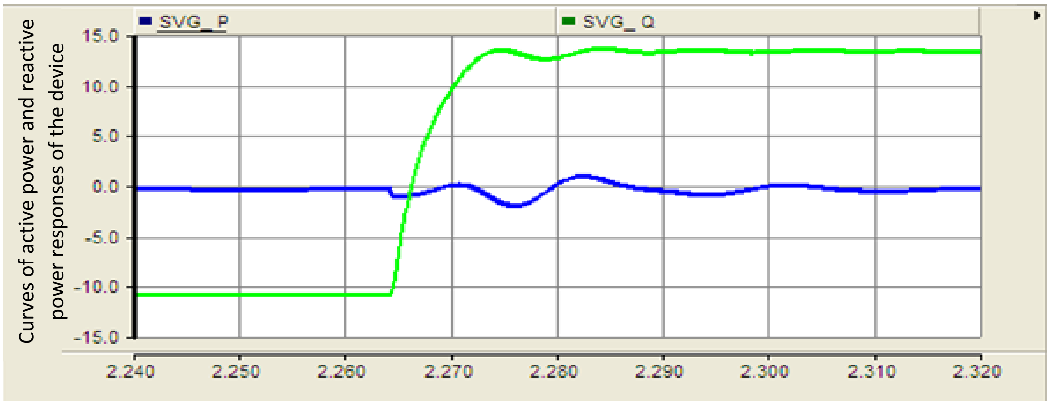

Fig. 9.18 Curves of active power and reactive power responses of the device (reactive power output stepping from the capacitive maximum to the inductive maximum)

The step responses of reactive power output (reactive power output stepping from the inductive maximum to the capacitive maximum) of the STATCOM are shown in the following figures:

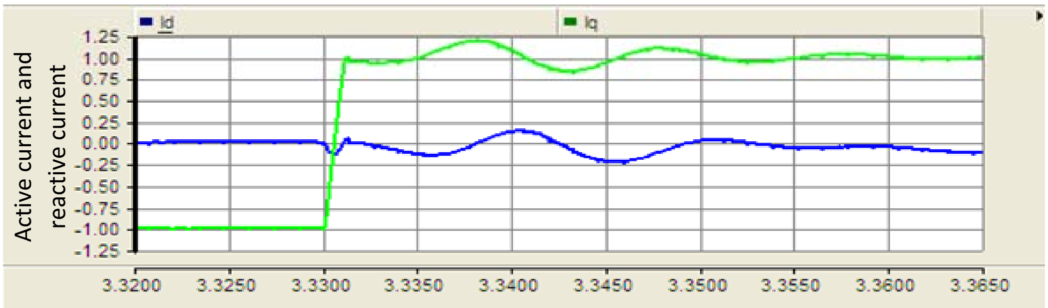

Fig. 9.19 Active current and reactive current (reactive power output stepping from the inductive maximum to the capacitive maximum)

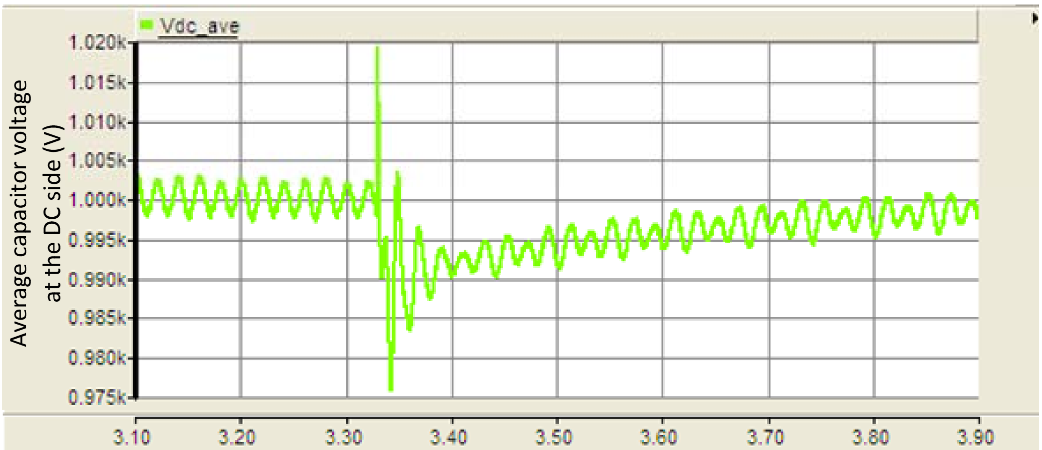

Fig. 9.20 Average capacitor voltage at the DC side (reactive power output stepping from the inductive maximum to the capacitive maximum)

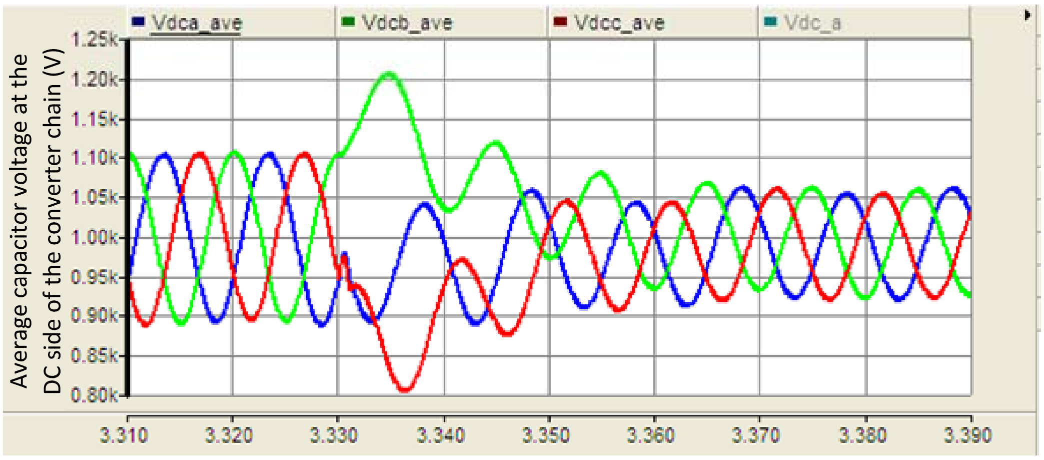

Fig. 9.21 Average capacitor voltage at the DC side of the converter chain (reactive power output stepping from the inductive maximum to the capacitive maximum)

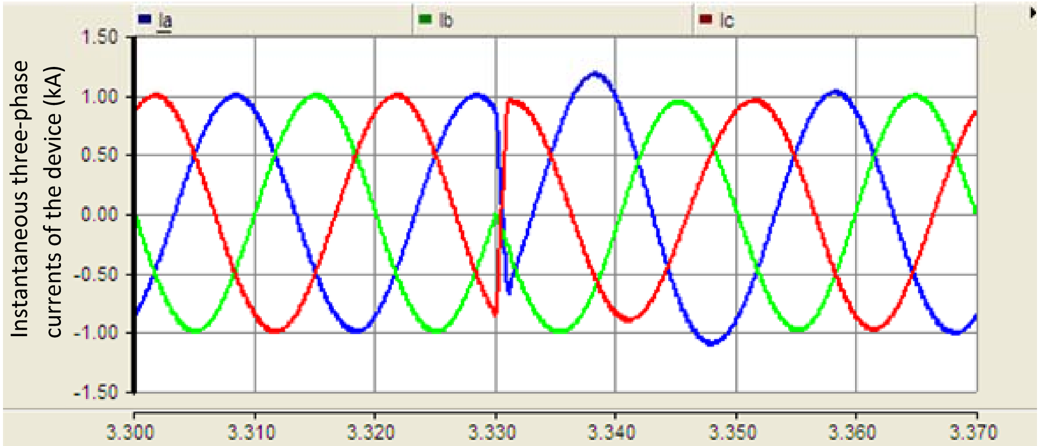

Fig. 9.22 Instantaneous three-phase currents (in kA) of the device (reactive power output stepping from the inductive maximum to the capacitive maximum)

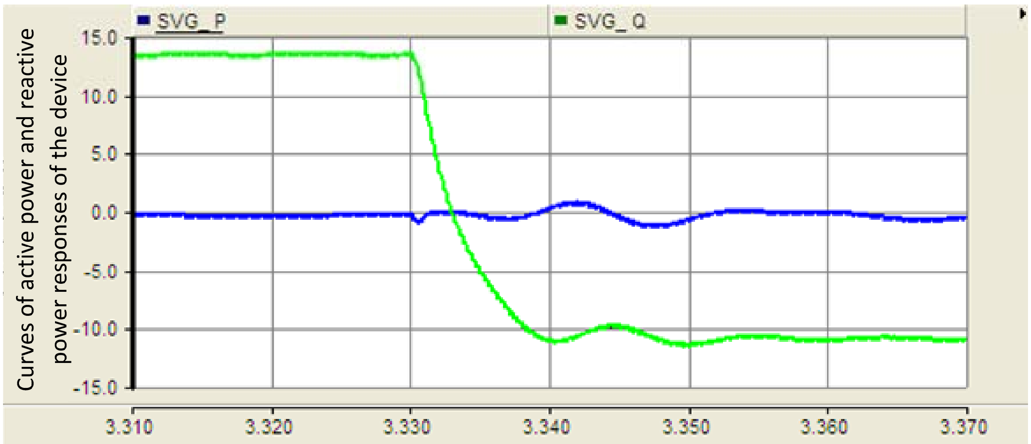

Fig. 9.23 Curves of active power and reactive power responses of the device (reactive power output stepping from the inductive maximum to the capacitive maximum)

As can be seen from the above results, in time of the steps of given reactive current, the actual reactive current will keep close track of it, with the response time and response precision meeting the requirements.

9.7 Simulation Results under Abnormal Conditions

To ensure that the device can function at the crucial time of disturbances and faults in the power system, we find it necessary to conduct comprehensive and pertinent analysis of the operation characteristics of the cascaded STATCOM in the cases of disturbances, especially of large disturbances in the power system, and research the control strategies of the STATCOM under abnormal conditions, while taking the security of the device and its role in the power system in account.

In accordance with the case of three-phase voltage sags with controllable sag amplitudes and time, we will observe the operation characteristics of the device, whether the device can maintain stability in operation, and the performances of the device during fault restoration process.

9.7.1 Three-phase Voltage Sags to 20%

The voltage sag process:

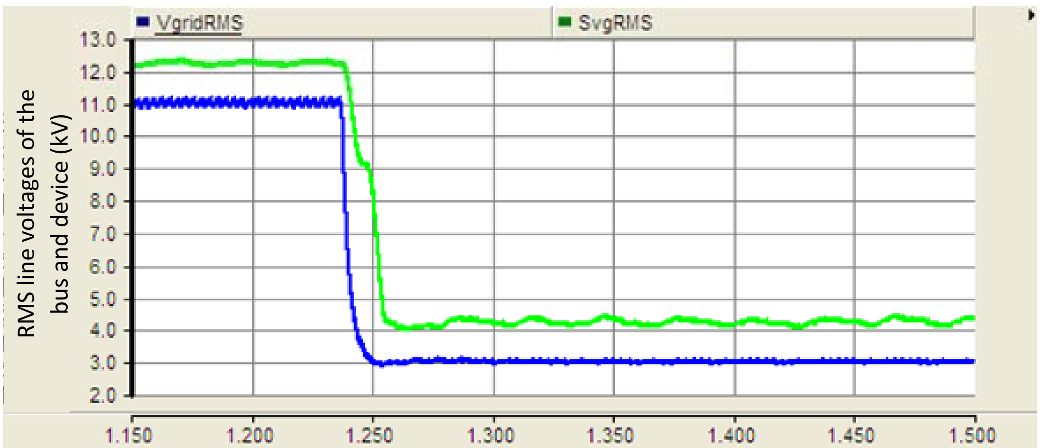

Fig. 9.24 RMS line voltages (in kV) of the bus and device (voltage sag)

Fig. 9.25 Average capacitor voltage at the DC side (voltage sag)

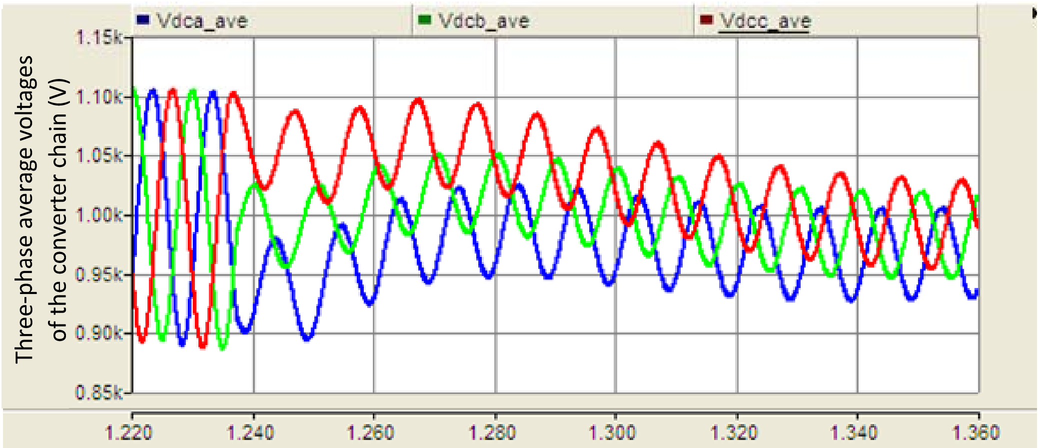

Fig. 9.26 Three-phase average voltages of the converter chain (voltage sag)

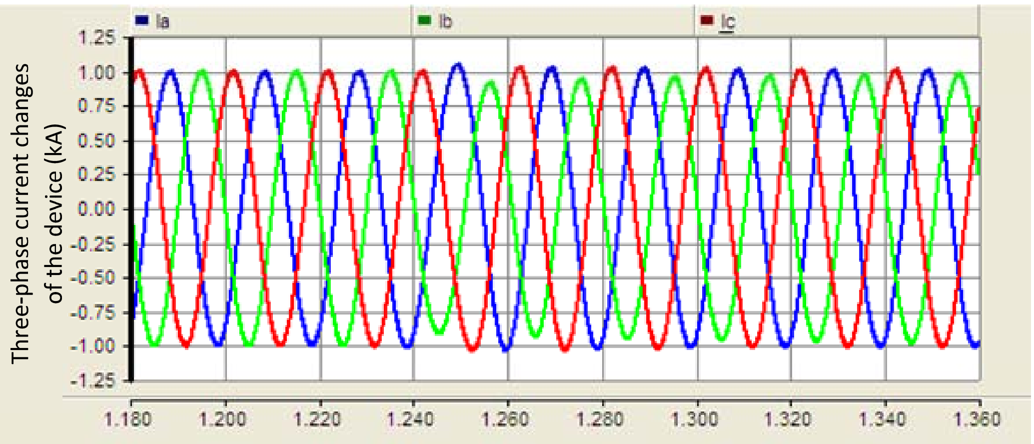

Fig. 9.27 Three-phase current (in kA) changes of the device (voltage sag)

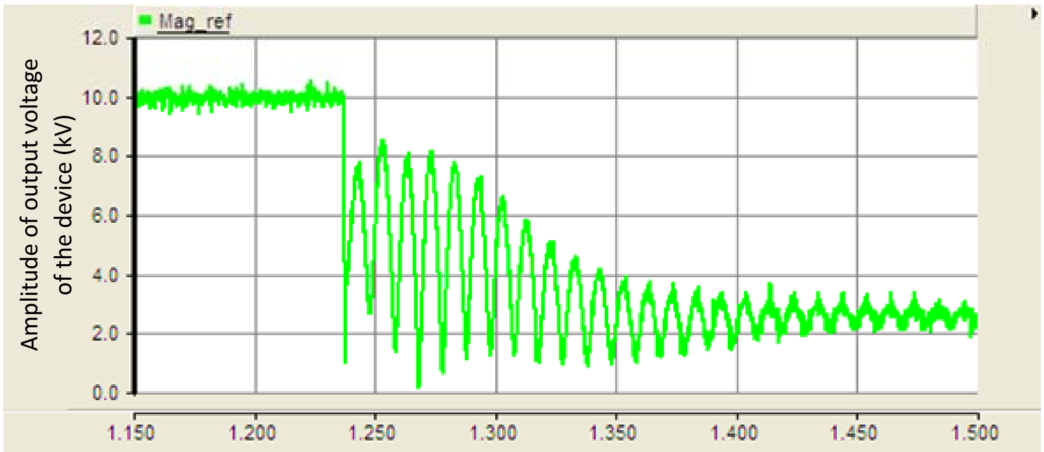

Fig. 9.28 Amplitude of output voltage (in kV) of the device (voltage sag)

As can be seen from the operation conditions of the device, when the voltage sags to 20%, there are no overcurrent and overvoltage phenomena. In the transient process of the system, there are fairly large fluctuations in the average voltage of the DC side, the fluctuations of the DC side capacitor voltages of the cascaded unit decrease, slight unbalances occur in the device current, and the output reference voltage drops quickly in amplitude so as to keep track of the grid voltage changes, but there are fairly large fluctuations in the transient process.

Summing up the above operation conditions of the device, we can see that when the grid voltage sags to 20%, the device can not only operate normally, but provide strong compensation of capacitive reactive power so as to support the grid voltage.

9.7.2 Single-phase Grounding Fault in the System

A single-phase grounding fault via a 0.1Ω resistor occurs at phase A of the lines at the instant of 1s, and is cleared at 1.2s. Observe the simulation results of the model from the occurrence to the clearance of the fault. Before the fault occurs, the STATCOM operates in the state of full reactive power output.

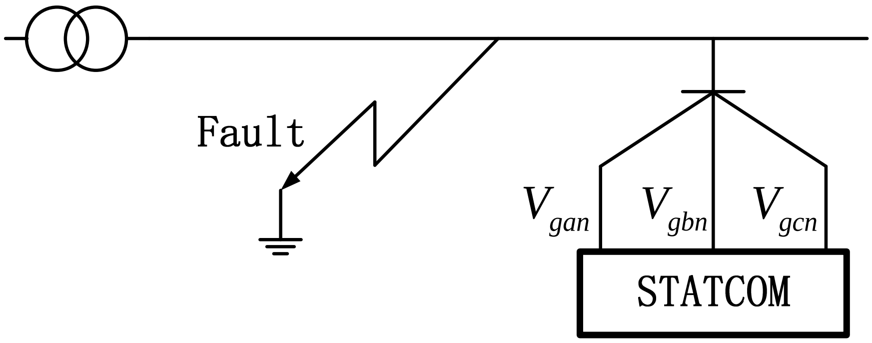

Fig. 9.29 Fault model diagram

(1) In the process from the occurrence to the clearance of the fault, the waveforms of the device voltages and the system voltages are as follows:

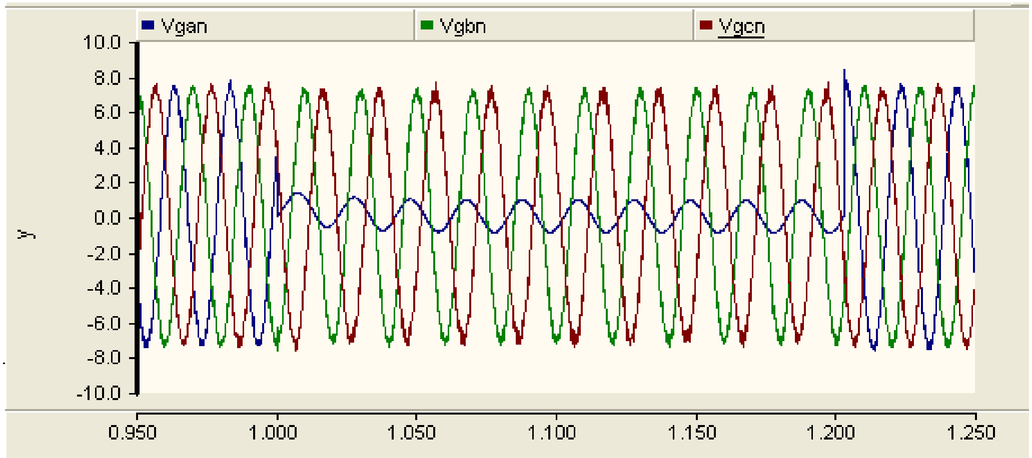

Fig. 9.30 Phase voltages of the three phases of the device

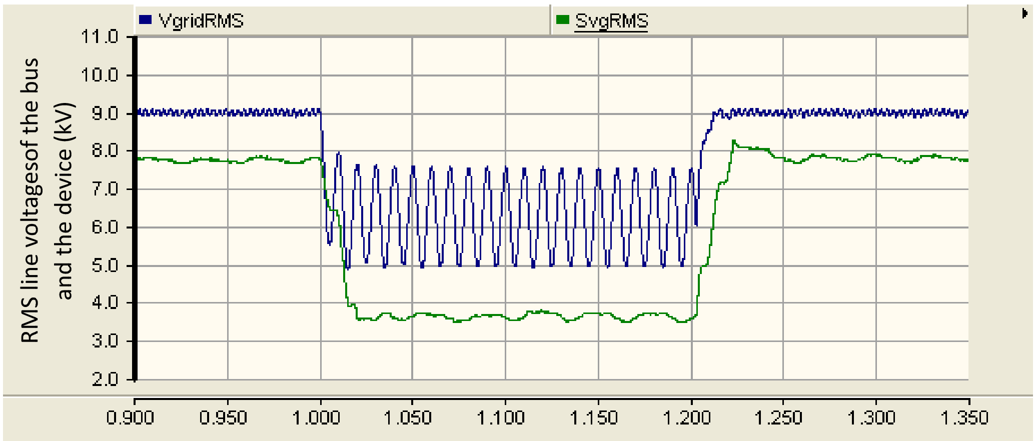

Fig. 9.31 RMS line voltages (in kV) of the bus and the device

When a single-phase grounding fault occurs at phase A of the lines, we can see that the phase voltage of phase A of the device becomes so small as to be close to 0, the output voltage of the device drops, and there are oscillations in the RMS voltage at the grid side. When the fault is cleared, the negative-sequence component of the voltage drops to 0 soon, the voltage oscillations at the grid side disappear, and the system voltages and the device voltages quickly recover to the pre-fault voltages.

(2) In the process from the occurrence to the clearance of the fault, the waveforms of the device currents are as follows:

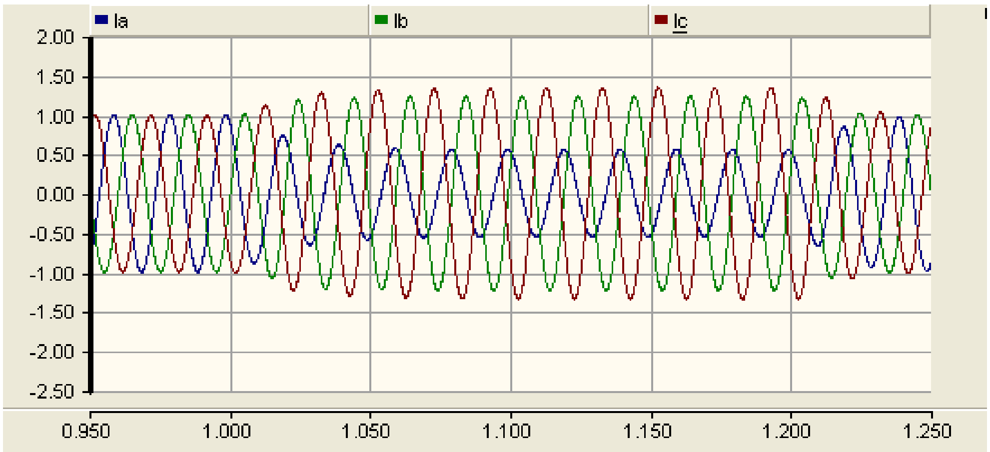

Fig. 9.32 Three-phase currents (in kA) of the device

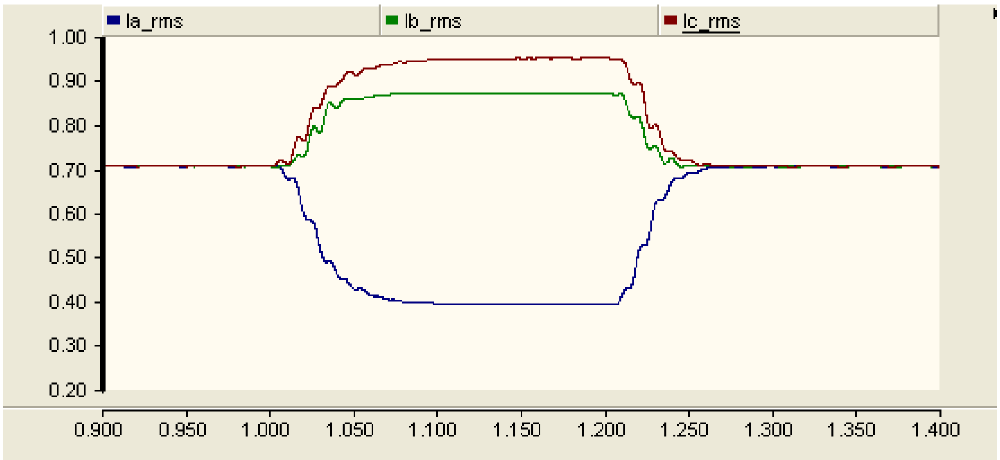

Fig. 9.33 Three-phase RMS currents of the device

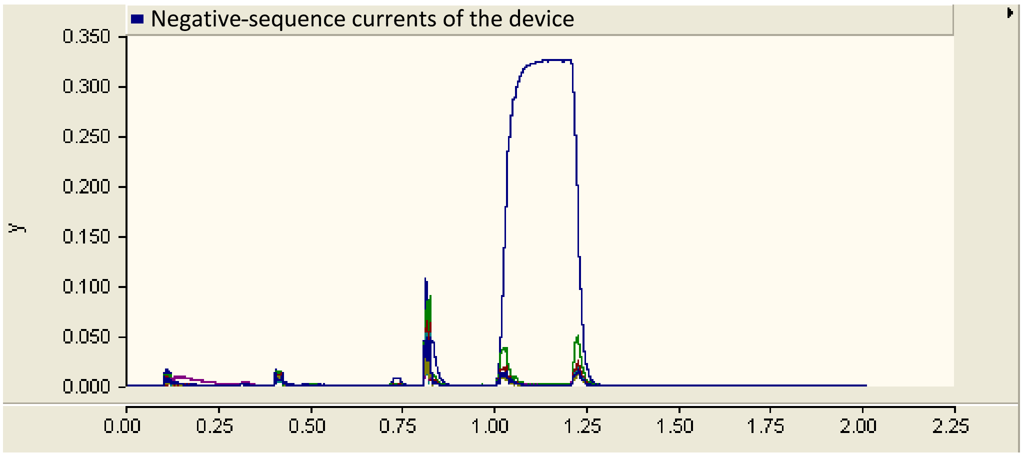

Fig. 9.34 Negative-sequence currents of the device

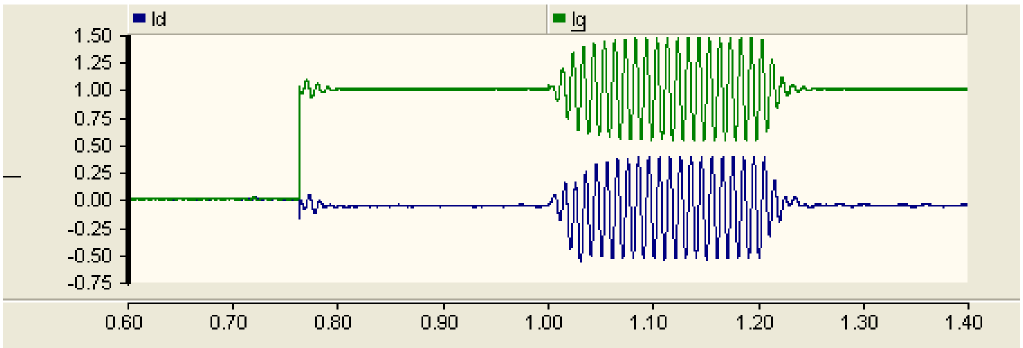

Fig. 9.35 Active current and reactive current of the device

When a single-phase grounding fault occurs in the lines, there are fairly large negative-sequence currents in the device currents with three-phase current unbalance, and there are oscillations in the active currents and reactive currents. When the fault is cleared, the negative-sequence current component drops to zero quickly, the oscillations in the active currents and reactive currents disappear, and the three-phase currents quickly recover to the pre-fault level and keep balanced.

(3) In the process from the occurrence to the clearance of the fault, the active power and reactive outputs of the device are as follows:

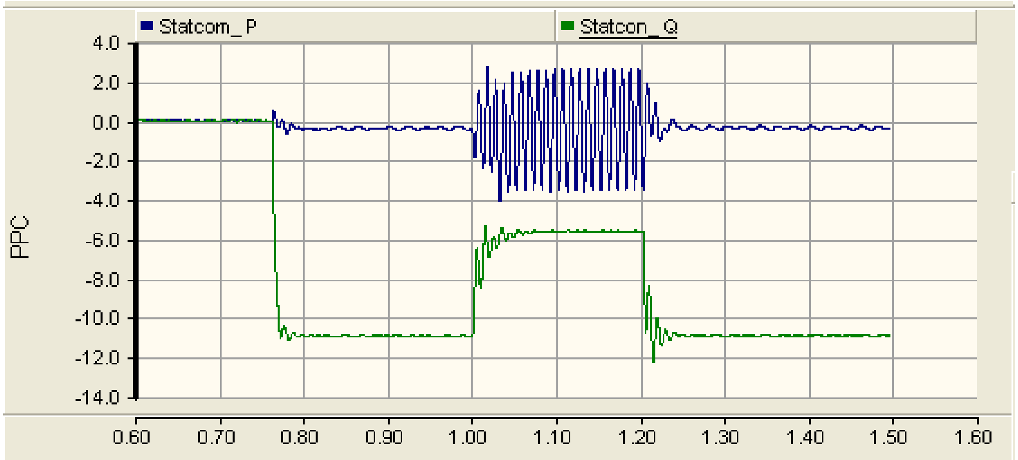

Fig. 9.36 Reactive power and active power outputs of the device

Before the fault occurs, the STATCOM sends out 100% reactive power; during the fault, the STATCOM sends out 50% reactive power, contributing to supporting the system voltages. During the fault, there are oscillations in the active power, and the oscillations disappear when the fault is cleared.

Compared with the certain type of STATCOMs that were manufactured and put into field industrial practice previously, the STATCOM based on this kind of directly decoupled control philosophy can still generate a certain amount of reactive power and provide dynamic reactive power and voltage support in a fast-response way in time of faults even though the voltage drops down to 20%. However, owing to the limitations of the actual conditions, no more STATCOMs that are in practical operation have been studied, so it is too early for us to arrive at any comparative conclusions between this type of STATCOMs and other types of STATCOMs.

9.8 Summary

This chapter presents the principle, algorithm and simulation results of the cascaded STATCOM, and the STATCOMs designed on this basis have been put into operation in Dongguan.

By virtue of the composite control structure of multiple sets in parallel operation (patented already) designed by LIN Yong, the 200Mvar STATCOMs in Dongguan set a new record in terms of capacity easily, and they are the STATCOMs with the highest voltage level of direct connection and the largest number of series levels worldwide.

So far, the STATCOM is the static reactive power compensator with the best performance. Compared with the SVC widely applied presently, the STATCOM is characterized by fast responses, small area, and generating no harmonics. Presently there are only more than ten sets of such devices in operation in the transmission grid and the largest capacity of the STATCOM was 150Mvar before the STATCOMs at 500kV Dongguan Substation of China Southern Power Grid.

CHAPTER 10 CONCLUSIONS AND FUTURE WORK

10.1 Conclusions

In the future construction of interconnected grids, with the increase of large-capacity generators and the wide applications of series capacitor compensators and long-distance HVDC systems, the subsynchronous oscillations will necessarily be a practical problem in urgent need of settlement. So, the studies on the theories and engineering technologies of power system stability enhancement and subsynchronous oscillations suppression are of great significance in engineering applications. And with the technological progress of high-voltage large-capacity power electronics devices and the reductions of their costs, it has become a practical and applicable way to provide dynamic reactive power compensation for the grid and to suppress subsynchronous oscillations.

This dissertation, in accordance with the applications of the SVC to the grids, especial to the interconnected grids, in providing reactive power compensation, enhancing voltage stability and suppressing subsynchronous oscillations and in combination with the engineering practices, discusses the approaches to the design of special SVC controllers, and performs simulation experiments and field engineering tests. This dissertation contributes to the research, engineering practice and innovations of the SVC mainly in the following aspects:

(1) Conducts modeling and simulation calculations in accordance with the China Southern Power Grid containing DC power transmission lines, and research the transient-state stability problems and the low-frequency oscillations brought about by small disturbances.

(2) Introduces the approaches to enhancing voltage stability with the SVC,

performs simulation calculations in combination with the practical data of China Southern Power Grid in accordance with the siting and capacity selection of the SVC, discusses the selection of the SVC capacity, and points out that it can enhance the voltage stability of the "Transmission of Power from the West to the East" channels to install 210Mvar SVC at Wuzhou Substation.

(3) Proposes an approach to designing the additional damping controller of the SVC based on Prony Identification, and simulation results indicate that this approach can effectively enhance damping and suppress dynamic oscillations. So far, this approach has been successfully applied in practical engineering design.

(4) Conducts simulation experiments for the SVCs at Wuzhou Substation, and the calculation results show that the SVCs can function correctly under various normal and faulty conditions. And the SVCs designed accordingly have been put into operation.

(5)Brings forward the control method of adding subsynchronous admittance regulations to the control system to suppress subsynchronous oscillations, and the methods of connecting the SVC directly to the 500kV bus while only taking the generator shaftings as the regulation control signals of the phase-controlled reactors, presents the algorithm implementation process, and the results of dynamic simulation experiment and field tests verify the correctness of SVC in suppressing SSR. This method has been leading worldwide.

(6) Conducts simulation experiments and analysis of the SVC in enhancing the voltage stability in the HVDC systems, providing references for the design and operation of HVDC systems, and two sets of SVCs designed accordingly for the Yunnan-Guangdong±800kV Ultrahigh-voltage DC Power Transmission lines have been put into operation at Chuxiong Converter Station.

(7) Analyzes the causes why two sets of SVCs based on traditional control structure may bring about reactive power oscillations when operating in parallel, puts forward a new composite control structure and makes simplifications in combination with the practice. The SVC controllers designed on the basis of this composite control structure have been tested by the RTDS simulation experiments and have been applied to the Yunnan-Guangdong ±800kV Ultrahigh-voltage DC Power Transmission lines.

And this was the first practical case that two sets of SVCs that are independently controlled respectively operate in parallel worldwide.

(8) The principle and algorithm of the decoupled control of a kind of cascaded STATCOM are put forward, and simulation experiments are conducted to verify the role of dynamic voltage support that the STATCOM plays. And the 200MVA STATCOMs designed according to the principle and algorithm have been in operation in Dongguan, and they are characterized by the highest voltage level of direction connection and the largest capacities all over the world.

10.2 Future Work

Some initial research results have been achieved in this dissertation and they have been successfully applied to the four world-leading actual large projects: the SSR-DSs in Guohua Jinjie Power Plant in Shanxi Province, the SVC at Wuzhou Substation in China Southern Power Grid, the SVCs at Chuxiong Converter Station of the Yunnan-Guangdong ±800kV Ultrahigh-voltage DC Power Transmission Lines, and the STATCOMs at the 500kV Dongguan Substation in China Southern Power Grid.

However, there is still much work for further research. For example,

(1) Theoretically, the SVC can be used to suppress the subsynchronous oscillations in the HVDC systems, and the controllers of the SVCs at Chuxiong Converter Station also have this function, but, owing to the limits of conditions, we did not have the Yunnan-Guangdong ultrahigh-voltage DC power transmission lines generate subsynchronous oscillations to test the effectiveness of this function. So, we still need to conduct more simulation calculations to research the effect of the SVC on the suppression of subsynchronous oscillations in HVDC systems.

(2) With the integration of new distributed energy sources into the grid in large scale, it becomes an important practical problem how to ensure the stability of the power systems that integrate a large quantity of wind power. According to the regulations of wind power integration into the grids, each wind farm must be furnished with a certain proportion of such static reactive power compensation devices as the

SVC and so on, so it will be a worthwhile research area how to control the large number of static reactive power compensation devices, such as the SVC and so on, in a clustering way.

REFERENCES

[2.1] Khoi T.Vu, Chen-Ching Liu, "Voltage Instability Mechanisms and Control Strategies," *Proceedings of The IEEE*, 1995, 83(11), pp.1442-1455.

[2.2] Carson W. Taylor, Power System Voltage Stability, New York, McGraw-Hill. Inc, 1994.

[2.3] Byung Ha Lee, Kwang Y. Lee, "A Study On Voltage Collapse Mechanism In Electric Power Systems," *IEEE Trans on PWRS*, 1991, 6(3), pp.966-974.

[2.4] C.D Vournas, P.W Sauer, et al., "Relationships Between Voltage And Angle Stability Of Power Systems," *IEEE Trans. on Electrical Power & Energy System*, 1996,18(8), pp.493-500.

[2.5] Kundur P., Power System Stability and Control, New York, McGraw-Hill Inc., 1994.

[2.6] CIGRE Task Force 38.02.10. "Modeling of Voltage Collapse Including Dynamic phenomena," Electra, 1993(147), pp.71-77.

[2.7] Π M Malkovich, Power system and operaion, USSR, 1965.

[2.8] V.A. VeniKov, Transient Processes In Electric Power Systems, V.A.Stroyev, Moscow Published, 1980.

[2.9] Sauer P.W, Pai M.A., "Power System Steady-Stability And The Load-Flow Jacobian," *IEEE Trans. on PWRS*, 1990, 5(4), pp.1374-1383.

[2.10] Kwatny H. G, et al., "Static Bifurcation on Electric Power System Networks: Loss of Steady-State Stability and Voltage Collapse," *IEEE Trans. on CAS,* 1986, 33(10), pp.981-991.

[2.11] E. Bompard, E. Carpaneto, "Asynchronous Motors Models For Voltage Stability Analysis," *Proceedings of The IEEE*, 1990, 78(11), pp.463-472.

[2.12] Chiang H.D, et al., "On voltage Collapse in Electric Power System," *IEEE Trans. on PWRS*, 1990, 5(2),pp.601-611.

[2.13] Sekine Y, Ohtsuki H, "Cascaded Voltage Collapse," *IEEE Trans. on PWRS*,1990,5(1).

[2.14] A. Borghetti, R. Caldon, et al. "On Dynamic Load Models for Voltage Stability Studies," *IEEE Trans. on PWRS*, 1997, 12(1), pp.293-303.

[2.15] Robert J, O'Keefe, Richard P. Schulz, "Improved Representation Of Generator and Load Dynamics in The Study of Voltage Limited Power System Operations," *IEEE Trans. on PWRS*, 1997, 12(1), pp.304-314.

[2.16] F.P. DeMello, J.W. Feltes, "Voltage Oscillatory Instability Caused By Induction Motor Loads," *IEEE Trans. on PWRS*, 1996, 11(3), pp.1279-1285.

[2.17] Yu Y.N., Zhang W.J., "Nature of Induction-Motor Load and Voltages Stability," *Proc. of Int Conf. on PST*, Beijing, 1992, pp.251-256.

[2.18] EL-Sadek M.Z, Abdelbarr F.N., "Effects of Induction Motor Load in Provoking Transient Voltage Instabilities in Power Systems," *Electrical Power System Research*, 1989(17).

[2.19] David J.Hill, "Nonlinear Dynamic Load Models With Recovery For Voltage Stability Studies," *IEEE Trans. on PWRS*, 1993, 8(1), pp.166-174.

[2.20] M.K. Pal, "Voltage Stability Conditions Considering Load Characteristics," *IEEE Trans. on PWRS*, 1992, 7(1),pp.243-249.

[2.21] Sekine Y., "Reverse Action of On-Load Tap Changer in Association With Voltage Collapse," *IEEE Trans. on PWRS*. 1990, 5(1).

[2.22] Larchs W.R., "Voltage Instability in Interconnected Power Systems: A Simulation Approach," *IEEE Trans. on PWRS*, 1992,7(2).

[2.23] Yu Y.N, Zhang W.J., "Simulation of Power System Voltage Stability Including Load and System Dynamics," *ICPST'94*, Beijing, China, 1994.

[2.24] Prabha Kundur, Kip Morison, Baofu Gao., "Practical Considerations in Voltage Stability Assessment," *International Journal of Electrical Power & Energy Systems*, 1993,15(4), pp.204-215.

[2.25] D.Popovic, I.A Hiskens, D.J Hill. "Investigations of Load-Tap Changer Interaction," *International Journal of Electrical Power & Energy Systems*, 1996, 18(2), pp.81-97.

[2.26] R.J Koessler. "Dynamic Simulation of static Var Compensators in Distribution System," *IEEE Trans. on PWRS*, 1992,7(3), pp.1285-1291.

[2.27] EPRI Final Report TR-108256 "System Disturbance Stability Studies for

WesternSystem Coordinating Council (WSCC)", September 1997.

[2.28] Elices, et al., "Design of robust controllers for damping interarea oscillations: application to the European power system. IEEE Trans. On Power Systems", Vol.19, No.2, May 2004, pp.1058-1067.

[2.29] M. Kurth, et al., "Oscillation behaviour of the enlarged European power system under deregulated energy market conditions," *Control Engineering Practice*, vol. 13, 2005. pp. 1525-1536.

[2.30] Johansson T, Wrang B, et al., "Stability problems in the Nordic power system," *CIGRE*, paper 31-06, 1982.

[2.31] Fairney W, Myles A, et al., "Low frequency oscillations on the 275kV interconnectors between Scotland and England," *CIGRE*, paper 31-08, 1982.

[2.32] Bolden R L, Wallace P J, Grainger A W, "Consideration in The Improvement of System Damping on The Southeast Australian Interconnected System," *CIGRE*, paper 31-05,1982.

[2.33] Kosterev D N, Taylor C W, et al., "Model Validation for The August 10, 1996 WSCC System Outage". *IEEE Trans. on Power Systems*, 1999, 14(3), pp.967-979.

[2.34] Xue Wu, Li Wenyun, Cao Kunnan, et al., "Improving Dynamic Stability of Yunnan Provincial and South China Power System by PSS", *Electricity*, 2001(2), pp.25-30.

[2.35] KleinM, Rogers G J , Kundur P, "A Fundamental Study of Inter 2 area Oscillations in Power Systems," *IEEE Trans on Power Systems*, 1991, 6 (3), pp.914-921.

[2.36] Jinyu Xiao, Xiaorong Xie, Yingduo Han and Jingtao Wu, "Dynamic Tracking of Low-frequency Oscillations with Improved Prony Method in Wide-Area Measurement System", presentation at 2004 *IEEE PES General Meeting*, pp.6-10, June 2004, Denver, Colorado, USA.

[2.37] F. Demello, "Concepts of Synchronous Machine Stability as Affected by Excitation Control", *IEEE Trans. on PAS,* No. 4, 1969.

[2.38] James Toal. "Learning to Live with Power System Oscillation", *IEE Colloquium on Power System Dynamics Stabilization*, 1998.

[2.39] Graham Rogers. "Power System Structure and Oscillations", *IEEE Computer Applications in Power*, Apr. 1999.

[2.40] Jixiu Yuan.Power System Security and Stability Control. Beijing: China Electric Power Press, 1996.

[2.41] Jingde Gao, Linzheng Zhang. Basic Theories and Analysis Methods of Transitional Processes of Electric Machines (A, B). Beijing: Science Press, 1983.

[2.42] K. Kim, et al., "Methods for Calculating Oscillations in Large Power Systems", *IEEE trans. on P. S.*, Vol. 12, No. 4, Nov. 1997.

[2.43] Qiang Lu, Yuanzhang Sun, "Nonlinear Stabilizing Control of Multimachine Systems", *IEEE/PES*, Vol. 4, No. 1, Feb., 1989.

[2.44] E. Z. Zhou, "Functional sensitivity concept and its application to power system damping analysis", *Trans on PWRS*, Vo1.9, No.1, Feb. 1994.

[2.45] Ahmed S S, "A Robust Power System Stabiliser for an Overseas Application," *IEE Colloquium on Generator Excitation Systems and Stability*, 6 Feb 1996, pp.1-4.

[2.46] Lu Q, Sun Y, Xu Z., Mochizuki T., "Decentralized Nonlinear Optimal Excitation Control," *IEEE Trans. on Power Systems*, 1996, Vol.11, No.4, pp.1957-1962.

[2.47] Yuangzhang Sun, Qiang Lu and Jingde Gao, "A New Nonlinear Modulation Control for HVDC Power Transmission Systems," *CSEE/IEEE International Conference on Power System Technology*, Beijing, Sept., 1991.

[2.48] Hauer J F, Demeure C J, Scharf L L, "Initial Results in Prony Analysis of Power System Response Signals," *IEEE Trans. on Power Systems*, 1990, 5 (1), pp.80-89.

[2.49] Hauer J F， "Application of prony analysis to the determination of modal content and equivalent models for measured power system response," *IEEE Trans on Power Systems*, 1991, l.6(3), pp.1062 -1068.

[2.50] T.Van Cutsem, C.D. Vournas, "Voltage Stability Analysis in Transient and Mid-Term time Scales," *IEEE Trans. on PWRS*, 1996, 11(1), pp.146-154.

[2.51] T.Van Cutsem, Y.Jacquemart, et al., "A Comprehensive Analysis of Mid-Term Voltage Stability," *IEEE Trans. on PWRS*, 1995,10(3), pp.1173-1182

[2.52] Baillieul J, Byrnes C I, "Geometric critical point analysis of lossless power system models," *IEEE*, Vol.CAS-29, No. 11, Nov. 1982, pp.724-737

[2.53] Tamura Y, Nakanishi Y, "On The Multiple Solution Structure, Singular Point And Existence Condition Of The Multiple Load Flow Solution," *IEEE PES Winter Meeting*, No A800448, 1980.

[2.54] Tamura Y, Sakamoto Y, Tayama Y, "Voltage Instability Proximity Index(VIPI) Based On Multiple Load Flow Solutions In Ill-conditioned Power Systems," *Proc IEEE CDC*, FP2-4, NOV, 1988.

[2.55] Ma. W M, Throp J S, "An Efficient Algorithm To Locate All The Load Flow Solutions," *IEEE Trans. on PWRS*, 1993, 8(3).

[2.56] Galiana F.D., "Load Flow Feasibility And The Voltage Collapse Problems," Proc of 23rd Conference On Decision And Control, Dec, 1984.485-487

[2.57] Galiana F D, "Analytic Properties Of The Load Flow Problem," *IEEE Proc. of ISCAS*, 1977.802-806.

[2.58] Yu. Y N, Huang C H, "Reactive Power Steady-State Security Region-Analysis and Computation," *Proc of Int on High Voltage Transmission*, China.

[2.59] V.A. Venikov, V.A Stroev, "Estimation of Electrical Power System Steady-State Stability In Load Flow Calcultaions," *IEEE Trans. on PAS*, 1974, 94(3).

[2.60] Tiranuchit A, Thomas R.J., "A Posturing Strategy Against Voltage Instabilities In Electric Power System," *IEEE Trans. on PWRS*, 1988, 3(2).

[2.61] Tiranuchit A., "Towards A Computationally Feasible On-Line Voltage Instabilities Index," *IEEE Trans. on PWRS*, 1988, 3(2).

[2.62] Bogovic M.M, Phadke A.G., "Voltage Stability Assessment Through Measurement of A Reduced State Vector," *IEEE Trans. on PWRS*, 1990, 5(4), pp.198-203.

[2.63] S.A be, et al., "Criteria For Power System Voltage Stability by Steady-State Analysis". Presented at the *IEEE PES Summer Meeting*, San Francisco, Calif, 1975, 20(25).

[2.64] Canizares C.A, Alvarado F.L., "Point of Collapse and Continuation Methods for Large AC/DC Systems," *IEEE Trans. on PWRS*, 1993, 8(1), pp.1-8.

[2.65] Canizares C.A, Alvarado F.L, et al., "Point of Collapse Methods Applied to AC/DC Power Systems," *IEEE Trans. on PWRS*, 1992, 7(2), pp.673-683.

[2.66] Obadina O.O, Berg G.J., "Determination of Voltage Stability Limit in Multimachine Power Systems," *IEEE Trans. on PWRS*, 1988, 3(4).

[2.67] Deuse J, Stubbe M, "Dynamic Simulation of Voltage Collapse," *IEEE Trans. on PWRS*, 1993, 8(3).

[2.68] El-Sadek M.Z. Voltage Instabilities Subsequent to Short-Circuit Recoveries. Electric Power System Research, 1991(21).

[2.69] Demarco C.L, Overbye T.J. An Energy Based Security Measure for Assessing Vulnerability to Voltage Collapse. *IEEE Trans. on PWRS.*, 1990, 5(2).

[2.70] Overbye T.J, Demarco C.L. Use of Energy Methods for On-Line Assessment of Power System Voltage Security. *IEEE Trans. on PWRS.*, 1993, 8(2), pp.452-458.

[2.71] H.R Pota, P.J Moylan, "A New Lyapunov Function For interconnected Power Systems," *IEEE Trans. on Automatic Control*, 1992(37), pp.1192-1195.

[2.72] Dobson I, Chiang H.D., "Towards a Theory of Voltage Collapse In Electric Power System," *Systems and Control Letters*, 1989(13), pp.253-262.

[2.73] I.A Hiskens, et al., "Analysis Tools For Power systems Contending With Nonlinearityes". *Proceeding of the IEEE*, 1995, 83(11), pp.1573-1587.

[2.74] Brucoli M, et al., "A Probabilistic Approach to the Voltage Stability Analysis of Interconnected Power System,". *Electric Power System Research*, 1986(10), pp.157-166.

[2.75] Sharaf T.A.M, Berg G.J., "Probabilistic Voltage Stability Indexed". *IEE. Proc. C*, 1991, 138(6).

[2.76] DeMarco C.L, Bergen S.R., "A Security Measure of Random Load Disturbances in Nonlinear Power System Models," *IEEE Trans. On CAS.*, 1987, 34(12), pp.1546-1557.

[5.1] Mithulananthan, N., Canizares, C.A., Reeve, J., Rogers, G.J, "Comparison of PSS, SVC, and STATCOM controllers for damping power system oscillations," Power Systems, *IEEE Transactions on Power Systems*, Volume 18, Issue 2, May

2003, pp.786-792

[5.2] Hammad A., Boshoff S., Van der Merwe W.C., Van Dyk C.J.D., Otto W.S. and Kleyenstüber U.H.E., "SVC for Mitigating 50 Hz Resonance of a Long 400 kV ac Interconnection", 1999, *CIGRE Symposium Singapore*

[5.3] Liu, J. Jia, J. C, “Research of Wind Farm SVC Control System Based on Real-Time Operation System”, *Power and energy engineering conference* 2010, pp.96-99

[5.4] Innocent Kamwa, Giles Trudel, Luc Gérin-Lajoie, " Robust Design and Coordination of Multiple Damping Controllers Using Nonlinear Constrained Optimization", *IEEE Transactions on Power Systems*, Vol. 15, No.3, August 2000. pp.1084-1092

[5.5] XIAO Jin-yu,XIE Xiao-rong,HAN Ying-duo,et al. "Dynamic Tracking of Low-frequency Oscillations with Improved Prony Method in Wide-area Measurement System," *IEEE Power Engineering Society General Meeting*, 2004.1104-1109.

[5.6] Dermentzoglou, J. C.,Karlis, A. D.,"Development of linear models of static var compensators and design of controllers suitable for enhancing dynamic/transient performance of power systems including wind farms", *Electric Power Systems Research*, Vol.8, No.4, 2011, pp.922-929.

[7.1] Putman, T. H. and Ramey, D. G., "Theory of modulated reactance solution for subsynchronous resonance". IEEE Trans., PAS-101(6)(1982):1527-1535.

[7.2] HSU Y Y, WU C J, "Design of PID static var controller for the damping of subsynchronous oscillations". *IEEE Trans on Energy Conversion*, 1988 , 3 (2), pp.210-216.

[7.3] PADIYAR K R, VARMA R K, "Static var system auxiliary controller for damping torsional oscillations," *International Journal of Electrical Power and Energy Systems*, 1990 , 12 (4), pp.271-286.

[8.1] J.M.Guerrero, L. G de Vicuna, Jose Matas, Miguel Castilla and Jaume, "Output Impedance Design of Parallel-Connected UPS Inverters With Wireless Load-Sharing Control,' *IEEE Transaction on Industrial Electronics*, 2005, 52(4), pp.1126-1135.

[8.2] Xiao Sun, Yim-Shu Lee and Dehong Xu, "Modeling, Analysis and Implementation of Parallel Multi-Inverter Systems With Instantanceous Average-Current-sharing Scheme," *IEEE transactions on power electronics*, 2003, 18(3), pp.844-856.

[8.3] Zhang Chunjiang, Zu Feng, GU Herong, Zhao Qinglin, Chen guitao, "An Interactive Following Current-Sharing Control Strategy for Paralleled Inverters in Full Digital," *IEEE ICEMS*, 2005, pp.1080-1083

[8.4] Pei Yunqing, Jiang Guibin, Yang xu, Wang Zhaoan, "Auto-Master-slave control technique of parallel inverters in distributed AC power systems and UPS," *IEEE 35th Annual Power Electronics Specialists Conference, PESC04*, 2004, Vol.3, pp.2050-2053

[8.5] S.J.Chiang and J. M. Chang, "Parallel Control of the UPS Inverters with Frequency-dependent Droop Scheme," *IEEE Annual Power Electronics Specialists Conference*, 2001, Vol.2, pp.957-961.

[8.6] KIM J W, CHOI H S, CHO B H, "A novel droop method for converter parallel operation," *IEEE Trans on Power Electronics*, 2002, 17(1), pp.25-32.

[8.7] CHANDORKAR M C, DIVAN D M, ADAPA R, "Control of parallel connected inverters in standalone ac supply sytem," *IEEE Trans on Industry Application*, 1993, 29(1), pp.136-143.

[8.8] IEEE Special Stability Controls Working Goup, "Static Var Compensator Models for Power Flow and Dynamic Performance Simulation," *IEEE Transaction on Power Systems*, Vol. 9, No. 1, February 1994, pp.229-239.

[9.1] CIGRE, "Static Synchronous Compensator," working group 14.19, September 1998.

[9.2] L. Chun, J. Qirong, X. Jianxin, "Investigation of Voltage Regulation Stability of Static Synchronous Compensator in power system," *IEEE Power Engineering Society, Proceedings of the Winter Meeting 2000*, IEEE Vol. 4, pp. 2642-2647

[9.3] H. F. Wang, "Applications of damping torque analysis to StatCom control," Electrical Power and Energy Systems, Vol. 22, 2000, pp. 197-204

[9.4] B. Han, S. Back, H. Kim, G. Karady, "Dynamic Characteristic Analysis of SSSC bases on multibrige inverter," *IEEE Trans. on Power Delivery*, Vol. 17, no. 2, April 2002, pp. 623-629

[9.5] P.W. Lehn, "Exact modeling of the Voltage Source Converter," *IEEE Trans. on Power Delivery*, Vol.17, No. 1, pp. 217-222, January 2002

[9.6] N. Mohan, T. M. Undeland, W. P. Robbins, "Power Electronics: Converters, Applications, and Design," John Wiley and Sons, 1995

BIOGRAPHY

LIN Yong was born on January 25, 1977, in Fuzhou, China. He received the BE and MSc degrees in Electrical Engineering both from Tsinghua University, Beijing in 1999 and 2002 respectively. He accomplished the control strategy of the SVC at Chuxiong Converter Station to improve the voltage stability of Yunnan-Guangdong HVDC system which is the first project of shunt 2 self-governed SVCs in the same site for ±800kV UHVDC system in the world and became a certified senior engineer in 2010. And this novel shunt control structure was also applied to the 200MVA STATCOM at 500kV Dongguan Substation of China Southern Power Grid. His research interests are power quality, wind power generation and high voltage power electronics, etc. His permanent alumni E-mail addresses are linyong@ & yong.lin@